

INFORMATION TO USERS

This manuscript has been reproduced from the microfilm master. UMI films the text directly from the original or copy submitted. Thus, some thesis and dissertation copies are in typewriter face, while others may be from any type of computer printer.

The quality of this reproduction is dependent upon the quality of the copy submitted. Broken or indistinct print, colored or poor quality illustrations and photographs, print bleedthrough, substandard margins, and improper alignment can adversely affect reproduction.

In the unlikely event that the author did not send UMI a complete manuscript and there are missing pages, these will be noted. Also, if unauthorized copyright material had to be removed, a note will indicate the deletion.

Oversize materials (e.g., maps, drawings, charts) are reproduced by sectioning the original, beginning at the upper left-hand corner and continuing from left to right in equal sections with small overlaps.

Photographs included in the original manuscript have been reproduced xerographically in this copy. Higher quality 6" x 9" black and white photographic prints are available for any photographs or illustrations appearing in this copy for an additional charge. Contact UMI directly to order.

**Bell & Howell Information and Learning
300 North Zeeb Road, Ann Arbor, MI 48106-1346 USA
800-521-0600**

UMI[®]

NOTE TO USERS

Page(s) not included in the original manuscript are unavailable from the author or university. The manuscript was microfilmed as received.

110

This reproduction is the best copy available.

UMI

**Moisture occurrence in
roof assemblies containing moisture storing insulation and
its impact on the durability of building envelope**

Dominique Derome

A thesis
In
The Department
of
Building, Civil and Environmental Engineering

Presented in Partial Fulfillment of the Requirements
for the Degree of Doctor of Philosophy at
Concordia University
Montreal, Quebec, Canada

October 1999

©Dominique Derome, 1999



**National Library
of Canada**

**Acquisitions and
Bibliographic Services**

**395 Wellington Street
Ottawa ON K1A 0N4
Canada**

**Bibliothèque nationale
du Canada**

**Acquisitions et
services bibliographiques**

**395, rue Wellington
Ottawa ON K1A 0N4
Canada**

Your file Votre référence

Our file Notre référence

The author has granted a non-exclusive licence allowing the National Library of Canada to reproduce, loan, distribute or sell copies of this thesis in microform, paper or electronic formats.

The author retains ownership of the copyright in this thesis. Neither the thesis nor substantial extracts from it may be printed or otherwise reproduced without the author's permission.

L'auteur a accordé une licence non exclusive permettant à la Bibliothèque nationale du Canada de reproduire, prêter, distribuer ou vendre des copies de cette thèse sous la forme de microfiche/film, de reproduction sur papier ou sur format électronique.

L'auteur conserve la propriété du droit d'auteur qui protège cette thèse. Ni la thèse ni des extraits substantiels de celle-ci ne doivent être imprimés ou autrement reproduits sans son autorisation.

0-612-47707-X

Canada

ABSTRACT

Moisture occurrence in roof assemblies containing moisture storing insulation and its impact on the durability of building envelope

Dominique Derome, Ph.D.
Concordia University, 1999

Moisture storing insulation such as cellulose has gained a large segment of the residential market, both in new and retrofit construction. Moisture deposited by exfiltration and adsorbed within the envelope reduces the thermal performance of the envelope and favors fungus growth leading to deterioration of the materials and contamination of the indoor air. Roof assemblies thus insulated are particularly vulnerable to the mechanism of moisture accumulation.

The objective of this study is to investigate the pattern of moisture accumulation in single cavity flat roofs fully insulated with cellulose insulation. Through an extensive experimental program using two test huts in an environmental chamber, patterns of moisture movement and accumulation for a full wetting-drying cycle have been developed for the first time. Using these results for validation, a model using the water potential concept as the driving force for moisture movement was developed to simulate the complete wetting and drying of wood components within the envelope.

Within an Environmental Chamber, which allows for testing full scale specimens, a 190-day test with daily cyclic conditions was designed and performed during which moisture transfer was monitored with electronic sensors and gravimetry. The test consisted of eight flat roof assemblies fully insulated with cellulose subjected to one complete, quasi real-time wetting-drying cycle. The research presents a methodology to evaluate the performance of retrofitting energy efficiency measures using moisture storing insulation in residential buildings.

An hygrothermal model using the concept of water potential gradient as the driving force for moisture movement in wood has been developed for flat roofs insulated with cellulose and integrated into an existing finite element computer model. The model includes the geometrical representation of the wood component, moisture content-water potential relationships, effective water conductivity and mass and heat transfer coefficients. The results from the computer model compare favorably with the experimental results and validate the use of the water potential approach in predicting moisture movement through building envelope assemblies.

The experimental and modeling data document the moisture condition of the assemblies. This moisture condition is an indicator of durability in terms of fungus growth. Design guidelines have been derived from this study for flat roof assemblies incorporating moisture storing materials. This information can be used by the designer to evaluate the hygrothermal performance and the durability of his/her design.

Acknowledgements

The pursuit of a PhD has been a dream of mine for a long time. My husband has always been confident that I would proceed to continue my graduate studies. Dr. Paul Fazio, in his quest to introduce the architectural dimension to building engineering, created the right environment for me to pursue the PhD while on faculty. The last four years have been filled with a lot of work, but also with a feeling of accomplishment.

I would like to thank my supervisor, Paul Fazio, who believed in me. I had the privilege to design and execute the first experiment to be held in the Environmental Chamber. He has been patient yet knew how to keep alive the sense of urgency. He has been understanding yet challenging and thought-provoking. He provided, through the NSERC and FCAR funding, the support to develop the Environmental Chamber and keep the facility operational. I would also like to gratefully thank my co-supervisor, Yves Fortin, who has been willing to stretch out of his domain of wood science to follow my work in building engineering. His support has been constant. Even at distance, I know I kept him busy with e-mails and special delivery packages and I want him to know how I appreciate his timely suggestions and valuable insight.

I would like to thank the many people who have contributed to this success: my colleagues, and specially Drs. Radu Zmeureanu, Dorel Feldman, Andreas Athienitis, Hugues Rivard, Fariborz Haghighat and Claude Bédard, for their availability in answering questions; Dean Nabil Esmail to have trusted me to finish my thesis while being a faculty member; my students of the last four years who showed respect and understanding for my time required by research; the people at Siricon, Dino Gerbasi, Sebastiano Depani, Linda

Farinaccio, who brought this challenging experimental project to us, shared their field experience and database with me and participated in the project; and finally the whole staff of the department, and specially Olga Soares, Rosie Meldonian, Vivianne Majeau and Sheila Anderson for their words of encouragement all along.

The testing was a huge endeavor and benefited from the technical support of a wonderful team. Jiwu Rao implemented and operated the data acquisition system during the test. My thanks goes also to Jacques Payer, Luc Demers, Joe Hrib, Joseph Zilka and Guylaine Desmarais for their support through the project.

In demanding times, family is utmost important. I want to thank my father, Jacques H. Derome, who listened and helped me order my thoughts all along the project, by asking the good questions in a field he did not even know, as the excellent educator he has always been and to have performed the editing of the whole thesis. The support from my family was always felt and appreciated. Thank you also to my mother, Francine Scott, who babysat so much, my brothers and sister, Pierre, Richard and Michèle, and my mother-in-law, Geneviève Voisard, who took so often care of my children.

I would like to recognize and thank my biggest fan and supporter, my husband Normand Voisard. He had to sacrifice a lot to allow me to focus on my research. He has been supporting and encouraging all along. I want also to thank my children, Gabrielle, Frédéric and Brigitte Voisard, to have shared their mother with building science. They have been so understanding and yet, for four years, they did not have a mother as available as she wished she could have been.

Table of contents

List of Figures.....	xi
List of Tables	xv
Nomenclature	xvii

Chapter 1. Statement of research problem 1

1.1 Introduction.....1

1.1.1 Current state of knowledge1

1.1.2 Problem.....4

1.1.3 Proposed approach.....5

1.2 Research objectives.....6

1.3 Literature review7

1.3.1 The envelope as a system.....7

1.3.1.1 Function and constituents8

1.3.1.2 Impact and interrelationships of moisture related parameters11

1.3.1.3 Standard test methods for the envelope14

1.3.2 Moisture transfer through the envelope16

1.3.2.1 Theoretical framework.....16

1.3.2.2 Moisture transfer by diffusion19

1.3.2.3 Moisture transfer by convection22

1.3.2.4 Moisture storage.....24

1.3.2.5 Capillary and supersaturated regions29

1.3.2.6	Thermodynamic approach – water potential.....	31
1.3.3	Computer modeling of heat and moisture transfer	34
1.3.3.1	Approaches for the modeling of heat transfer.....	35
1.3.3.2	Combined moisture and heat transfer modeling	36
1.4	Summary.....	49
Chapter 2.	Experimental procedure	50
2.1	Context.....	50
2.1.1	Objectives and plan of experiment	53
2.1.2	The testing facility	54
2.2	The experimental procedure.....	55
2.2.1	Description of a typical building.....	55
2.2.2	Reproduction of the typical roofs in the test chamber	58
2.2.3	Description of test hut construction	60
2.2.4	Simulated testing conditions	66
2.2.5	Parameters monitored.....	68
2.3	Running of the test.....	77
2.3.1	Preparation work	77
2.3.2	The running of the test	78
2.3.3	Dismantling of the set-up	80
2.4	Results	81
2.4.1	Wood plank and joist moisture content.....	83
2.4.2	Cellulose insulation moisture content	90
2.5	Conclusion	98

Chapter 3. Model development and validation	100
3.1 Physical phenomena and processes in the flat roof planks	100
3.1.1 Physical parameters.....	101
3.1.2 Choice of the moisture movement modeling approach.....	104
3.1.3 Description of the proposed physical model and the resulting modifications on the computer model	108
3.2 Determination of the parameters of the physical model	112
3.2.1 Nondimensional determination of the convective heat transfer coefficient.....	113
3.2.2 Experimental determination of the convective heat transfer coefficient	117
3.2.3 Analytical determination of the convective mass transfer coefficient ...	122
3.2.4 Experimental determination of the convective mass transfer coefficient.....	124
3.2.5 Sorption curves.....	127
3.2.6 Determination of the effective water conductivity.....	134
3.3 Modifications to the computer model	139
3.4 Validation of model for the simulation of the drying process.....	140
3.4.1 Determination of the actual conditions during the drying period	141
3.4.2 Determination of the simulation conditions	144
3.4.3 Computer model simulations	150
3.4.4 Observations on the simulation results.....	154
3.5 Validation of model for the simulation of the wetting process	156
3.5.1 Determination of the actual conditions during the wetting period.....	156
3.5.2 Determination of the simulation conditions	158

3.5.3	Computer model simulations	160
3.6	Conclusion	161
Chapter 4.	Guidelines derived from the research program	163
4.1	How to transfer building science to the designer	163
4.2	Knowledge transfer at the conceptual level of flat roof design.....	164
4.3	Knowledge transfer at the detailing level of flat roof design	167
4.4	Conclusion	171
Chapter 5.	Conclusion	172
5.1	Contributions of the research	173
5.2	Recommendations for further work.....	174
5.3	Related publications	176
References		177
Appendix A.	Conversion calculations	190
Appendix B.	Legend of sensors used during the experimental test.....	195
Appendix C.	Calculations results of the convective heat and mass transfer coefficients above the wood in a 10 mm high tunnel	197
Appendix D.	Schematic representation of the finite-element mesh	207

List of figures

Figure	Title	Page
1.1	Phases of moisture adsorption (after Ojanen <i>et al.</i> 1989).....	18
1.2	Schematic diagram of the sorption of a hygroscopic material showing the hysteresis between the adsorption and desorption curves.....	26
1.3	Schematic representation of moisture regimes after Burch and Thomas (1992).....	30
1.3.1	Schematic representation of moisture regions according to Künzle (1995).....	31
2.1	Testing configuration for the flat roof test.....	55
2.2	Typical structure of plank framing structure or “carré de madrier” (after Auger et Roquet 1998).....	56
2.3	Schematic view of part of building subjected to testing via test hut	59
2.4	Comparison of site (left) and test hut detail (right) of roof/wall junction.....	60
2.5	Typical hut and composition of roof assemblies	61
2.6	Schematic views of thermos and lambourdes test huts showing all 10 cavities	64
2.7	Exfiltration path schematic from inside to roof cavity	65
2.8	Typical thermos assembly during construction	65
2.9	Typical lambourdes assembly during construction.....	66
2.10	View of the cavity L5, which has lateral leakage all along lateral wall	66
2.11	Specimens on cold side of assembly, referred to as R in Figure 2.15	74
2.12	Specimens on interior side of assembly, referred to as J in Figure 2.15.....	75
2.13	Specimen in cavity T4 – gypsum board and polyethylene sheet, referred to as J in Figure 2.15	75
2.14	Specimens in the side of the header joists of T5 and L5 referred to as X in Figure 2.15	75
2.15	Schematic plan and corresponding details for monitoring	76

2.16	Typical layout of instrumentation in a thermos cavity	76
2.17	Results from airtightness measurements of cavities prior to insulation ..	77
2.18	Temperature profiles for period 1 to 7 – showing average temperature reproduced in the environmental chamber for each hour of each period vs. planned conditions	80
2.19	Comparison of gravimetric and moisture pin data in T3	82
2.20	Comparison of gravimetric and moisture pin data in T5	82
2.21	Comparison of gravimetric and moisture pin data in L3	83
2.22	Average moisture content in wood planks for length of test in thermos	84
2.23	Average moisture content in wood planks for length of test in lambourdes	85
2.24	Moisture content in T3 during length of test	86
2.25	Moisture content in L3 during length of test	87
2.26	Moisture content in L3 vs L2.....	87
2.27	Levels of exposure to moisture content and temperature in thermos roof	89
2.28	Levels of exposure to moisture content and temperature in lambourdes roof.....	90
2.29	Moisture content distribution in cellulose insulation during test in the diffusion only cavities.....	92
2.30	Moisture content distribution in cellulose insulation during test in the long exfiltration path cavities.....	93
2.31	Moisture content distribution in cellulose insulation during test in short exfiltration path cavities.....	94
2.32	Comparison of the moisture content distribution in cellulose insulation during test in the two diffusion driven cavities	95
2.33	Comparison of the moisture content distribution in the long exfiltration path cavities	95
3.1	Schematic of parameters	102
3.2	Schematic representation of heat flow through a wood surface	117
3.3	Photos of the experimental setup for convective coefficients	120

3.4	Sorption curves function of the relative humidity	127
3.5	Sorption curves function of water potential.....	128
3.6	Desorption curves for spruce at 5°C, 21°C and 35°C.....	129
3.7	Adsorption curves for spruce at 5°C, 21°C and 35°C.....	130
3.8	Full adsorption and desorption curves for spruce at 5°C, 21°C and 35°C illustrating the hysteresis.....	131
3.9	Full and intermediary sorption curves for yellow poplar as per Peralta (1995), as function of relative humidity on left and water potential on right.....	132
3.10	Intermediate desorption curves from 30%, 25% and 20%M at three temperatures.....	133
3.11	Effective water conductivity of red pine and epicea as function of moisture content and temperature.....	136
3.12	Effective water conductivity coefficients as function of moisture content and state of sorption.....	137
3.13	Conditions measured below and in the planking of cavity T3 during the test.....	142
3.14	Schematic representation of a situation with pure heat conduction.....	145
3.15	Sorption curves for non-treated cellulose insulation	147
3.16	Comparison of modeling and experimental data from 28% M in T3. .	151
3.17	Comparison of modeling and experimental data from 24% M in T3. .	151
3.18	Comparison of modeling and experimental data from 20% M in T3 ...	152
3.19	Sensibility analysis by varying the convective heat transfer coefficient	153
3.20	Sensibility analysis by varying the convective mass transfer coefficient	154
3.21	Moisture gradient across the thickness of the plank during simulation	155
3.22	Schematic representation of the daily periodic mass transfer with an overall drying direction.....	155
3.23	Conditions measured below and in the planks of cavity T3 during the wetting part of the test.....	157

3.24	Comparison of modeling and experimental data for wetting period in T3	160
4.1	Schematic representation of the four basic layers of a flat roof system	164
4.2	Schematic representation of the different flat roof assemblies for wood-framed buildings	165
4.3	Schematic representation of air leakage through a building from basement to roof.....	168
4.4	Parapet details before and after the installation of the insulation with detailing in order to minimize air flow through the roof	169
4.5	Party wall details before and after the installation of the insulation.....	170
4.6	Roof/parapet details before and after the installation of the insulation	170
4.7	Electrical outlet details before and after the installation of the insulation	170
4.8	Roof drain details before and after the installation of the insulation....	171
B.1	Diagrams of layout of sensors.....	196
C.1	Temperature profiles for run 1	198
C.2	Heat per square meter of wood as a function of time for run 1	198
C.3	Temperature profiles for run 2	199
C.4	Heat per square meter of wood as a function of time for run 2	200
C.5	Temperature profiles for run 3	201
C.6	Heat per square meter of wood as a function of time for run 3	201
C.7	Temperature profiles for run 4	203
C.8	Heat per square meter of wood as a function of time for run 4	203
C.9	Temperature profiles for warming in wet conditions	205
C.10	Heat per square meter of wood as a function of time for warming on wet conditions	205
C.11	Results of the drying test to determine the convective mass transfer coefficient	206
D.1	Schematic representation of finite-element mesh	207

List of tables

Table	Title	Page
1.1	Environmental barriers and driving forces (Bomberg and Brown 1993) .9	
1.2	Moisture transfer processes in building materials and components (after Kumaran 1992)18	
1.3	Classification used by HAMTIE-task 1 for HAMCaD-codes38	
2.1	Typical assemblies62	
2.2	Characteristics of cavities63	
2.3	Summary of basis for simulated conditions.....67	
2.4	Typical vs tested conditions.....68	
2.5	Accuracy of moisture readings in wood with pins from manufacturer ..70	
2.6	Correction table provided by pins manufacturer for the range of temperatures70	
2.7	Correction table provided by pins manufacturer for species71	
2.8	Depths of pins in this study.....71	
2.9	Synoptic table of test progress79	
3.1	Constant and variable parameters101	
3.2	Various moisture movement scenarios103	
3.3	Schematic representation of the physical model.....109	
3.4	Developments and modifications of the physical and computer model111	
3.5	Calculation of the convective heat transfer coefficient based on forced convection ($T = 20^{\circ}\text{C}$, $k_f=0.026$)).....115	
3.6	Calculation of the convective heat transfer coefficient based on free convection ($T = 20^{\circ}\text{C}$).....116	
3.7	Summary of nondimensional analysis on convective heat transfer coefficient117	

3.8	Summary of experimental convective heat transfer coefficients values	122
3.9	Convective mass transfer coefficient using water potential as the driving force	122
3.10	Mass transfer convective coefficients from conversion using Lewis analogy	123
3.11	Summary of the experimental convective heat and mass transfer coefficients	126
3.12	Equivalence of diffusion coefficients	135
3.13	Summary of the values retained for each parameter of the physical model	138
3.14	Measured conditions for short intervals of time within each period	144
3.15	Extrapolated temperatures for each sub-period	146
3.16	Relative humidity inferred from measured vapor pressures	146
3.17	Relative humidity in equilibrium with measured moisture content in wood and cellulose per period	147
3.17.1	Relative humidity extrapolated from measured moisture content per sub-period	149
3.18	Drying simulation conditions.....	150
3.19	Measured conditions for short intervals of time within each period during wetting.....	158
3.20	Temperature and relative humidity inferred from measured vapor pressure	159
3.21	Extrapolated relative humidity for T3-6	159
3.22	Wetting simulation conditions	160
C.1	Summary of data calculated from run 1	197
C.2	Summary of data calculated from run 2.....	199
C.3	Summary of data calculated from run 3	200
C.4	Summary of data calculated from run 4.....	202
C.5	Summary of data calculated from run 5.....	204

Nomenclature

Symbol	Parameter	Units
C	water concentration in wood	$[\text{kg}_{\text{water}}/\text{m}^3_{\text{moist wood}}]$
C'	electrical capacitance	[F]
g	density of mass flow rate	$[\text{kg}/\text{m}^2\cdot\text{s}]$
G	specific Gibbs free energy	
G _m	specific gravity of wood	$[\text{kg}_{\text{oven-dry wood}}\cdot\text{m}^3_{\text{water}}/\text{kg}_{\text{water}}\cdot\text{m}^3_{\text{moist wood}}]$
h	transfer coefficient	
h _h	convective heat transfer coefficient	$[\text{W}/\text{m}^2\cdot^{\circ}\text{C}]$
h _ψ	convective mass transfer coefficient	$[\text{kg}^2_{\text{water}}/\text{m}^2\cdot\text{s}\cdot\text{J}]$
h	specific enthalpy or heat	$[\text{J}/\text{m}^3 \text{ or } \text{kJ}/\text{kg}]$
H	total enthalpy	[J]
J	flux	
k	transport coefficient	
\tilde{k}	effective thermal conductivity tensor	$[\text{W}/\text{m}\cdot\text{s}\cdot^{\circ}\text{C}]$
\tilde{K}	effective moisture conductivity tensor	$[\text{kg}^2_{\text{water}}/\text{m}_{\text{moist wood}}\cdot\text{s}\cdot\text{J}]$
m	mass	[kg]
M	moisture content	$[(\text{kg}_{\text{water}}/\text{kg}_{\text{dry material}}) \times 100]$
p	pressure	[Pa]
Δp	pressure difference	[Pa]
q	moisture flux	$[\text{kg}_{\text{water}}/\text{m}^3_{\text{moist wood}}\cdot\text{s}]$
Q	volumetric airflow	$[\text{m}^3/\text{s} \text{ or } \text{l}/\text{s}]$
R	thermal resistance	$[\text{m}^2\cdot^{\circ}\text{C}/\text{W}]$

R	gas constant	[J/mol·°K]
U	thermal conductance	[W/m ² ·°C]
t	time	[s]
T	temperature	[°C]
w	weight	[N]
Z	vapor resistance	[Pa·m ² ·s/kg]

Greek Alphabet Symbols

β	factor function of moisture content	
ε	ratio of vapor diffusion to total moisture movement	
Φ	potential	
μ	vapor permeability	[s]
ρ	density	[kg/m ³]
ψ	water potential	[J/kg _{eau}]

Subscripts

a	air
c	condensation, condensation plane
$e.f.$	external force
g	gravitational
h	heat
in	interior
m	matric
$moist$	moist
p	pressure

o	dry
osm	osmotic
out	exterior
sat	saturation
sorp	sorption
t	temperature
T	thermal
v	vapor
vap	vaporisation
w	water
ψ	mass

Abbreviations

FSP	Fiber saturation point of wood
M	Moisture content
NBCC	National Building Code of Canada
RH	Relative humidity of the air

Chapter 1

Statement of research problem

1.1 Introduction

As the movement of moisture in walls and roofs under varying daily and seasonal conditions has not been totally characterized, the prediction of moisture occurrence in envelope assemblies still lacks accuracy. However, more and more assemblies are built with materials able to store moisture like cellulose insulation. An estimation from the Quebec house builders association evaluates cellulose and glass fiber insulation having an equal share of the new housing market (Gagné 1997). The performance of assemblies incorporating moisture storing insulation, under moisture and heat transfer, called hygrothermal performance, is not yet fully understood.

1.1.1 Current state of knowledge

The envelope is a subsystem of the building, composed of a large number of constituents that together must separate the indoor conditioned environment from the outdoor environment. Since the conditions are different on each side, differentials in terms of partial vapor pressure, air pressure and temperature create driving potentials for moisture, air and heat transfer through the envelope. Moisture movement through the envelope has two major driving potentials: (i) differential in vapor partial pressure, causing moisture diffusion, and (ii) differential of air pressure, causing moisture-laden air to move. On its way through the assembly, moisture is partially adsorbed by some of the building

materials where it may accumulate. This type of material is said to be hygroscopic. Excessive moisture within the assembly may decrease its thermal resistance, augments the risk of fungus development and biodegradation under appropriate temperature and time exposure and multiply shrinkage and swelling effects. To resist the vapor, air and heat flows, vapor retarder materials, air barrier strategies, and thermal insulation have been developed.

Good practice of building envelope assembly construction has been traditionally based on experience and rules of thumb. The scientific approach to building envelope assessment started around the late 30's, *e.g.* with research in the Prairies on air leakage (Bomberg and Brown 1993), and in the United States on attic ventilation (Rose 1995a). In 1947, the Division of Building Research of Canada was set up by the National Research Council of Canada. Soon, other countries set up their research body dedicated to building. Over the years, case and field studies led to a general surveying of good and bad envelope construction practices. In parallel, experimental work was performed in laboratories. Early work focused on heat transfer and building materials. The scope was then enlarged to include building envelope systems, such as windows, wall and roof assemblies, and was widened to examine the moisture issue. First, diffusion only was studied, then air movement and air exfiltration were included. Tests are now increasingly complex and experimental setups simulate conditions close to the real ones. This half-century of research has provided knowledge in terms of material properties and transfer mechanisms. This knowledge has been partially embedded in several heat and moisture transfer computer models using the finite-difference method. All these models simulate moisture diffusion. Several models take into account capillary flow and some codes have provisions to accommodate air movement. However, none of the models accounts in reality for the spatial distribution of the convective mass transfer due to air exfiltration. Although a lot of work is performed on theoretical modeling of combined heat and

moisture transfer, the validity of the resulting data depends entirely on the experimental measurements of the properties of the materials. Based on these measurements, coefficients are determined and fed into the computer models.

The approach applied in most models divides moisture transfer into separate regimes, each acting under a different driving potential: the hygroscopic regime (vapor and bound water), the capillary one (liquid) and the above saturation point one (viscous flow). This separation requires transfer coefficients for each regime and a transition module between regimes. In wood science, for wood drying, another approach in modeling has been developed using the difference in the free energy state of water, *i.e.* the water potential gradient, as the driving force. This approach has the advantage of encompassing all the above mechanisms with one driving potential. The energy state of water within the matrix of the wood cell is defined in relation to the energy state of free water in a pool, *i.e.* in a standard reference state. Depending on the amount of water within the cells and the walls of the cells, the water is more or less free. The gradient in the energy state of water causes moisture flow at a rate given by the moisture transport coefficient, called the effective water conductivity.

With the present state of knowledge, the long term performance of the building envelope subjected to moisture transfer cannot be assessed solely with computer models but is rarely the object of testing. On the other hand, on-site investigations are often limited, as not all parameters can be controlled. More specifically, for envelope assemblies integrating hygroscopic insulating materials, little experimental work has been performed, especially in a retrofitting context.

1.1.2 Problem

Without means to predict the long term hygrothermal performance of the envelope components, requirements of standards and codes cannot be enforced effectively. Verification of designs is usually performed with simple engineering methods. Consequently, the requirements regarding moisture control in envelope assemblies stemming from codes, like the National Building Code of Canada, cannot reflect the total complexity of the hygrothermal performance of the building envelope. It will be shown that the actual knowledge in terms of prediction of moisture behavior is limited. Simple engineering methods are too conservative and limited (dew point method and Glaser scheme, Glaser 1959) and simulations with computer models too restricted. Only models that would effectively take into account all the moisture driving forces and integrate a complete database on material moisture related properties could allow such total performance assessment. In the mean time, testing remains the main means of performance assessment. However, as the industry, and in particular the renovation industry, intervenes in more and more complex situations, testing all possible assemblies is not feasible. Therefore, an analytical model validated by experimental data is required to predict the long term moisture conditions of envelopes, leading to the establishment of guidelines to be incorporated in codes and standards. The main challenge regarding the use of models is having access to accurate and available material properties. The water potential approach minimizes the material data required. However, it has not been used yet in building envelope application.

Both modeling and experimental works face challenges when dealing with moisture storing materials because of the difficulties in measuring and monitoring the performance of the materials. Moisture transfer involves complex processes. Diffusion and

adsorption of moisture is dependent on local relative humidity and temperature and also on the material's moisture content. Convection is difficult to assess quantitatively. And the interrelation between path of air movement and moisture deposit and removal along the path is just beginning to be addressed. Wood frame envelope assemblies retrofitted with hygroscopic insulating materials have not been documented yet.

1.1.3 Proposed approach

This thesis combines measurements and simulations. This combined approach is recognized to allow the use of measurements to calibrate, adapt or check the simulation model, and of modeling as a means to explain and interpret the experimental results (Geving *et al.* 1997). As no model can yet calculate all moisture transfer mechanisms and as experiments are still the main mode of investigation of moisture transfer while being very time and energy consuming, the combination of the two modes of investigation is the approach that yields the best insight.

This project studies the moisture occurrence in wood-frame flat roofs with cellulose insulation from a combined experimental and modeling approach. In terms of modeling, the current frame of reference in building science is the use of driving potentials. This work proposes to use the gradient of water potential as the driving force to model moisture movement in timber. The experimental data that documents the performance of eight roof assemblies insulated with a moisture storing insulation through one wetting-drying cycle is used to validate the model.

1.2 Research objectives

The scope of this research is to investigate the pattern of moisture accumulation within roof assemblies insulated with cellulose insulation during a complete wetting-drying cycle.

Specifically, the objectives are, in terms of experimental work:

- to develop a test procedure that includes methods of monitoring the moisture transfer, and
- to determine the level of exposure to high moisture conditions in different assemblies.

In terms of modeling work, the objective is:

- to predict the moisture and temperature profiles within the planks of a flat roof assembly insulated with high-density cellulose as a function of the ambient air conditions, during both the adsorption and desorption process.

And in terms of assembly design, the objectives are:

- to assess the impact of construction geometry and material selection on moisture transfer rate and storage, and
- to implement the findings of the research in terms of design guidelines and improved details.

The remaining part of this chapter presents the fundamentals of the building envelope field and previous experimental and modeling work performed to understand and predict the hygrothermal behavior of envelope assemblies. The second chapter describes the test set-up and procedure and relates the results and their analysis. The third chapter presents the model development and results. The fourth chapter extracts design guidelines from

the results of the preceding chapters. The main results of this study are summarized in the conclusion.

1.3 Literature review

In the last 20 years, many studies on the building envelope subjected to combined heat and moisture transfer have been published. These efforts have led to a better understanding of the interrelations of phenomena occurring within the building envelope. Although the work presented later, in Chapters 2 and 3, was undertaken on wood-framed flat roofs, the following literature review considers works on different envelope assemblies. This aims at describing the field of knowledge of moisture transfer in the building envelope. This literature review first presents the envelope system and its components. Then, the phenomenon of moisture transfer is covered by describing its many aspects. This theoretical overview is followed by a presentation of the existing research on modeling moisture movement.

1.3.1 The envelope as a system

Together, the constituents of the building envelope form a barrier between the outdoor and the indoor climates. The analysis of the performance of envelope assemblies must consider the envelope as an integrated system, where constituents are connected to each other and where air, heat and moisture have interrelated effects.

1.3.1.1. Function and constituents

The building envelope must, among others, control heat flow, air flow and vapor flow; prevent ingress of rain; and control solar radiation, noise, airborne pollutants, and smoke and fire propagation (Hutcheon 1966). Furthermore, the envelope must be structurally sound, durable, aesthetically pleasing and economical and have a correct functionality. To accomplish this, the envelope is composed of several components intended to fulfill different functions. Bomberg and Brown (1993) list the environmental barriers required by opaque walls and roofs to control vapor, water, air and heat transfer across the assembly as shown in Table 1.1.

In the case of residential or commercial buildings, the components of the envelope controlling air, heat and vapor flow are attached to or supported by the structural elements of the envelope: *i.e.* concrete slab, steel deck or wood deck on wood trusses in the case of roofs; and wood studs, steel studs, masonry or concrete blocks in the case of walls. In the case of a wall, these components together form the backwall or inner layer. This layer is covered by an exterior veneer that acts as a rain screen. For a roof, the waterproofing membrane can either be placed over the whole assembly or be located below the insulation layer. On their interior face, assemblies are covered with interior finish.

Table 1.1. Environmental barriers and driving forces (after Bomberg and Brown 1993).

Driving Forces	Environmental Barrier	Design Goals
Vapor pressure	Vapor retarder	Vapor diffusion control
Wind pressure and rain	Pressure equalized rain (PER) screen	Eliminates wind pressure difference across rain screen
Rain	Air gap with weather barrier and flashing	Provides capillary break and leads water away
Ground water	Damp proofing, gravel or crushed stone layer	Provides capillary break
Air pressures (wind loads, stack effect, etc)	Air barrier (continuous airtight materials and load support)	Carries wind loads to the desired location
Air pressure and high indoor humidity	Air barrier	Controls moisture flow due to air leakage
Wind pressure difference	Weather barrier with load support	Eliminates effects of windwashing
Temperature difference	Thermal insulation	Reduces the rate of heat flow
High temperature, <i>e.g.</i> fire	Thermal barrier, <i>e.g.</i> drywall	Prevents rapid temperature rise on susceptible materials

The control of air is achieved with a succession of airtight materials, tightly joined one to the other. The air barrier is, in effect, a strategy applied to the whole envelope assembly, and more importantly, to all junctions encountered in the envelope, *e.g.* wall/window, floor/wall, wall/roof, wall/mechanical exhaust, roof/drain, etc. The plane of the air barrier can be positioned at any depth of the wall provided its vapor retarder properties do not cause moisture accumulation. When the air barrier is placed on the inner side of the insulation layer, a wind-sensitive insulation might require the addition of a wind barrier on its outside to prevent air movement through its thickness. Acceptable air barrier materials must have an air leakage lower than $0.02 \text{ l/(s}\cdot\text{m}^2)$, measured under a differential pressure of 75 Pa (NBCC, 1995, art. 5.4.2.1). Gypsum board, steel sheet, elastomeric bituminous membranes, concrete can act as air barrier. In the annex of the code, overall

system airtightness is recommended to be $0.15 \text{ l}/(\text{s}\cdot\text{m}^2)$ at 75 Pa or below, depending on the indoor relative humidity.

The control of vapor movement by diffusion across the assembly in a cold climate is achieved through the use of a vapor retarder material that is generally placed on the warm side of the insulation layer, in order to prevent condensation. Recent changes in the National Building Code of Canada (1995) allow for the positioning of the vapor retarder in the wall in relation to the heating degree-days of the location of the building. For example, in Montreal, the minimum ratio of the thermal resistance on the cold side of the vapor retarder to the thermal resistance on its warm side is of 0.20. The ratio increases with increasing heating degree-day values. Vapor retarder materials must have a permeance of $15 \text{ ng}/(\text{Pa}\cdot\text{s}\cdot\text{m}^2)$ or less (art. 9.25.4.2.2, NBCC, 1995); polyethylene sheets of different thickness, aluminum foil and paints can act as vapor retarder.

The control of heat transfer across the assembly is achieved by using thermal insulation. This may consist of one or many layers. Insulation can be installed between structural members as in wood and steel stud walls, or in wood structure roofs. It can also be installed on the exterior side of the structure, *e.g.* on top of the concrete slab or on the cold side of concrete blocks. Depending on the mode of installation, insulation can be blown or sprayed in place, or installed in batt, semi-rigid or rigid form. Current insulation materials are glass fiber, cellulose, extruded and expanded polystyrene and polyurethane. Other insulation materials include polyisocyanurate, glass foam, vermiculite and perlite. Levels of insulation in Quebec are set by the Regulation respecting energy conservation in new buildings since 1983, and the Model national

energy code of Canada for houses (1997) should replace the Regulation in the near future. Present requirements for residential buildings are of RSI-3.4 m²·°C/W for above ground walls and RSI-5.3 m²·°C/W for roofs for the Montreal area.

1.3.1.2 Impact and interrelationships of moisture related parameters

As the envelope is a complex assembly exposed to various phenomena, research has been focused at studying the impact of individual parameters and their interrelationships or cross effects on the performance of the building envelope. These studies can be experimental, analytical or a combination of both.

The importance of controlling vapor diffusion has been demonstrated by several studies. For example, in an experimental study to validate a computer model (Zarr *et al.* 1995), 12 specimens of approximately one square meter in area each were exposed to winter conditions. The presence of a vapor retarder material on the warm side of the glass fiber insulation reduced the moisture content in the wood exterior panel from 24 % to 8 %. The absence of insulation also had an impact on moisture content of the exterior panel, decreasing the moisture from 24 to 14 %, due to the resulting warmer temperatures. Verschoor (1986) conducted a study to investigate the migration and accumulation of water vapor and the effect of moisture on the thermal performance of a typical insulated wood-framed residential wall under various conditions of vapor retarder and total pressure differential. The wall that had an excellent vapor retarder (polyethylene) had insignificant moisture accumulation in the insulation whereas the use of a poor vapor retarder (paint) with the addition of point-source defects led to moisture accumulation in

the insulation and on the sheathing. The thermal resistance of the glass fiber insulation was not influenced by the slight moisture accumulation. This study shows that all condensation does not occur at the theoretical plane of vapor saturation within the mineral wool batt layer, but that vapor flow continues until it meets a material that is not as permeable. Ojanen and Kohonen (1995) observed the lack of correlation between permeance derived from dry cup/wet cup methods and from mean flux at temperature differentials and conditions that could lead to condensation. This observation illustrates that material properties measured in certain conditions do not reflect necessarily the behavior of the material under different conditions.

Site surveys and case studies rarely document envelope failures that are caused mainly by vapor diffusion (Tsongas and Olson 1995). Kumaran (1996) has pointed out that the amount of moisture brought in the assembly due to exfiltration can be many times larger than that due to diffusion and is therefore of much greater concern. The phenomenon of air bringing moisture in assemblies is three-dimensional and contingent on the quality of construction and climatic elements. This makes air leakage and its impact on the assembly difficult to forecast. Tsongas (1987) has shown that moisture problems tend to appear around warm and moist air leakage location, as moisture condenses on the cold adjacent surfaces.

To study the impact of exfiltration, Janssens *et al.* (1992) tested three cavities for three consecutive tests. In the first test, which lasted nine weeks and subjected the assemblies to vapor diffusion only, the differentials maintained were 20.5°C for temperature and 750 Pa for vapor pressure. This was followed by six weeks in diffusion-convection mode

with tight construction, with 18.5°C temperature differential, 590 Pa vapor pressure differential, and 10.5 Pa air pressure differential. Finally, the last test consisted of five weeks in diffusion-convection mode with intentional air leakage, with 19°C temperature differential, 325 Pa vapor pressure differential and 4.5 Pa air pressure differential. This series of tests demonstrated how convection is able to transport larger amounts of moisture through a construction than diffusion and how the amount of condensation is proportional to the amount of vapor that reaches a cold surface. Simpson and O'Connor (1994) showed the direct link between air barrier perforation and moisture content increase within the wall. The sensitivity of the assembly to air leakage was studied by Ojanen and Kohonen (1989) who, by modeling air leakage, found that limits for critical exfiltration rates should be analyzed case by case because they depend both on the hygrothermal properties of the structure and on the inside air and climate conditions.

The effect of the presence of moisture on the thermal properties of insulating material has also been the object of investigation. Epstein *et al.* (1977) and Larsson *et al.* (1977) approximated that each rise of 1% in moisture content in insulation is matched by a 3 to 5% increase in heat flux. An even more important heat flux effect is found in assemblies experimenting daily reversal of heat flux (Hedlin 1988, Shuman 1980).

Moisture transfer through the assembly can be further complicated if the assembly has the marked capacity to retain some of the moisture passing through. In an experimental study, Rose (1994) studied the impact of ventilation and vapor retarder in a series of cathedral roofs insulated with glass fiber. Holes of 38 mm were in each cavity. Results were given in hours of exposure for different moisture content level. A correlation was

found between the numbers of hours where the roof deck was above fiber saturation point and the area of the deck affected by molds. More molds were in vicinity of the hole in the cavities facing north (no sun). The absence of vapor retarder and ventilation led to the most severe situations.

1.3.1.3 Standard test methods for the envelope

To test the airtightness of envelope assemblies, two standard test methods, ASTM E 283 (1991a) and E 1424 (1991b), call for subjecting assemblies to a pressure differential and measuring the air flow required to maintain the differential. The setup of these standard methods incorporates data for extraneous leakage while the specimen is not moved between the two measurements. The resulting air leakage rate at given pressure differentials or air leakage rate at given pressure and temperature differentials may then be converted into an equivalent leakage area (ELA). This procedure provides quick information of air leakage rate at pressure differentials larger than the ones naturally occurring.

For low air pressure differentials, tracer gas decay can be used to measure air change rates. Used mainly on site, this method may use one or two gases to monitor air movement from one room to the other or from inside to outside.

The two methods mentioned above, used in conjunction, provide a relationship between air movement at small pressure differentials and air leakage rate at relatively important pressure differentials. In the laboratory, pressurization is used as a technique to compare

the airtightness of an assembly before and after a parameter is applied, *e.g.* gust of wind, wood drying (Rousseau 1992, Onysko and Jones 1989), and to compare materials (Rousseau 1992). Pressurization effects can be monitored using temperature, infra-red, moisture content (Trechsel *et al.* 1985a) or tracer gas to detect induced air movement (Trechsel *et al.* 1985b). Site measurements provide whole building and building components air leakage rate data using fan pressurization techniques. On site, because of the small pressure differentials, tracer gas methods can be affected by weather, occupancy and operation (Persily *et al.* 1988). No method has been developed so far that allows characterizing of the air leakage path and flow within the assembly.

To assess the thermal resistance, two standard test methods, ASTM C236 (1983) and ASTM C976 (1990), using a guarded hot box or a calibrated hot box, provide a measured thermal resistance of a wall or roof assembly under the steady-state mode. The same setup has been used to measure values of the dynamic heat transmission characteristics of walls (Brown and Stephenson 1993a, 1993b). To measure thermal resistance over small area, heat flux sensors may be used.

The moisture content of materials can be monitored using different methods. One straightforward method to measure the moisture content of a material is to weigh it when moist, let it dry and then weigh it dry. This method is called gravimetry. Previous work in moisture transfer monitoring has used gravimetry of material specimen taken out of the experiment setup (*e.g.*, Timusk and Doshi 1986, Verschoor 1986, Burch *et al.* 1989; and more recently, Janssens *et al.* 1995).

The other approach is the use of moisture content pins in the wood (developed by Duff 1968, used by Burch *et al.* 1989, and more recently by Desjarlais *et al.* 1993, Dumont 1993, Zarr *et al.* 1995, Rose 1995b, Rose and McCaa 1998). The common wood moisture content pin sensor consists of two pins inserted in a known type of wood. The resistance to electrical current between the two pins is measured. This value is inversely proportional to the wood moisture content, and thus can be converted to a moisture content reading. Variations include use of custom-made moisture content probes consisting of small maple blocks with electrodes fastened to opposite sides (Rose, 1992).

1.3.2 Moisture transfer through the envelope

Moisture transfer is a complex phenomenon that involves materials and moisture in terms of quantity and phase. Compared to heat transfer, moisture transfer has a slower time of response. The time constant of moisture movement for a house has been evaluated to be around 72 hours (Tsongas *et al.* 1995). The many parameters involved in moisture movement, *i.e.* time, temperature, relative humidity, moisture content of material, etc, make the description of its physical process complex.

1.3.2.1 Theoretical framework

Transfer processes can be construed as due to a driving force that induces a transfer resisted by the medium. For an entity B, the rate of transfer, J_B , is proportional to the gradient of the driving force, Φ_B , as shown in the general form of transfer equations (Kumaran 1992):

$$J_B = -k \cdot \text{grad } \Phi_B \quad (1.1)$$

where k is a quantity, called transport coefficient, characteristic of the medium through which the transfer occurs.

The rate, J_B , is expressed as the magnitude of B transported across a plane of unit area normal to the direction of transport in unit time. It is also called flux or flux density of B .

The gradient, also represented by ∇ (del), is a vector representing the rate of change for any direction of a given function, f , as shown below:

$$\text{grad } f = \nabla f = \frac{\partial f}{\partial x} \mathbf{i} + \frac{\partial f}{\partial y} \mathbf{j} + \frac{\partial f}{\partial z} \mathbf{k} \quad (1.2)$$

In three dimensions, J_B has three components, J_{Bx} , J_{By} , J_{Bz} , each with an equation :

$$J_{B_A} = k_A \cdot \left(\frac{d}{dA} \Phi_{B_A} \right) \quad (1.3)$$

where $A = x, y$ or z .

If the medium is truly isotropic, then $k_x = k_y = k_z$. However, many building materials are generally anisotropic and nonhomogeneous, so transfer coefficients show spatial variability. Furthermore, k is rarely independent of Φ_B . For example, the thermal conductivity of insulation material is linearly dependent on temperature within the temperature range in which buildings operate. In moisture transfer, most transfer coefficients are complex functions of the corresponding driving force to be determined experimentally.

Moisture transfer is complex because, at the conditions to which the envelope may be subjected, water may be present in four different phases: ice, water, vapor and adsorbate film. Figure 1.1 illustrates how vapor and liquid move through the matrix of a

hygroscopic material. Table 1.2 classifies the driving potential of each transport process. It indicates that several forces may affect one phase: i.e. vapor may be moved due to vapor pressure, air pressure or temperature gradient. Although the properties of water in the air are well known, e.g. equilibrium between the three phases of moisture, saturation pressure for different temperatures, no exact relationship is known for moisture in the pores of materials. Experimental work encounters difficulties in identifying the process responsible for the measured moisture transfer.

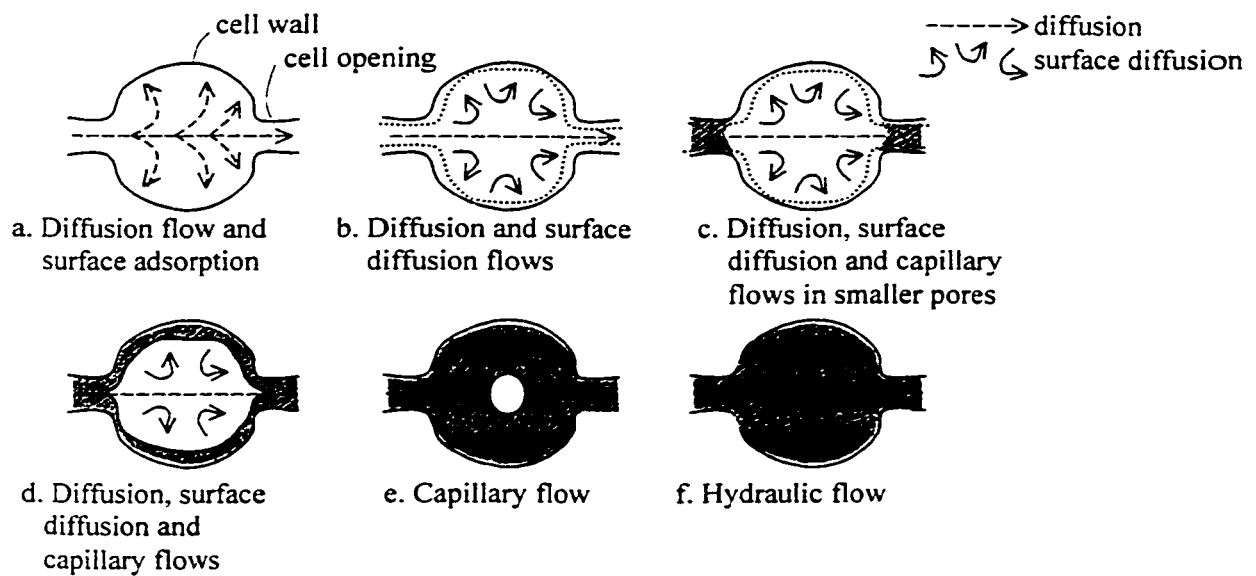


Figure 1.1 Phases of moisture adsorption (after Ojanen *et al.* 1989).

Table 1.2 Moisture transfer processes in building materials and components (after Kumaran 1992).

Process	Participating state	Potential difference
gas diffusion	vapor	vapor pressure difference
liquid diffusion	liquid	concentration
adsorbate diffusion	adsorbate	concentration
moisture thermodiffusion	vapor & liquid	temperature
capillary flow (unsaturated)	liquid	suction
convective flow	vapor	air pressure
gravitational flow	liquid	height
Poiseuille flow	liquid	liquid pressure

For light weight building envelope studies, the two main moisture transfer modes are diffusion and convection, but each mode may actually encompass several processes. As a result, this traditional split, which simplifies driving forces, explains that the moisture transfer through an envelope assembly occurs via the slow process of diffusion through the material or via the faster movement of moisture laden air through the discontinuities in the building materials. Once displaced within the building envelope, moisture may condense as vapor pressure approaches its saturation point due to a decreasing temperature.

1.3.2.2 Moisture transfer by diffusion

Vapor transfer within building materials may occur through two processes: gas phase diffusion in air contained in the interconnected pores of materials, and by adsorption of the vapor by the inner surfaces of the pores of polar (electrically charged) materials.

In the case of gas phase diffusion, materials allow moisture to pass through their matrix at a rate that is proportional to their permeability. The gradient in vapor pressure is the driving potential of this diffusion process. The magnitude of the permeability depends on the structure of the matrix and of the polarity of the molecules forming the matrix. Non-polar molecules do not attract water molecules allowing vapor to go through a maze of neutral corridors. Non-polar building materials include the polyethylene sheet, elastomeric bituminous membranes, insulation like polystyrene and polyurethane. Tight matrix, non-polar materials are often used in weatherproofing applications. These materials have none or very low vapor permeability. When moisture succeeds in passing

through, it is by gas diffusion only, *i.e.* by reaching equilibrium of vapor pressures from one surface through each pore of the material molecular structure to the other surface. As no storage occurs in these materials, the response to partial pressure differential changes is almost instantaneous in terms of change of rate of vapor flow.

The diffusion movement can also be due to the movement of bound water; this is referred to as surface diffusion. At the surface of polar material, polar ions, *e.g.* Cl^- , OH^- , display forces of attraction on the polar molecules of water (van Krevelen and Hoftyzer 1972, Birley *et al.* 1991). This process is called adsorption, a term which reflects that water is attached to the surface of the material including inner pore surfaces. Water travels by jump in a maze of corridors with attracting walls. Depending on the local partial pressure of water, the film of water at the surface of the pores can be of different thicknesses, one or more molecules thick (as shown in drawings a, b and c of Figure 1.1). Polar materials with very large inner areas are said to be hygroscopic and show a characteristic affinity for water. For example, wood has a high affinity for water due to the hydroxyl groups in its lignocellulosic cell walls (Viitanen and Ritschoff 1991). The porous structure of wood allows for a piece of wood after a 12 week stay in ambient conditions at 98% relative humidity (RH) to have the same moisture content (M) as if it had been immersed in water for 15 minutes; and at 100% RH, a piece of pine has a moisture content of 57% compared to 38 %M after the same 15 minute stay in water. This indicates the importance of surface diffusion in porous materials.

At the steady state, moisture transfer by diffusion, including surface diffusion, can be represented by the transfer equation (1.4) with the gradient in vapor pressure as the driving potential (Kumaran 1992):

$$J_v = -\mu \cdot \text{grad } p_v \quad (1.4)$$

where: J_v is the vapor flux [$\text{ng}/\text{m}^2 \cdot \text{s}$],

μ is the transport coefficient called water vapor permeability of the medium through which vapor is transported [$\text{ng}/\text{m}^2 \cdot \text{s} \cdot \text{Pa}$], and

p_v is the partial pressure of vapor [Pa].

The coefficient μ is not a constant, but depends on relative humidity (p_v), temperature and on the moisture content of the material. Experimental methods developed for the determination of μ usually provide an average value for the coefficient in a range of relative humidity.

A differential in temperature can also act as a driving potential for vapor transport. At non isothermal conditions, thermodiffusion occurs and the resultant vapor flux can be expressed as:

$$J_{v,T} = -\mu_T \cdot \text{grad } T \quad (1.5)$$

where : μ_T is the thermal vapor permeability.

Building physicists have largely disregarded this quantity assuming that this part of the vapor flux is negligible in comparison with J_v . Hence, there are no well-developed experimental techniques accepted for the determination of μ_T (Kumaran 1992).

The simplified version of equation (1.4) for unidirectional vapor diffusion uses the vapor permeability as measured according to ASTM E96 (1980) commonly referred to as the wet-cup/dry-cup method. This standard method calls for a setup where permeability is measured for steady-state conditions for the material. The measured permeability values are normally average coefficients for the 0 to 50 % or 50 to 100% relative humidity ranges. As mentioned above, permeability is dependent on relative humidity, temperature and on the moisture content of the material. This dependency explains in part that data from different sources do not always agree.

1.3.2.3 Moisture transfer by convection

Air within a cell, where any dimension is larger than 12 mm, can be induced to move if the walls of the cell are not at the same temperature. Air heated up in contact with one side of the cell moves up as its density decreases, until it reaches a colder surface that increases its density. This loop movement may transport moisture as well as heat. On a larger scale, moisture laden air can be introduced into the building envelope through orifices, cracks and open materials. The driving potential for this process is the air pressure differential. This may be caused by either the stack effect created by air temperature differential across the envelope, the wind inducing varying pressures on the exterior of the envelope or mechanically driven air movements, as performed mainly by the heating, ventilating and air conditioning (HVAC) system. As temperature and wind velocity vary, air pressure differentials vary as well. Another factor that complicates the exact determination of the air leakage rate and pattern is the difficulty of assessing the geometry of the discontinuities of the materials within the building envelope.

Although Shaw (1980) indicates preferences for site measurements for global assessment, Colliver *et al.* (1994) have pointed to the lack of data in building construction joints. There is no exact quantification of air flow through the building envelope, even though this information is required for the assessment of the performance of assemblies in terms of moisture. Approximations used are average leakage per area of envelope, estimated size of cracks or expected air leakage path through the envelope. If air movement in terms of geometry and flow rate could be determined, the amount of moisture in contact with materials could then be assessed.

Present knowledge on air leakage characteristics of envelope assemblies stems from two sources: global assessment of buildings using infiltrometry test, and individual tests on specimen (Brown and Poirier 1988, Bumbaru *et al.* 1988, Leblanc and Patenaude 1991, Lawton and Quirouette 1991, McKay *et al.* 1993). Both occur at higher pressure differential than normally occur in buildings. The relationship between airflow through an orifice and pressure differential is normally expressed by:

$$Q = c (\Delta p_a)^n \quad (1.6)$$

where Q is the air flow [m^3/s],

c is the coefficient of air flow [$\text{m}^3/(\text{s} \cdot \text{Pa}^n)$],

Δp_a is the pressure differential across opening [Pa] and

n is the exponent of air flow.

From this relationship, an equivalent leakage area can be approximated through correlations. For example, ASHRAE (1997) uses:

$$ELA = Q / C_d [2 / \rho \Delta p_a]^{1/2} \quad (1.7)$$

where ELA is the equivalent leakage area [m²],

ρ is the air density [kg/m³], and

C_d is the discharge coefficient, 0.6.

The blower door equipment is used to perform infiltrometry tests at 50 Pa pressure differential that yield a global assessment of the air leakage of a house. The air leakage of a material is defined as the airflow during one second for one square meter of material subjected to a pressure differential of 75 Pa (CBN 1995). Values for assemblies are also averaged over area for a given pressure differential. Information of the type of air flow, *i.e.* laminar vs turbulent, can be deduced from the value of the exponent n in equation (1.6) with tests at different pressure differentials.

1.3.2.4 Moisture storage

Hygroscopic materials slowly accumulate the diffusing moisture on their pore surface. The exact process of the moisture accumulation is not known and is affected by several driving potentials. The rate of storing depends on temperature, ratio of surface to volume and relative humidity. Because of this multitude of variables, the measurement of the rate of moisture movement is not practical. The moisture content at equilibrium for a given relative humidity and temperature can be measured. Sorption curves relate the equilibrium moisture content as a function of relative humidity and are developed with an experimental setup that employs steady-state conditions. In this manner, a given material is exposed to an environment at steady temperature and relative humidity. When the material mass is stable, it indicates that its moisture content is in equilibrium with the

ambient conditions. The moisture content of the material is expressed as a percentage of its dry mass:

$$M = \frac{m_{\text{moist}} - m_o}{m_o} \times 100 \quad (1.8)$$

where: M is the moisture content [%],

m_{moist} is the mass of the moist material [kg], and

m_o is the mass of the dry material [kg].

Then the relative humidity of the air is increased and moisture content assessed again until there is no more mass gain, and so on. The same method is used for a wet material exposed successively to dryer conditions. Sorption curves are developed for the full range of relative humidity at one set temperature.

The processes of desorption and adsorption of the same specimen, at the same temperature yield different sorption curves. During desorption, a wet porous material retains more moisture than it can adsorb at any given relative humidity. This difference in moisture content at the same relative humidity between the adsorption and desorption curves is called hysteresis. In some materials, this is due to the shape of pores. During desorption, these pores present bottle necks full of liquid. The meniscus at the surface of the liquid is of smaller radius than the one present at the start of adsorption at the bottom of the cell. As the radius is smaller, the partial pressure of vapor above the meniscus is lower and less evaporation may take place. As the global vapor pressure is reduced further, the bottle neck will eventually be cleared and evaporation of the rest of the free water in the bottle-shape pores will occur. At that point, the desorption and adsorption isotherms converge (Gregg and Sing, 1982). Figure 1.2 illustrates the hysteresis.

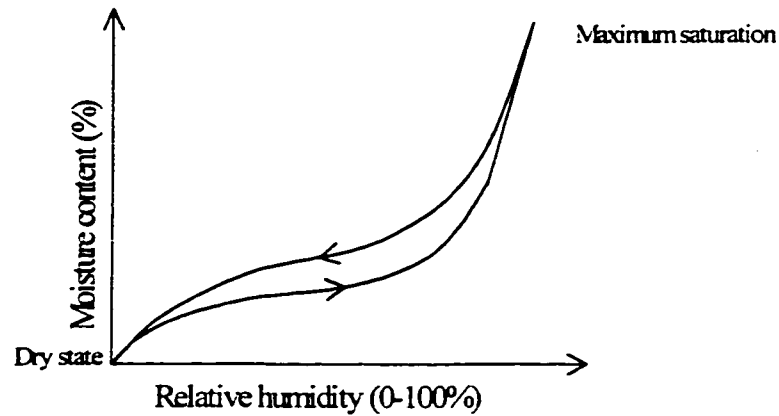


Figure 1.2 Schematic diagram of the sorption of a hygroscopic material showing the hysteresis between the adsorption and desorption curves.

The hygroscopic range refers to the range from dry state to the point of droplet formation within pores of material, when adsorption is no longer the only process involved.

There has been some work on hygroscopic insulation materials, mainly related to cellulose insulation. Sandberg (1992) worked with cellulose insulation because of its hygroscopic nature and studied the impact of moisture on the thermal conductivity of the insulation. Within the hygroscopic range (up to 98% RH), the impact was found to be less than 3% ($0.001 \text{ W/m} \cdot ^\circ\text{K}$ / $0.375 \text{ W/m} \cdot ^\circ\text{K}$). Along the same lines, Kumaran (1988) demonstrated that, in cellulose insulation, moisture is distributed through out the insulation layer and contributes to the heat flux. This contrasts with the non-hygroscopic glass fiber insulation in which, where under a temperature gradient, moisture moves to the coldest side of the test specimen and, once there, does not contribute any longer towards heat transfer.

The impact of moisture storage within building envelope assemblies comprising hygroscopic materials has not been studied extensively. Stewart (1982) noticed that few tests reproduce daily and seasonal cycling that potentially has a great impact on transient moisture transfer because the time constant of moisture accumulation is very long. The literature review made in conjunction with the design of the test procedure presented in chapter 2 found no study similar to the one proposed. This absence is mainly due to the technical difficulty of maintaining the desired controlled environment for the long term testing of moisture transfer and the cost involved.

A well-used hygroscopic material is wood. Canadian low-rise housing has traditionally used wood-frame construction due to its advantages of economy, durability, speed of erection, flexibility of design, ease of renovation, and availability and renewability of materials (Robinson 1992). Skaar (1988) explains the growing of wood in terms of moisture content:

Newly formed wood cells in a living tree are born in a water-saturated environment, and the cell walls themselves are presumably also fully saturated with water. Those wood cells which function primarily as channels for conducting water from the roots to the branches and foliage may remain essentially water-saturated in order to provide continuous unbroken water columns from roots to leaves.

When the wood cells no longer function primarily as water transport media, the cell-cavity may become partially or fully displaced by gases, including water vapor. The cell wall itself, however, remains fully saturated. Therefore, green wood generally contains water in three forms, liquid water partially or completely filling the cell cavities, water vapor in the empty cell cavity spaces, and water in the cell wall.

The bound water found in cell walls is attracted to wood with stronger forces than the free water held within the cell. When wood is dried, the free water is lost first, as it is held with weaker forces due to capillary action. The moisture content at which all free water of a cell has exited, but the cell walls are still saturated with water, is called fiber-saturation point (Tiemann 1906). It ranges from 20% to 40% of the dry weight. It

follows that moisture movement above FSP is due to capillarity action and is a function of the vapor pressure above the meniscus. This is used to explain the hysteresis above FSP with the ink bottle analogy. The drying process below FSP continues through water exiting the cell walls. This process occurs at the molecular level of the wood matrix. Spalt (1958) explained that during the cell formation, cellulose is formed in a glucose solution to precipitate on the cell walls. Cellulose is thus dispersed in water and there are few lateral cohesive bonds between cellulose fibers. During drying, the gel gets more compact and lateral bonds develop. The more the bonds, the less the mobility. Further removal of water produces distortion due to shrinkage. Cellulose has therefore exchanged bonds with water to lateral bonds with cellulose fibers. This reduction of available sites explains the hysteresis below the FSP. Comstock (1963) linked shrinkage of the matrix to the differences of diffusion coefficients through desorption and adsorption.

The relationship between moisture storage and moisture transfer is not completely understood since the moisture storage or release rate is not known for all sets of conditions. However, transient moisture transfer in the building envelope is more common than steady state moisture transfer due to the diurnal cycling of temperature and relative humidity. With changing conditions, equilibrium is never reached. The rate of storing or releasing moisture as a function of the ambient conditions should also be taken into account, like is the sorption isotherm. Transient moisture transfer properties are not yet developed. As a parallel, one can point at the effort of transient characteristics developed in the domain of heat transfer with z-transfer function coefficients (Stephenson and Mitalas 1971, Mitalas and Arsenault 1972) or harmonic function (Athienitis *et al.*

1990). One application of transient heat transfer including storage is the study of thermal mass used in passive solar heat gain. One way to describe transient phenomena is to use the concept of time constant.

1.3.2.5 Capillary and supersaturated regions

As shown in Figure 1.1, liquid water may be found within the envelope due to contact of the material with a liquid pond, occurrence of condensation at interfaces within the assembly, or simply the slower process of moisture accumulation within materials. It is difficult to separate the different physical causes of water movement and measure how each contributes to the amount of water in the material. Therefore, the water content is assessed as a whole. To predict the actual moisture storage process of materials, there is a need to establish a relationship between the water content of a material and the ambient conditions. To derive this relationship, many (Salonvaara and Karagiozis 1994, Rode Pedersen 1990) include in their analysis of moisture transfer capillary related properties and relationships, in addition to the sorption curves described above. Two approaches, in particular, are well defined.

In the first approach, Burch and Thomas (1992) split the moisture related material properties into three regimes, as shown in Figure 1.3: 1) the diffusion regime, which takes place below the maximum sorption occurring at 97% RH; 2) the capillary regime, which occurs when a continuous path of liquid exists within the porous material, the first path of liquid occurring at irreducible saturation; and 3) a transition regime, located in between the two, i.e. from maximum sorption to irreducible saturation. In the transition

regime, liquid water exists but it is not continuous, and “the capillary attraction between discrete liquid particle and pores is so strong that this liquid cannot be separated from the porous material by ordinary mechanical means”. For the transition and capillary regime, Burch proposes the use of liquid diffusivities, capillary pressure and unsaturated liquid permeability to model moisture transfer.

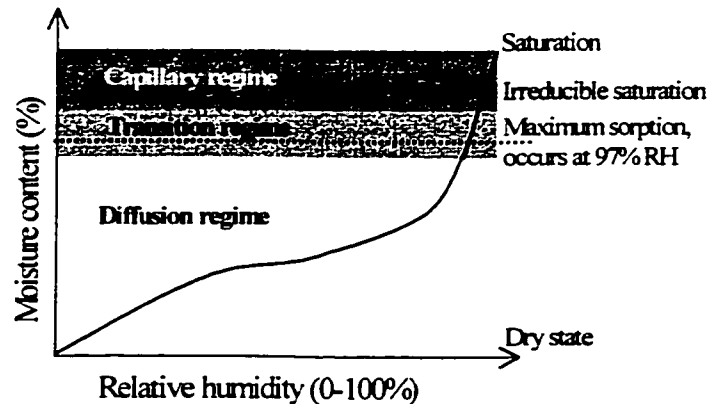


Figure 1.3 Schematic representation of moisture regimes after Burch and Thomas (1992).

In the second approach, Künzle (1995) derives three moisture regions due to the increasingly intensive moisture conditions. As shown in Figure 1.4, he defines them as: 1) the hygroscopic region, which goes from 0 to 95% RH and is dealt with the sorption curves described above; 2) the capillary water region, also called super-hygroscopic region, which starts at 95% RH and reaches free water saturation; and 3) the supersaturated region, where the relative humidity is always 100% and water is found in the pores of hygroscopic materials. The moisture transfer in the capillary region is modeled by a relationship between relative humidity and capillary forces. In the supersaturated region, the moisture transfer is described by the moisture storage capacity, which is the difference between maximum and free water saturation.

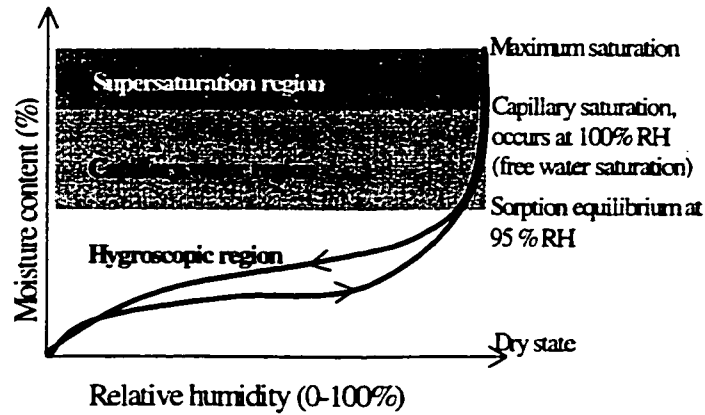


Figure 1.4. Schematic representation of moisture regions according to Künzle (1995).

1.3.2.6 Thermodynamic approach - water potential

The split between regimes or regions is arbitrary and inaccurate. Boundaries existing between the various forms of water are not sharp. One approach for porous media reconciles the different forms of water. Water potential is a characterization of the energy state of the water within the wood. Siau (1984) mentioned that the gradient in water potential can be regarded as the driving force for the transport of water in both liquid and vapor phases including bound water in wood. The factor of proportionality is determined experimentally to estimate moisture flux resulting from a given gradient in water potential.

The concept of water potential is derived from classical thermodynamics. It is defined as:

$$\psi = \bar{G} - \bar{G}_0 \quad (1.9)$$

where ψ is the water potential [J/kg_{water}],

\bar{G} is the specific Gibbs free energy of water in the state under consideration, and

\bar{G}_0 is the specific Gibbs free energy of water in the standard reference state.

The standard reference energy state generally used is a hypothetical pool of pure free water in atmospheric pressure, at a given elevation, and at the same temperature as that of the water in wood. The water potential may be thought of as the sum of the separate contributions of the various force fields acting on the water in wood:

$$\psi = \psi_m + \psi_o + \psi_p + \psi_g + \psi_{e.f.} + \dots \quad (1.10)$$

where ψ_m is the matric potential due to the combined effect of the capillary and sorptive forces,

ψ_o is the osmotic potential due to the presence of solutes in the water,

ψ_p is the pressure potential describing the effect of a system bulk pressure either greater or less than the reference bulk pressure,

ψ_g is the gravitational potential,

$\psi_{e.f.}$ is a component potential representing the integrated sum of the effects of all external force field exclusive of gravity, and

... the dots on the right-hand side of the equation indicate that additional components potentials are theoretically possible.

The mass conservation equation used is:

$$\frac{\partial C}{\partial t} + \bar{\nabla} \cdot \bar{q}_m = 0 \quad (1.11)$$

where C is the water concentration in wood [$\text{kg}_{\text{water}}/\text{m}^3_{\text{moist wood}}$],

t is time [s], and

q_m is the total moisture flux (liquid water + water vapor + bound water)
 $[kg_{water}/m^2_{moist wood}\cdot s]$.

Similar to the general driving potential equation (1.4), the water potential gradient induces a moisture flow as follows :

$$\bar{q}_m = - \underline{K}(M) \cdot \bar{\nabla} \psi \quad (1.12)$$

where $\underline{K}(M)$ is the effective water conductivity tensor $[kg^2_{water}/m_{moist wood}\cdot s\cdot J]$, and

$\bar{\nabla} \psi$ is the gradient of water potential in the three dimensions.

The effective water conductivity is the proportional factor linking the moisture flux to the water potential gradient.

The gradient in water potential as the driving force of moisture in wood was proposed by Fortin (1979). To use the gradient in water potential as the driving force of moisture in wood, the moisture content-water potential ($M-\psi$) relationship and the appropriate moisture transport coefficient must be developed. Water is held in porous hygroscopic materials, like wood, through two types of mechanisms: specific attraction forces between the water molecules and the material molecules, and capillary attraction forces due to superficial tension of water. These molecular sorption and capillary forces can be expressed in term of water potential (Cloutier and Fortin 1991). There is therefore a link between moisture content and water potential. To measure ψ when capillary forces are present, the techniques used are the tension plate, the pressure plate and the pressure membrane. For ψ corresponding to molecular sorption forces, i.e. for moisture content below fiber saturation point, equilibration over saturated salt solutions is used. The $M-\psi$

relationship can then be established for the whole range of moisture contents, covering the processes of diffusion and mass flow of water in wood.

As it considers the water potential gradient as the driving force for the complete range of moisture content, the effective water conductivity term encompasses the two main modes of mass transfer in wood: convection, or capillary flow, where permeability is the proportional factor between moisture flux and the pressure gradient, and conduction or, more commonly, diffusion. Diffusion refers to vapor transfer in the air within the lumen of the wood cells and bound water transfer within the cell walls.

The effective water conductivity is measured in adsorption and desorption considering the gradient in water potential as the driving force, and is measured for the three main directions of wood: longitudinal, radial, tangential. The conductivity varies by several orders of magnitude from unsaturated to saturated conditions.

1.3.3. Computer modeling of heat and moisture transfer

The simulation of the heat and moisture performance of the building envelope using existing physical models and material properties is a complex and extensive activity that is better performed by computer models. Several computer models are presented in the following sections.

A general distinction must be made between computer model and computer tool. A computer tool can be understood to be constituted of a model, a controller and a view,

where the controller accepts the input and activates the tool and the view controls the visual representation of all or parts of the model (Lewis *et al.* 1995). The computer model is the part of the computer tool that represents the problem at hand and contains the related data. In heat and moisture transfer simulation in the building envelope, the computer model includes the description of the elements and their properties, the physics of their interaction and the mathematical method used to translate this model for computer application.

1.3.3.1 Approaches for the modeling of heat transfer

The study of the thermal behavior of the envelope assemblies is well developed. One of the reasons for this advancement is the relative facility of measuring the thermal properties of materials. Steady-state computer models have been applied to study different parts of the building envelope, from thermal bridges due to the presence of concrete slabs to thermal behavior of window frames. Modeling is also very useful in dynamic heat transfer and has as basic equation for conservation of heat:

$$\text{heat}_{\text{in}} = \text{heat}_{\text{out}} + \text{heat}_{\text{stored}} \quad (1.13)$$

When the applied heat_{in} varies sinusoidally, a similar variation in the temperature profile occurs through the building envelope. Because the flow of heat is resisted by the different materials of the envelope, the resulting temperature profile on the other side has less magnitude. Also, during transfer, heat may be stored and heat flow slowed by some materials. As a result, the peaks of the temperature profiles on both sides of the envelope do not occur simultaneously. This delay is named the time lag, which is one of the parameters used to define transient heat transfer.

In assessing heating and cooling loads, the transient heat conduction through the building envelope must be taken into account as the effects of the changes in indoor and outdoor conditions on the envelope are not instantaneous. Several modeling methods have been developed based on different mathematical approaches. In the finite element method, the wall is seen as a series of elements to which parameters are attached. In the harmonic analysis, the changes in conditions are assumed to be periodic (Athienitis *et al.* 1990). And the z-transfer function coefficients are the characterization parameters of the transient heat conduction performance of a specific wall assembly (Mitalas and Arsenault 1972, Brown and Stephenson 1993a, 1993b).

1.3.3.2 Combined moisture and heat transfer modeling

A natural extension of the body of knowledge in moisture transfer presented so far is the development of computer models to simulate heat, air and moisture transfer and their implementation into computer tools. The main advantage of modeling moisture transfer through the building envelope comes from the reduced time and cost efforts involved as compared to the hygrothermal testing of assemblies. However, developing models is a challenge in terms of balancing the demands of building science to reproduce accurately all aspects and conditions of moisture transfer versus the scarcity of data on material properties, the limitation of calculation techniques, and their implementation into computer codes. In the framework of the Annex 24 of the International Energy Agency (Hens 1996), the interdependence of experimental and modeling work has been expressed as follows:

“For the research community, the limits must make clear that HAM (heat, air and moisture)-modeling is only one of the instruments to be used. Experimental work on heat, air and moisture response is the other one. Both are complementary. Models help in understanding experiments and experiments help in verifying, validating and upgrading models.”

This was part of the conclusion of the final report of Task 1- Modeling, one of the five tasks set by Annex 24 which mandate, *Heat, air and moisture transfer through new and retrofitted insulated envelope parts* (Hamtie), had been initiated by the International Energy Agency. Task 1 focused on improvements in modeling and testing of simplified models with a potential to predict the combined effects of heat, air and moisture transport on thermal performance, hygrothermal responses and durability. From 1991 to 1995, a total of 37 Heat, air and moisture transport computer codes (abbreviated to HamCaT) from 12 countries were reviewed and six common exercises were performed comparing results from six to ten different models, depending on the exercise. These codes were classified into nine types, as presented in Table 1.3, based on Hens and Janssens (1992).






Very few models have included all the important transport physics; obstacles being primarily of a computational/numerical nature (Karagiozis and Salonvaara 1995). This paper lists the four most sophisticated models in the mid-90's: TRATMO2, developed mainly first by Kohonen and then by Salonvaara and Ojanen, LATENITE, a development of the TCCC2D of Ojanen and Salonvaara by Karagiozis and Salonvaara, MATCH, by Pederson and FSEC, by Kerestecioglu. TRATMO2 and FSEC were classified as type 9 by the Annex 24; LATENITE and MATCH, classified as type 4 by the Annex, have now a version of type 9. The following section will look at these models. Three type 4 models are described: MOIST, the main commercial transient state tool, WUFIZ and MATCH. Finally, four models of type 9, FSEC, TRATMO2, TCCC2D and LATENITE,

are briefly presented. To start with, two simple steady-state methods are briefly presented to describe the tools most used presently in practice.

Table 1.3. Classification used by HAMTIE-task 1 for HAMCaD-codes.

Features	Glaser scheme	Steady state	Constant mat. prop.	Heat transfer	Vapor diffusion	Non steady state	Air transfer	Mat. prop. f moisture ratio	Link heat-mass transfer	Liquid transfer
Class type number										
1 (1D)										
2 (1D)										Capillary
5 (2 or 3D)										
6 (1 or 3D)										
7 (1D)										
3 (1D)										
4 (1 or 2D)										
8 (1 or 2D)										
9 (1 or 2D)										

Legend : For link heat-mass transfer

	p_{sat} equation of state
	p_{sat} equation of state, latent heat
	enthalpy transfer and stack effect
	p_{sat} equation of state, latent heat, enthalpy transfer
	p_{sat} equation of state, latent heat, enthalpy transfer and stack effect

1D one-dimensional]

ss steady state

nss nonsteady state

+T and function of temperature

For other parameters



Yes



No

- Simple steady-state methods.

These methods can be performed by hand but several codes have implemented them. The two more used methods are the dew-point method (ASHRAE 1993) used mainly in North-America and the Glaser scheme (Glaser 1959) in Europe. The assumption of these methods is that the only mechanism to be considered is vapor diffusion, so any storage is entirely due to the difference between vapor flow towards and away from a location. Heat transport is according to the Fourier equation and there is no account of air transport. For each point across the assembly, the temperature and the corresponding vapor pressure are calculated given thermal conductivity and wet cup/dry cup permeability. The methods compare vapor pressure versus saturation vapor pressure for steady-state conditions. Condensation may occur when the partial pressure is greater than the vapor saturation pressure. The information is not quantitative, but can be used for design guidelines.

The main difference between the two methods is in the graphical solution of the condensation calculation. The Glaser scheme method translates “multi-layered building components into a virtual homogeneous element in terms of vapor diffusion resistance through a geometrical representation proportional to the differences in vapor diffusion resistance of layers” (Mahdavi and Lam 1993). The dew-point method uses the scale cross-section drawing of the assembly. Both the dew-point method and the Glaser scheme assess the condensation rate without taking airflows into account.

The Glaser scheme is presented, among other, in Janssens *et al.* (1995). Heat is transferred by conduction and vapor by diffusion. The amount of condensation is calculated according to equations (1.14) and (1.15).

$$T_c = T_{out} + (T_{in} - T_{out}) \cdot \frac{R_c^{out}}{R_{tot}} \quad (1.14)$$

$$g_c = \frac{p_{in} - p_{sat, c}}{Z_{in}^c} - \frac{p_{sat, c} - p_{out}}{Z_c^{out}} \quad (1.15)$$

where T is the temperature [$^{\circ}\text{C}$],

R is the thermal resistance [$\text{m}^2 \cdot ^{\circ}\text{C}/\text{W}$],

p is the partial pressure of vapor [Pa],

Z is the vapor resistance [$\text{Pa} \cdot \text{m}^2 \cdot \text{s}/\text{kg}$], and

g is density of vapor flow rate [$\text{kg}/\text{m}^2 \cdot \text{s}$],

subscripts : a= air, c = condensation, out = exterior, in = interior, sat = saturation.

This diffusion-only approach has been proved to be far away from reality and may lead to misestimated condensation prediction (White 1989). This method and the dew-point method have been implemented in several computer codes that have the same limitations. For example, CONDENSE (1998), widely used in Quebec by practitioners, is coupled with an extensive material database.

• Heat, vapor and liquid transfer computer models

The first attempts to model with computer the combined transfer of heat and moisture through envelope assemblies were simple but they have been used as stepping stones by their successors. Early on, differential equations were solved using finite difference methods and implemented into computer models. TenWolde (1985) developed a steady-state one-dimensional model for moisture movement by diffusion and convection.

Andersson (1985) is an example of early transient state attempts. These two authors focused on modeling heat transfer combined with moisture transfer due to diffusion.

One computer model using diffusion as the main moisture transfer process is MOIST developed at NIST (National Institute of Standard and Technology). In 1989, Burch *et al.* proposed a one-dimensional finite-difference computer model with distributed moisture capacity that could predict time-dependent moisture diffusion. The driving potential for moisture transfer was water vapor pressure and its range of application was for moisture content lower than fiber saturation (also named free water saturation). Moisture transfer properties were independent of moisture content of material or conditions of the environment. In 1992, Burch and Thomas presented an extension to the model to include capillary and some convective transfer. The model stayed one-dimensional. The driving force for heat transfer remained temperature differential and the heat transfer properties were kept constant. The extension consisted of adding the possibility of including non-storage layers, where steady-state transfer would occur but that could be coupled with indoor or outdoor air. This allowed including one-dimensional convective transfer, thereby simulating averaged effect of air leakage over a studied surface. Also, the model was extended to model moisture conditions in its full range. The three regimes of material properties were described above in section 1.3.2.5. The model was validated through a diffusion-only experimental program subjecting 12 specimens to similar conditions (Zarr *et al.* 1995). Measured results and model predictions were very close.

Another heat, vapor and liquid transfer model, named WUFIZ, was developed by Künzeli (1995). The implicit finite-volume model was developed for the calculation of simultaneous one and two-dimensional transient heat and moisture transfer in multi-layered building components. This method assumed that vapor diffusion resistance is not moisture-dependent, and that the transfer phenomena observed in higher moisture regions are allocated to liquid transfer. Liquid transfer was differentiated in two capillary transfer intensities, depending on whether the material is in contact with water or not. The model included transfer below the freezing point and in organic polymers in the form of solution diffusion. The driving potentials used for vapor and liquid transfer were vapor pressure and relative humidity. The model used simple hygrothermal material parameters, i.e. thermal conductivity, liquid conduction coefficient, vapor permeability, heat storage capacity, moisture storage capacity. Moisture movements based on air flows, gravitation, hydraulic pressure differentials, osmotic and electrokinetics effects were disregarded. Moisture storage in building components was divided into three regions presented in section 1.3.2.5. This resulted in a continuous storage function that can be defined throughout the entire moisture region from 0 to 100% RH. The model results compared well with experimental results involving mainly stone, concrete and masonry assemblies.

Rode Pedersen (1990) developed a computer program MATCH – Moisture and Temperature Calculations for Constructions of Hygroscopic Materials - based on the theory for combined heat and moisture transport which takes advantage of the similarities between the governing equations for transient transfer of heat, vapor and liquid moisture. The original version was one-dimensional and did not account for air movement. It modeled moisture transfer by diffusion, using Fick's relationship. It was also possible to

calculate liquid moisture transport. The model results were validated with experimental results on airtight roof assemblies.

The three computer models presented above have added other modes of transfer, such as the capillary and convection transfer to the simple diffusion process. However, building envelopes are subjected to conditions that are even more complex than the ones simulated by these models due to the presence of air movements. This is why Kumaran (1992) puts that, “any calculation method should consider moisture, heat and air transport simultaneously and respect the following axioms: transfer equations and equations of conservation of energy (heat transport), of mass (moisture and air transport) and of momentum (air and vapor transport)”. The following section will present the most advanced models that strive to incorporate air transfer.

- Heat, vapor, liquid and air transfer computer modeling

Kerestecioglu (1989) describes how a detailed finite element code called Florida Software for Engineering Calculations (FSEC) was used to study moisture transfer through a wall assembly. Because the main difficulties in understanding moisture transfer are associated with the fact that moisture migrates in each of its physical states and is driven by various vapor, liquid and thermal forces, Kerestecioglu pointed out that the most common treatment is to select a measurable driving force (*e.g.* vapor pressure or moisture content) and lump the separate mechanisms using a single overall effective diffusivity. This treatment can be improved upon by segregating the vapor and liquid transport mechanisms and lumping each separately, where vapor transport mechanisms are defined by partial vapor pressure, and liquid transport mechanisms are defined by

liquid pressure. Sorption isotherms in the hygroscopic region and moisture retention curves in the capillary region are used to relate the various driving forces and moisture capacities to each other. Kerestecioglu emphasized the difficulty to obtain good quality material property data for use in such simulations that, even though large amounts of data have been compiled from the literature, there is little certainty as to their accuracy. The software results were not validated against experimental results.

The approach by Kerestecioglu integrates all known relationships into one, two or three dimensional analysis implemented into a finite element code. Although the same software was used for studies in other areas, like contaminant transport, this theoretical analysis approach was never developed further.

Kohonen (1984) describes a model that was implemented into a computer code called TRATMO (Transient Analysis Code for Thermal and Moisture Physical Behavior of Constructions) using the local volume averaging technique. The energy balance equation integrated conduction, convection, accumulation of heat and generation of heat due to phase changes. The moisture balance equation integrated accumulation of moisture, diffusion in gas phase, surface diffusion and viscous flow of water vapor, as well as capillary and viscous flow of liquid water. The hygrothermal transfer included diffusion coefficient of water vapor, moisture diffusivity and permeability, as well as thermal conductivity and capacity. TRATMO2 (Ojanen *et al.* 1989) solves the equation in a 2-dimensional case. It contains three main parts : solutions for the temperature, moisture and flow fields.

Another numerical model, TCCC2D (Transient Coupled Convection and Conduction in 2-Dimensions) developed first by Ojanen (1988), aimed at analyzing the hygrothermal effects of forced and natural convection in building structures. In this 2-dimensional non-steady-state numerical model, a building structure could consist of several hygroscopic layers of materials with given flow resistances on the interfaces. The variables used for the solution of the flow, temperature and moisture field were total pressure, temperature and partial pressure of water vapor. The moisture content of each material was coupled with partial vapor pressure and temperature by sorption isotherms. Ojanen and Kohonen (1989) described that the moisture flow was divided into diffusion and convective mass flows. The diffusive moisture flow included pure vapor diffusion and the surface flow in liquid phase (both mechanisms were measured in the determination of the material property 'vapor diffusivity'). The effects of convection on the moisture movement in envelope assemblies can be analyzed numerically in different convection cases, especially in exfiltration flows which may most change the hygrothermal behavior of a building envelope from that of a non-convective case.

In the early 1990's, the Institute for Research in Construction, IRC, of the National Research Council of Canada and the Technical Research Centre of Finland (VTT) started to work jointly. The TCCC2D model was further developed into a model called LATENITE (Salonvaara and Karagliozis 1994), for the hygrothermal analysis of residential walls of light weight constructions. It solved two-dimensional heat, air and moisture transport and conservation equations that represent hygrothermal behavior of multilayer building structures, using the finite difference. Transport equations were based on temperature, air pressure and water vapor pressure as driving potentials. Local

thermodynamic equilibrium was assumed between stagnant and flowing phases. Allowance was made for phase changes. Material properties included sorption isotherm, vapor diffusion coefficient as a function of moisture content, air permeability, thermal conductivity as a function of temperature and moisture content. It can use weather data for outdoor conditions. Geving *et al.* (1997) relates the investigation of a set of experimental results, generated from laboratory controlled measurements on a wood frame wall construction, with the hygrothermal model LATENITE where the model has been upgraded to include porous air flow through insulation and cracks.

It is repeatedly said across the referenced research that the reliability of the results obtained from these codes depends on the modeling capabilities and, even more so, on the “accuracy and reliability of the material properties used, such as sorption and desorption isotherms, dry and moist thermal conductivity, wet and dry heat capacity, and suction curves, water vapor permeability, moisture diffusivity, thermal moisture diffusivity and air permeability in both dry and wet stages” (Karagiozis and Salonvaara 1995). Some standard methods for dry materials exist but knowledge of these properties at the dry state is not enough. More research is required to define measurement procedures of hygrothermal properties of materials. In some cases, results for the same properties, such as liquid diffusivity, in a round-robin testing, show disagreement in the order of 40% (Kumaran 1992, referred in Karagiozis and Salonvaara 1995). The moisture content and the geometry of the different building materials composing the envelope assembly may have an effect on some properties. Another problem, in the case of air convection related modeling, is the absence of 3-dimensional data. Approximations, like determination of the approximate inner leakage path, can be made to bypass this lack of

data. Similarly, airflows cannot be easily used as they are measured, for the most part, at pressure differentials of 50 to 75 Pa compared to the ± 10 Pa normally experienced on site. Spolek and Oosternout (1989) have pointed to the need of 2-D convection coefficients for inner leakage. TenWolde (1989) estimates that moisture transfer can be determined with exact quantification of air flow.

The challenge presented by the lack of material data has not hampered the development of computer models and their validation. Hokoi and Kumaran (1993) acknowledge the difficulties in deriving detailed materials physical properties, but stress the importance of research in this field to allow computer model calculations to become part of predictive methods for assessing long term behavior of the building envelope. Kumaran (1992) also stresses the need for more large-scale measurements on envelope components and systems to compare simulation results and to generate the much needed hygrothermal properties of materials in components and assemblies. Attempts could be made to characterize each phenomenon individually, and to study the cross effects of phenomena. One of the main advantages of models is this possibility to vary parameters one by one. For instance, in Karagiozis and Salonvaara (1995), in studying the impact of varying moisture transport properties, it was found that varying the sorption isotherm had a great impact on results, while changes in vapor permeability and liquid diffusivity had much less impact.

The models presented above use sets of driving potential, which are summarized in the final report of Annex 24 (Hens 1996): 1) temperature, relative humidity and air pressure; 2) temperature, generalized suction (including capillary suction, gravity and external

forces) and air pressure, and 3) temperature, suction, vapor pressure and air pressure. Chemical potential can be used instead of suction, as proposed by Matsumoto (1994). Hens (1996) acknowledges that such approach opens the way to include effects such as osmosis and adsorption, but concludes that chemical potential does not offer real benefits in practice. A slightly different concept, water potential, may present some advantages.

• Water potential modeling approach for drying of wood

Researchers at Université Laval (Cloutier *et al.* 1992, Cloutier and Fortin 1993) developed a two-dimensional finite element code to model industrial kiln drying of wood based on the water potential concept as the driving force.

One possible gradient to be used as the driving force for moisture transfer is the water potential gradient, which was first used in soil studies. It has been applied for moisture transfer in wood. Although some material properties are required, the utilization of a potential term to characterize water in wood allows a simplification of the physical model since a separate treatment for each phase is avoided.

This approach requires the experimental determination of the:

- relationship between moisture content and water potential ($M-\psi$), in desorption and adsorption for a complete range of moisture content and temperature for the wood species;
- relationship of the effective water conductivity, \underline{K} , moisture content and temperature in the radial and tangential directions;
- mass transfer and heat transfer coefficients for the wood-air interface;

- ratio of vapor/total moisture movement inside the wood material.

The effective conductivity is available for several species (Fortin 1979, Cloutier and Fortin 1993, Tremblay *et al.* 1998a) and sorption curves are also available. The model was implemented using a finite element method as described at length in Cloutier (1991). This approach is explained in more detail later in chapter 3.

1.4 Summary

The most fruitful approach for moisture related studies is the combination of modeling and measurements. The measurements of moisture-related material properties and of the moisture content need careful analysis which may complicate the interpretation of experimental results. On the other hand, all available models do not stand on their own and require calibration and validation as moisture movement is a very complex phenomenon. This complexity stems from the fact that the four phases of water may be found in envelope assemblies and the hygrothermal properties are a function of the moisture content of the material and the conditions of its environment.

In this thesis study, moisture movement is studied with the combined approach where experimental data are used to validate a physical model. The next chapter presents the experimental setup exposing different roof types to day-night conditions through a complete winter-summer cycle. The results are presented and later compared with the results of a computer model developed and presented in Chapter 3.

Chapter 2

Experimental procedure

This chapter presents the experimental work performed to study the moisture patterns in flat roof assemblies and examines the experimental results. The experimental program used an environmental chamber and was carried out on two large-scale flat roof huts fully insulated with cellulose fiber. These two huts incorporated the two most representative types of single-cavity flat roofs for urban houses found in the Montreal area and built between 1930 and 1970. The insulating technique consisted of packing cellulose insulation to a density of approximately 67 kg/m^3 , commonly referred to as 4 lbs/cubic foot in the industry, in a single cavity roof between the roof planking and the ceiling plaster. The behavior of the assemblies was documented with an extensive monitoring plan. The results show the moisture accumulation and egress in the assemblies. Specifically, the moisture content in wood and in the cellulose insulation is presented for the duration of the 190-day test. The wood wetting-drying patterns are used to validate a model developed and presented in the next chapter.

2.1 Context

The experimental work drives from a project carried out in collaboration with local industry in the context of a weatherization program for one to three-unit residential buildings. The study was carried out to determine the feasibility of insulating flat roofs, common in the Montreal area, with cellulose. This program represented potential annual

energy savings of over 100 GWh for the province of Québec. Among flat roofs, single-cavity roofs were challenging due to their relatively low height (150 to 450 mm). A proposed method suggested that cellulose insulation be installed at a high density to reduce air movement to a level which would avoid condensation problems. To attain high density, the whole cavity from roof deck to ceiling finish had to be filled. Although this approach had been used in some weatherization programs in the United States, it remained untested and undocumented in Canada where all wood frame roofs should be ventilated as required by the National Building Code (1995 art. 9.19.1.1 par. 1). Without ventilation above the insulation, the proposed insulating method could lead to moisture accumulating within the assembly. To study this complex multi-dimensional process involving vapor diffusion, air movement, capillary flow and moisture storage, a comprehensive model was necessary. The existing available models (*e.g.* CONDENSE 1998, MOIST- Burch *et al.* 1989, Zarr *et al.* 1995) were one-dimensional, limited to vapour diffusion and capillary flow, and therefore too limited. Hence, an in-situ study was considered but an experiment allowing control over all parameters was preferred. The test set up had to simulate the winter and summer climate for full-scale roofs.

Published work related to experimental work of similar scale was lacking. Stewart (1982) found that variations to daily cycling (*e.g.* solar radiation) are rarely reproduced in laboratory conditions due to the long time constant of moisture accumulation. Most works involving the long-term monitoring of the moisture-related performance of assemblies use field setup exposed to natural conditions, *e.g.* Rose (1994). Some experimental work was found in the line of the proposed test. Ojanen and Simonson

(1995) had a 50-day laboratory experiment, but with constant conditions selected arbitrarily. Simpson and O'Connor (1994) ran a test for 66 days of wetting steady state conditions followed by 176 days at drying steady state conditions until equilibrium was attained. Another large scale test (Zarr *et al.* 1995) included 12 panels of 1m by 1.1 m, in which one panel was insulated with cellulose. No large-scale cellulose tests were found in the literature.

A new testing procedure had to be developed. The roof assemblies of the two test huts were built to reproduce actual site conditions. The transposition process from real conditions to the experimental set up is presented below. A methodology, using a weather data file, was developed by others to define the testing conditions. Finally, a monitoring plan was developed using both electronic and manual methods.

To evaluate the consequences of exposing wood-framed assemblies to conditions leading to moisture accumulation, acceptable levels of wood exposure to moisture were developed as limits beyond which rot would develop. In recent work, Viitanen (1996) found that one fungus of the brown rot decay family, a family of decay fungi found typically in wood structure exposed to moisture and water damage, required moisture content (M) of 25 to 28% for growth. These moisture content values result from equilibrium with air at relative humidity (RH) of 94 to 96%. For these moisture conditions, it was found that growth was activated at temperatures as low as 5°C after several months of exposure and was more rapid at 20°C after several weeks of exposure. In terms of temperature exposure, reported temperature limits for growth of decay fungi

vary between -5° and $+45^{\circ}$ C. Lethal temperatures for fungi vary between 35°C and 80°C . At the conditions of 100% RH and 20°C to 30°C , the decay rates of wood accelerate. The minimum moisture requirement, for brown rot fungi to develop, is about the fiber saturation point of wood which corresponds to a relative humidity above 94 to 98%, depending on temperature.

The widespread rule-of-thumb, as noted by Viitanen (1996), is that from a practical point of view, the general rule for wood protection in construction is to keep the wood moisture content below 20% independently of temperature and duration of moisture exposure. No fungi can grow at conditions below 20% M. In the next range from 20% to fiber saturation point or around 27% M, it is possible that, locally, a wood specimen has its fibers saturated with moisture. In these locations, fungi growth would be possible. Above fiber saturation, and with temperatures in the 10° to 40°C range, conditions become very favorable for rot development. These values are in the same range as the ones identified by Trechsel (1994) which indicate decay to occur at moisture content above 27% in the 10 to 32°C range.

2.1.1 Objectives and plan of the experiment

The insulation measure consists of dense packing cellulose insulation in the entire cavity of a flat roof. The high density insulation is expected to prevent convection of moisture laden air. To determine the level of exposure to high moisture conditions in the different assemblies insulated in this manner, the objectives of the experiment were twofold:

- to determine what net moisture gain would occur in the cavities after one wetting-drying cycle, simulating conditions from November to July in the environmental chamber, and
- to evaluate the potential for the development of wood rot.

The test had a duration of six months: the first three months simulating November to March steady periodic winter conditions and the last three months simulating April to July spring and summer conditions. Two different roof assemblies were tested in an Environmental Chamber. The main variables were the mode of moisture transfer (diffusion and convection), the type of vapor barrier, and the geometry of the air exfiltration path.

2.1.2 The testing facility

The Environmental Chamber, commissioned in 1996 (Fazio *et al.* 1997), has been designed to recreate climatic conditions to test building envelope performance. This facility can accommodate wall specimens of up to 4.1 m by 7.2 m, which is equivalent to approximately two commercial storeys or three residential storeys high. It also permits the evaluation of roof specimens of 3.5 m by 4.5 m. It allows for the study of the hygrothermal aspects of the building envelope performance and its interaction with the indoor environment when subjected to controlled simulated outdoor and indoor conditions.

This test used the facility as one large environmental chamber. The two boxes were joined and the two testing huts were built inside, one on top of the other, as shown in Figure 2.1. There was no heat transfer from one hut to the other as they were separated by a 900 mm open air space.

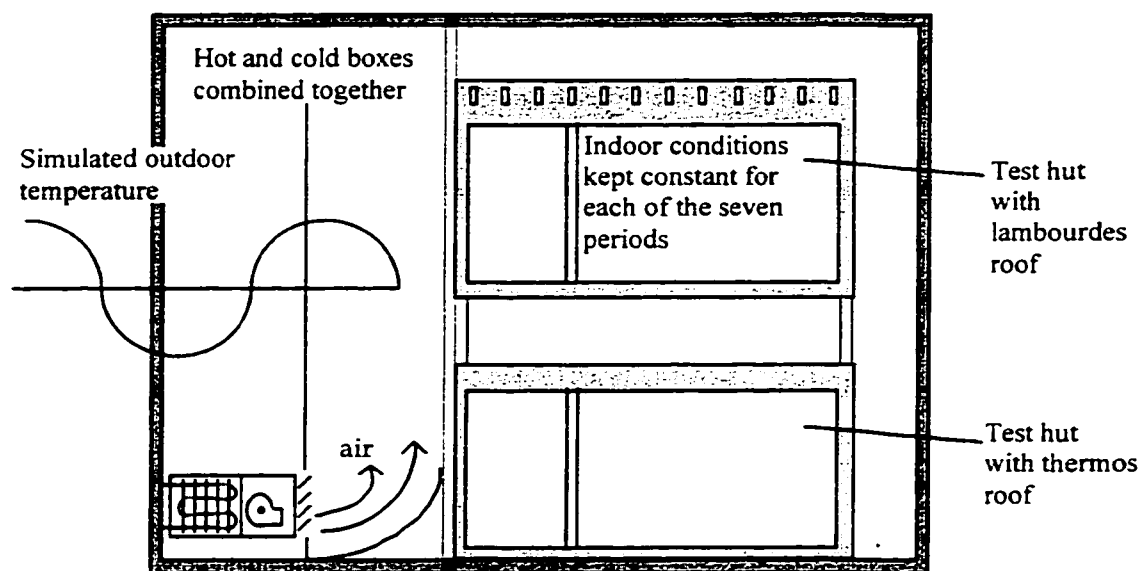


Figure 2.1. Testing configuration for the flat roof test.

2.2 The experimental procedure

2.2.1 Description of a typical building

For the purpose of this study, the author was given access to an industry-owned database of 500 buildings, all admissible to the weatherization program and mostly built between 1930 and 1960, that had been compiled. From this, a statistically average building was defined and used to derive the parameters for the testing hut.

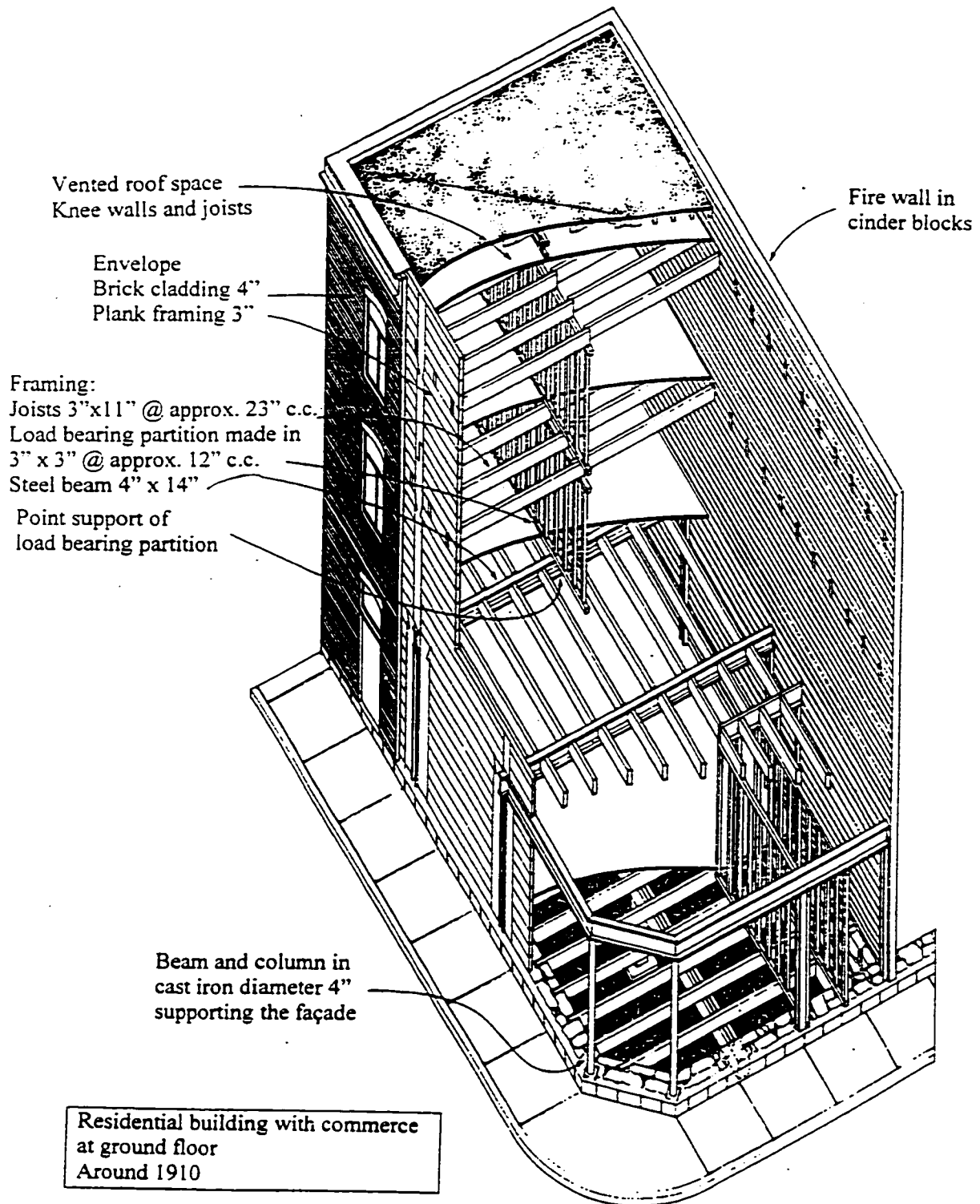


Figure 2.2 Typical plank framing structure or "carré de madrier" (after Auger and Roquet 1998).

At the time of the construction of these buildings, the platform construction using 2"x4" was not allowed in the city of Montreal. The structure of these houses was composed of 50 mm to 75 mm thick by 200 mm to 300 mm high wood timber horizontally installed, one on top of the other (see a typical building in Figure 2.2). This urban adaptation of the log cabin, called "carré de madrier" (timber square) or plank framing, was covered by brick for fire protection. In the case of row houses, a masonry firewall would separate two houses. Of the 500 houses in the database, 50% were row houses and 40% were semi-detached. Roof joists were generally parallel to the front façade and thus 50% of the joists had both ends resting in masonry walls and 40 % had one end in the masonry wall and the other within the wood wall.

Of the 500 buildings, the majority had roof assemblies high enough to get proper ventilation above the added insulation. However, 25% of the buildings had single-cavity roofs, requiring complete insulation of the cavity. 15% were of thermos type assembly, i.e. with joists directly between the ceiling plaster and the roof planking, and 8% were of the lambourdes type; this french word designates wedged joists perpendicular to the main ones used to create the drainage slope of the roof. The wood deck was 19 mm or 25 mm thick tongue and groove planks.

The database showed a great variety of roof membrane assemblies. Some roofs had up to three different wooden deck, each with several layers of roof membranes. In terms of ventilation, the older houses had none, while, for more recent houses, the presence of ventilation goose neck was not always logical. In fact, 50% of thermos roofs, which is a

series of independent cavities, had goose necks, while lambourdes roofs, which had the potential for air movement under the membrane, were not all ventilated. More generally, roofs that had been retrofitted in the last 20 to 25 years were ventilated whether or not it was appropriate to their frame type.

Cross bridging (croix St-André) was more common than wood blocking for bracing. As it does not restrict air movement, cross bridging was not built in the huts. The plaster used in the houses was composed of one or two coats of base plaster often reinforced with horse hair and a finish coat of Paris plaster. Plaster was typically applied either on wood or metal lath and finished with several coats of oil paint which acted as the vapor barrier.

2.2.2 Reproduction of the typical roofs in the test chamber

The test huts were designed to reproduce the main construction conditions found on site. Figure 2.3 shows a typical end of the row building. As the corner of the building possesses one wall that supports joist and another that is parallel to the joists, it formed the basis of the design of the test huts. The huts were thus conceived as having two exterior walls and two interior walls offering adiabatic conditions, i.e. boundaries considered to have no heat and moisture transfer.

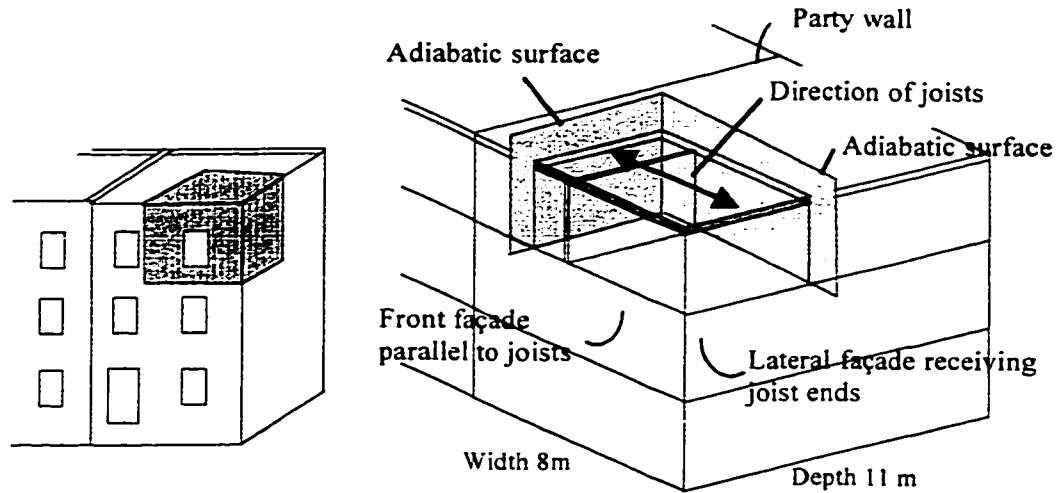


Figure 2.3. Schematic view of part of building subjected to testing via test hut.

The selection of the assembly components was then based on two precepts: the final construction would closely reproduce one section of the building modeled and the dimensions of the wood members would be determined by the averages compiled by the database of 500 buildings. As an example, Figure 2.4 shows the result of the transposition for roof/wall detail from the average existing detail to the test hut detail. For the objectives of the study, the brick veneer and the parapet wall were not built and the focus was on the insulated roof structure and its airtightness. As shown, the walls were not part of the study and were built as to not interfere with air movement and moisture transfer.

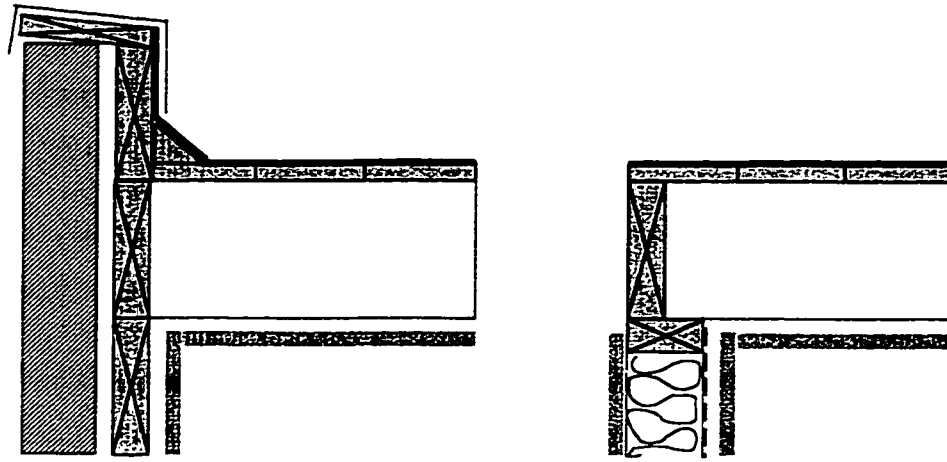


Figure 2.4 . Comparison of site (left) and test hut detail (right) of roof/wall junction.

2.2.3 Description of test hut construction

Each test hut was 4.8 m long and had a load bearing wall at 1.2 m from one end, as shown in Figure 2.5. The 1.2 m joists rested on an exterior wall. That end of the hut was considered to provide adiabatic indoor conditions. The 3.6 m joists rested on the opposite wall, an exterior wall considered to be of the timber type. The total width of the huts was 3.5 m, the thermos hut was 2.5 m high, the lambourdes hut 2.65 m high and there was a 0.9 m open space in between the huts. Walls and floors were not part of this study and were therefore as airtight as possible and very well insulated to allow constant indoor temperature and relative humidity.

Each hut was divided into five longitudinal cavities. The average joist spacing measured on site was 409 mm for thermos joists and 459 mm for the lambourde joists; the median for both types was 400 mm. This was the spacing used in the testing huts for each pair of

joists. Four cavities had a width of 735 mm each, leaving 150 mm of insulation on the non-monitored sides of the joist, insuring adiabatic conditions. Cavities were separated by a 12 mm exterior grade plywood, covered with a self-adhesive bituminous membrane to insure no moisture or air transfer between cavities.

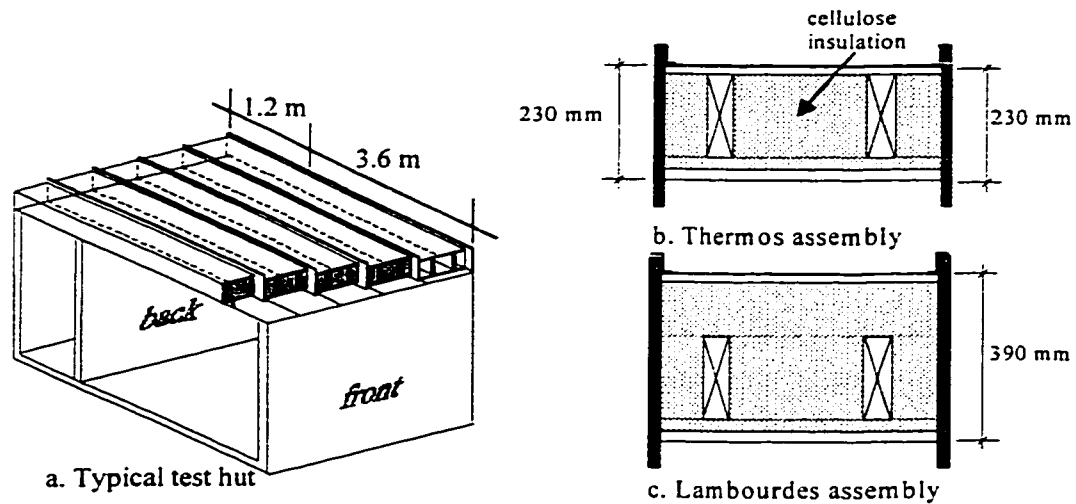


Figure 2.5 Typical hut and composition of roof assemblies.

Furthermore, in accordance with the database, the ceiling finish consisted of plaster on wood lath, which was installed on 19 mm furring strips. Metal lath was also used to provide grip for the plaster. The plaster used consists of two coats of double use plaster and one finish coat of gaging plaster, equivalent to, but setting slower than plaster of Paris. The roof deck was composed of 19 mm by 150 mm planks covered with a roofing membrane, without tongue and groove as it was not available on the market. 90% of the roofs in the database did not have fiber board below the membrane. To simulate a built-up roof, a self-adhesive modified bituminous membrane was chosen since mopping hot asphalt might have been hazardous in the chamber. The membrane was lapped over the

plywood separator, insuring continuity of air barrier. Table 2.1 presents the composition of each roof assembly.

Table 2.1. Typical assemblies.

Thermos (T)	Lambourdes (L)
Self-adhesive bituminous membrane	
Planking – spruce – 19 mm x 150 mm	
n/a	Cross member “lambourdes” – spruce – 45 mm x 150 mm @ 400 mm c/c
Joist – spruce – 45 mm x 190 mm @ 400 mm c/c	
Dense packed cellulose Total height 210 mm.	Dense packed cellulose Total height 360 mm
Furring 19 mm x 38 mm @ 400 mm c/c	
Wood lath – 12 mm x 25 mm @ 35 mm c/c	
Metal lath	
Plaster – 2 coats, 19mm	
Paint – alkyde 2 coats	

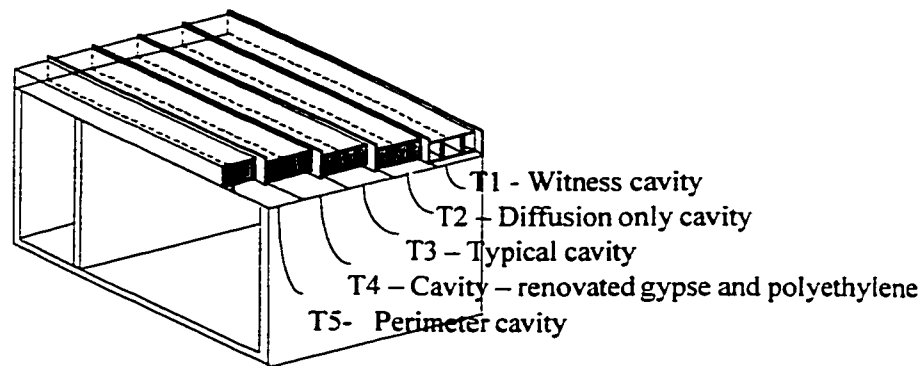
Note : in T4 – plaster is replaced by a polyethylene sheet and gypsum board.

Temperature in each hut is maintained by two baseboards heaters (2 kW) controlled by one electronic thermostat, and an air conditioning unit; temperature settings were changed manually at the beginning of each period. The test huts are equipped also with a humidifier and a dehumidifier. As buildings in the database were two or three story high, the air pressure differential due to the stack effect was simulated with a pressurization system. It was composed of an air pump, located outside of the chamber so the air pumped was at indoor conditions, connected to two pipes, each equipped with a manual flowmeter and linked to one hut.

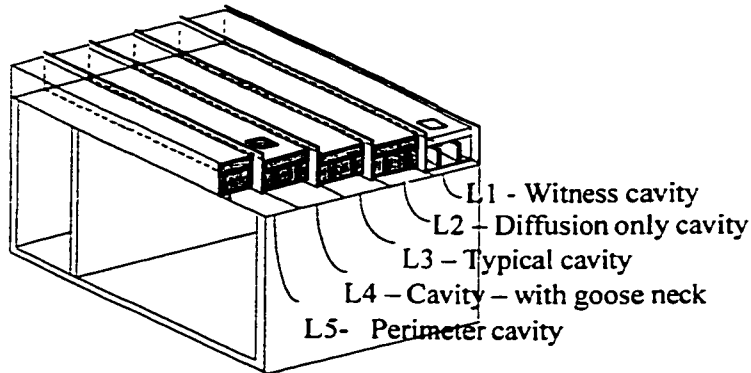
Each hut contained 5 roof cavities - one reference cavity without insulation and four insulated with high density cellulose, as shown in Figure 2.6. Of these four, one was subjected to moisture diffusion only (little or no air leakage); the three others, to both diffusion and air exfiltration. Table 2.2 summarizes the characteristics of each cavity.

Table 2.2. Characteristics of cavities.
Black squares indicate parameters applied in each cavity.

Parameters Assemblies						
	Insulation	Moisture Diffusion	Air Exfiltration	Moisture Diffusion	Moisture Diffusion	Moisture Diffusion
Thermocouples						
T1						
T2						
T3						
T4						
T5						
Barbometer						
B1						
B2						
B3						
B4						
B5						



a. Thermos hut



b. Lambourdes hut

Figure 2.6. Schematic views of thermos and lambourdes test huts showing all 10 cavities.

Diffusion only cavities have no air path and all apparent openings were sealed with polyurethane. As shown in Figure 2.7, for the cavities 3, 4 and 5 of both huts, air could enter the cavities in four modes: 1- through the partition, 2- through ceiling electrical outlet, 3- from behind the gypsum board of the exterior wall to the joining roof space, and 4- for cavities T-5 and L-5, there was also a continuous lateral leakage all along the side wall, behind the gypsum board. The air could exit through: A- the cracks between the structural members of the outside wall, B- through the goose neck, and C- all along the cavity through the cracks between the wood frame members. The goose neck is simulated by a 150 mm x 200 mm opening in the deck surrounded by a 200 mm high box filled with glass fiber insulation used as a filler to maintain cellulose during its

installation and often left in place in practice. Figures 2.8, 2.9 and 2.10 show the actual cavities during construction.

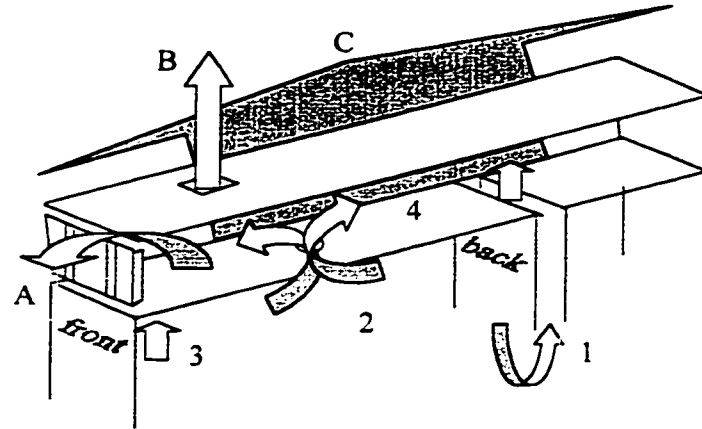


Figure 2.7. Exfiltration path schematic from inside to roof cavity : 1. through mid-room partition, 2- at lighting fixture, 3- at exterior wall connection, 4- all along side. From roof cavity to outside: A- through cracks between structural members, B-through goose neck, C- lateral exfiltration along length of cavity.

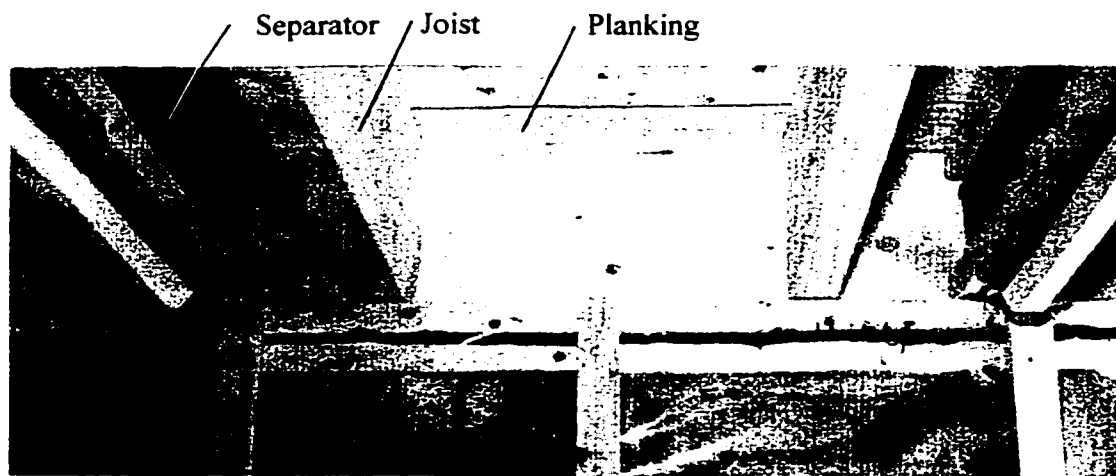


Figure 2.8. Typical thermos assembly during construction. The end of the cavity against the exterior wall is shown. Air leakage occurs in between wood members.

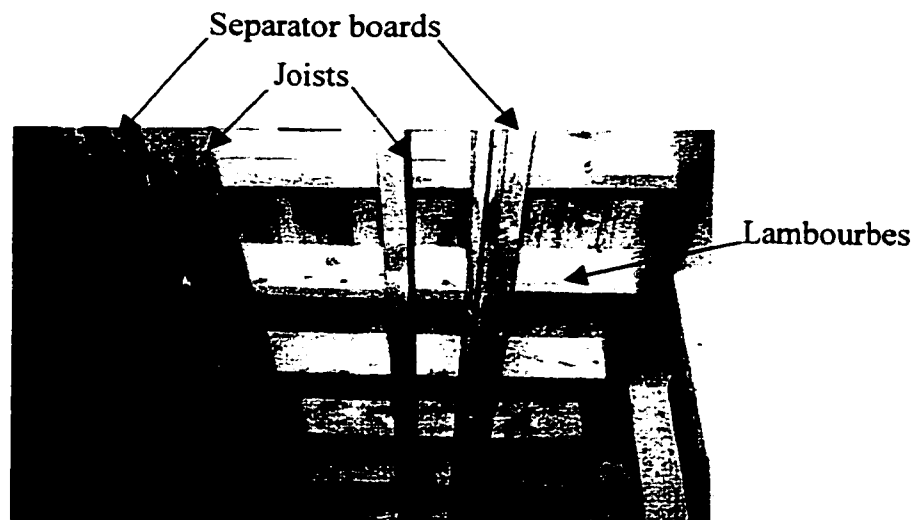


Figure 2.9. Typical lambourdes assembly during construction. Long joists receive cross members called lambourdes. Black panels are dividers between cavities.



Figure 2.10. View of the cavity L5, which has lateral leakage all along lateral wall. The furring on top of the polyethylene sheet leaves a space for air leakage behind gypsum board. At bottom right of picture, the interior partition can be seen. Leakage occurs through that partition as well.

2.2.4 Simulated testing conditions

To meet the project objectives, a methodology was developed to determine the conditions to be simulated during the test (Gerbasi, to be published). The goal was to define testing conditions that would expose the roof cavities to wetting and drying conditions equivalent to conditions experienced by roofs on site. The present section presents briefly the main hypotheses used in the process.

The first step was to determine the approximate duration of the wetting season and its corresponding wetting potential for a house located in Montreal. A simple one-node computer spreadsheet was developed to approximate the hourly condensation and drying rates due to diffusion and air leakage for a typical insulated flat roof based on its material properties, and given indoor and outdoor conditions. The seasons were defined as :

Wetting season: November 8 to April 8 => 5 months approximately
Drying season: April 9 to November 7 => 7 months approximately

Then, the wetting season was compressed to 3 months by increasing the humidity content of the indoor air in respect to average site conditions. The experiment's wetting season consisted of three periods of 30 days, each represented by a sinusoidal outdoor temperature profile and constant relative humidity and indoor temperature. The drying season was not reduced or compressed. The three wetting periods and the four drying periods are presented in section 2.3. Table 2.3 presents the factors that were used.

Table 2.3. Summary of basis for simulated conditions

Conditions to be simulated	Site conditions assumed	Conditions reproduced
Indoor temperature	Constant setpoint, slightly above normal, air conditioning	Constant setpoint
Indoor relative humidity	Constant setpoint, several occupants or some use of humidifier	Constant setpoint
Outdoor temperature	According to Montreal weather file	Daily temperature cycling
Solar radiation	Solar radiation as per weather file. Roof membrane with absorptance of 0.9, without snow cover	Equivalent sol-air temperature integrated in temperature cycling
Outdoor relative humidity	According to Montreal weather file	Constant moisture content
Roof is at second or third floor of building	Stack effect. No account for wind effect or mechanical ventilation	One or two setpoints daily for pressure differential

The test hut's indoor temperature and RH levels as compared to the typical site conditions are presented in Table 2.4. This table also shows the time compression in the duration column.

Table 2.4 - Typical vs. tested conditions

#	Period Duration	Period simulated		Typical site conditions		Procedure requirements	
		From	To	Indoor Temperature (°C)	Indoor Relative Humidity	Indoor Temperature (°C)	Indoor Relative Humidity
1	54 days simulated in 30 days	Nov. 8	Dec. 31	21	40%	23	50%
2	39 days simulated in 30 days	Jan. 1	Feb. 8	21	35%	22	40%
3	59 days simulated in 30 days	Feb. 9	April 8	21	40%	23	55%
4	21days	April 9	April 29	21	45%	21	45 %
5	30 days	April 30	May 29	21	45%	21	45 %
6	30days	May 30	June 28	23	50 %	23	50 %
7	14 days	June 29	July 14	23	50 %	23	50 %

2.2.5 Parameters monitored

Overall, 262 points were monitored electronically throughout the test and 120 specimens were periodically removed from the test huts for gravimetric measurement.

Temperature and air pressure measurements were done with conventional equipment. All temperature measurements used thermocouples, type T, copper and constantan, 30 gage, with 0.3°C accuracy. Air pressure differential was measured across the wall, with both taps at the same level, at 12 locations, *i.e.* in each hut and inside the five cavities. Measurements were made by a pressure transducer that sent the electronic reading to the data acquisition system. A scanner valve allowed for the rotation of 12 readings against the two reference pressures, just outside of the huts.

Three methods were used to monitor the variations in moisture content due to moisture transfer: 1) measurement of the moisture content of the wood with moisture content pins, 2) measurement of the relative humidity in the cellulose insulation, and 3) gravimetry measurement on samples in the planks, the joist and the cellulose insulation. The implementation of the three methods was proposed to fully document moisture movement.

- Wood moisture content sensor.

Moisture content in terms of percentage is defined as the ratio of the mass of the moisture within a given volume of wood to the mass of the same volume of dry wood, times a hundred. The moisture content present within a material affects its electrical resistance. Studies have achieved specific correlations between the electrical resistance of wood and its moisture content, for different wood species in a range of temperature. In this study, 101 pairs of insulated pins were inserted in the wood. The pins were at a defined distance one from the other. The resistance to electrical current between the two pins was

measured. The sensed resistance was converted to a current (4 to 20 mA) signal which was read by the data acquisition system. The readings were calibrated at the beginning of the test. To prevent any electrodeposition on the pins, the direction of the current was switched with a relay for each measurement and the current was maintained for only a few seconds. A thermocouple was inserted with each pair of pins in the wood at the same depth. The measured temperature was used to correct the moisture content readings which are temperature dependent.

The probes measure moisture content ranging from 6% to fiber saturation (25-30%) as explained in chapter 1. Wood with very low moisture content has high electrical resistance. Readings at low moisture content are expected to be more accurate than at high moisture content. Above the saturation point of the fiber, readings are of limited value.

Table 2.5. Error of moisture readings in wood with pins from manufacturer.

Moisture content	Error
from 6 to 12 %	$\pm 0.5\%$
from 12 to 20 %	$\pm 1\%$
from 20 % to fiber saturation point	$\pm 2\%$

Correction tables are provided by the manufacturer for temperature correction and wood species correction. The base relation is for Douglas fir at 20°C, while white spruce is used in the experiment. Excerpts from the tables are shown in Tables 2.6 and 2.7.

Table 2.6. Correction table provided by pins manufacturer for species.

Wood species	Meter readings by moisture content pins										
	7	8	9	10	12	14	16	18	20	22	24
Spruce Sitka	0.0	0.2	0.3	0.3	0.5	0.6	0.8	0.9	1.0	1.4	1.7

Table 2.7. Correction table provided by pins manufacturer for the range of temperatures.

Wood T [°C]	Meter readings by moisture content pins						
	6	7	10	15	20	25	30
-20	+3	+4	+5	+7	+11**	+13	+18
-10	+2	+3	+4	+5	+8	+9	+16
5	+1	+1	+2	+3	+4	+5	+6
15	0	0	+1	+1	+1	+2	+2
20	0	0	0	0	0	0	0

*the manufacturer estimates that corrections below 10% can be disregarded.

**values in the shaded area are indicative only as being above the fiber saturation point

Insulated pins provide a contact only with their uncoated portion at the tip. The contact area with the wood is most probably uniform in terms of moisture content independently of the depth of the penetration. Uninsulated pins increase the contact area, thus creating a rise in meter readings. The reading of moisture pins is local so care must be applied to extrapolate on moisture distribution. Several local conditions may affect the reading. All the readings in this experiment are taken perpendicular to the wood grain. The wood resistance to electrical current is greater across the wood grain than parallel to it. For moisture content below 10%, readings are similar in the two directions. But, for moisture content of 20%, readings across the grains are approximately 2% lower than readings taken parallel to the grain. Readings across the grain, by traversing many layers, provide an average moisture content, whereas readings parallel to the grain reflect one layer of wood cells and may therefore not be representative of the entire sample. The depths of readings for this project are given in Table 2.8.

Table 2.8. Depths of pins in this study.

Location of moisture content reading	Pins inserted	Distance from tip of pins to the surface of wood in contact with cellulose
In 19 mm roof planking	from outside	6 mm
At top of joist	from outside	20 mm, at middle of joist
At bottom of joist	from inside	6 mm

The presence of inorganic salts, like fire retardant compounds that electrolyze rapidly, may affect the readings by indicating a much higher moisture content than is actually present. The presence of borax in the cellulosic fiber was thus a concern, as it has caused problems to Zarr *et al.* (1995). In order to prevent contact with the insulation, all the pins were either driven from the outside or embedded into the wood pieces. Also, as the moisture content probes in wood had a chance to loosen over time due to wood contraction and expansion caused by temperature and moisture content variations, a PVC strip was installed over the pins in the planking to provide constant pressure, and therefore constant contact area between the pins and wood.

- Relative humidity sensor in cellulose insulation. The relative humidity in the cellulose was measured using relative humidity sensors of the capacitive type. These probes were installed in the center of the insulated cavity and at 50 mm below the plank, with the transmitters on the warm side of the assembly. A thermocouple was integrated with the probe. The relative humidity sensors used the principle that the dielectric constant of the polymer thin film changed with atmospheric relative humidity, resulting in linear capacitance changes as a function of relative humidity. This type of sensor is not affected by water condensate once evaporated and is immune to most chemically reactive vapors. This sensor had to be small so as to minimize its effect on the moisture distribution. All sensors were calibrated at 30% and 60% RH within a precision relative humidity generator designed to be used as an RH calibration test chamber.

- Gravimetry is an indirect method of measuring moisture content which consists of comparing the weight of a specimen before and after it is oven dried. This can be done for an assembly or with small samples taken within the assembly. To monitor variation

in the moisture content over time, the same sample can be weighed and replaced within the assembly during the length of the test. The samples were retrieved and weighed at the end of the experiment. This procedure allows long term monitoring of moisture accumulation at regular intervals as a ratio of the dry mass of the wood specimen. As opposed to the electronic methods described above, the net mass of moisture for a defined volume of wood can be obtained by gravimetry. To compare the results from gravimetry with the results from the moisture pins, almost all gravimetry specimens were taken from the same plank that was undergoing electronic monitoring. This set up allowed to use the gravimetry results to complete the electronic results for moisture content above the fiber saturation point.

For this project, 40 samples of spruce wood and 80 samples of cellulose insulation were measured at regular intervals, during the experiment. Moisture content was determined at the end of the experiment by weighing the completely dried specimens. Drying was not done before the completion since the sorption history of the hygroscopic materials would be modified and therefore be different from the properties of the wood and cellulose remaining in the hut. Cellulose insulation specimens were contained in small bags, 40 mm x 40 mm x 10 mm, which were made of the same highly vapor permeable paper used for teabags. Specimens were always put back into place according to the same orientation and positioning. The weighing of all the specimens was carried out approximately every two weeks, *i.e.* at the beginning and middle of each of the seven periods and at the end of the test.

Specimens were accessible either from inside or from outside the hut. In each case, one opening provided access to several specimens. For specimens situated on the cold side of the assembly, the wood specimen were cut out directly of the plank, at 200 mm from the location of the moisture content sensors in the same plank. Two cellulose tea bags were positioned below, as in Figure 2.11.

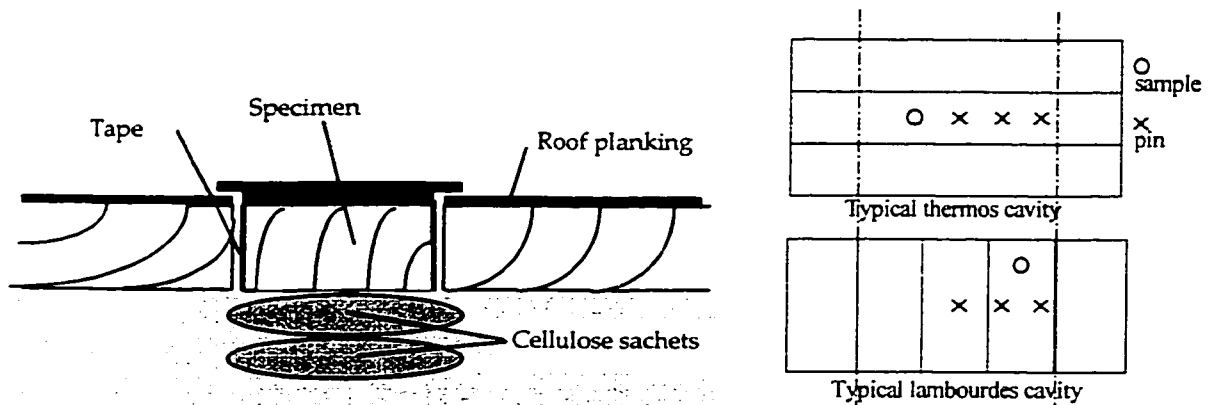


Figure 2.11. Specimens on cold side of assembly, referred to as R in Figure 2.15 and position of these specimens on the planks.

Access to specimens on the warm side of the assembly was provided through a gypsum board plug. These specimens included two cellulose tea bags and one wood cube which was inserted in the bottom of the joist (Figure 2.15). This cube was of the same wood species as the joist, installed with grain in same direction and maintained in place with a rubber band. The cubes were at the same height as the wood moisture pins in the facing joist. Figure 2.12 illustrates the specimens at the bottom of the joist. Figure 2.13 depicts specimens located in the cavity T4, which has gypsum board and polyethylene sheet and Figure 2.14 presents specimens found in the header joist of T5 and L5. Figure 2.15 shows the distribution of the moisture content probes and the gravimetric samples in both roofs. Finally, Figure 2.16 illustrates a typical layout of the instrumentation as seen in cross section.

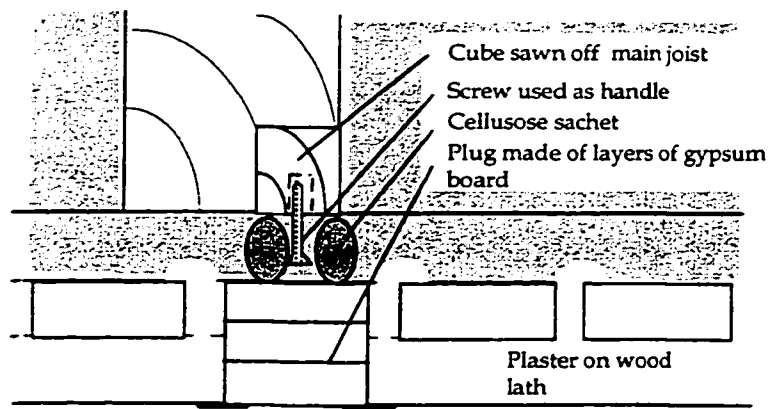


Figure 2.12. Specimens on interior side of assembly, referred to as J in Figure 2.15.

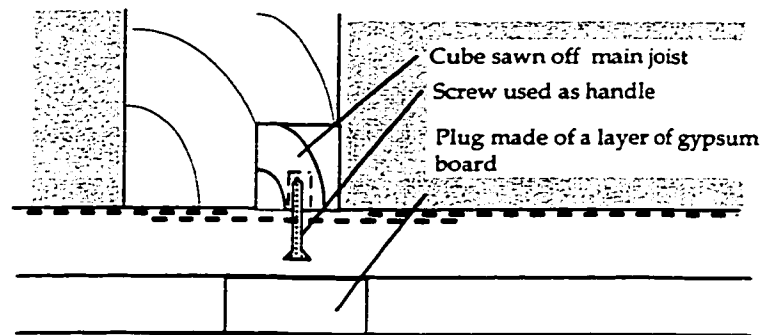


Figure 2.13. Specimen in cavity T4 – gypsum board and polyethylene sheet, referred to as J in Figure 2.15.

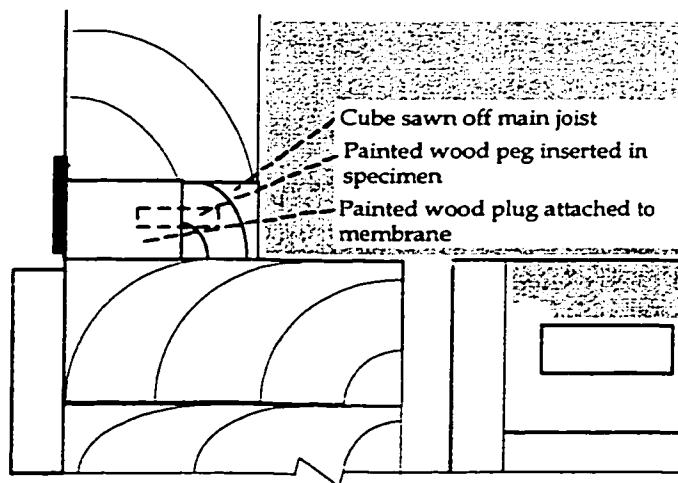


Figure 2.14. Specimens in the side of the header joists of T5 and L5 referred to as X in Figure 2.15.

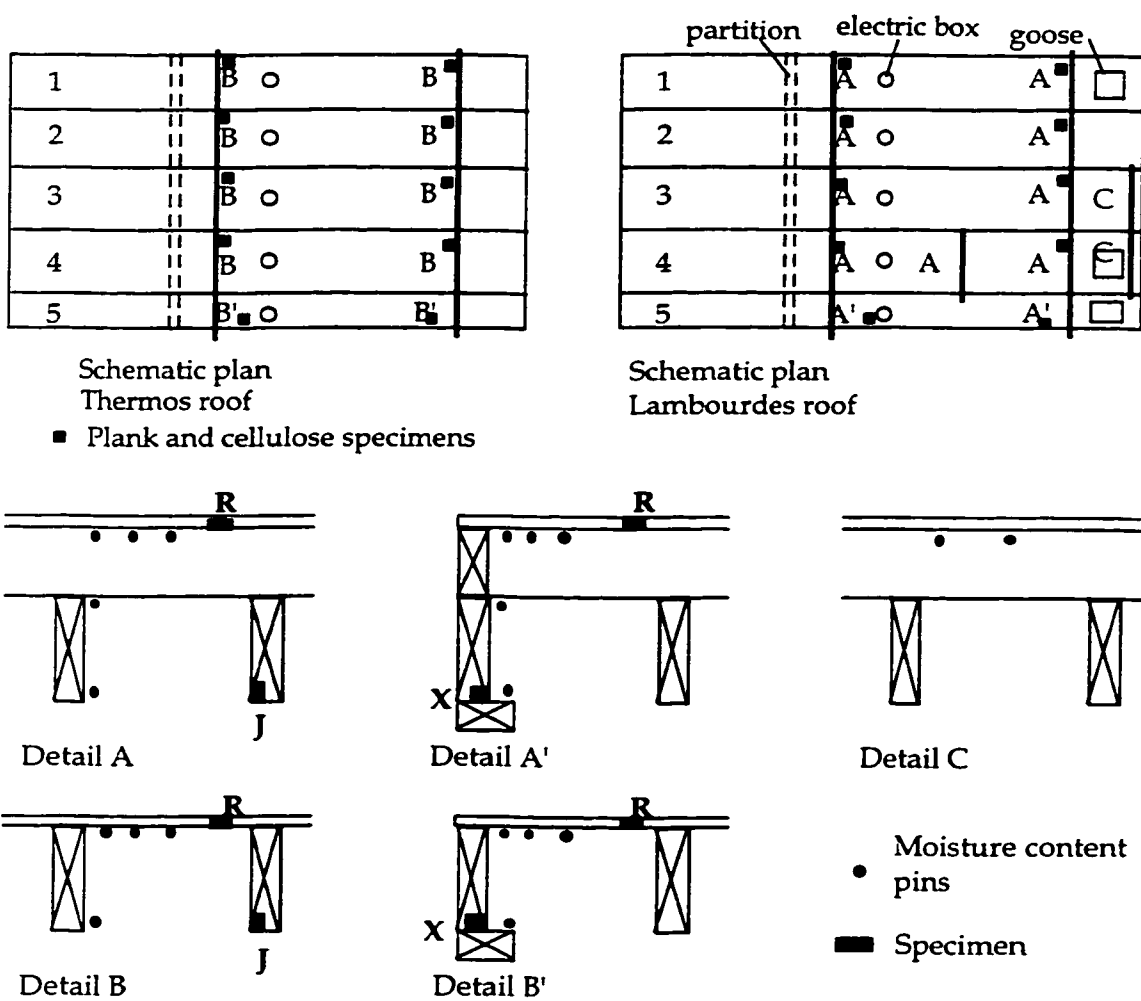


Figure 2.15. Schematic plan and corresponding details for monitoring

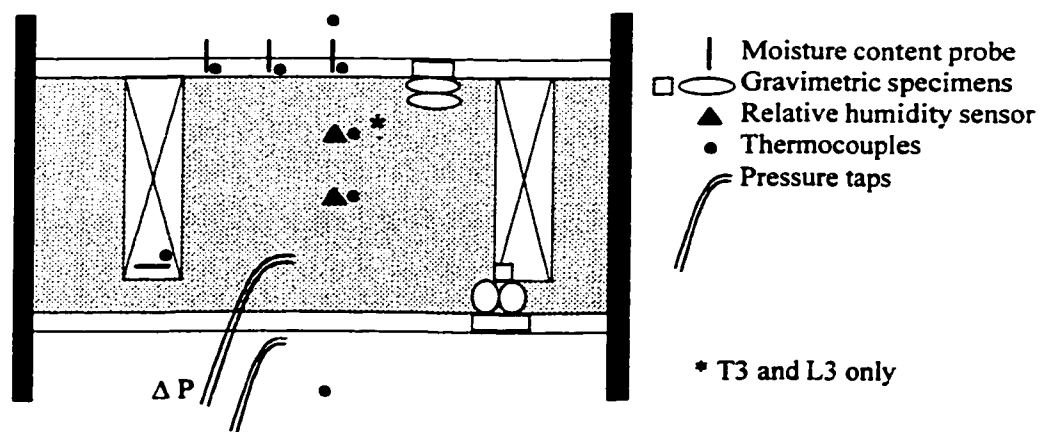


Figure 2.16. Typical layout of instrumentation in a thermos cavity.

2.3 Running of the test

2.3.1 Preparation work

The wood used for the construction of the huts arrived in the laboratory at normal lumberyard conditions, *i.e.* with a moisture content higher than 20%. The construction occurred from January 6 to January 13, 1997. Instrumentation took a longer period from January 14 until March 25. On March 10 and 11, the airtightness of the uninsulated cavities was assessed as shown in Figure 2.17. The method consisted of progressively sealing the exterior cracks of each cavity and, for each levels of sealing, measuring the volume of air exfiltrating through the hut pressurized at different pressures using a blower door.

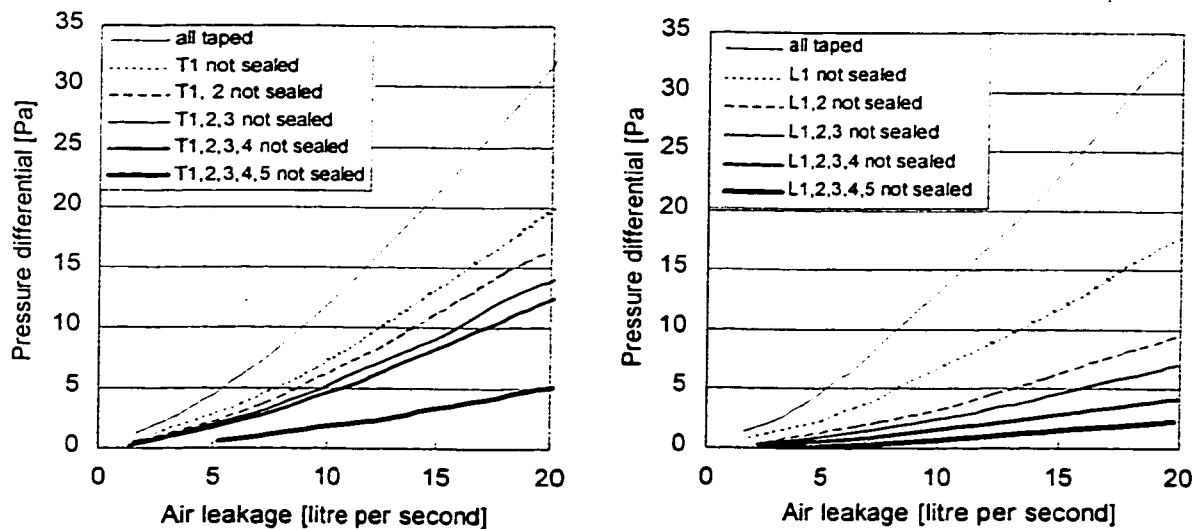


Figure 2.17. Results from airtightness measurements of cavities prior to insulation.

The test was started when the moisture content sensors in the wood were all below 6%. The chamber, the instrumentation and the data acquisition system were checked for 5 days from March 26 to April 1st. When the trouble shooting was completed, the

insulation was installed on April 2. The installed cellulose moisture content was measured to be at 5%. This was followed by another five-day trouble-shooting period.

2.3.2 The execution of the test

From April 7, the test was executed without interruption for 190 days. Only two out of the 262 sensors did not work properly. The conditions obtained compared very favorably with those planned for the procedure. Table 2.9 and Figure 2.18 show that the planned procedure was closely respected. The causes of discrepancies between planned test conditions and actual tests conditions were considered. For outdoor simulated temperature, some differences are due to the fact that during the first three periods, the cooling coil of the environmental chamber was defrosted at regular frequency. The effect was a rise of temperature of few degrees for a period of 20 minutes. In the coldest period 2, when defrosting was required on a more frequent basis, its impact explains the differences found at the bottom of the curves. This defrosting procedure was always performed during the ascending part of the cycle. Due to the fans present within the environmental chamber, there was little temperature stratification. The outdoor relative humidity was not controlled and the value was measured without possibilities for adjustment. Indoor conditions were sometimes one or two degrees cooler than required. In terms of percentage, the most important differences come from the air pressure differentials. The very low pressure differentials required were difficult to maintain and measure, but absolute discrepancies of one pascal or less are considered low. The impact

of the differences between the planned procedure and the actual testing conditions on the moisture transfer was found to be insignificant.

Table 2.9 - Synoptic table of test progress.

T – refers to Thermos assemblies and L refers to Lambourdes assemblies.

0 and 3 means 0 Pa during the day, 3 Pa during the night.

	Day number and date of actual test	Duration (days)	Indoor Temp. (°C)	Indoor RH (%)	Pressure differential (Pa)	Outdoor Temp. (°C)	Outdoor RH (%)
Preparation		5	23	50		-3.5	90
	Days -5 to 0 April 2 -7		T 21.9 L 20.9	T 50.9 L 50.1		-3.6	64
Period 1.		30	23	50	3.1	-3.5	90
Planned							
Actual	Days 0 to 28 April 7 to May 5	28	T 21.9 L 20.9	T 50.9 L 50.1	T 3.8 L 4.3	-3.6	64
Period 2		30	23	40	3.6	-7.0	80
Planned							
Actual	Days 28 to 60 May 5 to June 6	32	T 22.4 L 21.4	T 40.1 L 40.7	T 3.8 L 3.25	-6.7	64.4
Period 3		30	23	55	3.1	-1.2	90
Planned							
Actual	Days 60 to 91 June 6 to July 6	31	T 23.5 L 22.7	T 53.7 L 53.9	T 3.3 L 3.6	-1.4	70.9
Period 4		21	21	45	0 and 3	10.5	45
Planned							
Actual	Days 91 to 112 July 7 -28	21	T 21.9 L 20.9	T 46.5 L 48.4	T 1.7 L 1.3	10.6	56.6
Period 5		30	21	45	0 and 2	18.2	40
Planned							
Actual	Days 112 to 143 July 28 to Aug. 28	31	T 21.9 L 20.7	T 45.1 L 44.3	T 1.3 L 2.2	18.3	48.8
Period 6		30	23	50	0 and 1	24	50
Planned							
Actual	Days 143 to 172 Aug. 28 to Sept.26	29	T 21.9 L 21.2	T 47.7 L 45.5	T 0.2 L 0.1	25.2	46
Period 7		As needed	23	50	0 and 0.5	27.4	72
Planned							
Actual	Days 172 to 190 Sept. 26 to Oct. 14	18	T 21.6 L 21.5	T 47.3 L 46.6	T 2.5 L 2.7	27.3	41.8
Total		190					

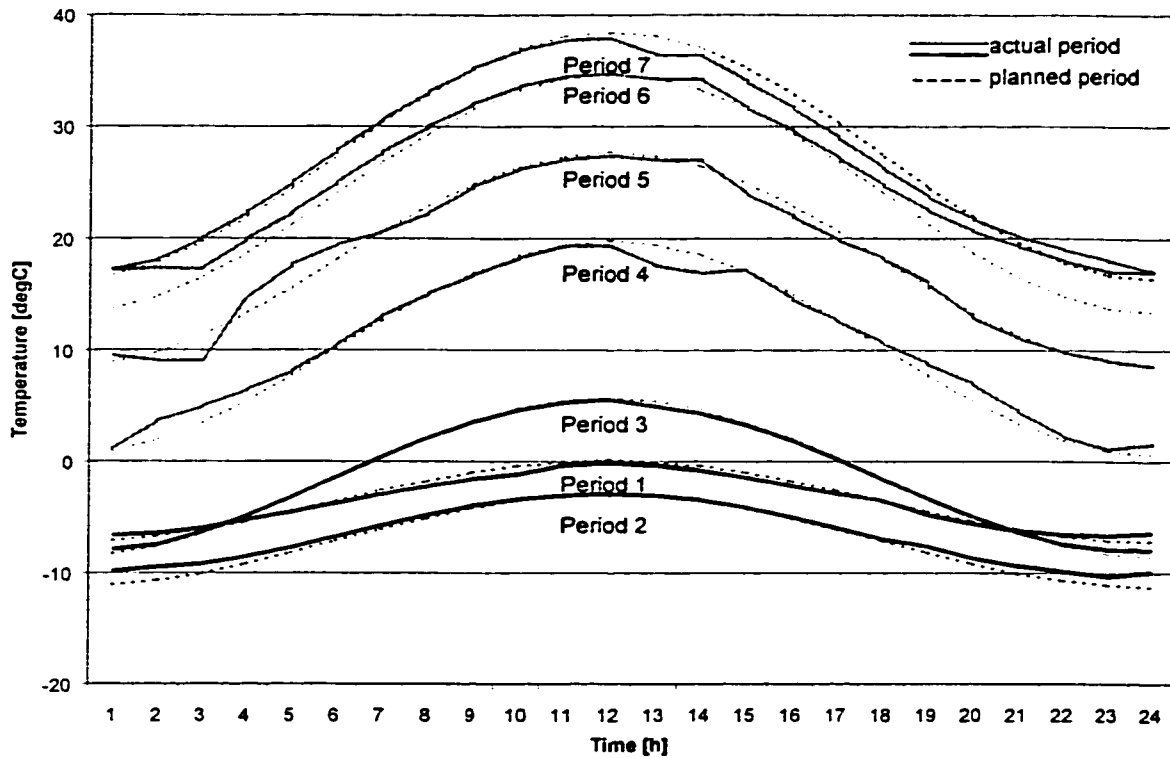


Figure 2.18. Temperature profiles for periods 1 to 7 – showing average temperature reproduced in the Environmental chamber for each hour of each period vs. planned conditions.

2.3.3 Dismantling of the set-up

Special care was taken during the removal of the moisture content pins to try to detect changes on the pins or in the wood. Almost all pins of cavities T2, T3, T4 and L2, L3, L4 were spotless, only a few had loosened in their holes. By comparison, all pins in T1, T5 and L1, L5 were either tarnished, rusted and/or had wood dust stuck to them while the holes in the wood were darker. The high moisture content present in the latter cavities caused reactions at the pins surfaces. There is no indication that the measurements were affected by this change.

Dismantling then focused on removing the wood planks without altering the cellulose insulation. Notes were made on the aspect of each wood plank and these observations are presented later. Then followed the removal of the insulation and plaster. Once this was completed, the inspection of the wood joists and lambourdes members was performed.

2.4 Results

The electronic data from the moisture content pins was corrected for temperature as presented in section 2.2.5. The name of sensors used during the test for the database is used in the following graphs. Appendix B explains the meaning of the nametags of the sensors. The wetting and drying curves from the moisture pins and from the gravimetry have the same overall shape. However, the values of moisture content offer discrepancies of up to 5%M. The tendency is for gravimetric results to be higher than the electronic data in the thermos roof and lower in the lambourdes roofs. This remains to be explained. Examples of these differences are in the following graphs, Figures 2.19, 2.20 and 2.21.

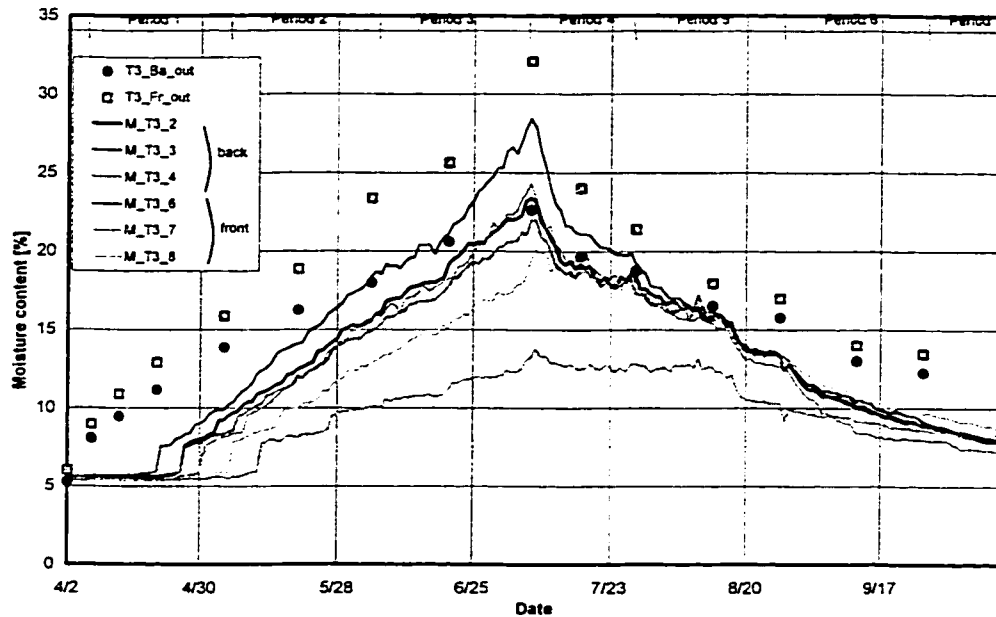


Figure 2.19. Comparison of gravimetric and moisture pins data in T3. The gravimetric specimen at the front of the cavity (T3_Fr_out) has a moisture content systematically above the pins 6,7 and 8 while the specimen at the back of the cavity (T3_Ba_out) starts with a higher moisture content but at the end of the wetting coincides with the measurements from pins 1, 2 and 3.

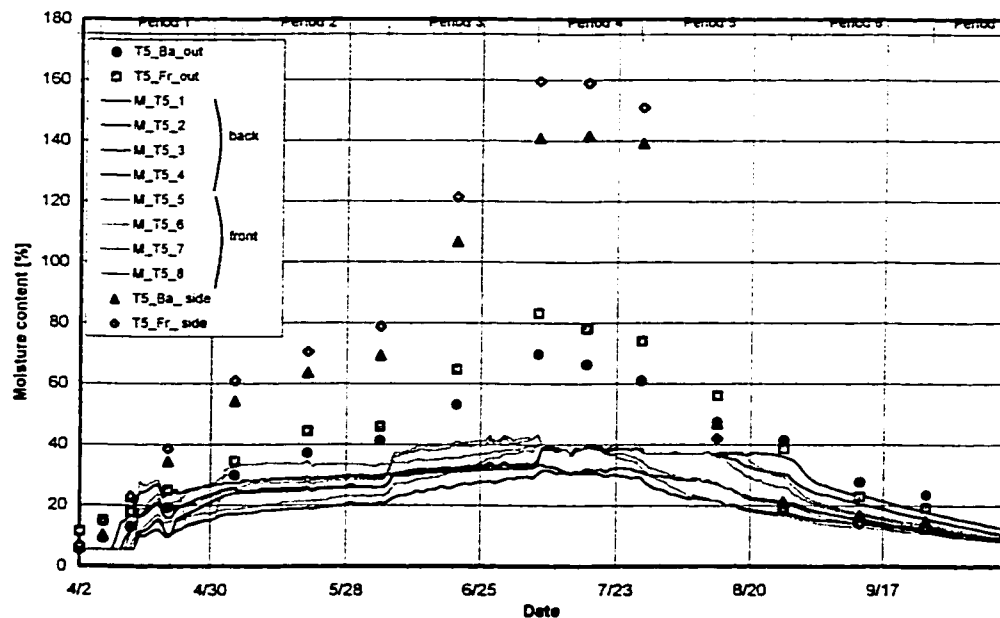


Figure 2.20. Comparison of gravimetric and moisture pins data in T5. This graph shows the significance of the gravimetric results when the moisture content rises above the FSP.

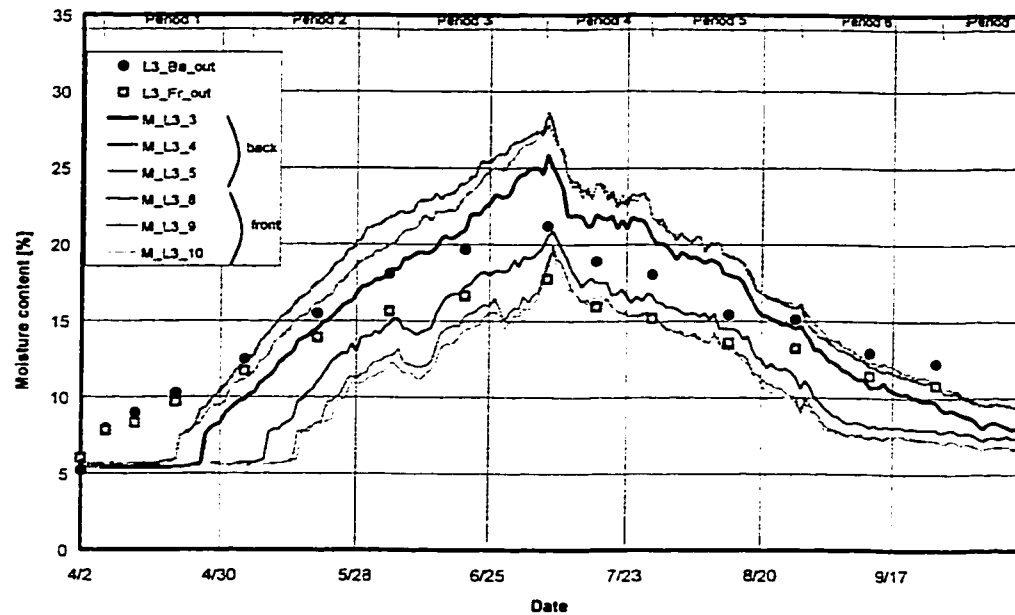


Figure 2.21. Comparison of gravimetric and moisture pins data in L3. In this case, in both locations, the gravimetric measurements are lower than the electronic measurements during the middle section of the test.

2.4.1 Wood plank and joist moisture content

To present the overall results of the test, Figures 2.22 and 2.23 show the average moisture content for the planking of the 5 cavities of each hut. As predicted, each cavity has a different moisture content curve which illustrates the impact of the different parameters. The average construction was found in T3 and L3. Using these as base line, the diffusion only cavities, T2 and L2, had low moisture content level, even at the end of the wetting periods. Average maxima of 16 and 14% were found respectively. The fourth cavities, T4 and L4, were used to monitor the impact of two different parameters. In the thermos roof, the assemblies had a polyethylene sheet and gypsum board as if the ceiling had undergone a major retrofitting. The moisture content measured in that cavity is the

lowest of all. The vapor barrier prevented moisture diffusion and moisture convection. During demolition, it was also found that the polyethylene sheet was installed in a way that restricted air exfiltration.

In the lambourdes roof, the fourth cavity had an extra hole in the roofing deck to simulate the presence of a goose neck. The higher moisture content of that cavity could be accounted for by the extra air movement induced by the opening. The side exfiltration found in T5 and L5 have resulted in very high moisture content. The cavities T1 and L1 were not insulated but were exposed to exfiltration conditions found in insulated houses in terms of relative humidity. As a result, the high moisture content levels monitored in those cavities are not representative of those found in actual roofs of uninsulated houses.

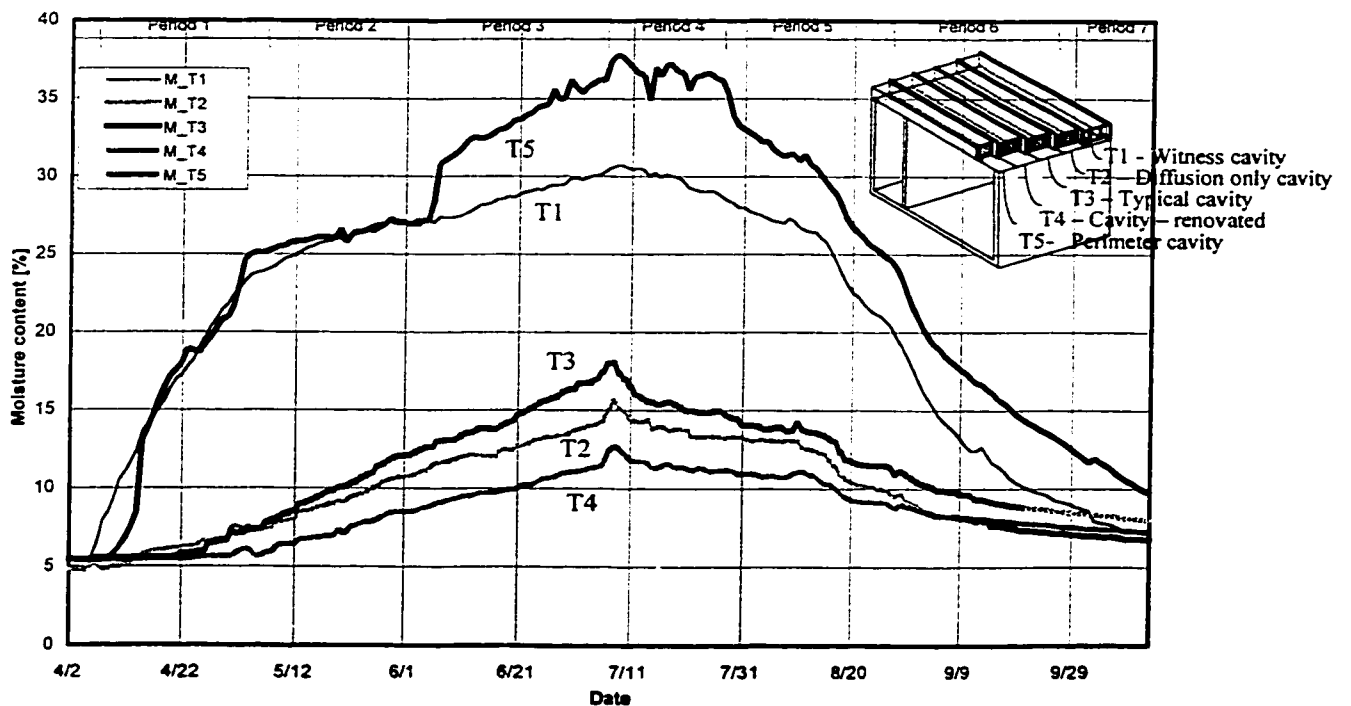


Figure 2.22. Average moisture content in the wood plank for length of test in thermos.

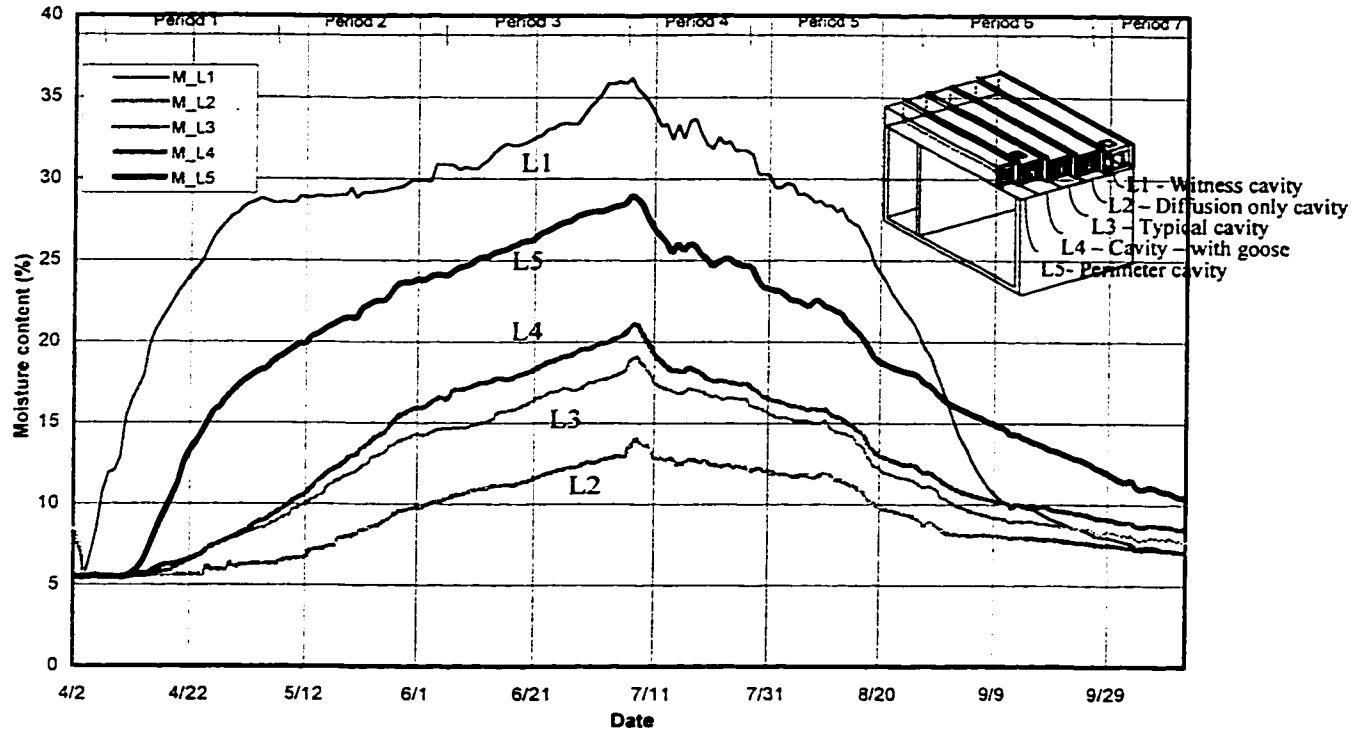


Figure 2.23. Average moisture content in wood plank for length of test in lambourdes.

The graphs in Figures 2.24 and 2.25 show the level of moisture content monitored with the moisture pins in the planks and in the joists at two locations : at back, close to the main source of exfiltration in the roof, *i.e.* the interior partition, and at front, close to the way out through the exterior wall. The planks experienced a steady moisture accumulation from two weeks after the start of test. Both cavities saw some of their planks with high moisture content, *i.e.* above 20%. The jump in moisture content at the beginning of the curve from 6 to 7.5% is explained by the location of the pins in the middle of the planks, and the time required for the moisture to penetrate into the wood and reach the moisture pins level.

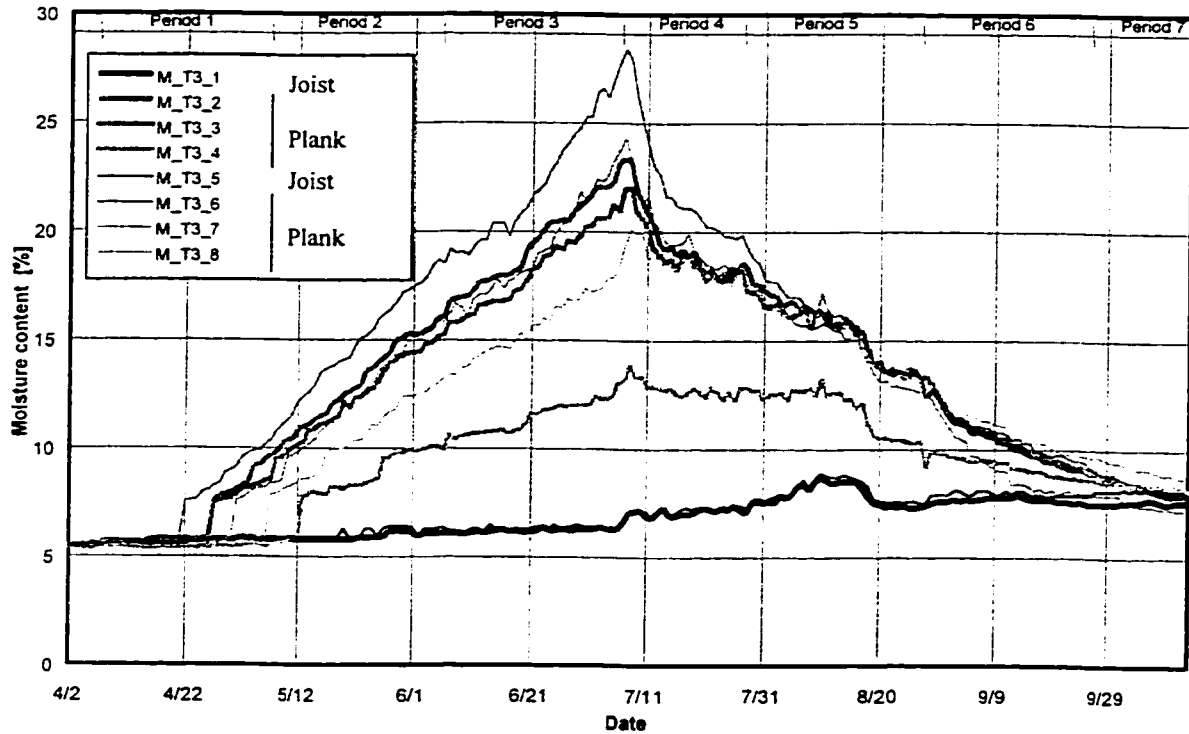


Figure 2.24. Moisture content in T3 during length of test.

Wetting of joists started at period 4, *i.e.* at the start of the drying season. The explanation for this moisture accumulation pattern is that during the wetting periods, the moisture condenses under the face of the planks in which it accumulates. During the drying periods, higher temperature gets the moisture out of the planks. As this moisture cannot move out through the roofing membrane, it is redistributed in the whole assembly as the rise in moisture content in the bottom of the joist shows.

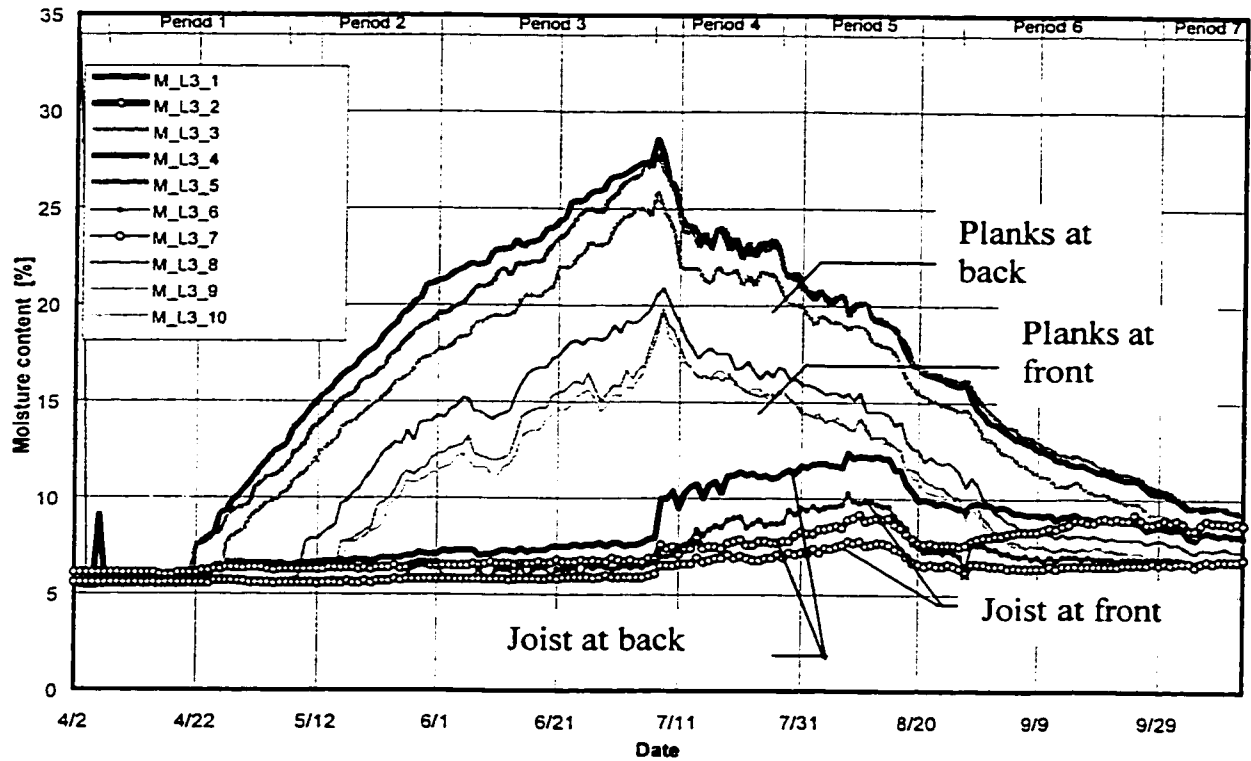


Figure 2.25. Moisture content in L3 during length of test.

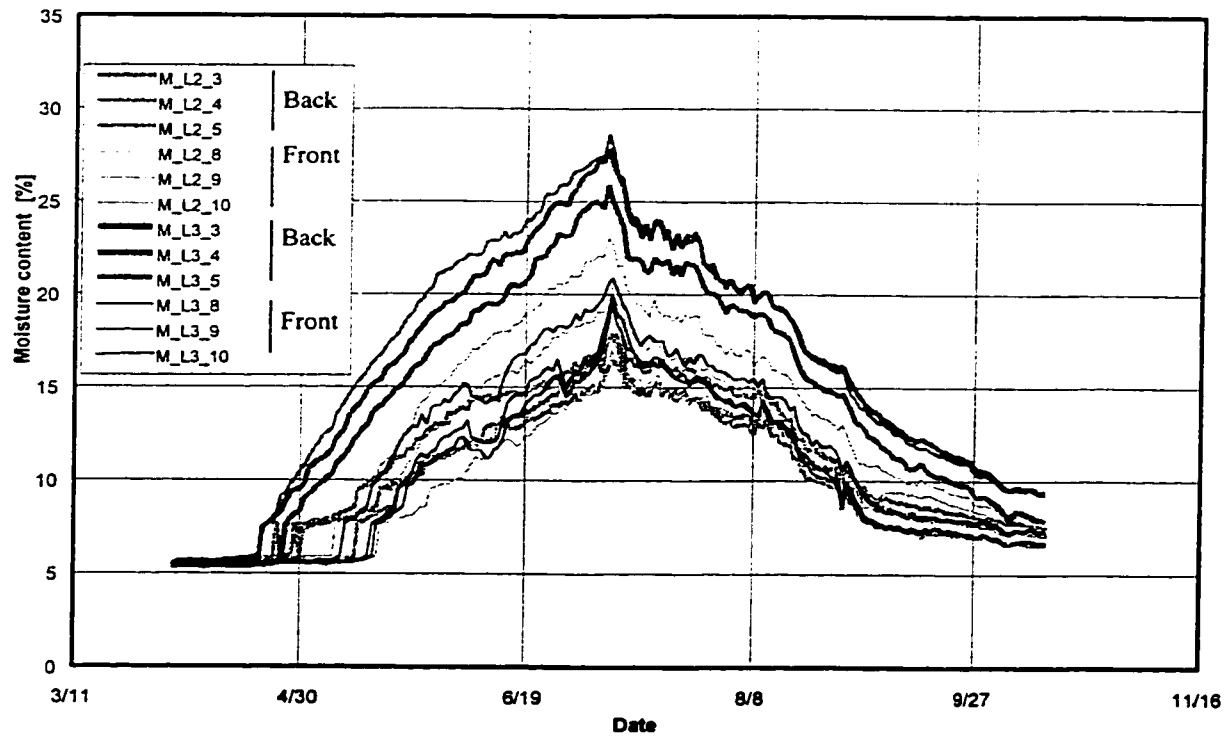


Figure 2.26. Moisture content in L3 vs L2.

Figure 2.26 shows the difference in moisture content in L3 vs L2. The difference is important for the moisture content level close to the exfiltration source.

A visual inspection of the cavities was performed at the end of the experiment. Except for T1 and L1, no visible fungi growth was found once the insulation was removed. However during dismantling, fungi were found in between wood members. In L5 and T5, staining fungi were present on wood surfaces that were facing other wood surfaces during the test. Surfaces in contact with the cellulose seemed to have been protected by the borax and the boric acid added to cellulose as ignifuge and pesticide.

To summarize levels of exposure to moisture, the following diagrams of Figures 2.27 and 2.28 present duration of exposure to moisture content and temperature for each cavity. Conditions leading to fungi growth are in gray, i.e. for temperature above 20°C and for moisture content above 20%.

Cavities with exfiltration, i.e. T3, T5, L3, L4 and L5, are exposed to conditions that can lead to biological degradation. Among these, T5 and L5 exhibit a very important exposure which explains the findings of fungi in between the wood members of these cavities.

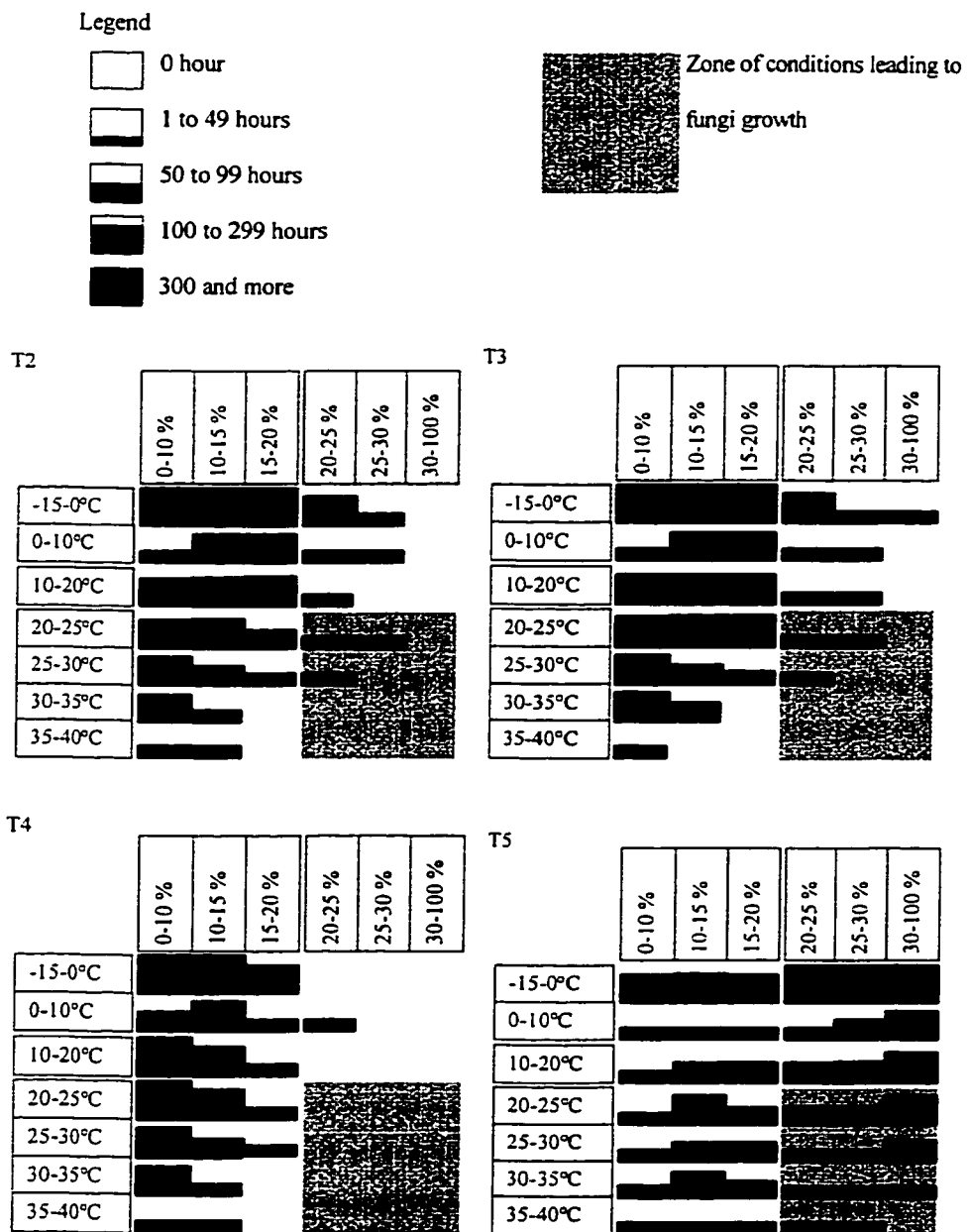


Figure 2.27. Levels of exposure to moisture content and temperature in thermos roof.

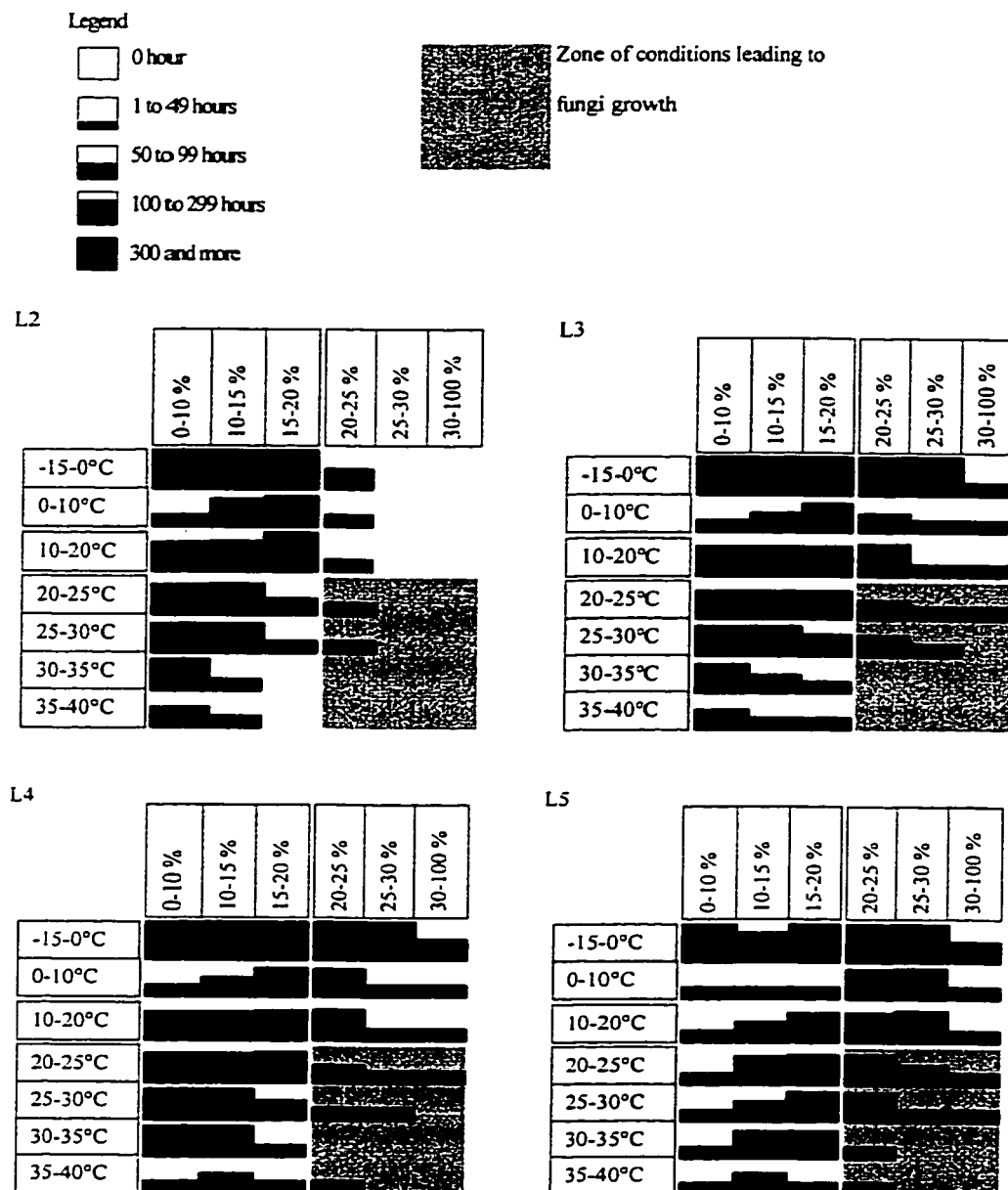


Figure 2.28. Levels of exposure to moisture content and temperature in lambourdes roof.

2.4.2 Cellulose insulation moisture content

It has been found that the low air permeability of cellulose improves the airtightness of houses (Wilkes and Child 1992). It was then hoped that cellulose could prevent air

convection. The wetting and drying patterns of the insulation in the different assemblies of the following figures clearly illustrate moisture accumulation which was due to air movement, either humid air moving through the insulation or through the air space after settling of the insulation. During the six months and half test, the moisture content was monitored in the cellulose using gravimetry.

- Wetting and drying patterns of insulation

The following graphics compare moisture content wetting and drying patterns of the cellulose insulation throughout the execution of the test. Each cavity had eight gravimetric samples. The nametags “bot and “top” refers to the samples below the wood deck and “left” and “right” to the samples above the plaster. The nametag “Ba” indicates that the samples were at the back of the huts, close to the infiltration location, and “Fr” that the samples were at the front of the huts, close to the exfiltration location along the length of the cavity. The same nametags were used for cavities 5 even though the air exfiltration path was not longitudinal.

It is of interest to compare the behavior of the two huts to see the impact of the amount of cellulose on accumulating moisture. In the cavities subjected to diffusion only, as seen in Figure 2.29, there is no significant pattern difference, except for slightly higher moisture content maxima in the shallow roof. At low moisture exposure, the two roofs have almost the same behavior. For the long exfiltration path cavities, Figure 2.30, the cavity with less insulation demonstrates jumps in the moisture content at the end of the second and third period. These two period transition were accompanied with warmer

temperature, indicating a possible thaw of accumulated frost. This did not occur in the thicker roof. The cavities exposed to short exfiltration paths, see Figure 2.31, experienced important moisture accumulation in the cellulose, with very high moisture content at the bottom of the cavity, where the exfiltration path above the top sill was about 10 cm long. There is little overall difference between the two huts, indicating that, in both cases, the moisture accumulation occurs within a small fraction of the total volume of the cellulose.

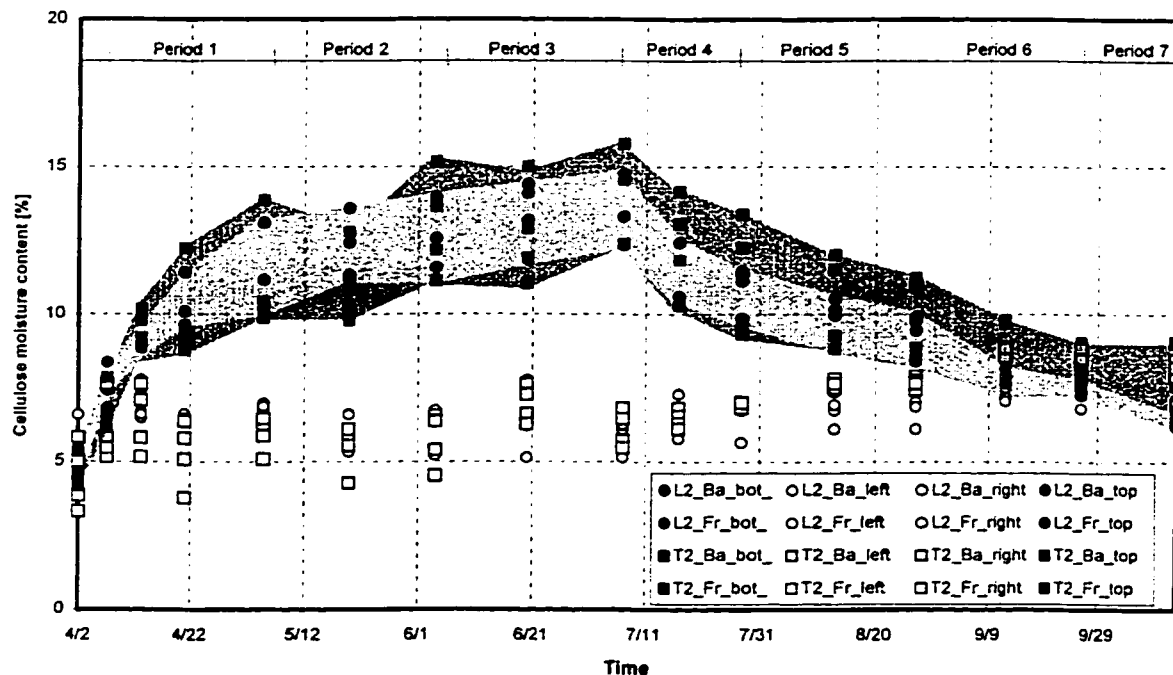


Figure 2.29. Moisture content distribution in cellulose insulation during test in the diffusion only cavities. Darker zone groups the cellulose samples that were under the deck in the 200 mm high roof (T2). Lighter zone groups the samples in the 350 mm high roof (L2). The samples that were at the bottom of the assemblies are left blank.

Figure 2.30 shows a very slender drying profile for the whole assembly. This indicates that everything is exposed to the same conditions which yield the same equilibrium moisture content. There is no such uniformity during the wetting. This confirms that during drying, the moisture source is local, therefore easier to predict. In wetting, moisture comes from further away and is brought in. It is less likely that moisture gets to the cellulose at the same uniform rate throughout the assembly.

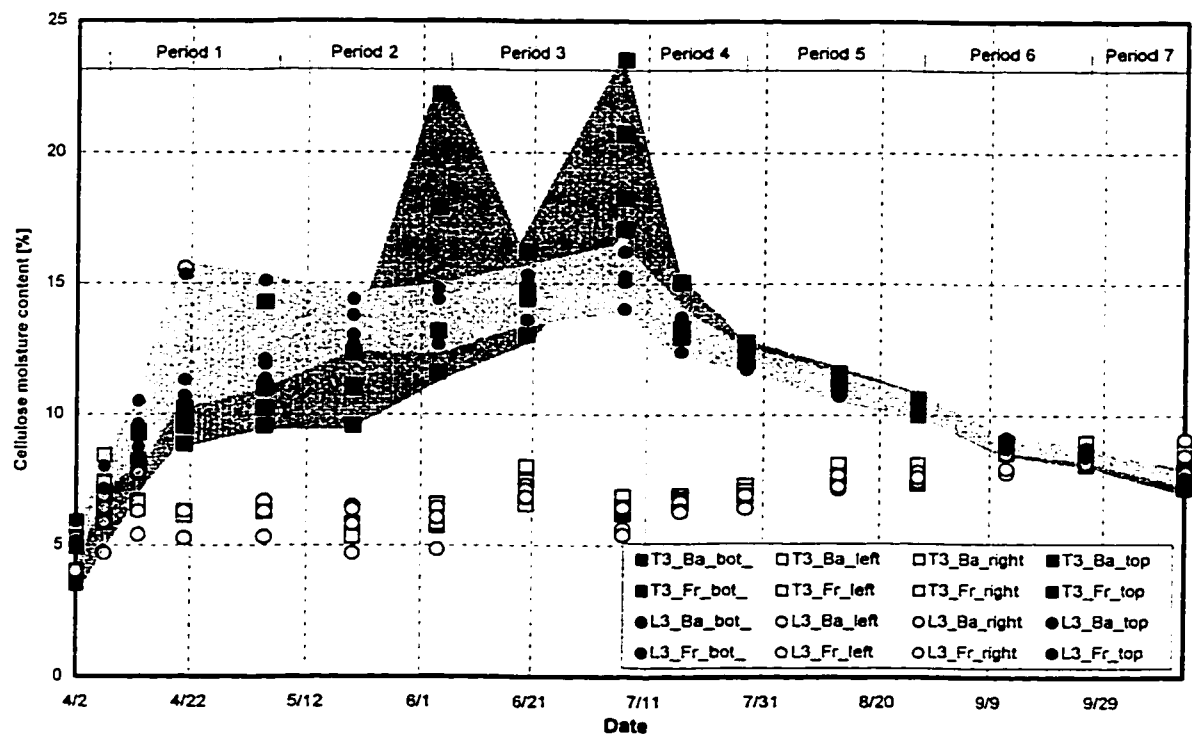


Figure 2.30. Moisture content distribution in cellulose insulation during test in the long exfiltration path cavities. Darker zone groups cellulose under deck in 200 mm high roof (T3). Lighter zone groups samples of the 350 mm high roof (L3).

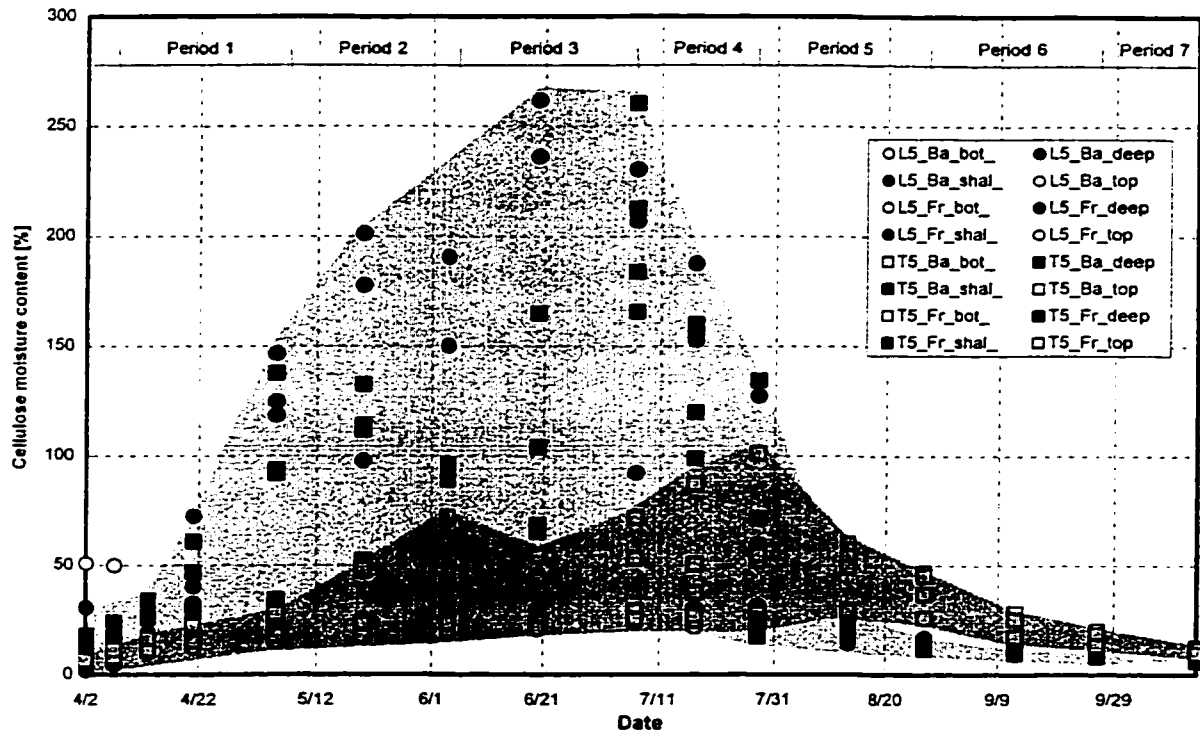


Figure 2.31. Moisture content distribution in cellulose insulation during test in short exfiltration path cavities. Darker zone groups cellulose samples under the deck, corresponding to air path of about 25 cm. Lighter zone groups cellulose samples at the bottom of the assembly, corresponding to air path through the insulation of about 10 cm.

The impact of varying parameters for the same assembly can be seen in the following two cases. Figure 2.32 compares the moisture content of the cavities where the main mode of transfer was diffusion, with and without polyethylene. The addition of polyethylene reduces slightly the moisture accumulation but does not affect the rate of drying. Figure 2.33 lets compare two long path cavities, where one had an opening in the roof deck to simulate a goose neck. The total moisture content was raised by 5%, which means a significant impact of the increased flow due to the opening.

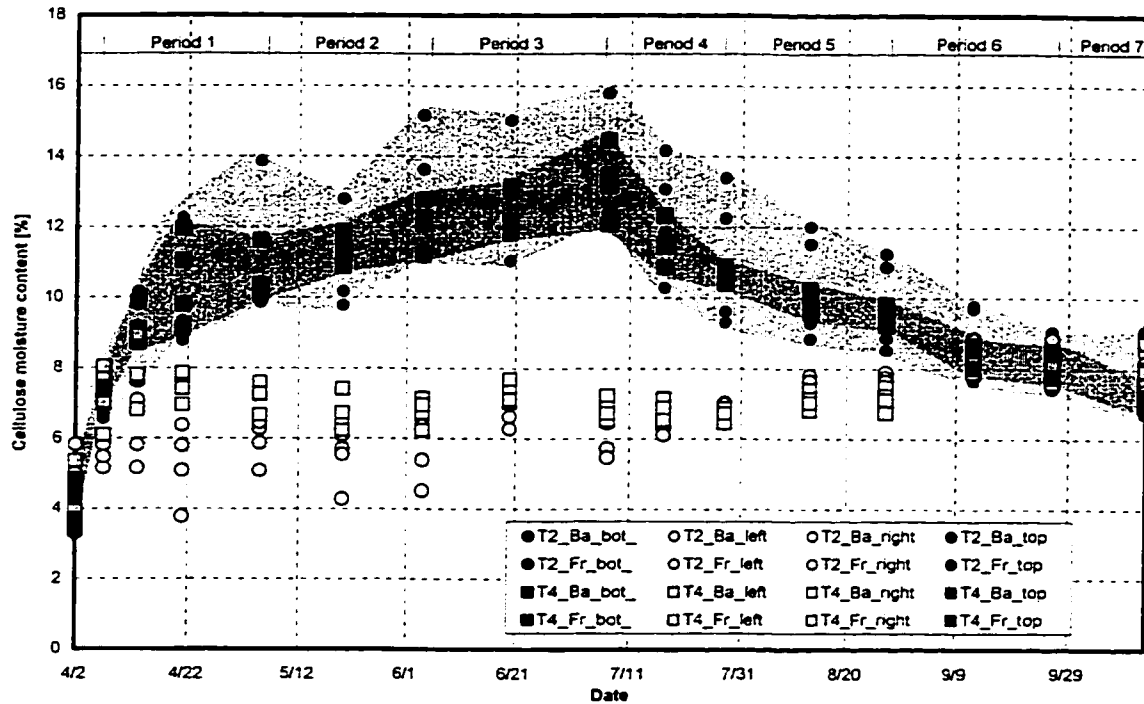


Figure 2.32. Comparison of the moisture content distribution in cellulose insulation in the two diffusion driven cavities. Samples in polyethylene T4 grouped in darker zone and samples in the plastered and painted only diffusion cavity (T2) grouped in light zone.

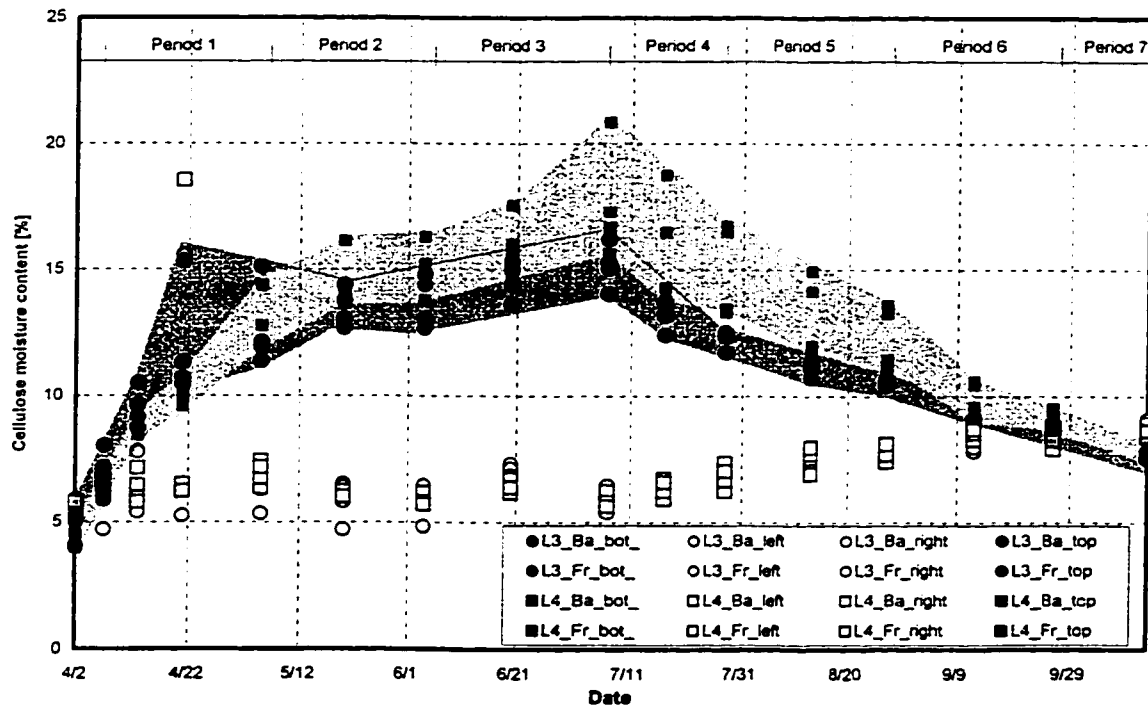


Figure 2.33. Comparison of the moisture content distribution in the long exfiltration path cavities: L4 with a gooseneck opening (in light zone) and L3 (in darker zone).

In cases of diffusion only and long exfiltration path, the cellulose at the bottom of all the cavities remained at a moisture content level close to its initial value, until the onset of the drying season where moisture released from the upper part of the assembly was forced down to dry towards the interior as the deck was covered with a vapor tight roofing membrane. This vapor on its way out was adsorbed by the cellulose at the bottom of the cavities, raising slightly its moisture content. At the end of the test, the moisture content was apparently uniform from top to bottom of the assemblies, for an average moisture content of 8%. This final moisture content indicates the capacity of cellulose insulation to dry within the summer time.

The procedure developed permitted the assessment of the moisture accumulation patterns in the cellulose insulation in flat unvented roof assemblies subjected to one complete wetting/drying cycle with precisely environmental known conditions. The moisture patterns obtained demonstrate the complexity of moisture transfer as being dependent on the thickness of the moisture storing insulation and on the different construction details.

- Impact of wetting-drying cycle on the texture of the insulation

To inspect the cellulose insulation, the planks of roof deck were carefully removed to uncover the upper surface of the insulation. This process did not disturb the insulation except in cases where insulation had adhered to the underside of some planks of the L roofs. The texture of the cellulose insulation was not uniform over the whole surface. The insulation in T2, T4 and L2 did not manifest important change of texture. The other cavities exhibited different levels of texture changes. This change of texture is due to the

binding of some cellulose molecules during the drying of the moist cellulose insulation and has been named “caking” by Rose and McCaa (1998). Light level of caking was present in cavities T3, L3 and L4 with a more pronounced hardening above the exfiltration inlets, *i.e.* the partition, the light fixture and the exterior wall. Some cellulose had adhered to the planks of L3 and L4 above the partition in both cases, above the light fixture in L3 and between the gooseneck and exterior wall in L4. The most important changes of texture occurred in T5 and L5, where the insulation along the joist had almost the appearance of papier-mâché. Cloisters of cellulose of 50 to 75 mm thick had adhered to the planks of L5 above the partition. The remainder of the surfaces of L5 and T5 exhibited caking.

The removal of the cellulose from cavity T5 and L5 revealed the presence of caking at bottom of the cavity whereas no caking was found at the bottom of the other cavities. This is explained by the fact that these cavities were exposed to outdoor conditions on their side. The change of texture in T5 led to the uniform clogging of the insulation. The thicker L5 had some loose insulation which allowed to reveal caking of insulation formed into a geometry of interest. The caking above the partition clearly demonstrated the path of the exfiltrating air with a pyramidal cone starting at the partition and increasing in cross area towards the front exterior wall. Also of interest was the quarter sphere of caked insulation just downstream of the light fixture opening, illustrating once again the air exfiltration path.

2.5 Conclusion

The test exposed two types of single cavity roofs, completely insulated with cellulose insulation, to a full winter/summer heating/cooling cycle. A testing method was developed using the capabilities of an environmental chamber. The simulated conditions compared favorably with the conditions required by the procedure. 98% of the expected data was actually monitored and recorded, which reflects the effectiveness of the acquisition of data. The long duration of the test was required to adequately account for the slow process of moisture accumulation. A total of 380 points both on the cold and warm sides of the assembly were monitored, in a quasi continuous mode with electronic instrumentation and in a periodic mode for the gravimetry measurements. The data allowed for a close monitoring of the conditions of the wood structure and the cellulose insulation. The data collected documented the moisture transfer process through two types of single cavity roof with different variables. The new methodology could be used as a base to develop of a standard test method. The assemblies tested show no sign of accumulated moisture from one season to the next after one cycle. Some wood members had high level of exposure to moisture and temperature conditions that could induce fungi growth. The cellulose insulation exhibited changes of texture that indicate important moisture accumulation. Very little mould was found in the insulated cavities, which is explained by the presence of borax, a fungicide, in the cellulose. The cavities with the long air exfiltration paths had an acceptable performance with controlled moisture accumulation and complete drying. The two cavities with short air exfiltration paths did not exhibit an acceptable behavior.

The next chapter presents the development of a physical model to represent moisture transfer in wood. The experimental data are used for the validation of the model.

Chapter 3

Model development and validation

This chapter presents the development of a model based on building physics, referred to herein as physical model, that describes the movement of moisture in the roof wood planks and the adaptation of a computer model to simulate their hygrothermal behavior. First, the physical parameters and scenarios of moisture transfer to be modeled are defined. The physical model describes the physical phenomena through the use of physical laws expressed in mathematical equations. The model requires the development and the determination of the convective heat and mass transfer coefficients, the sorption curves and the water effective conductivity in regards to the conditions and the wood species. Once integrated in a computer model, this approach is then validated for the simulation of the drying process. Finally, the model is applied for the simulation of the wetting process.

3.1 Physical phenomena and processes in the flat roof planks

In order to examine further the moisture movement within the roof assembly tested, the moisture transfer process is represented into a physical model. The resulting model can be used to predict the movement of the moisture content in the wood plank of the roof assembly under different conditions.

3.1.1 Physical parameters

The situation to be analyzed is illustrated in Figure 3.1 and is based on the experimental setup presented in the previous chapter. Some of the parameters are kept constant and some vary as seen in Table 3.1.

Table 3.1. Constant and variable parameters.

Constant parameters	Variable parameters	Resulting changes
Geometry	Indoor temperature	Moisture content of wood
Materials	Indoor relative humidity	
Air leakage path	Outdoor temperature	
	Outdoor relative humidity	
	Pressure differential, and resulting velocity below the plank	
	Drying conditions below planks	
	Initial moisture content of wood	

For analysis purposes, the configuration is simplified. As the wood planks of the roof assembly are covered by the roof membrane, it is assumed that no moisture movement occurs through that membrane. It is also assumed that each plank is entirely at the same initial temperature and moisture content, which are the temperature and the moisture content measured at the core of the plank. Using the temperature measured in the planks takes indirectly into account the heat loss and heat gain of the assembly to the outside. It is assumed that a narrow air space allows air movement between the wood and the insulation. As explained in more details further below, the temperature and relative humidity of the air below the plank are extrapolated from the measurements taken in the cellulose insulation below the planking with a thermocouple and a relative humidity

sensor. The velocity of the air is estimated from the total pressure differential and the geometry of the air tunnel.

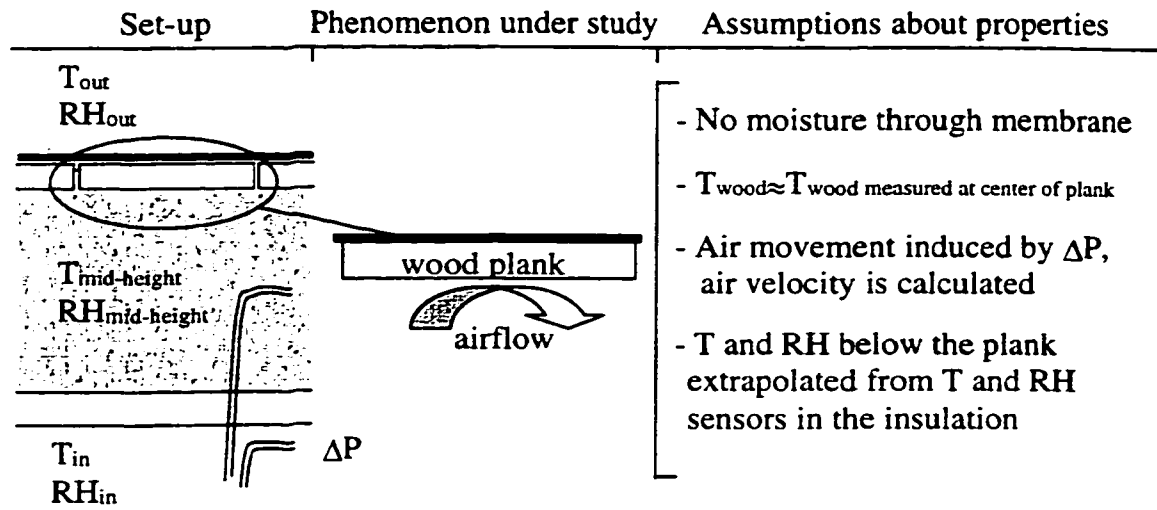


Figure 3.1. Schematic of parameters.

The change of moisture content (M) in the wood is a function of the characteristics of air and wood as expressed in the following relationship:

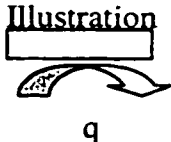
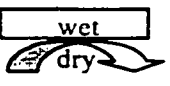
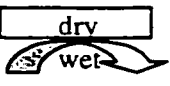



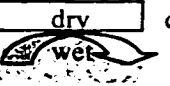


$$M_{final} = M_{initial} + \text{moisture in/out } f(\text{air velocity, T and RH of air, M and T of wood, length of exposure and wood species}) \quad (3.1)$$

The wood-air interface below the plank is the plane through which all moisture must flow. At this boundary, the air layer offers some resistance to the heat and mass flow. This resistance is expressed by the heat and mass transfer coefficients, which are derived using available correlations based on experimental data or can be measured. The conductivity of moisture in the wood is inferred from existing material properties of similar species. In this study, the moisture movement through the wood planking is predicted at a location where moisture content and temperature data have been measured.

Eight scenarios are developed to represent the different moisture transfer modes across the interface, as shown in Table 3.2. The computer model is used to investigate scenarios

1 to 3. These three scenarios require the conditions at the wood-air interface. Scenarios 5 to 8 where the wood is in contact with cellulose insulation are not considered in this study due to the complexity of the wood/cellulose interface and the lack of data on cellulose properties. Scenario 4, not investigated in this study, is where wood is in contact with a film of condensation and could be part of a simulation of the wetting of wood.

Table 3.2. Various moisture movement scenarios.

Scenario	Illustration	Resulting moisture movement
	 <p>wood plank airflow moisture flux q</p>	
1. Wet wood in contact with dry air Desorption	 <p>$q \downarrow$</p>	Difference in water potential induces flux (q) outward
2. Dry wood in contact with humid air Adsorption	 <p>$q \uparrow$</p>	Difference in water potential induces flux inward
3. Equilibrium between wood and air	 <p>$q = 0$</p>	Equilibrium in water potential. No flux
4. Presence of a film of water at surface of wood Imbibition	 <p>$q \uparrow$</p>	Difference in water potential induces flux inward
5. Wet wood in contact with drier cellulose Desorption	 <p>$q \downarrow$</p>	Difference in water potential induces flux outward
6. Dry wood in contact with very humid cellulose Adsorption	 <p>$q \uparrow$</p>	Difference in water potential induces flux inward
7. Equilibrium between wood and cellulose	 <p>$q = 0$</p>	Equilibrium in water potential. No flux
8. Presence of a film of water at surface of wood Imbibition	 <p>$q \uparrow$</p>	Difference in water potential induces flux inward

3.1.2 Choice of the moisture movement modeling approach

The modeling of the scenarios 1 to 3 described in Table 3.2 requires the calculation of the moisture content resulting from the moisture movement within and at the surfaces of the wood planking. This moisture may be in the forms of vapor, bound water, or liquid water. The water potential approach described in section 1.3.2.6 integrates these three phases of water by relating the state of the free energy of water under any phase compared to the free energy of water in a reference state. Water potential gradients therefore induce moisture movement in the same manner an electrical potential induces a current or a temperature differential results in heat flux. This approach (Cloutier *et al.* 1992, Tremblay *et al.* 1999a, 1999b) is used in this study and is summarized below.

In the transient state, a change in moisture storage results from a moisture flux and is expressed by the mass conservation relationship presented previously in equation (1.10):

$$\frac{\partial C}{\partial t} + \bar{\nabla} \cdot \bar{q}_m = 0 \quad (3.2)$$

where C is the moisture concentration [$\text{kg}_{\text{water}}/\text{m}^3_{\text{moist wood}}$] in the moist wood and

q_m is the total moisture flux (liquid water + water vapor + bound water)

[$\text{kg}_{\text{water}}/\text{m}^2_{\text{moist wood}} \cdot \text{s}$].

The symbol ∇ , denotes the divergence of the mass flux in the three dimensions. For practical reason, C may be substituted by its moisture content equivalent which is:

$$C = G_m \rho_w \frac{M}{100} \quad (3.3)$$

where G_m is the specific gravity of wood [$\text{kg}_{\text{oven-dry wood}} \cdot \text{m}^3_{\text{water}} / \text{kg}_{\text{water}} \cdot \text{m}^3_{\text{moist wood}}$],

ρ_w is the density of water [$\text{kg}_{\text{water}}/\text{m}^3_{\text{water}}$] and

M is the moisture content of wood [$(\text{kg}_{\text{water}}/\text{kg}_{\text{dry wood}}) \times 100$].

Substituting 3.3 into 3.2, the following is obtained:

$$\frac{\partial(G_m \rho_w M/100)}{\partial t} + \bar{\nabla} \cdot \bar{q}_m = 0 \quad (3.4)$$

which, assuming a constant wood volume, can be simplified to:

$$\frac{\partial M}{\partial t} + \frac{100}{G_m \rho_w} \bar{\nabla} \cdot \bar{q}_m = 0 \quad (3.5)$$

From soil science and the work of Darcy (1856), a proportional relationship was found between moisture flux and the driving potential, *i.e.* the gradient of the free energy state of water. A differential in the water potential will cause moisture movement from the point of highest energy to the point of lowest energy, as shown in equation (1.11) and reproduced here:

$$\bar{q}_m = - \underline{K}(M, T) \cdot \bar{\nabla} \psi \quad (3.6)$$

where $\underline{K}(M, T)$ is the effective water conductivity tensor [$\text{kg}^2_{\text{water}} / \text{m}_{\text{moist wood}} \cdot \text{s} \cdot \text{J}$], and

$\bar{\nabla} \psi$ is the gradient of water potential in the three dimensions.

The Soret effect is not considered in equation (3.6). The temperature gradient effect on moisture flow is partly taken into account by considering the temperature dependency of \underline{K} and ψ . When equation (3.6) is substituted into equation (3.5), the change in moisture content is linked to the change of the gradient of water potential. A one-directional relation is shown below:

$$\frac{\partial M}{\partial t} - \frac{100}{G_m \rho_w} \left[\frac{\partial}{\partial x} \left(K_x(M, T) \frac{\partial \psi}{\partial x} \right) \right] = 0 \quad (3.7)$$

In terms of transient heat transfer within wood, heat flux results in a change of the enthalpy of the system. The heat flux occurs due to two main phenomena: conduction induced by a thermal gradient and phase changes of water causing absorption or release of energy. Heat flux due to moisture movement is considered negligible. The energy equation that represents these phenomena proposed by Cloutier (1995) and Tremblay *et al.* (1999c) is:

$$\frac{\partial H}{\partial t} = -\bar{\nabla} \cdot \bar{q}_h + \varepsilon(\beta \Delta h_{\text{sorp}} + \Delta h_{\text{vap}}) \frac{\partial C}{\partial t} \quad (3.8)$$

where H is the total enthalpy of the system wood-water-atmosphere [$\text{J}/\text{m}^3_{\text{moist wood}}$],

\bar{q}_h is the conductive heat flux vector [$\text{W}/\text{m}^2_{\text{moist wood}}$],

ε is the ratio of vapor diffusion to total moisture movement varying from 0 when all moisture is liquid to 1 when it is all gas,

Δh_{sorp} is the differential heat of sorption [$\text{J}/\text{kg}_{\text{water}}$] and is function of M ,

Δh_{vap} is the latent heat of vaporization [$\text{J}/\text{kg}_{\text{water}}$], and

$\varepsilon(\beta \Delta h_{\text{sorp}} + \Delta h_{\text{vap}}) \frac{\partial C}{\partial t}$ represents the heat transfer due to phase change where $\beta=0$

for $M > \text{FSP}$ or $\beta=1$ for $M \leq \text{FSP}$.

By substituting equation (3.3) in equation (3.8), the result is:

$$\frac{\partial H}{\partial t} + \bar{\nabla} \cdot \bar{q}_h = \varepsilon(\beta \Delta h_{\text{sorp}} + \Delta h_{\text{vap}}) \frac{G_m \rho_w}{100} \frac{\partial M}{\partial t} \quad (3.9)$$

Heat flux, as per Fourier's law, is proportional to the gradient of temperature:

$$\bar{q}_h = -\underline{k}(M, T) \cdot \bar{\nabla} T \quad (3.10)$$

where $\underline{k}(M, T)$ is the thermal conductivity tensor for moist wood [$\text{W}/\text{m}_{\text{moist wood}} \cdot ^\circ\text{C}$], and

$\bar{\nabla} T$ is the temperature gradient [$^\circ\text{C}$].

Substituting equation (3.10) in equation (3.9) yields the following equation that links the change of enthalpy to the temperature gradient and the moisture content change rate, shown here in one dimension:

$$\frac{\partial H}{\partial t} - \frac{\partial}{\partial x} \left(k_x(M, T) \frac{\partial T}{\partial x} \right) = \varepsilon (\beta \Delta h_{\text{sorp}} + \Delta h_{\text{vap}}) \frac{G_m \rho_w}{100} \frac{\partial M}{\partial t} \quad (3.11)$$

The boundary conditions describe the heat and moisture flux normal to the wood surface due to convection. The heat flux at the surface has two components: the heat flux due to the temperature gradient and the heat involved in the phase changes of water. The following equations express the conditions at the wood-air interface:

$$q_h = h_h (T_{\text{surf}} - T_{\infty}) + (1 - \varepsilon) (\Delta h_{\text{vap}} + \beta \Delta h_{\text{sorp}}) q_m \quad (3.12)$$

where h_h is the convective heat transfer coefficient [$\text{W}/\text{m}^2 \cdot ^\circ\text{C}$],

T_{surf} is the temperature at the surface of wood [$^\circ\text{C}$], and

T_{∞} is the temperature of the ambient air [$^\circ\text{C}$].

$$q_m = h_{\psi} (\psi_{\text{surf}} - \psi_{\infty}) \quad (3.13)$$

where h_{ψ} is the convective mass transfer coefficient [$\text{kg}^2_{\text{water}}/\text{J} \cdot \text{m}^2 \cdot \text{s}$],

ψ_{surf} is the water potential at the surface of wood [J/kg], and

ψ_{∞} is the water potential of the ambient air [J/kg].

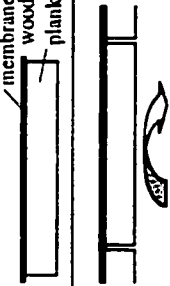







This model has been developed to represent industrial wood drying in kiln, and uses as initial condition green wood.

3.1.3 Description of the proposed mathematical model and integration of this model into a computer model

A mathematical model has been developed herein which describes the movement of moisture in the wood planks of flat roofs. Represented in Table 3.3, the model consists of the following components:

1. The process of drying and wetting of wood planks. Moisture movement within the wood is represented with the two equations, (3.7) and (3.11). The wood properties used by the physical model must correspond to the wood species and wood conditions during drying and wetting. The following relationships were therefore required:
 - Full adsorption and desorption curves, which are the $M_{\text{Equilibrium}}$ vs. RH relationships, were developed for the species used, spruce. The hysteresis required the development of intermediary curves.
 - The effective water conductivity was recalculated for spruce, as a function of moisture content and temperature, especially for low moisture content.
2. The heat and moisture exchanges at the surface of the wood plank were modeled with boundary conditions, as listed below:
 - The convective heat and mass transfer coefficients, h_h and h_ψ , were calculated and experimentally determined for the conditions found in the roofs. These coefficients are used in equations (3.12) and (3.13).
 - Other boundary conditions were defined: mean temperature and relative humidity of air, velocity of air flow, direction of air flow vs. grain of wood, dimensions of air tunnel, presence of membrane on planking, possibility of water film on lower face of planks and determination of the ratio ε during wetting of wood.

Table 3.3. Schematic representation of the mathematical model.

Physical phenomena	Mathematical model Equations	Material properties	Other parameters $f(\cdot)$ is used to indicate dependency
WETTING PROCESS			
	Initial moisture content and temperature are uniform		$M_{\text{initial}}, T_{\text{initial}}, \text{species and size of wood piece}$
	No moisture across membrane Still air between planks Air movement below plank		Velocity of air, $RH_{\text{air}}, T_{\text{air}}$
	Some moisture transfer from air to wood surface which results in a wetter surface and a change of surface temperature	$q_{\text{li}} = h_{\text{li}}(T_{\text{surf}} - T_{\infty}) + (1 - \epsilon)(\Delta h_{\text{vap}} + \beta \Delta h_{\text{sorp}})q_{\text{m}}$ $q_{\text{m}} = h_{\psi}(\psi_{\text{surf}} - \psi_{\infty})$	Heat transfer coefficient Mass transfer coeff. Condensation film
	This causes a water potential gradient across plank and moves moisture inward. Temperature gradient and phase change induce change of enthalpy of system	$\frac{\partial M}{\partial t} - \frac{100}{G_m \rho_w} \left[\frac{\partial}{\partial x} \left(K_s(M, T) \frac{\partial \psi}{\partial x} \right) \right] = 0$ $\frac{\partial h}{\partial t} - \frac{\partial}{\partial x} \left(k_s(M, T) \frac{\partial T}{\partial x} \right) = \epsilon \left(\beta \Delta h_{\text{vap}} + \Delta h_w \right) \frac{G_m \rho_w}{100} \frac{\partial M}{\partial x}$	Enthalpy of sorption $f(M)$ Enthalpy of vaporization
DRYING PROCESS			
	Initial moisture content and temperature are uniform		$MC_{\text{initial}}, T_{\text{initial}}, \text{size of wood piece}$
	No moisture across membrane Still air between planks Air movement below plank		Velocity of air, RH, T
	Some moisture transfer from wood surface to air which results in a dryer surface and a change of surface temperature	$q_{\text{li}} = h_{\text{li}}(T_{\text{surf}} - T_{\infty}) + (1 - \epsilon)(\Delta h_{\text{vap}} + \beta \Delta h_{\text{sorp}})q_{\text{m}}$ $q_{\text{m}} = h_{\psi}(\psi_{\text{surf}} - \psi_{\infty})$	Heat transfer coefficient Mass transfer coeff.
	This causes a water potential gradient across plank and moves moisture outward. Temperature gradient and phase change induce change of enthalpy of system	$\frac{\partial M}{\partial t} - \frac{100}{G_m \rho_w} \left[\frac{\partial}{\partial x} \left(K_s(M, T) \frac{\partial \psi}{\partial x} \right) \right] = 0$ $\frac{\partial h}{\partial t} - \frac{\partial}{\partial x} \left(k_s(M, T) \frac{\partial T}{\partial x} \right) = \epsilon \left(\beta \Delta h_{\text{vap}} + \Delta h_w \right) \frac{G_m \rho_w}{100} \frac{\partial M}{\partial x}$	Enthalpy of sorption $f(M)$ Enthalpy of vaporization

NOTE TO USERS

Page(s) not included in the original manuscript are unavailable from the author or university. The manuscript was microfilmed as received.

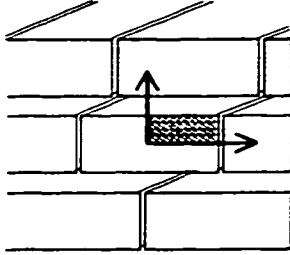
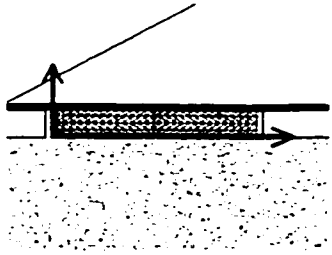
110

This reproduction is the best copy available.

UMI

To implement the mathematical model, several modifications were made to an existing finite element computer model, which had been developed to simulate wood drying in industrial kiln purposes (Cloutier *et al.* 1992, Tremblay *et al.* 1999b). Table 3.4 highlights the main advances made to the mathematical and computer models.

Table 3.4. Developments and modifications of the mathematical and computer models.

			
	Starting point	Developments of the mathematical model	Modifications to the computer model
Geometry	One quarter of a nominal lumber Air space all around	<i>Planking covered with roofing membrane</i> <i>Air space below</i>	<i>Development of the mesh and data file</i>
Wood species	Aspen or red pine	<i>Spruce</i>	
Air convection	Air speed Air temperature and relative humidity – steady state	<i>Air speed to be calculated/estimated</i> <i>Cycling air temperature and relative humidity evaluated as daily average</i>	<i>T and RH used in input file</i>
Wood parameters	Initial temperature and moisture content	Initial temperature and moisture content	<i>Used in input file</i>
Wood property	Moisture content-water potential relationship Effective water conductivity radial and tangential	Moisture content-water potential relationship and effective water conductivity radial, <i>developed for spruce</i>	<i>Development of datafiles</i>
Boundary conditions	Mass transfer coefficient Heat transfer coefficient	<i>Mass transfer coefficient and heat transfer coefficient, calculated from nondimensional analysis and measured</i>	<i>Integration of the coefficients to the code</i>

The modifications to the computer model included:

1. The mesh of the finite elements had to be defined for a plank of dimensions 19 mm by 140 mm, where one surface had no mass.
2. Incorporation of the proper coefficients within the code.
3. Development of the proper data files for the $M-\psi$ and $\bar{K}-\psi$ relationships. Moisture content was converted into saturation percentage.

3.2 Determination of the parameters of the physical model

Three parameters for the mass conservation equation and the boundary conditions of the model are determined. The parameters include the water conductivity of wood and the convective heat and mass transfer coefficients at the wood-air interface. They have to be determined for the ambient conditions in contact with wood and for the appropriate mode of sorption. The relevant sorption curves are determined using existing data. The convective transfer coefficients are determined with nondimensional analysis and experimental methods. The effective water conductivity is determined using existing data for similar wood species and moisture diffusion coefficients measured at low moisture content. As the available moisture diffusion coefficients are measured using different driving forces, the conversion of the coefficients requires the use of sorption curves.

3.2.1 Nondimensional determination of the convective heat transfer coefficient

Convective wood drying is a complex process involving heat and mass exchanges between air and wood. The net heat exchange at the surface of the drying wood is determined by the temperature differential and the mass transfer, as shown in equation (3.12). The heat and mass transfer convective coefficients used in a dozen of wood drying models were different (Tremblay *et al.* 1999b). In almost all cases, the coefficients were constant, independent of the surface moisture content. Recent measured values of convective heat and mass transfer coefficients for industrial drying conditions were constant above a surface at moisture content values of 60 to 80% but were proportional to the surface moisture content below these values (Tremblay *et al.* 1999b). As the moisture content in the roof planks in the experiment presented in chapter 2 is in large part below the fiber saturation point (FSP), it is important to determine the values of the convective coefficients in relation to the air velocity below the planks.

Nondimensional analysis has been used to provide general correlations for different convective heat transfer situations. The convective heat transfer coefficient can be calculated using the Nusselt number, Nu , by:

$$Nu_D = \frac{h_h D}{k} \quad (3.14)$$

where Nu is the Nusselt number [dimensionless],

h_h is the convective heat transfer coefficient [$W/m^2 \cdot ^\circ C$],

D is the characteristic length of the system [m], and

k is the thermal conductivity of air [W/m·°C].

The Nusselt number has been correlated for different sets of parameters with the aid of dimensionless groups such as Reynold's number, Re , Prandtl's number, Pr , and Grashof's number, Gr .

In the case where settling of the cellulose insulation occurs, the space below the deck allows air passage. The space is assumed to be a rectangular duct with three surfaces in wood and the remaining one in cellulose and is 360 mm wide by 2 to 5 mm high by 4 m long. The convective coefficients at the underside of the roof planks can be evaluated using nondimensional analysis. The air velocities based on the pressure differentials measured during the experiment vary from 0.2 m/s for a duct of 5 mm height to 0.02 m/s for a duct of 2 mm height using Hagen-Poiseuille equation. At such low velocities, Re is smaller than 2000 and the flow can be considered laminar.

Inside of a long circular duct with constant surface temperature, the relationship for the Nusselt number for forced convection and laminar flow can be evaluated as (Sieder and Tate 1936, in Kreith 1986):

$$\overline{Nu}_{D_H} = 1.86 \left(\frac{Re_D Pr D_H}{L} \right)^{0.33} \left(\frac{\mu_b}{\mu_{surf}} \right)^{0.14} \quad (3.15)$$

where D_H is the diameter,

L is the characteristic length,

μ_b is the viscosity of the air away from the wood surface, and

μ_{surf} is the viscosity of the air at wood surface temperature.

Table 3.5 presents values for the convective heat transfer coefficients calculated using this equation for air at 20°C. The first value is reasonable but the very low values of the

Nusselt number of the three other cases indicates that this equation might not be applicable. Indeed, this relationship is recommended for values of $(Re \cdot Pr \cdot D_H/L)^{0.33} (\mu_b/\mu_{surf})^{0.14}$ larger than 2 (Incropera et DeWitt 1996), condition that is not satisfied in all cases of table 3.5. For values of $(Re \cdot Pr \cdot D_H/L)^{0.33} (\mu_b/\mu_{surf})^{0.14}$ smaller than 2, the Nusselt number should tend towards 3.66, which yields a convective heat transfer coefficient of approximately $9 \text{ W/m}^2 \cdot ^\circ\text{C}$, a value too high for the present case as the calculated Nusselt numbers were closer to one.

Table 3.5 Calculation of the convective heat transfer coefficient based on forced convection ($T = 20^\circ\text{C}$, $k_f=0.026$).

Air velocity	Characteristic dimensions	Hydraulic diameter	Reynolds number	Prandtl number	Nusselt number	Heat transfer coefficient
v [m/s]	$b \times h \times L$ [m]	$D_H = 4A/P$ [m]	$Re = \rho_f v D_H / \mu_f$	$Pr = c_p \mu / k_f$	$Nu = 1.86 (Re \cdot Pr \cdot D_H/L)^{0.33} (\mu_b/\mu_{surf})^{0.14}$	$h_h = Nu \cdot k_f / D_H$ [W/m ² ·°C]
0.2	0.36x0.005x4	0.01	127	0.71	1.14	2.98
0.1	0.36x0.005x4	0.01	64	0.71	<1	undetermined
0.02	0.36x0.002x4	0.004	5	0.71	<1	undetermined
0.01	0.36x0.002x4	0.004	2.5	0.71	<1	undetermined

To evaluate the free convection case, the wood plank could be considered as a horizontal plane with heat loss at its underside. The following relationships apply then for the average Nusselt number (Incropera et DeWitt 1996):

$$\overline{Nu}_L = 0.54 (Ra_L)^{1/4} \quad (3.16)$$

when $10^4 \leq Ra_L \leq 10^7$, and

$$\overline{Nu}_L = 0.15 (Ra_L)^{1/3} \quad (3.17)$$

when $10^7 \leq Ra_L \leq 10^{11}$. The Rayleigh number (Ra_L) is the product of Gr_L by Pr . The characteristic length L to calculate Gr is A/P (Incropera and DeWitt 1996) where A is the plane surface area and P its perimeter, equivalent to approximately half of the width of

the surface, *i.e.* half the width of the wood deck. Table 3.6 presents the calculations using these relationships. The values of the convective heat transfer coefficient now lie between 2.15 and 4.62, *i.e.* of the same order of magnitude than the ones found with equation (3.15). Considering the modeling, a constant minimum h_h could be set, independent of the Reynold's and Prandtl's numbers, while equation (3.15) could be used when the condition, $(Re \cdot Pr \cdot D_H/L)^{0.33} (\mu_b/\mu_{surf})^{0.14} > 2$, is met.

Table 3.6. Calculation of the convective heat transfer coefficient based on free convection ($T_\infty = 20^\circ\text{C}$).

$(T_{surf} - T_\infty)$	Characteristic length	Grashof's number	Prandtl's number	Rayleigh's number	Nusselt's number	Heat transfer coefficient
$[\text{°C}]$	$L = A/P$ [m]	$Gr_L = \frac{\rho^2 g \beta (T_{surf} - T_\infty) L^3}{\mu_f^2}$	$Pr = c_p \mu / k_f$	$Ra_L = Gr_L Pr$	Nu	$h_h = Nu k_f / L$ [W/m ² .°C]
20	0.18	1.58×10^7	0.71	1.12×10^7	31.8	4.62
10	0.18	0.79×10^7	0.71	0.56×10^7	26.3	3.83
5	0.18	0.40×10^7	0.71	0.28×10^7	22.1	3.22
1	0.18	0.08×10^7	0.71	0.057×10^7	14.8	2.15

Combined free and forced convection must be considered when the ratio of the Grashof number to the square of the Reynold number is close to one (Incropera and de Witt 1996). For a duct of 5 mm of height, the Grashof number varies between 100 and 500×10^5 depending of the exfiltrating air temperature. For a duct of 2 mm high, Gr_L varies from 5 to 150×10^5 . The Reynold number calculated for the same temperature conditions varies between 2.5 and 150. Depending on the height of the duct and the temperature of the air, forced convection alone, free convection alone or a combined forced and free convection regime can be considered.

In the case where no cellulose insulation settlement occurs, *i.e.* case where all air flow is through the insulation layer, there is no nondimensional correlation for this situation.

Serkitjis (1998) measured the effects of forced convection on the heat transfer of porous insulation and found a Nu number very close to 1 for air flows of 0.2 to 3 m/s through cellulose insulation. This yields a heat transfer coefficient of about $2.9 \text{ W/m}^2\cdot^\circ\text{C}$, as shown in Table 3.7.

Table 3.7. Summary of nondimensional analysis on the convective heat transfer coefficient

	parameter	$h_h [\text{W/m}^2\cdot^\circ\text{C}]$
In air		
Forced convection	$v = 0.2 \text{ m/s}$	2.98
Natural convection	$\Delta T = 5 \text{ to } 10^\circ\text{C}$	3.22 – 3.83
In cellulose insulation	$Nu = 1.1$	2.9

3.2.2 Experimental determination of the convective heat transfer coefficient

Given that no nondimensional correlation corresponds closely to the low velocity conditions present in the roofs tested, the convective heat transfer coefficients were measured using an experimental setup with similar air movement and velocity as present in the roofs tested.

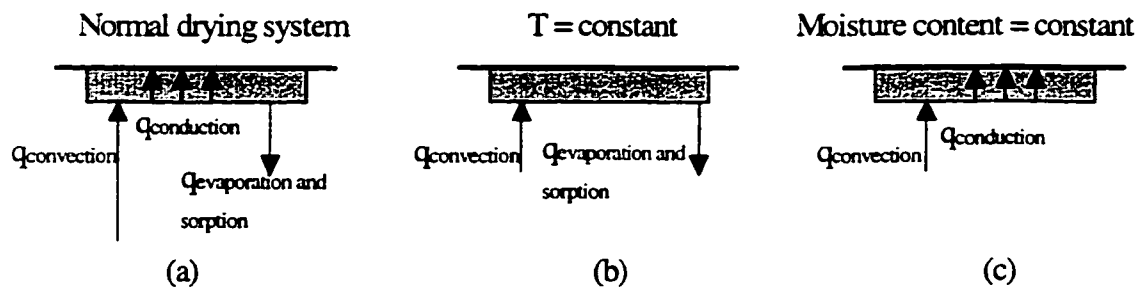


Figure 3.2. Schematic representation of heat flow through a wood surface.

The convective heat transfer coefficients at the wood-air interface may be a function of wood moisture content, air velocity and temperature and can be measured using two

methods: 1) under varying moisture content conditions at constant air temperature, case (b) of Figure 3.2 and; 2) under constant moisture content conditions (warming or cooling tests) at different air temperatures and humidities, case (c) of Figure 3.2. The first method is based on equation (3.12) (Tremblay *et al.* 1999a):

$$h_h = \frac{q_h}{(T_{surf} - T_{\infty})} - \frac{(1 - \epsilon)(\Delta h_{vap} + \beta \Delta h_{sorp})q_m}{(T_{surf} - T_{\infty})} \quad (3.18)$$

The heat flux q_h at the wood-air interface is calculated using enthalpy profiles established in the direction of the moisture flux for different drying times. The enthalpy profiles are calculated from the moisture content profiles determined with gravimetry of the sliced specimen and from the temperature profiles determined with thermocouples inserted at different depths. The mass flux, q_m , is obtained from equation (3.13) or by integrating the moisture profiles. In the second method, without any moisture flow, (*i.e.* $q_m = 0$), the following equation can be derived using equation (3.12):

$$h_h = \frac{q_h}{(T_{surf} - T_{\infty})} \quad (3.19)$$

The heat flux, q_h , is obtained by integrating the temperature profiles measured during warming of the wood specimen. When temperature profiles are systematically measured during warming or cooling of wood at different temperatures and equilibrium moisture contents, h_h can be determined as a function of T and M . This second method is much simpler and is used to determine the heat transfer coefficients above white pine specimens with a moisture content of 12 % and above red pine specimens in green condition, during the warming of cooled wood exposed to ambient room conditions. Two air velocities, 0.3 m/s and 0.15 m/s are considered. Temperature was not varied due to the relatively small range of temperature measured below the planks.

- Theoretical considerations

In this experiment, the warming of the wood occurred without mass change. All the heat that went through the surface of the specimen resulted in a change of its inside temperature. Therefore, the convective heat transfer at the surface is expressed by:

$$q_{h(x=0)} = -k \left(\frac{\Delta T}{\Delta x} \right)_{x=0} = h_h (T_\infty - T_{surf}) \quad (3.20)$$

where q_h is the heat flux at the wood surface [W/m^2]

k is the thermal conductivity of moist wood [$W/m \cdot ^\circ C$]

$\frac{\Delta T}{\Delta x}$ is the temperature gradient at $x=0$ [$^\circ C/m$], i.e. the slope of the temperature profile at the surface.

The heat flux in the wood, as shown in Frayret *et al.* (1995), is:

$$q_{cond} = \frac{\partial Q/A}{\partial t} = \frac{\partial (\rho_{moist\ wood} c_p \int_x T dx)}{\partial t} \quad (3.21)$$

where $\rho_{moist\ wood}$ is the density [$kg_{moist\ wood}/m^3_{moist\ wood}$], and

c_p is the specific heat of moist wood [$J/kg \cdot ^\circ K$].

Therefore, the integration of temperature profile at different times allows the determination of heat flux per conduction, q_{cond} , which in turn allows the determination of h_h .

$$h_h = \frac{q_{cond}}{(T_\infty - T_{surf})} \quad (3.22)$$

- Experimental setup for the determination of the convective coefficients

The experimental setup, used by the author at the department of Sciences du bois et de la forêt of Université Laval, is composed of a tunnel insulated on its four long faces in which three layers of eight wood pieces of 38 mm x 91 mm x 295 mm, inserted perpendicular to the air stream, are stacked with a space of 10 mm in between, as shown in Figure 3.3. Air is circulated through the tunnel and the measurements are made in the last wood specimen of the middle layer. A closed loop system is available for air conditions different than the ones found in the laboratory. In the first three tests, the wood specimens were at a moisture content of 12% which is in equilibrium with the laboratory environment of 20°C and 65% RH. In the last test, the last specimen of each layer was changed to a specimen at green wood condition.

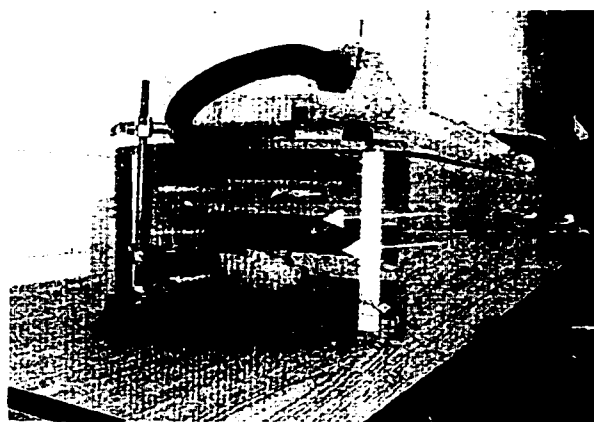


Figure 3.3. Photo of the experimental setup for convective coefficients. White arrows point to 10 mm space above and below the instrumented specimen.

No mass transfer was to occur and the specimens were weighed before and after each test as a verification. The four other sides of the wood specimen were isolated with duct tapes to have the heat transfer occur in one-dimension. To monitor the changes of temperature in the half-thickness of the wood, thermocouples were installed in five holes

drilled on the side at 3.8, 7.6, 11.4, 15.2 and 19 mm from the surface and held in place with a wooden peg plugging completely the hole. A sixth thermocouple was installed on the surface. Two other thermocouples were used as a psychrometer to monitor the dry bulb and wet bulb air temperature. The air was driven with a fan at one end of the tunnel. A jute tissue was introduced downstream of the fan as a diffuser to insure uniform air distribution. Measurements of the temperature and velocity of the air were achieved at the other end beside the instrumented specimen. Air velocity was measured with a manual anemometer. The thermocouples of copper-constantan were calibrated in a water bath at 13°C and 30°C.

For the first test conducted with wood at green condition, the humid atmosphere, desired to prevent drying, was obtained by having a closed air loop linking the tunnel to a vapor saturator consisting of a pan filled with water. However, it was not possible to avoid vapor condensation and the test specimen had a weight gain of 8 g over the two hours. The results, included in Appendix C under the heading Warming in wet conditions, show that all the heat transfer was due to the heat released by the condensation of vapor on the wood surface and that there was no convective heat transfer from the air to the wood. The second test, referred to as run 4, was therefore performed without the closed air loop, exposing the specimen to the laboratory conditions. This lower relative humidity resulted in the evaporation of the water at the surface of the wood and a decrease in weight. It was still possible to calculate a heat transfer coefficient by adding the heat of vaporization to the change of enthalpy in the wood to derive the total enthalpy change.

- Test results

Table 3.8 presents the main parameters of each test run and the convective heat transfer coefficient measured. The complete data and graphs are in Appendix C.

Table 3.8. Summary of experimental convective heat transfer coefficient values.

	M [%]	v [m/s]	Initial temperature gradient [°C]	Initial temperatures at center and on surface [°C]	Convective heat transfer coefficient, h_h [W/m ² ·°C]
Run 1	12	0.3	8.9	4.0 - 12.9	10.0
Run 2	12	0.3	8.6	0.2 - 8.8	9.6
Run 3	12	0.15	1.4	6.1 - 7.6	3.8
Run 4	75.5	0.15	1.5	11.4 - 13.1 plus a moisture flux=1.47x10 ⁻⁵ kg/s·m ²	12.0

The values given by the thermocouple at 15.2 mm from the surface were eliminated because they were systematically too high which indicated a malfunction of the sensor.

3.2.3 Analytical determination of the convective mass transfer coefficient

The convective mass transfer coefficient h_ψ as a function of moisture content has been determined for several conditions. Existing literature data are listed Table 3.9.

Table 3.9. Convective mass transfer coefficient using water potential as the driving force.

Authors	Convective mass transfer coefficient – h_ψ [kg _{water} ² /m _{air} ² ·s·J]	Drying conditions
Cloutier <i>et al.</i> (1992)	9.36 x 10 ⁻¹⁰	T _{d.b.} 50°C, T _{w.b.} 42.5°C v _{air} 1 m/s
	4.43 x 10 ⁻¹⁰	T _{d.b.} 20°C, T _{w.b.} 14°C v _{air} 0.5 m/s
	5.82 x 10 ⁻¹⁰	T _{d.b.} 35°C, T _{w.b.} 28°C v _{air} 0.5 m/s
Tremblay <i>et al.</i> (1999)	8.6 x 10 ⁻¹⁰ constant above 110% M decreasing to 0.8 x 10 ⁻¹⁰ between 15 and 20% M	T _{d.b.} 56°C, RH 52% v _{air} 1 m/s

Note: T_{d.b.} is the dry bulb temperature, T_{w.b.} is the wet bulb temperature and v_{air} is the velocity of air.

The convective mass transfer coefficient can also be inferred from the convective heat transfer coefficient, either calculated or measured, using the Lewis analogy, known in nondimensional analysis as:

$$h_h = h_{m(c)} \rho c_p Le^{2/3} \quad (3.23)$$

where ρ is the air density ($\text{kg}_{\text{air}}/\text{m}^3_{\text{air}}$),

c_p is the specific heat of air ($\text{J}/\text{kg}_{\text{air}}\cdot\text{K}$), and

Le is the Lewis number, approximately 1 for air (Tremblay *et al.* 1999a).

The convective mass transfer coefficient $h_{m(c)}$ [$\text{m}_{\text{air}}/\text{s}$] is different from the coefficient h_ψ [$\text{kg}_{\text{water}}^2/\text{m}_{\text{air}}^2\cdot\text{s}\cdot\text{J}$] of equation (3.13). Based respectively on moisture concentration and water potential, the two coefficients are related by the following equation:

$$h_\psi = h_{m(c)} \frac{(c_{\text{surf}} - c_\infty)}{(\psi_{\text{surf}} - \psi_\infty)} \quad (3.24)$$

where c_{surf} is the moisture concentration of air in equilibrium with the surface

[$\text{kg}_{\text{water}}/\text{m}^3_{\text{air}}$] and

c_∞ is the moisture concentration of ambient air [$\text{kg}_{\text{water}}/\text{m}^3_{\text{air}}$].

Using the values of the convective heat transfer coefficients determined in section 3.2.2, the corresponding h_ψ values vary from 2.9 to $8.6 \times 10^{-10} \text{ kg}_{\text{water}}^2/\text{m}_{\text{air}}^2\cdot\text{s}\cdot\text{J}$ as shown in Table 3.10.

Table 3.10. Mass transfer convective coefficients from conversion using Lewis analogy.

	h_ψ [$\text{kg}^2/\text{s}\cdot\text{J}\cdot\text{m}^2$]		
	Period 4	Period 5	Period 6
$h_h = 3.8 \text{ W}/\text{m}^2\cdot^\circ\text{C}$	2.9×10^{-10}	3.2×10^{-10}	3.3×10^{-10}
$h_h = 10 \text{ W}/\text{m}^2\cdot^\circ\text{C}$	7.7×10^{-10}	8.3×10^{-10}	8.6×10^{-10}

3.2.4 Experimental determination of the convective mass transfer coefficient

The experimental determination of the convective mass transfer coefficient h_ψ requires the determination of the mass flow and the water potential at the wood surface, as shown in equation (3.13). When the moisture content of the wood surface is above the FSP and under proper ventilation, the surface temperature corresponds to the wet bulb temperature of air. In such conditions, drying occurs at constant enthalpy, i.e. the energy from the air to the wood surface returns to air via the heat of vaporisation, as shown in Figure 3.2 (b).

The mass flux is calculated using the drying curve (mass vs. time):

$$q_m = \left(\frac{dM}{dt} \right) \frac{V_{\text{wood}} \rho_{\text{water}} G_m}{A} \quad (3.25)$$

where dM/dt is the slope of the drying curve [$\text{kg}_{\text{water}}/\text{kg}_{\text{dry wood s}}$],

V_{wood} is the volume of moist wood [$\text{m}^3_{\text{moist wood}}$],

ρ_{water} is the density of water [$\text{kg}_{\text{water}}/\text{m}^3_{\text{water}}$],

G_m is the specific gravity [$\text{kg}_{\text{dry wood}}/\text{m}^3_{\text{moist wood}}$], and

A is the area of wood specimen subjected to evaporation [m^2].

Then the mass transfer coefficient is calculated using:

$$q_m = h_\psi (\psi_{\text{surf}} - \psi_\infty) \quad (3.26)$$

where h_ψ is the mean mass transfer convective coefficient [$\text{kg}^2_{\text{water}}/\text{m}^2 \cdot \text{s} \cdot \text{J}$], and

$(\psi_{\text{surf}} - \psi_\infty)$ is the water potential differential between wood surface and air

[$\text{J}/\text{kg}_{\text{water}}$].

The water potential of the wood surface can be calculated from the moisture content of the wood surface, while the water potential of the air is calculated with the following equation:

$$\psi_{m+o} = \frac{RT}{M_w} \cdot \ln \frac{p_v}{p_{vs}} \quad (3.27)$$

where ψ_{m+o} is the sum of the matric and osmotic potentials of water [J/kg],

R is the universal gas constant [8.3143 J/mol·°K],

T is the absolute temperature [°K],

M is the molecular weight of water [0.0180153 kg/mol],

p_v is the partial pressure of vapor in equilibrium with the water in wood [Pa], and

p_{vs} is the partial pressure of vapor in equilibrium with pure free water [Pa].

The relative humidity divided by 100 is therefore equaled to p_v/p_{vs} .

• Experimental set up

The same experimental setup for the determination of the heat transfer coefficient was used. The initial moisture content of the tested wood specimen and its two vertical neighbors was at 76% and the rest of the upstream wood was at 12% and its surfaces impregnated with paraffin wax to prevent moisture adsorption. The test specimen has its four side faces sealed with duct tape. There was no space between pieces of wood in one layer. Pieces were conditioned to 14°C, close to the wet bulb temperature of the lab of about 16.5°C. The air velocity was about 0.15 m/s. The mass of the specimen was measured at time intervals of 8 to 15 minutes.

The moisture flux at the wood-air interface was calculated using the slope of the drying curve during the first stage of drying, the bulk of the specimen being at 76% M. The surface was assumed to be at 60% M at that stage, having its surface water potential

equaled to -800 J/kg , according to the sorption curve. Results are summarized in Table 3.11.

Table 3.11. Summary of the experimental convective heat and mass transfer coefficients

	M	Air velocity [m/s]	Initial temperature gradient [°C]	Initial temperatures at surface and center [°C]	Convective heat transfer coefficient, h_c [W/m ² ·°C]	Convective mass transfer coefficient, h_m [kg ² /J·s·m ²]
<u>Heat</u>					Measured	From Lewis analogy
Run 1	12	0.3	8.9	4.0 - 12.9	10.0	11.8×10^{-10}
Run 2	12	0.3	8.6	0.2 - 8.8	9.6	11.2×10^{-10}
Run 3	12	0.15	1.4	6.1 - 7.6	3.8	4.5×10^{-10}
Run 4	75.5	0.15	1.7	11.4- 13.1 plus a moisture flux= 1.47×10^{-5} kg/s·m ²	12.0	8.8×10^{-10}
<u>Mass</u>						Measured
Run 5	75.5	0.15	none	14	-	3.1×10^{-10}

A comparison of the calculated value of run 4 and the measured value of run 5 for the convective mass transfer coefficients confirms the statement of Salin (1996) to the effect that the Lewis analogy tends to overestimate the convective mass transfer coefficients. Comparing the Lewis analogy results of runs 1 to 3 with the values shown in table 3.9 supports the same conclusion. Although more measurements would be required to conclude, it is proposed to use the ratio of the heat transfer convective coefficients at 0.15 m/s for green and 12% M and to apply it to the mass transfer convective coefficient measured to deduce a mass transfer convective coefficient of a surface at 12% M. This ratio of 3.8 to 12.0 applied to 3.1×10^{-10} yields a convective mass transfer coefficient of $1.0 \times 10^{-10} \text{ kg}^2/\text{J} \cdot \text{s} \cdot \text{m}^2$ to be used for conditions below FSP at low air velocity instead of the $4.5 \times 10^{-10} \text{ kg}^2/\text{J} \cdot \text{s} \cdot \text{m}^2$ resulting from the Lewis analogy.

3.2.5 Sorption curves

Two properties of wood are required to model water movement in wood: the moisture content vs. air relative humidity or water potential relationships and the effective water conductivity of wood. In this section, adsorption and desorption full and intermediary curves are developed for spruce at three different temperatures using existing data.

Figure 3.4 shows typical sorption curves (wood moisture content vs. air relative humidity) of two well-known indigenous species, white spruce and sugar maple. These curves cover only the hygroscopic domain of wood, *i.e.* up to FSP. As generally the case for species with low extractive content, the sorption curves are very similar. The magnitude of the hysteresis is almost the same, and the PSF is around 30% M for typical ambient temperature.

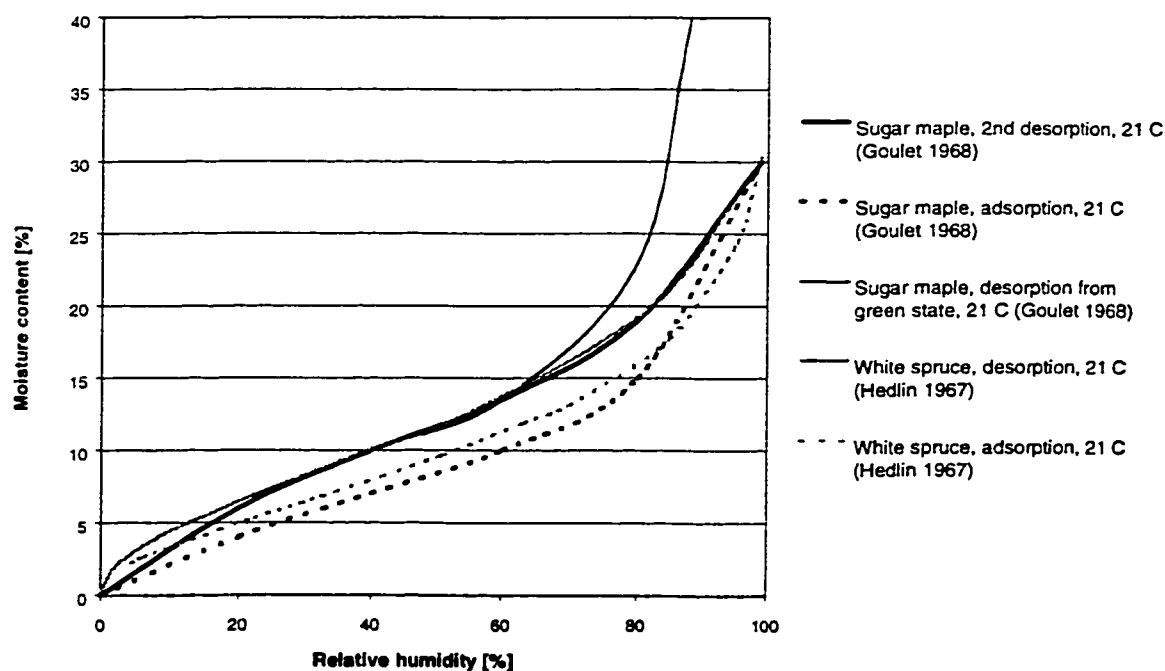


Figure 3.4. Sorption curves function of the relative humidity.

Figure 3.5 shows the sorption curves where the air relative humidity index has been replaced by its equivalent, the water potential of wood. The relation of water potential to air relative humidity is shown in equation (3.27). Replacing the air relative humidity index by water potential allows to consider the section of the sorption curve above FSP, which is difficult otherwise. The strong hysteresis between the desorption and adsorption has an important impact on moisture movement in wood. In Figure 3.5, the curves of Figure 3.4 are shown after conversion for the M between 0 and 30 %. They are continuous with the curves of Fortin (1979) and Tremblay *et al.* (1996). This continuity illustrates the advantage of using the water potential as the driving force for the entire range of moisture content.

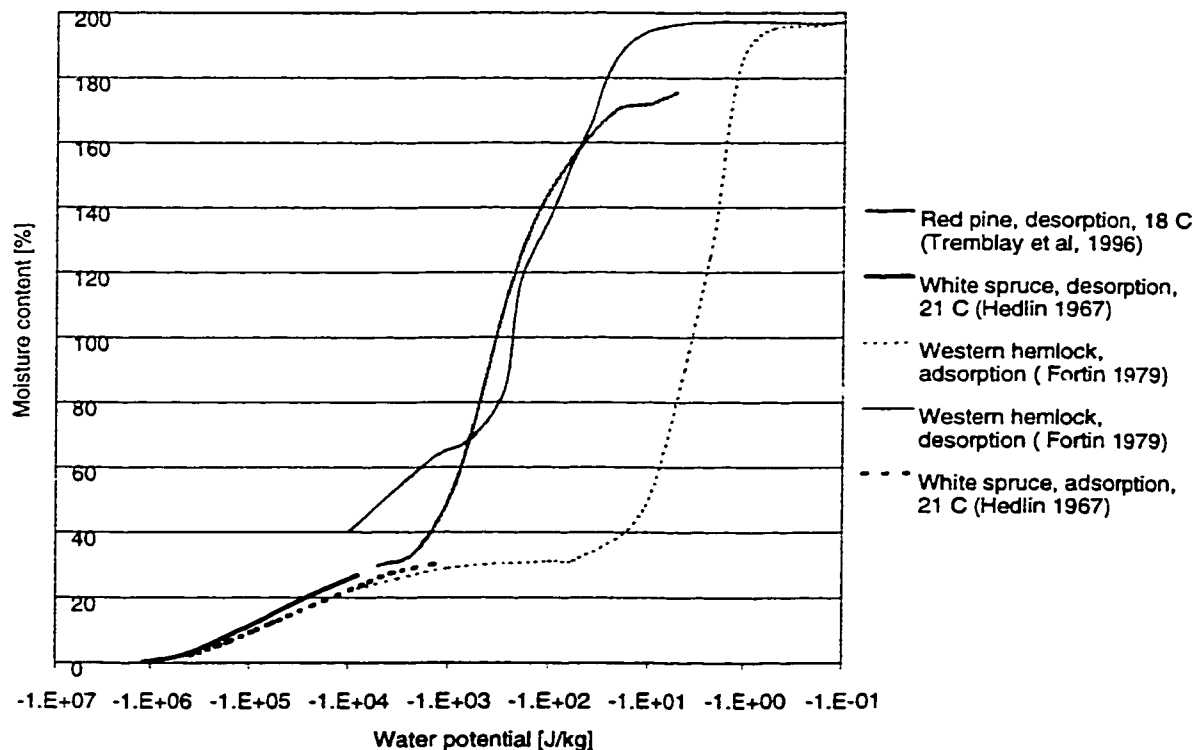
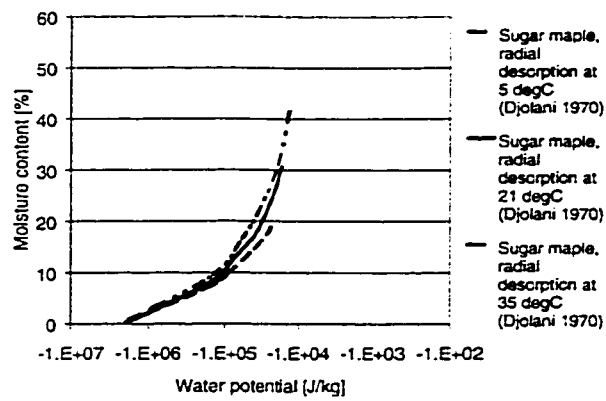
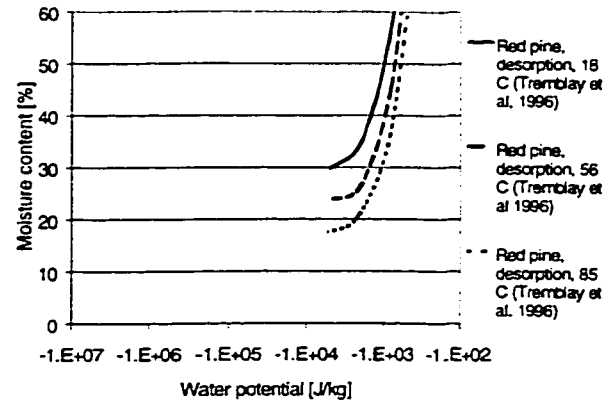


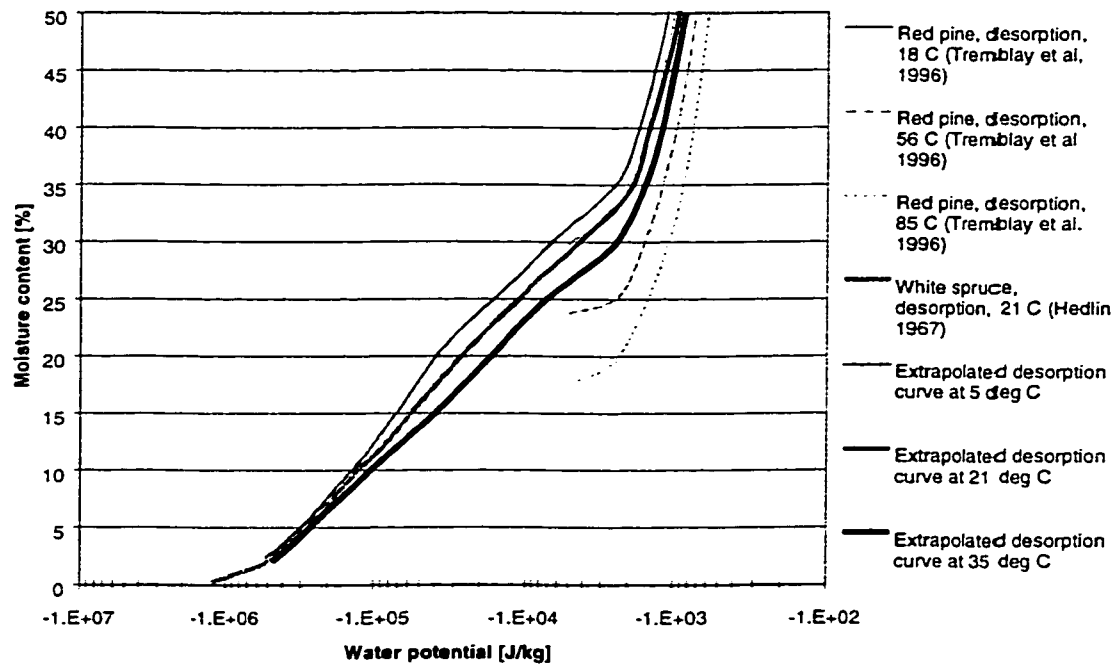
Figure 3.5. Sorption curves function of water potential.



(a) Desorption curves for sugar maple used to extrapolate below 30% M.



(b) Desorption curves for red pine used to extrapolate above 30% M.

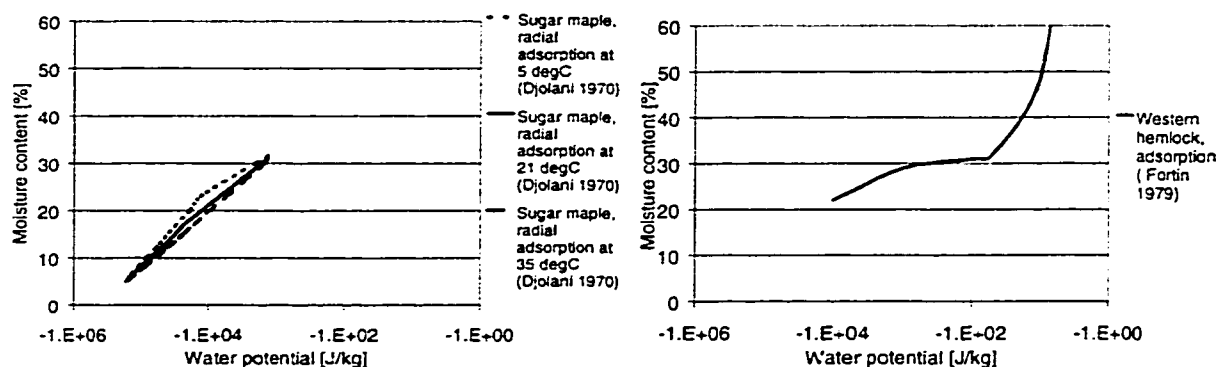


(c) Extrapolated desorption curves for spruce with base curve in grey.

Figure 3.6. Desorption curves for spruce at 5°C, 21°C and 35°C. Graph (a) is used to extrapolate the base curve below 30% M and graph (b) above 30 % M.

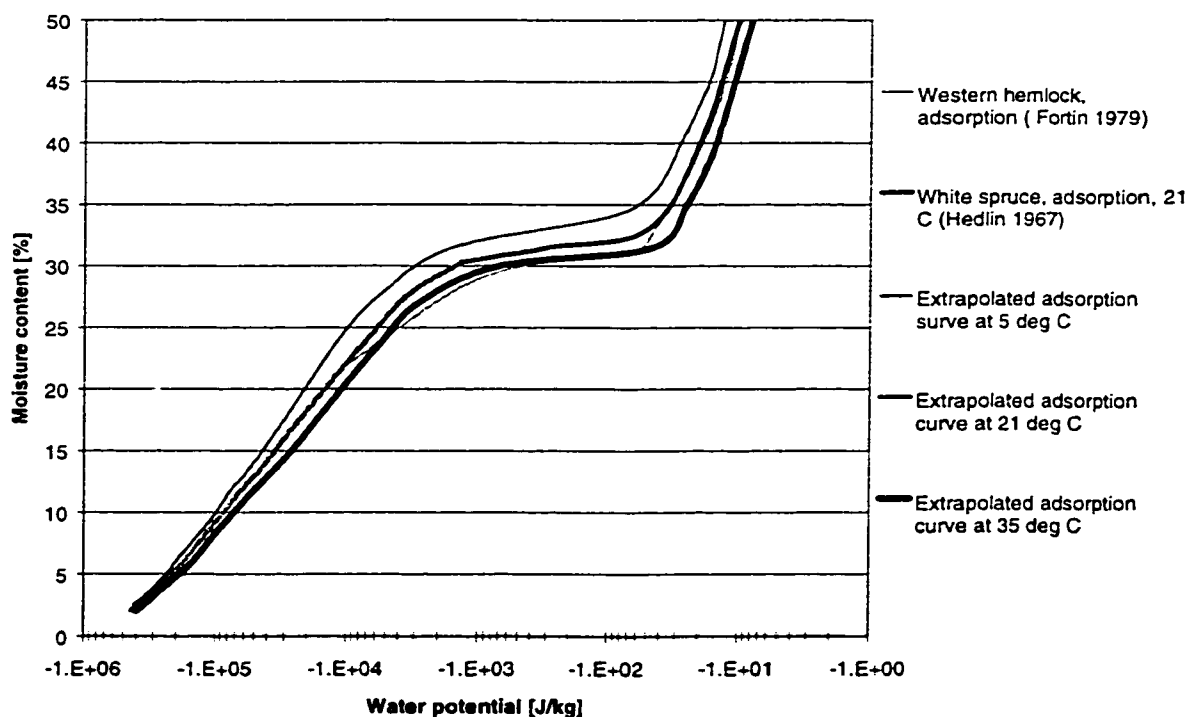
The desorption curves are then extrapolated for the temperature range of the test. Data from Djolani (1970), Stamm and Harris (1953) and Tremblay *et al.* (1996) show how sorption curves are a function of temperature. Figure 3.6 shows that the portion of the 21°C desorption curve that is below 30% M is extrapolated at 5°C and 35°C using the differential between the sorption curves at 5°C, 21°C and 35°C measured for sugar maple

by Djolani (1970). These resulting curves are in agreement with the sorption curves for Sitka spruce of Stamm and Harris (1953) for different temperature ranges. The upper part of the curves are extrapolated using the data measured for red pine by Tremblay *et al.* (1996). In Figure 3.7, the adsorption curve at 21°C is similarly extrapolated at 5°C and 35°C using Djolani measurements in adsorption.



(a) Adsorption curves for sugar maple used to extrapolate below 30% M.

(b) Adsorption curve for hemlock used as base curve above 30% M.



(c) Extrapolated adsorption curves for spruce with base curve in grey.

Figure 3.7. Adsorption curves for spruce at 5°C, 21°C and 35°C. Graph (a) is used to extrapolated the curve below 30% M and graph (b) is used as base above 30 % M.

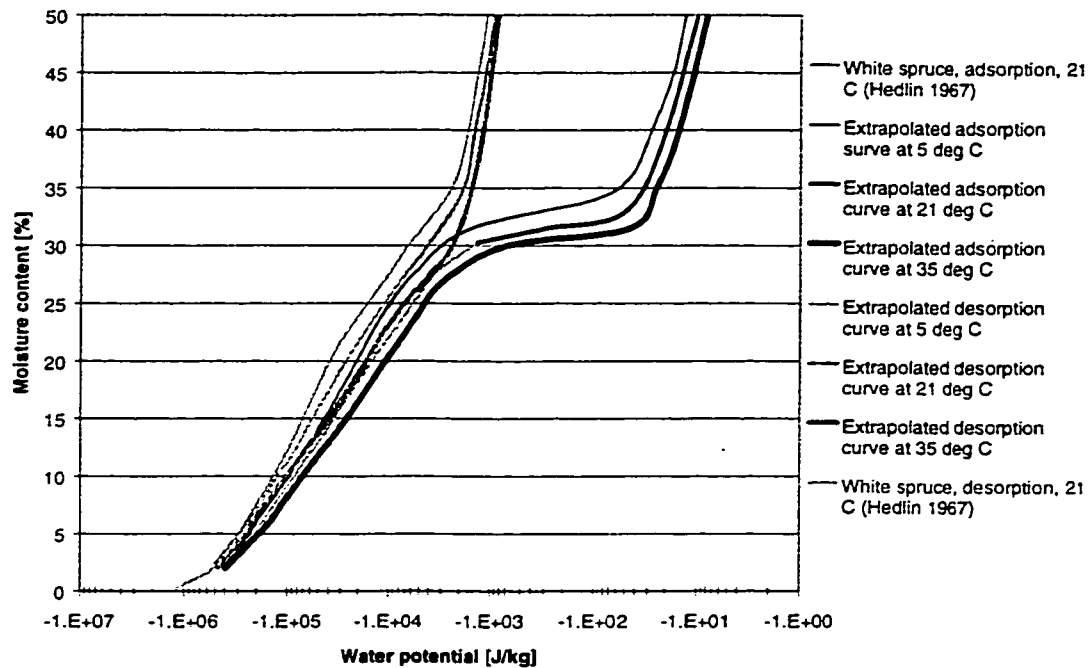


Figure 3.8. Full adsorption and desorption curves for spruce at 5°C, 21°C and 35°C illustrating the hysteresis.

The curves of Figures 3.6 and 3.7 are grouped in Figure 3.8. They are the full sorption curves from completely saturated or dry conditions. In the roof test, the wood planks started at 6% M, were progressively wetted to attain maxima varying from 12 to 120% M and then were dried. In most cases, the drying process started at conditions much lower than saturation, and closer to fiber saturation point. Examining the wood drying process from different starting point, Peralta (1995) has observed that intermediary sorption curves fall between the full desorption and adsorption curves as shown in Figure 3.9. This confirms the finding that the full curves should be considered as the boundary of the hysteresis (Urquhart 1960). Any point between the curves can be met depending on which conditions the material was subjected to. Therefore, temperature and relative humidity alone are not sufficient to determine moisture content. The sorption history is necessary. Starting on the adsorption isotherm, the intermediary curves of Figure 3.9 join

the desorption isotherm with a variation of the relative humidity of approximately 40%. The 92% intermediary curve is the only one with the characteristic sigmoidal shape. The other ones have a simple convex form. Peralta (1996) and Peralta and Bangi (1998a, 1998b) have attempted to model these intermediary curves without satisfactory precision.

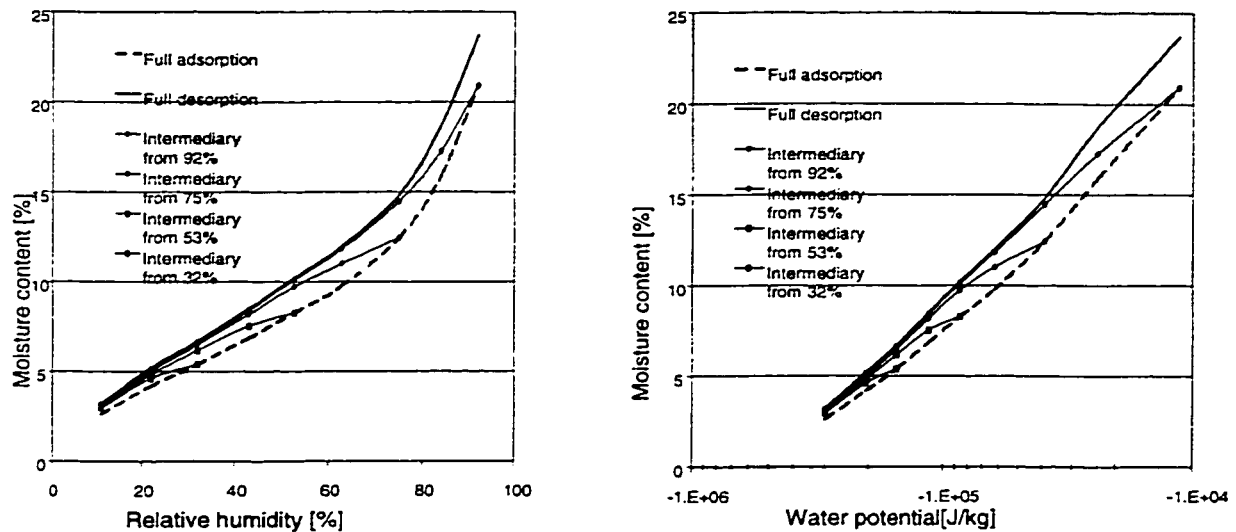


Figure 3.9 Full and intermediary sorption curves for yellow poplar as per Peralta (1995), as function of relative humidity on left and water potential on right.

Using each pair of desorption and adsorption curves defined at 5°C, 21°C and 35°C, three intermediate curves are determined from moisture contents of 30%, 25% and 20% on the full adsorption curves. The curves then join the desorption curves following the pattern determined by Peralta, as shown in Figure 3.10.

The curves as defined allow the modeling of the different situations found in the test. When the calculation requires values intermediate of the ones provided by the curves, a linear extrapolation is performed.

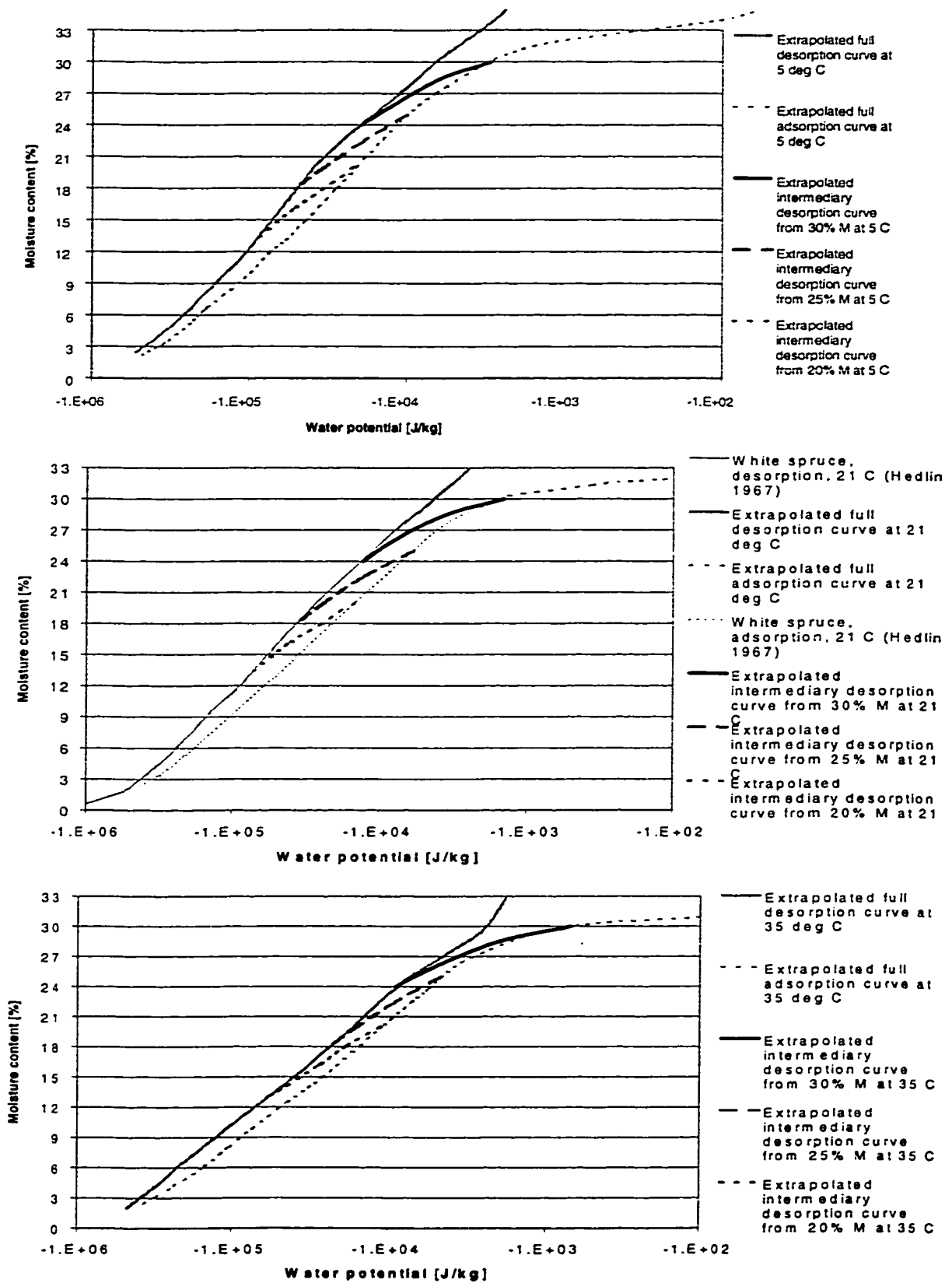


Figure 3.10. Intermediate desorption curves from 30%, 25% and 20% M at three temperatures: 5°C on top graph, 21°C in middle graph and 35°C on bottom graph.

3.2.6. Determination of the effective water conductivity

In order to model moisture movement with the water potential gradient as the driving force, the appropriate transfer coefficient, *i.e.* the effective water conductivity, must be determined. Cloutier and Fortin (1993) and Tremblay *et al.* (1999b) have measured respectively the effective water conductivity of aspen and red pine for the complete range of moisture content in wood. The method used, called instantaneous profile method, measures directly the effective water conductivity. Tremblay *et al.* present the two advantages of this method: 1) the flux-gradient proportionality can be verified directly, and 2) no specific set of boundary conditions need to be imposed since the gradient and the resulting flux are measured directly in wood. Moschler and Martin (1968) have used an equivalent method, the Matano method, but only below the FSP. The method uses edge coated specimens to impose a one-dimensional moisture flow. The specimens are allowed to dry in a conditioning cabinet at constant temperature, relative humidity and air velocity. The moisture concentration profiles are obtained from the moisture content profiles measured at different mean moisture content between complete saturation and 15% M. This is done by slicing the specimens and by determining the moisture content of each slice by gravimetry. The water potential is obtained with the sorption curve. The effective water conductivity is obtained with the following equation:

$$[K_x]_{x_i, t_j} = \frac{\left[\frac{\partial}{\partial t} \left(\int_{x_4=0}^{x_i} C dx \right) \right]}{\left[\frac{\partial \psi}{\partial x} \right]_{x_i, t_j}} \quad (3.28)$$

In the hygroscopic domain, *i.e.* between 0 and 30% M, another method to determine the diffusion coefficient *D* uses a vapometer cup assembly and is based on Fick's first law of

diffusion. During the test, the specimen is exposed on its two faces to two different moisture conditions. These conditions can be related in concentration of moisture or in vapor pressure, which is the case of most data available. To use these data in the context of water potential, some conversions must be made. Table 3.12 compares three equations using each a different driving force: concentration gradient for a coefficient D_c , moisture content gradient for a coefficient D_m and vapor pressure gradient for a coefficient D_{pv} . Comparing each with the equation using water potential gradient as the driving force allows to present the different conversion factors. For each conversion case, the sorption curve, water potential vs. moisture content, is required.

Table 3.12. Equivalence of diffusion coefficients.

Variations of Fick's law	Equivalence	Conversion factor $q_x = -K_{eff} \frac{\partial \psi}{\partial x}$
$q_x = -D_c \frac{\partial C}{\partial x}$ where $C \equiv [\text{kg}_{\text{water}}/\text{m}_{\text{wood}}^3]$, $D_c \equiv [\text{m}_{\text{wood}}^2/\text{s}]$	$q_x = -D_c \frac{\partial C}{\partial \psi} \frac{\partial \psi}{\partial x}$	$K_{eff, c} = D_c \frac{\partial C}{\partial \psi}$ or $K_{eff, c} = D_c \frac{\partial M}{\partial \psi} \cdot \frac{G_m \rho_{\text{water}}}{100}$
$q_x = -D_M \frac{\partial M}{\partial x}$ where $M \equiv [\%]$, $D_M \equiv [\text{kg}_{\text{water}}/\text{m} \cdot \text{s} \cdot \%]$	$q_x = -D_M \frac{\partial M}{\partial \psi} \frac{\partial \psi}{\partial x}$	$K_{eff, m} = D_M \frac{\partial M}{\partial \psi}$
$q_x = -D_p \frac{\partial p_v}{\partial x}$ where $p_v \equiv [\text{kg}_{\text{water}}/\text{m}^2]$, $D_{pv} \equiv [\text{m}/\text{s}]$	$q_x = -K_{eff, p} \frac{\partial p_v}{\partial \psi} \frac{\partial \psi}{\partial x}$	$K_{eff, p} = D_p \frac{\partial p_v}{\partial \psi}$ or $K_{eff, p} = D_p \frac{\partial p_v}{\partial M} \cdot \frac{\partial M}{\partial \psi}$ where $\frac{\partial p_v}{\partial M} = \frac{\partial \text{HR}}{\partial M} \cdot \frac{p_v}{100}$
where q_x is the intensity of the moisture flux $[\text{kg}_{\text{water}}/\text{m}^2 \cdot \text{s}]$ and K_{eff} is the effective water conductivity $[\text{kg}_{\text{water}}^2/\text{m} \cdot \text{s} \cdot \text{J}]$		

Figure 3.11 groups diffusion coefficients measured during desorption of wood. The values for epicea at 40°C, which is a Norwegian spruce, measured by Egner (1934)

(converted first by Kübler 1957, and reconverted here) fit very well with the values of Tremblay *et al.* (1999b) for red pine at 18°C and 56°C. This allows to extrapolate the values of Tremblay to low moisture content.

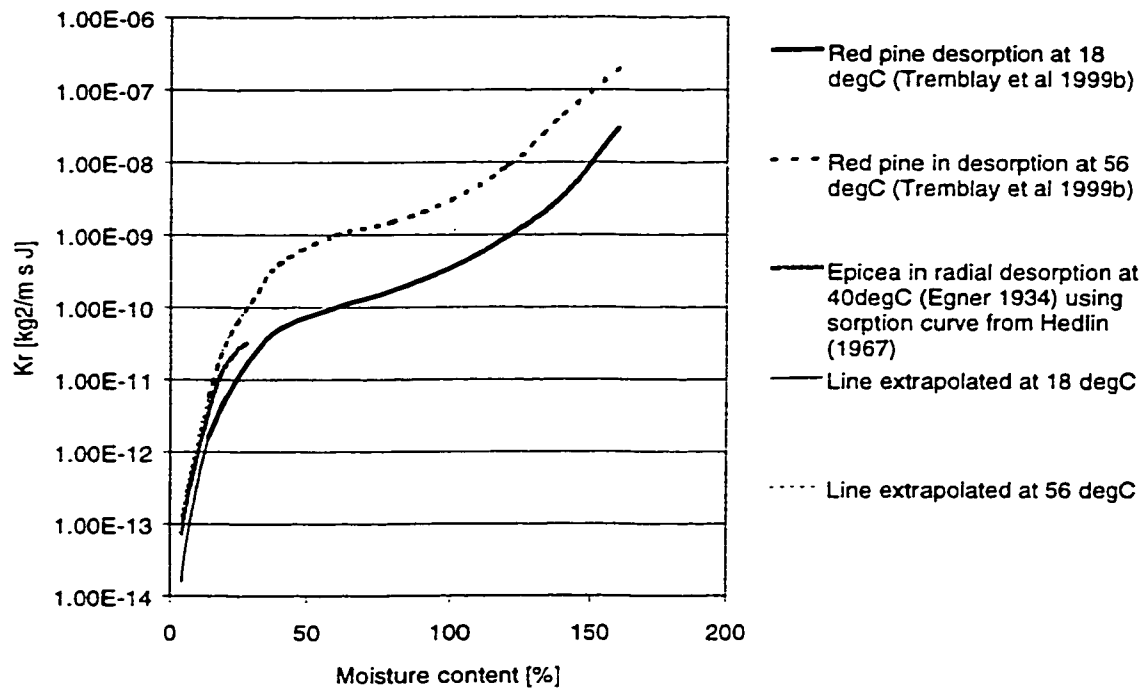


Figure 3.11. Effective water conductivity of red pine and epicea as function of moisture content and temperature.

The hysteresis of the sorption curve of wood indicates that wood properties, at a given moisture content, might be different in adsorption and desorption. However, little data is available to document the differences in values of the coefficient of diffusion of adsorbing or desorbing wood. Comstock (1963) measured the diffusion coefficient during adsorption and desorption, and in steady-state conditions following one of the two states of sorption and found the diffusion coefficients in adsorption to be lower than the value in desorption for wood between 6 and 16% M. Fournier (1976) has also measured the coefficient of diffusion of moisture in relationship with the state of sorption of wood.

The diffusion coefficient was found smaller in wood in adsorption than in desorption. The difference was more pronounced at lower temperature. Fournier notes that moisture content per se does not influence the coefficient of diffusion as it is the gradient of vapor pressure across the wood that determines its moisture content in the same time as it induces a moisture flow. Wood in adsorption has a greater cohesion and density than wood in desorption and, as a result, lets through less moisture.

Figure 3.12 compares the Egner curve with data measured for sugar maple by Fournier (1976). This wood was of a higher density than spruce which explains the lower diffusion coefficient. The two curves by Fournier do not provide enough basis to extrapolate reliably the effective water conductivity for wood in adsorption.

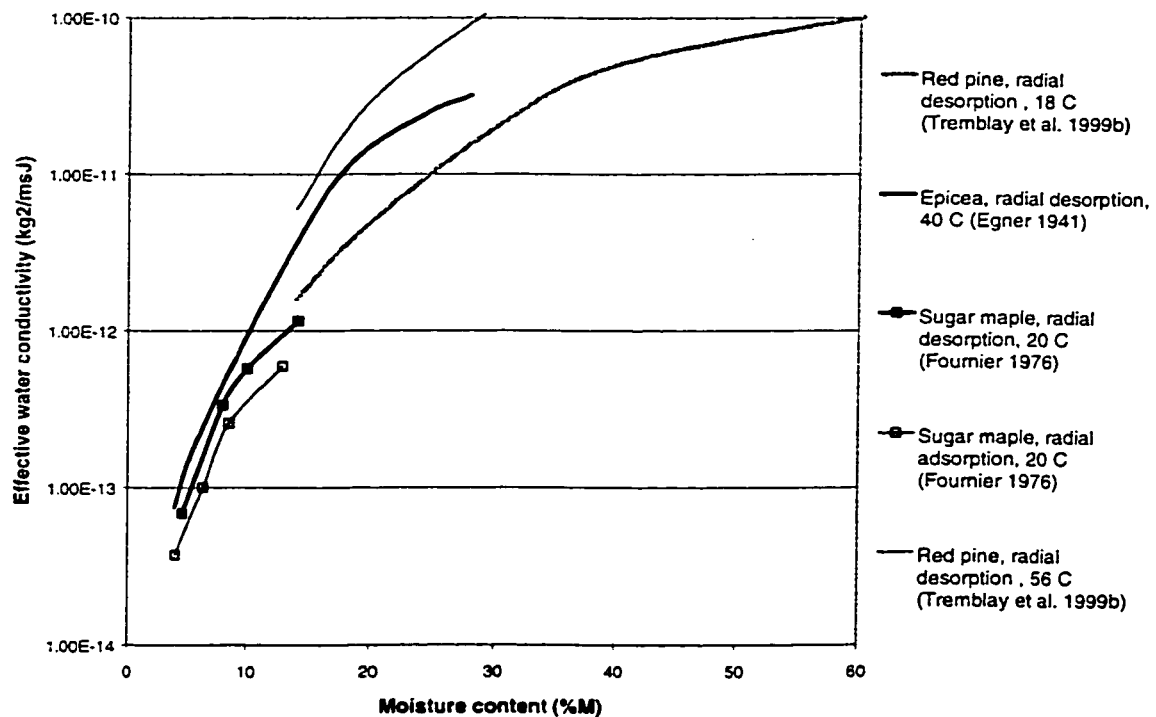


Figure 3.12. Effective water conductivity coefficients as function of moisture content and state of sorption.

The whole section 3.2 shows the scarcity of available data in the literature and the complexity of unit conversion to compare data related to the drying and wetting of wood at moderate temperature and low air velocity. However, sufficient information, data and measurements have been presented to select the parameters to be used in the simulation as listed in Table 3.13.

Table 3.13. Summary of the values retained for each parameter of the physical model.

	From analytical results	From experimental results	Retained values or relationships
Convective heat coefficient h_h below wood plank	Between 2 and 4.6 W/ m ² .°C Independent of moisture content	Serkitjs (1998) $Nu \approx 1$ Tremblay <i>et al.</i> (1999b) at $v=1$ m/s. 8 W/m ² .°C, but proportional to M below 30% Measurements in this study at 12%M 3.8 W/m ² .°C at 0.15m/s and 10 W/m ² .°C at 0.3 m/s Measurements in this study at 75%M 12 W/m ² .°C at 0.15m/s and	$h_h = 3.8$ W/m ² .°C constant
Convective mass transfer coefficient h_ψ below wood plank	Above values converted with Lewis analogy 3 to 8.6 x10 ⁻¹⁰ kg ² /s·J·m ² _{air}	Tremblay <i>et al.</i> (1998b) at $v=1$ m/s, 14 x10 ⁻¹¹ at M=30 %, to 8 x10 ⁻¹¹ at M=15% Measurements in this study at 75%M 3.1x10 ⁻¹⁰ W/m ² .°C at 0.15m/s	$h_\psi = 1.0 \times 10^{-10}$ kg ² /s·J·m ² _{air} constant
Complete sorption curves	-	Tremblay (1996) Red pine in desorption Fortin (1979) Hemlock in adsorption Hedlin (1967) White spruce below 30% M desorption and adsorption	Set of extrapolated curves Figure 3.8
Intermediary sorption curves	-	From above curves, intermediary curves are drawn following Peralta results below 30%	Set of extrapolated curves Figure 3.10
Effective water conductivity	-	Assume all radial movement In desorption, Tremblay <i>et al.</i> (1999a) for red pine and Egner (1934) for epicea Use same value in adsorption	Set of extrapolated curves Figure 3.11

3.3 Modifications to the computer model

To implement the mathematical model, the following modifications were made to the computer model (Cloutier *et al.* 1992, Tremblay *et al.* 1999a, 1999b). The first modifications regarded the definition of the grid. A 225 point triangular mesh defined the 19 mm x 149 mm cross section of the plank. The schematic representation of the finite element mesh can be found in Appendix D. The second type of modifications consisted in the insertion of the proper coefficients within the code. The code was modified in order to maintain the convective heat and mass transfer coefficients, h_h and h_ψ , constant and not a function of conditions as in the base code. The third type was the development of the data files. The specific gravity of wood, G_m (oven dry weight to green volume), varies substantially from one specimen to the other for the same wood species. For example, the specific gravity of red pine was found to vary from 0.360 to 0.460 (Tremblay *et al.* 1999a). Moisture content at full saturation is a function of G_m and it is not possible to use the relationship of moisture content vs. water potential ($M-\psi$) and the effective water conductivity function of moisture content and temperature, $K(M,T)$, directly without introducing a significant error (Cloutier *et al.* 1992). To avoid this error, the saturation percentage, Sp , was used as an indicator of the degree of wetness in wood. Sp relates the volume of water present in a porous medium relative to the total pore volume (Hillel, 1971). For wood, the following applies:

$$Sp = \frac{M}{\frac{1}{G_m} - \frac{1}{G_{ws}}} \quad (3.29)$$

where G_{ws} is the specific gravity of the wood substance defined as $G_{ws} = m_o/V_{ows} \cdot \rho_w$, and V_{ows} is the oven-dry volume of the wood substance.

Therefore, the $M-\psi$ relationship and the $\tilde{K}(M,T)$ function are expressed in terms of S_p instead of M in the datafiles. The $M-\psi$ relationship datafiles allow to take into consideration the intermediary sorption curves, which was not the case in the base code.

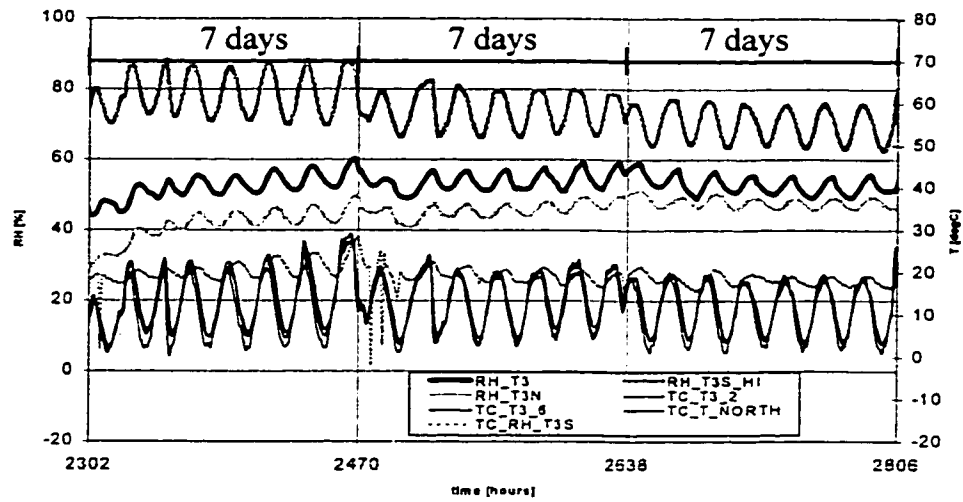
3.4 Validation of model for the simulation of the drying process

In this section, the computer model is validated for its capacity to simulate the drying process of the wood plank. After a wetting season, it is the drying ability of the assembly that determines whether the wood structure is exposed to conditions leading to fungi degradation. Therefore, the drying ability is of prime importance. For the validation, the data measured during the wetting and drying of the plank in cavity T3, the base case, were used as the presence of one-dimensional air flow was preferred. This condition was not found in the other thermos cavities. For the validation, one set of moisture data in T3 was used, *i.e.* the data measured towards the front of the test hut where air was exiting the cavity. Three moisture content pins were inserted across the cavity. The resulting three different wetting/drying patterns measured may be explained by cellulose being more dense along the sides of the cavity, resulting in less air movement.

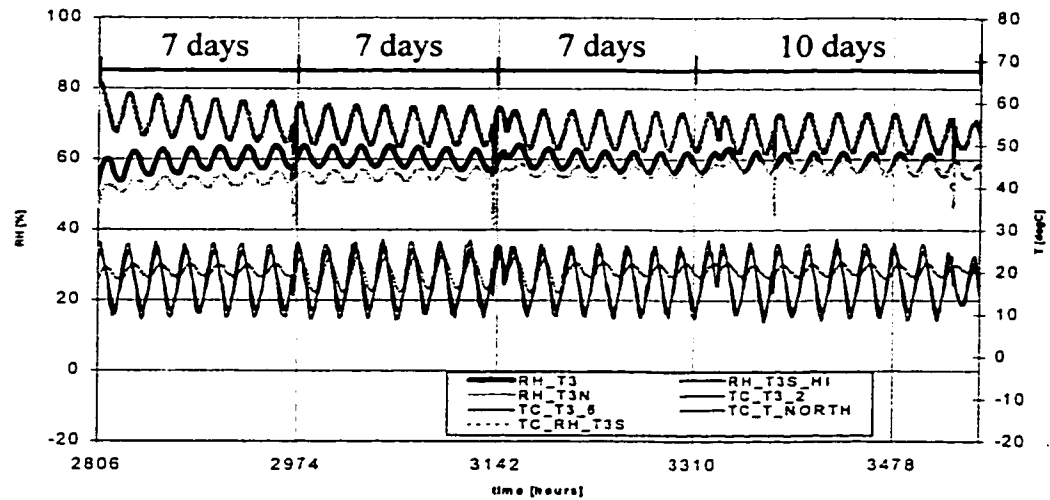
3.4.1 Determination of the actual conditions during the drying period

To perform the simulation so that its results could be compared with the experimental results, the conditions prevailing at the underside of the wood deck during the test had to be assessed. The measurements provided the following information: local temperature and moisture content in the middle of the plank, average moisture content of the plank, temperature and relative humidity above the roof, and temperature and relative humidity approximately 50 mm and 100 mm below the planks. These last two sensors were inserted gropingly after the insulation was installed.

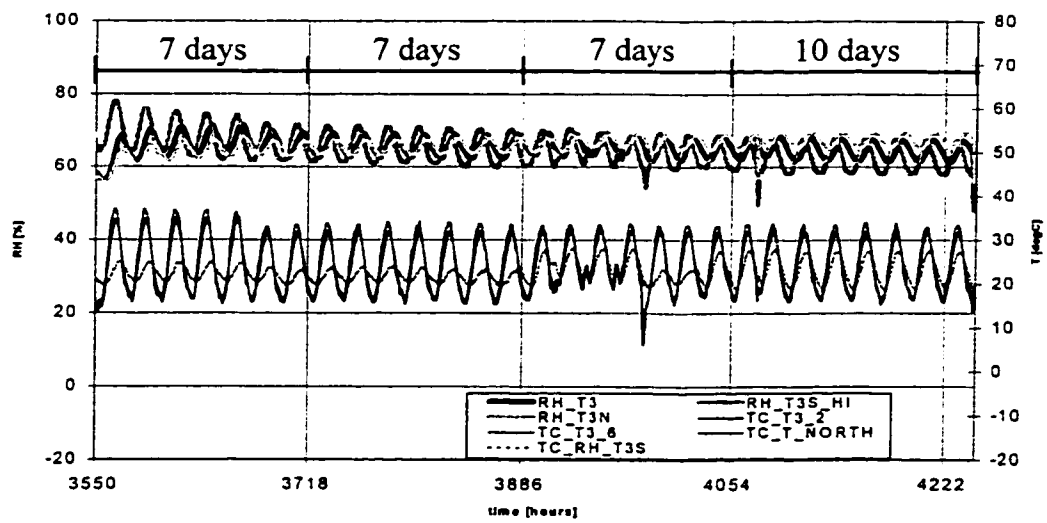
The wood planks were exposed to the outdoor temperature conditions. This resulted in their temperature cycling in phase with the daily periods simulated in the chamber. The temperature measured in the cellulose at 50 mm below the planks also varied in phases with the exterior conditions, but to a lesser degree. The relative humidity measured varied in phase with the temperature cycle, the amplitude of the variation being more prominent at 50 mm below the planks than 100 mm below. No data was taken exactly at the underface of the deck. It was necessary to determine the boundary conditions at that interface during the drying simulation. To do so, each drying period was split into short sub-periods with mean relative humidity and temperature. The following graphs show the relative humidity and the temperature in the insulation together with the plank temperature from period 4 to 6.



(a) Period 4



(b) Period 5



(c) Period 6

Figure 3.13. Conditions measured below and in the planks of cavity T3 during the test.

The examination of Figure 3.13 leads to the following observations on the interrelated effects of temperature and relative humidity:

- the temperature (TC_RH_T3S) in the insulation 50 mm below the planks was rather constant.
- the temperature (TC_T3_6, TC_T3_2) of the wood plank varied considerably and in phase with the outdoor air temperature daily cycle (TC_T_NORTH). There was heat transfer on the outside side of the plank. The presence of the membrane prevented any mass transfer. The set of boundary conditions on the topside of the plank was then different than the one present on its underside.
- the relative humidity (RH_T3S_HI) below the plank varied in phase with the outdoor temperature air cycle. This is explained as follows. In a closed system, a rise of temperature would result in a decrease of the relative humidity. However, the system was open. Each temperature increase induced moisture to egress the wood plank and the cellulose insulation. As soon as it was released, this moisture was likely evacuated outside through the faint but existing air movement.
- the relative humidity in the center of the cellulose (RH_T3, RH_T3N) had its variation dampened and delayed, as the amplitude of the temperature cycle was also reduced in the center of the assembly.

Examining the whole length of the drying period, it is observed that the values of RH in the center of the assembly increased gradually from the start of period 4 to the end of period 6. This indicates that moisture was released into the roof cavity. Relative humidity was higher towards the exit end of the cavity. This can be explained by the

accumulation of more moisture towards the end of the cavity or by the convective movement of vapor towards the end of the cavity due to air exfiltration. Table 3.14 summarizes these measurements as mean values for each sub-period.

Table 3.14. Measured conditions for short intervals of time within each period.

	Period 4 Subdivided in 3 (7, 7 and 7 days)	Period 5 Subdivided in 4 (7, 7, 7 and 10 days)	Period 6 Subdivided in 4 (5, 7, 7 and 10 days)
T_{mean} in wood planks [°C]	14.1 11.9 10.2	17.6 18.6 17.8 17.9	25.2 24.4 24.2 24
T_{mean} in insulation 50 mm below wood planks [°C]	20.1 19.1 18.1	20.3 19.35 20.4 19.3	22.7 21.8 22.4 23.4
Relative humidity max/min [%]	86.5/71.2 80.5/66.1 75.6/63.9	78.0/68.0 74.6/64.7 73.1/63.0 72.0/62.8	74.5/63.5 70.9/62.0 69.6/59.9 68.1/58.2
Mean vapor pressure at 50 mm below planks [Pa]	1880 1645 1460	1716 1615 1643 1528	1914 1750 1784 1889

3.4.2 Determination of the simulation conditions

The simulation requires the input of the conditions of the air below the plank in term of temperature and relative humidity which are used to calculate the water potential in the air. As mentioned earlier, the model used in this study does not allow to deduce the hygrothermal conditions of the air below the planks from the prevailing inside and outside hygrothermal conditions. The conditions below the planks have to be calculated from the measurements conducted in the cellulose and in the wood planks. Water

potential is proportional to temperature and relative humidity as shown in equation (3.27). Of the two parameters, relative humidity is more determinant. For example, a change of the relative humidity from 80% to 90% increases by 50% the water potential, while a change of temperature of 10°C leads to a variation of $\pm 4\%$ of the water potential. Using the measured data, the temperature and relative humidity are set for each sub-period.

- Temperature conditions

The temperature of the air below the plank could be calculated in two ways: by considering conduction only, using the convective heat coefficient as one element, as shown in Figure 3.14, or by evaluating the heat transported to the wood surface by convection. As the exfiltration rate is quite restricted, the first option is used.

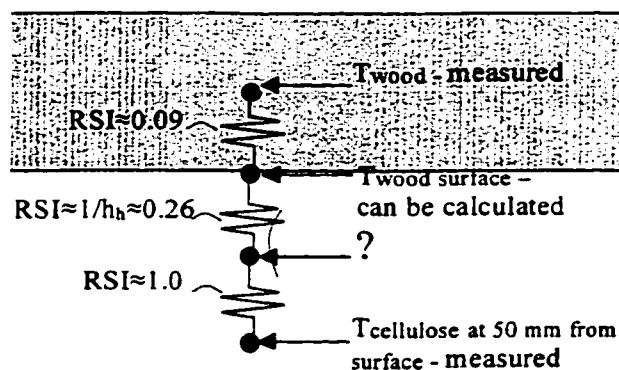


Figure 3.14. Schematic representation of a situation with pure heat conduction.

Table 3.15. Extrapolated temperatures for each sub-period.

	Period 4 Subdivided in 3 (7, 7 and 7 days)	Period 5 Subdivided in 4 (7, 7, 7 and 10 days)	Period 6 Subdivided in 4 (5, 7, 7 and 10 days)
T_{mean} extrapolated	15.7	18.3	24.6*
below wood	13.8	18.8	23.7*
surface [°C]	12.3	18.5	23.7*
		18.3	23.8*

*note that temperature gradient direction is reversed.

• Relative humidity conditions

As noted above, there was no measurement of relative humidity directly below the planks. Relative humidity had to be inferred from the given data. Two methods of determining the actual relative humidity are proposed. In the first method, the relative humidity measured at 50 mm below the planks is given in local vapor pressure. The same vapor pressure is assumed to be found just below the planks and, together with temperature extrapolated for the underside of the plank, is converted into relative humidity. Table 3.16 presents the deduced relative humidity conditions.

Table 3.16. Relative humidity inferred from measured vapor pressures.

Period 4		Period 5		Period 6	
T	RH	T	RH	T	RH
[°C]	[%]	[°C]	[%]	[°C]	[%]
15.7	96.0	18.3	82.8	24.6	61.9
13.8	93.7	18.8	74.5	23.7	61.1
12.3	91.2	18.5	74.3	23.7	59.8
		18.3	72.5	23.8	59.2

This method gives the same conditions for the whole width of the cavity and cannot explain the differential moisture content measured from the center to the side of the cavity. A second method uses the moisture content measured during the test at the three locations. Assuming equilibrium, the corresponding relative humidity is determined from

sorption curves. Figure 3.15 presents the sorption curves from three different sources for non-treated cellulose. In the range of moisture content considered, the relationship is rather flat. This poses an uncertainty that favors the consideration of the moisture content in the wood due to the more important changes in moisture content as seen in Figure 3.4. Table 3.17 summarizes the equilibrium relative humidity.

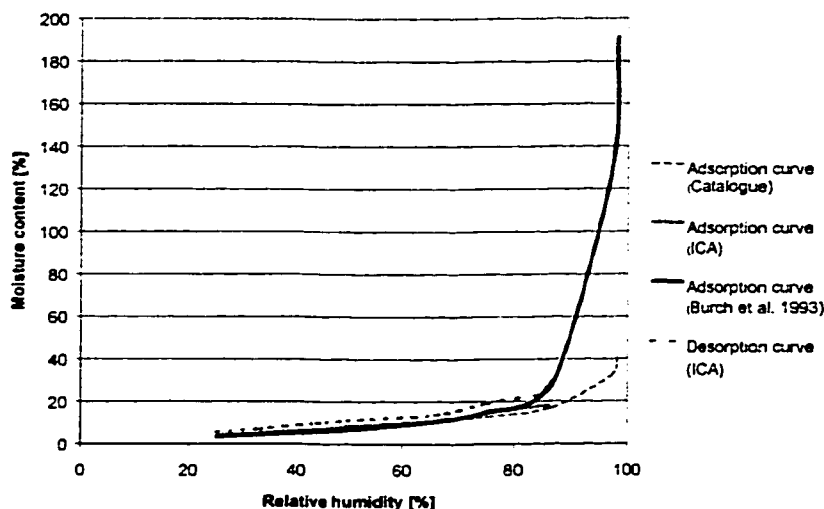


Figure 3.15. Sorption curves for non-treated cellulose insulation.

Table 3.17. Relative humidity in equilibrium with measured moisture content in wood and cellulose per period

	Conditions in and below planks			Conditions 50 mm below planks	
	Measured moisture content from start to end of period[%]	Relative humidity at equilibrium from sorption curves [%]	Measured temperature [°C]	Measured relative humidity [%]	Measured temperature [°C]
Period 4					
In cellulose	15→ 12.5	72 → 66	15.5*	73	19
In wood	28 → 19	94 → 78	12	n/a	n/a
Period 5					
In cellulose	12.5→ 10	66 → 47	18.5*	70	20
In wood	18 → 13	78 → 56	18	n/a	n/a
Period 6					
In cellulose	10 → 8	47 → 38	22.5*	66	21
In wood	13 → 9	56 → 36	24	n/a	n/a

*: mean value of planks and insulation measured temperature

Table 3.17 shows that the direction of sorption was the same for cellulose and wood. The relative humidity measured in the cellulose during period 4 and 5 was similar to the relative humidity to be expected according to the sorption curve using the measured moisture content. In period 6, the measured relative humidity 50 mm from the deck is high compared to the relative humidity given by the sorption curve. This can be explained by the fact that the high temperatures above the planks would warm the insulation located just below the planks, inducing a faster drying.

The equilibrium relative humidity was derived from the measured moisture content of wood and the desorption curve of Figure 3.4 for the three moisture content sensors, T3_6 located at the center of the spacing between the two structural joist, and T3_7 and T3_8 located respectively at 100 mm and 25 mm from the joist. This derivation of the relative humidity using the moisture content measured at the center of plank was based on the assumption that there was no or little moisture content gradient across the thickness of the plank. The results are listed in the Table 3.18 for the three sets of measured moisture content available.

Table 3.18. Relative humidity extrapolated from measured moisture content per sub-period.

Period	Day	T3-6			T3-7			T3-8		
		Moisture content [%]	Corresponding RH from sorption curve [%]	Average RH for the sub-period [%]	Moisture content [%]	Corresponding RH from intermediary sorption curve [%]	Average RH for the sub-period [%]	Moisture content [%]	Corresponding RH from intermediary sorption curve [%]	Average RH for the sub-period [%]
Period 4	1	28.4	97		24.4	93.5		20	88	
	8	22.1	85.5	91.2	20	82	89.5	18.5	83	86
	15	20.5	81	83.2	18.8	76.5	80.5	18	81	82
	21	19.8	79.5	80.2	18.2	75	75.7	17.5	79.5	80.2
Period 5	1	19.8	81.5		18.2	76.5		17.5	80.5	
	8	17	72.5	77	16	68.5	72.5	16.5	75.5	77.7
	15	16.5	70.5	71.5	15.8	67.5	68	16.2	73.5	74.2
	22	14	60.5	65.5	13.7	59	63.2	13.9	60	66.7
	31	13	56	58.2	12.6	53.5	56.2	13	56	58
Period 6	1	13	58		12.6	56		13	58.5	
	6	11.5	51.5	54.7	10.6	45.5	50.7	12	53.5	56
	13	10.8	46.5	49	9	36	40.7	11	46	49.7
	20	10	41	43.7	8	30	33	10.3	43	44.5
	30	9.1	36	38.5	8	30	30	9.8	40	41.5

3.4.3 Computer model simulations

Table 3.19 lists the data used to simulate the drying of three sensor locations in cavity T3.

Table 3.19. Drying simulation conditions

Conditions used for each simulation								
K = desorption conductivity - same for all h_h = assumed constant at $3.8 \text{ W/m}^2\text{°C}$			v_{air} = assumed constant at 0.1 m/s for all h_w = assumed constant at $1 \times 10^{-10} \text{ kg}^2/\text{s}\cdot\text{J}\cdot\text{m}^2$					
	Initial M [%]	Appropriate sorption curve	Period 4 T RH [°C] [%]		Period 5 T RH [°C] [%]		Period 6 T RH [°C] [%]	
T3-6	28.4	Intermediate	15.7	96.0	18.3	82.8	24.6	61.9
RH from		curve from	13.8	93.7	18.8	74.5	23.7	61.1
measured vapor		30%	12.3	91.2	18.5	74.3	23.7	59.8
pressure					18.3	72.5	23.8	59.2
T3-6	28.4	Intermediate	15.7	91.2	18.3	77	24.6	54.8
Extrapolated		curve from	13.8	83.2	18.8	71.5	23.7	49
RH from		30%	12.3	80.2	18.5	65.5	23.7	43.8
measured M					18.3	58.2	23.8	38.5
T3-7	24	Intermediate	15.7	96.0	18.3	82.8	24.6	61.9
RH from		curve from	13.8	93.7	18.8	74.5	23.7	61.1
measured		25%	12.3	91.2	18.5	74.3	23.7	59.8
vapor pressure					18.3	72.5	23.8	59.2
T3-7	24	Intermediate	15.7	89.5	18.3	72.5	24.6	77.8
Extrapolated		curve from	13.8	80.5	18.8	68	23.7	74.2
RH from		25%	12.3	75.8	18.5	63.2	23.7	66.8
measured M					18.3	56.25	23.8	58
T3-8	20	Intermediate	15.7	96.0	18.3	82.8	24.6	61.9
RH from		curve from	13.8	93.7	18.8	74.5	23.7	61.1
measured		20%	12.3	91.2	18.5	74.3	23.7	59.8
vapor pressure					18.3	72.5	23.8	59.2
T3-8	20	Intermediate	15.7	88	18.3	77.8	24.6	56
Extrapolated		curve from	13.8	82	18.8	74.2	23.7	49.8
RH from		20%	12.3	80.2	18.5	66.8	23.7	44.5
measured M					18.3	58	23.8	41.5

Depending on the given initial moisture content, a desorption curve with the appropriate history is selected. The table also specifies the values of the other parameters used by the simulation. The resulting drying curves are shown in the Figures 3.16, 3.17 and 3.18.

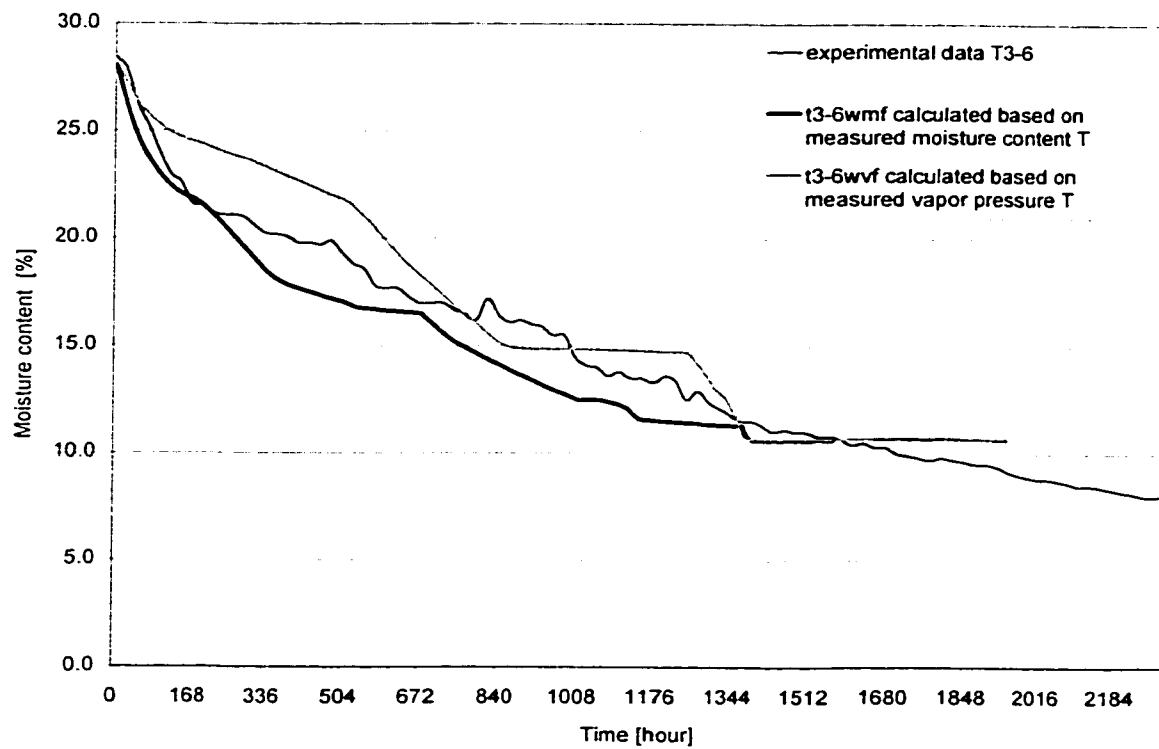


Figure 3.16. Comparison of modeling and experimental data from 28% M in T3.

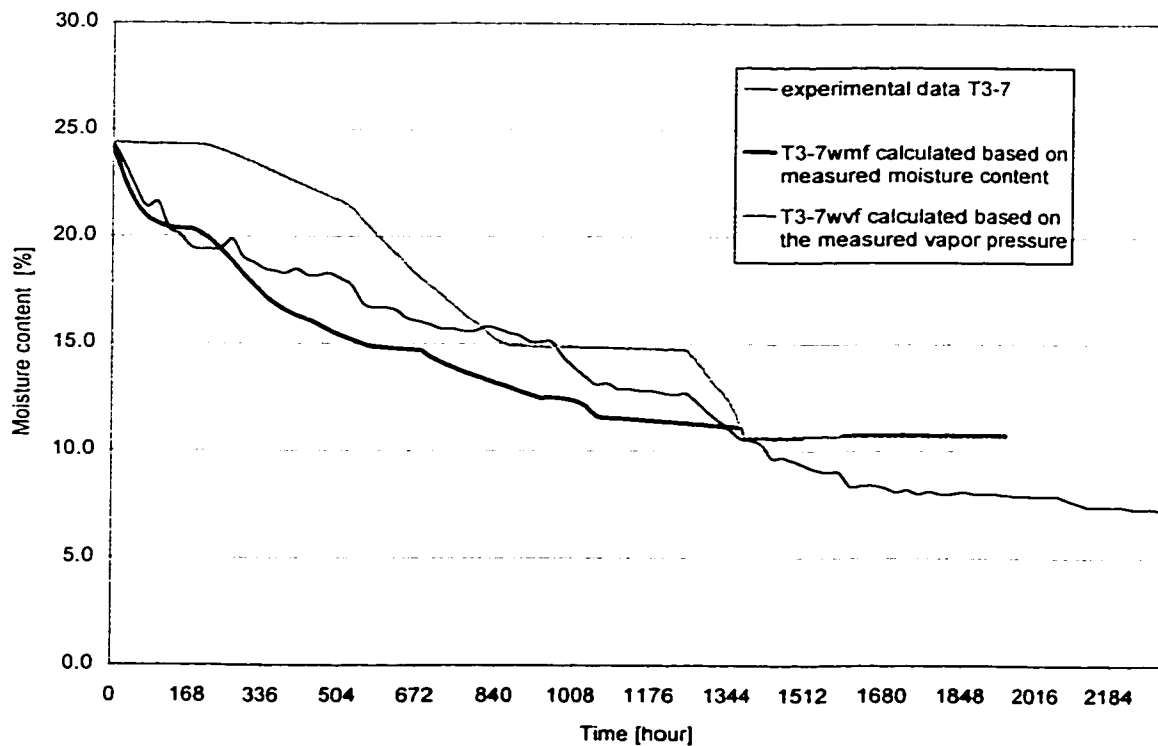


Figure 3.17. Comparison of modeling and experimental data from 24% M in T3.

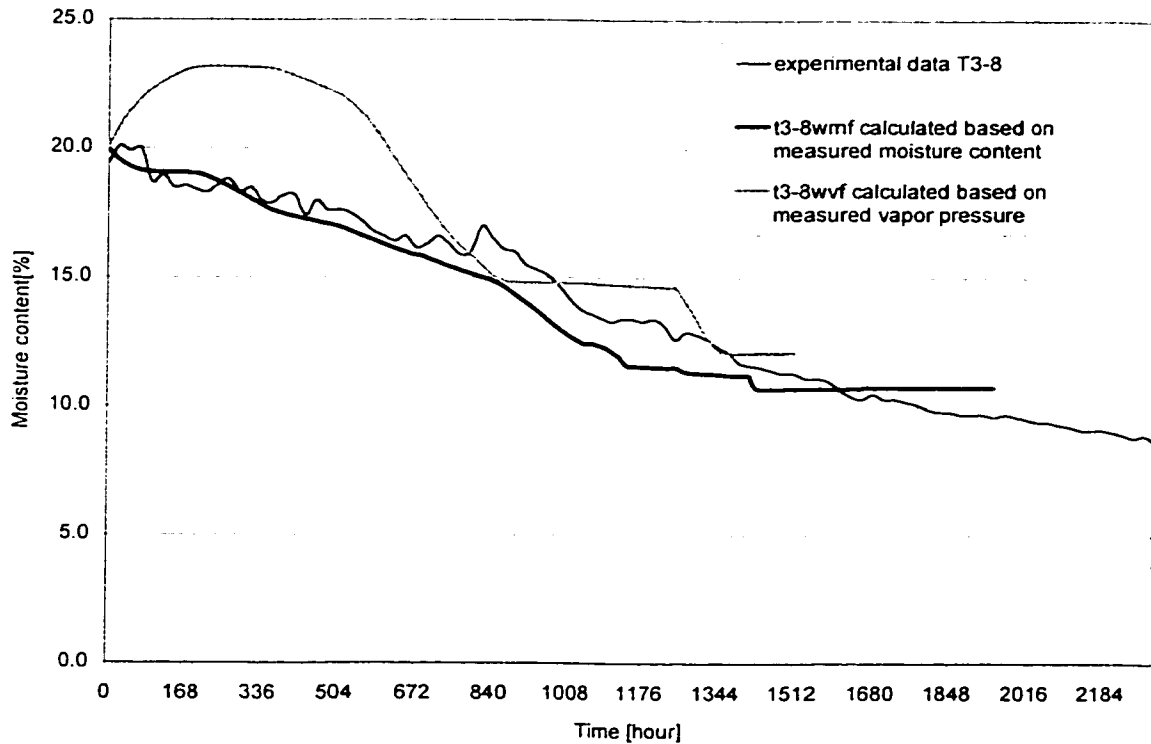


Figure 3.18. Comparison of modeling and experimental data from 20% M in T3.

The simulated drying curves using the conditions derived from the measured moisture content show a close fit for their first part, while slightly underestimate the moisture content for most of the rest of the drying. The simulated curves using the conditions derived from the measured vapor pressure show a slower drying process in the first part of the curves to then demonstrate a good fit in the middle part of the curves. The curve using the measured vapor pressure in Figure 3.18 demonstrates that the measurements done at the center of the cavity must not reflect the conditions on the side of the cavity.

• Sensitivity analysis

As the actual air velocity could not be known, the impact of the estimation of the air velocity was assessed by varying the heat and mass convective coefficients. Figure 3.19

shows a sensitivity analysis using the same input data except for the convective heat transfer coefficient, h_h , which was set successively at 2, 3.8 and 8 $\text{W/m}^2\text{°C}$. This variation has little impact on the drying curve. This result was expected as, in reality, a change of h_h would imply a change of h_ψ . The next analysis is more conclusive in this respect. Figure 3.20 shows a similar sensitivity analysis setting the mass transfer coefficient, h_ψ , at 0.5×10^{-10} , 1×10^{-10} and $2 \times 10^{-10} \text{ kg}^2/\text{m}^2 \cdot \text{s} \cdot \text{J}$. This variation results in a noticeable impact on the first part of the drying curves. Therefore, the difficulty in determining the actual air velocity has a low impact on the drying from a heat transfer point of view but an important one on drying from a mass transfer point of view. This may explain in part the differences found across the same planks as seen by the moisture content of three side by side locations at the start of the drying period. The lower moisture content in the plank near the joist could result from restrictions imposed on the air movement by the cellulose.

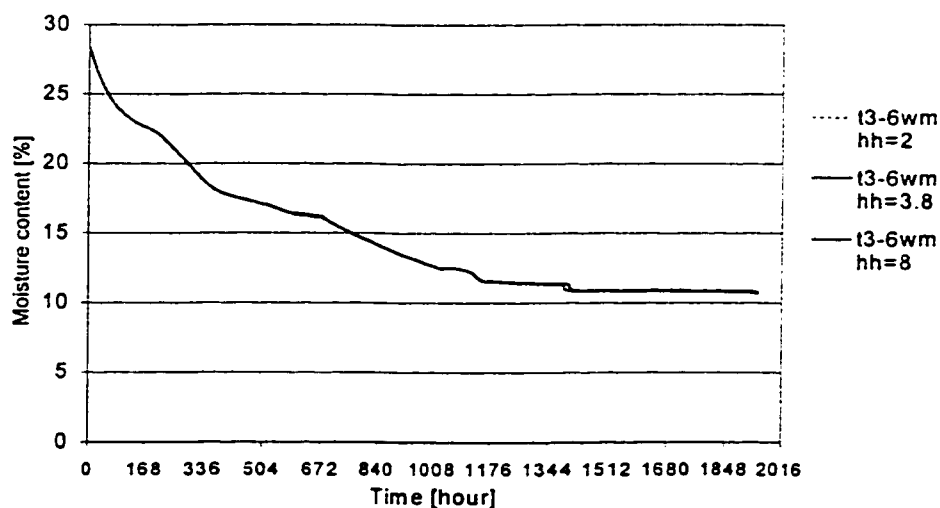


Figure 3.19. Sensitivity analysis by varying the convective heat transfer coefficient.

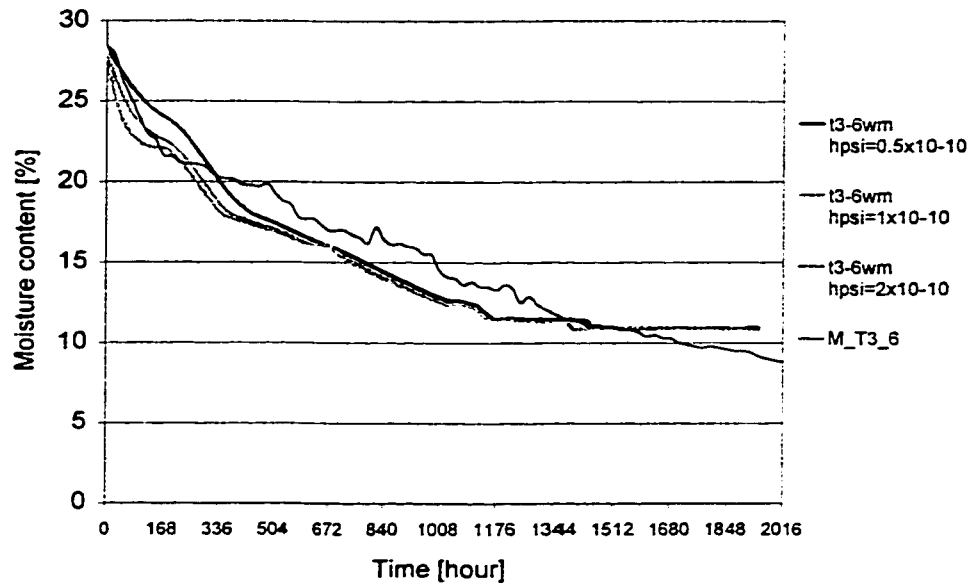


Figure 3.20. Sensitivity analysis by varying the convective mass transfer coefficient.

3.4.4 Observations on the simulation results

• Drying profiles

From the drying profiles across the thickness of the plank throughout the simulation as shown in Figure 3.21, it can be seen the gradient of moisture content is very small. The slow variation of the average relative humidity throughout drying allows the moisture content to approach equilibrium levels through the thickness of the plank. This tends to show that the long time constant associated with moisture transfer is linked to the large quantities of moisture adsorbed and desorbed within the assemblies but that relatively instantaneous uniform conditions may be maintained given a uniform source of moisture during wetting and a uniform source of heat during drying. Within the wood plank itself, the transient effect of change of conditions was minimized. The low moisture content gradients across the plank reinforce the importance of the sorption curves as one of the most valuable data used in the simulation.

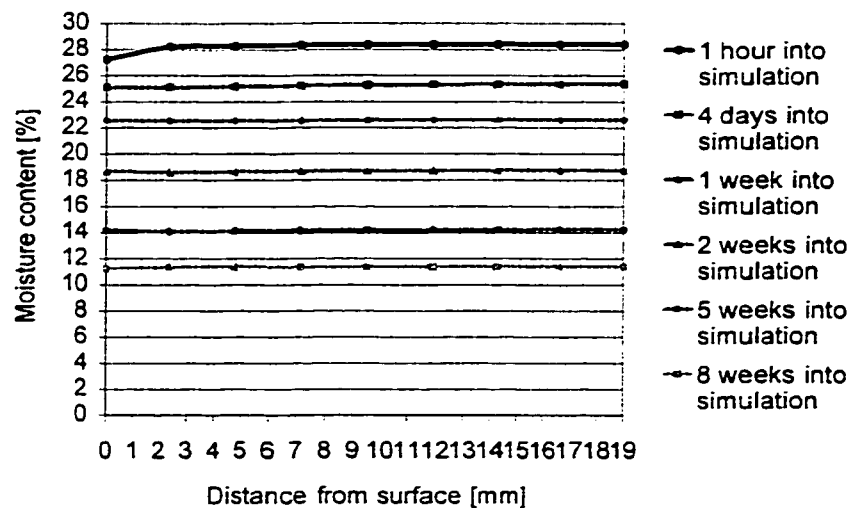


Figure 3.21. Moisture gradient across the thickness of the plank during simulation.

• Conditions cycles

This test uses steady periodic daily conditions whereas the simulation uses constant conditions. In terms of relative humidity cycling, a look at period 4 indicates that the conditions may yield a periodic mass transfer, i.e. drying during day conditions and readsorption of vapor or condensate during the night conditions. To model such a case requires the specific history of the wood to allow the use of the proper sorption curve. This periodic reversal is shown schematically in Figure 3.22. The local relative humidity may then rise and condensation may occur, decreasing the vapor pressure.

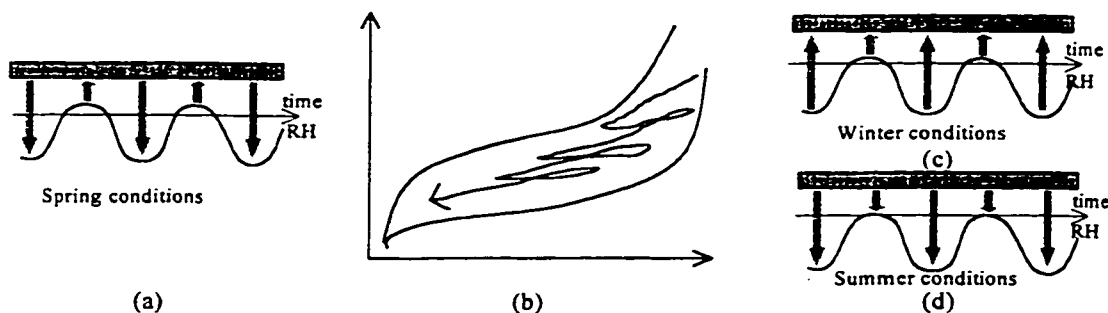


Figure 3.22. Schematic representation of the daily periodic mass transfer with an overall drying direction, (a) shows the moisture movement in and out of the plank; and (b) the corresponding sorption history. The diagrams (c) and (d) represent winter and summer conditions where no daily reversal takes place.

- Impact of warming of wood with warmer air

Due to the code structure, the temperature of the wood during simulations is a result of the interaction of the wood with the air below the plank. In reality, the wood plank is warmed by air on one side but is cooled on the other, so there is constantly a temperature gradient across the plank. The impact of this approximation is estimated to be low as the air temperature used was close to the temperature measured in the plank and also due to the fact that water potential is slightly dependent on temperature.

3.5 Validation of model for the simulation of the wetting process

The process of the wetting of wood has not attracted a lot of research effort. This thesis proposes a first attempt at modeling the moisture accumulation process using the model developed previously.

3.5.1 Determination of actual conditions during the wetting period

To model the wetting of the wood plank, the method developed in section 3.4.1 to present the actual conditions in and below the plank during the test is applied here for the first three periods of the test. The graphs of Figure 3.23 presents the data measured during the three wetting periods of the test. Table 3.20 presents the mean values for the sub-periods.

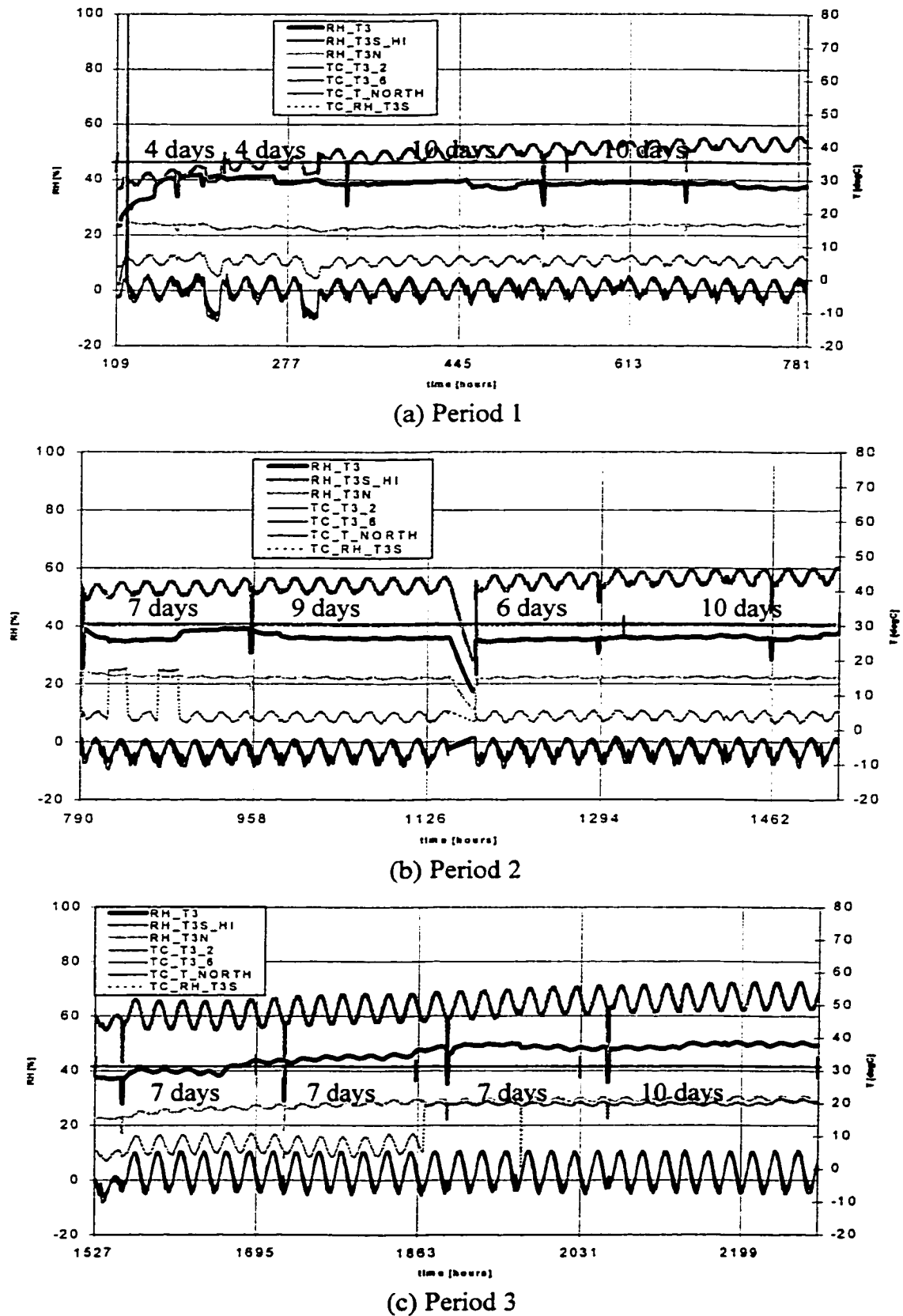


Figure 3.23. Wetting conditions measured below and in the planks of cavity T3.

Table 3.20. Measured conditions for short intervals of time within each period during wetting

	Period 1 Subdivided in 4 (4,4,10 and 10 days)	Period 2 Subdivided in 4 (7, 9, 6 and 10 days)	Period 3 Subdivided in 4 (7, 7, 7 and 10 days)
T_{mean} in wood planks [°C]	-2.0 -2.0 -3.0 -2.25	-6.25 -6.25 -6.25 -6.0	-1.0 -0.5 -0.75 -1.0
T_{mean} in insulation 50 mm below wood planks [°C]	6.0 6.0 5.5 6.0	3.25 3.75 3.75 3.85	7.5 7 7.5 7.5
Relative humidity max/min [%]	39/44 44/48 48/52 51/55	51/55 52/55 53/57 54.5/59	55/65 57/67 59/69 62/72
Mean vapor pressure at 50 mm below planks [Pa]	391 437 458 501	413 436 442 458	635 638 643 667

3.5.2 Determination of simulation conditions

The methods to extrapolate the measured conditions used in section 3.4.2 to derive the conditions below the plank were applied to the three first periods of the test and presented in Tables 3.21 and 3.22.

Table 3.21. Temperature and relative humidity inferred from measured vapor pressure.

	Period 1 Subdivided in 4 (4,4,10 and 10 days)	Period 2 Subdivided in 4 (7, 9, 6 and 10 days)	Period 3 Subdivided in 4 (7, 7, 7 and 10 days)
T_{mean} extrapolated	0.1	-3.8	1.2
below wood	0.1	-3.6	1.4
surface [°C]	-0.8	-3.6	1.4
	-0.1	-3.4	1.2
RH_{mean}	68	75.5	82.5
extrapolated	64.4	78.5	82.5
below wood	68	80.4	84.2
surface [%]	71.5	81.4	87.6

Table 3.22. Extrapolated relative humidity for T3-6.

Period	Day	Moisture content [%]	Corresponding RH from sorption curve [%]	Average RH for the sub-period [%]
Period 1	1	6	21.5	
	5	6.2	22.5	22
	9	6.7	25.5	24
	19	8	34	29.8
	29	10.4	49	41.5
Period 2	1	10.4	48	
	8	12.5	60	54
	17	14.9	70	65
	23	16.4	75.5	72.8
	33	18.6	82.4	79
Period 3	1	18.6	82.4	
	8	19.7	84.4	83.4
	15	21	86.5	85.4
	22	23.8	91	88.8
	32	28.4	96	93.5

3.5.3 Computer model simulation

The conditions used for the simulation are listed in Table 3.23 for the sensor in the center of the cavity T3. The resulting curves are presented in Figure 3.24.

Table 3.23. Wetting simulation conditions

Conditions used for each simulation							
M- ψ = adsorption curve – same all K = desorption conductivity - same for all							
h_c = assumed constant at $3.8 \text{ W/m}^2\text{°C}$ v_{air} = assumed constant at 0.1 m/s for all							
h_{ψ} = assumed constant at $1 \times 10^{-10} \text{ kg}^2/\text{s} \cdot \text{J} \cdot \text{m}^2_{\text{air}}$							
	Initial	Period 4		Period 5		Period 6	
	M	T	RH	T	RH	T	RH
	[%]	[°C]	[%]	[°C]	[%]	[°C]	[%]
T3-6	28.4	0.1	68	-3.8	75.5	1.2	82.5
RH from measured vapor pressure		0.1	64.4	-3.6	78.5	1.4	82.5
		-0.8	68	-3.6	80.4	1.4	84.2
		-0.1	71.5	-3.4	81.4	1.2	87.6
T3-6	28.4	0.1	22	-3.8	54	1.2	83.4
Extrapolated		0.1	24	-3.6	65	1.4	85.4
RH from		-0.8	29.8	-3.6	72.8	1.4	88.8
measured M		-0.1	41.5	-3.4	79	1.2	93.5

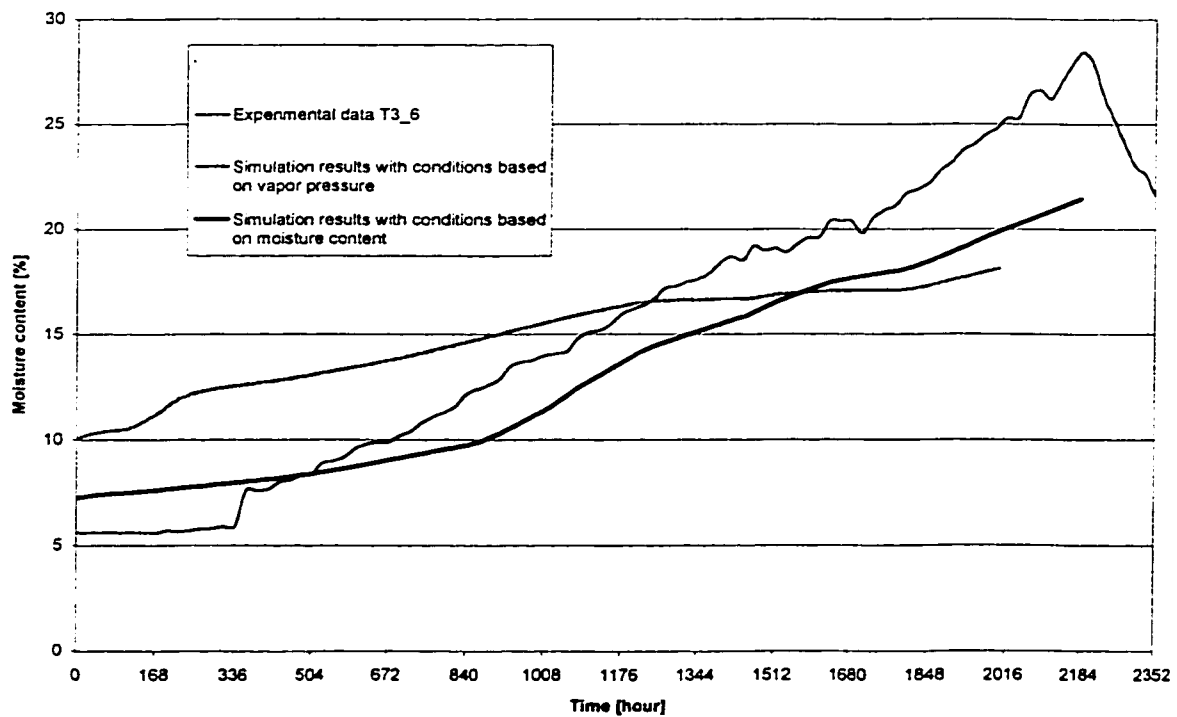


Figure 3.24. Comparison of modeling and experimental data for the wetting period in T3

The two methods developed for the drying curves do not provide satisfying fit in terms of prediction of the wetting curves. The grey curve based on the vapor pressure overestimates the moisture contents in the early portion and underestimates them in the remaining part. This may indicate that the relative humidity measured at 50 mm below the plank in winter time is very different that the relative humidity that could have been measured just underneath the plank. The thick black line curve uses the conditions based on the measured moisture content. This curves follows the general shape of the experimental curve but is markedly below, especially in the last few weeks.

The expected presence of condensation was not taken into account in the determination of the conditions and can explain some of the discrepancies between the simulated curves and the experimental data. To take condensation into consideration would require an analysis of the boundary conditions and the evaluation of the appropriateness of the equations, with special attention required to determine the factor ϵ used in equation (3.12).

3.5 Conclusion

A mathematical model was developed to describe the moisture movement of a wood plank drying within a roof assembly. The resulting computer model can predict the drying of such roofs. The use of the water potential concept lets the model focus on moisture movement as opposed to focus on the phase of the moisture required by the other approaches in modeling. The sorption history of the wood was taken into

consideration by the development of appropriate intermediary desorption curves. The results show that the model can predict the drying of the wood planks. The same methods were applied to the wetting of the planks. The results of the model point to the need to know the precise boundary conditions and to further development of the description of the physical phenomena to include the formation and presence of condensation.

This model has opened the way to the use of the gradient of water potential in the field of building envelope. One of the next developments of the model should be to integrate heat flow through the roofing membrane. This will subject the wood plank to a temperature gradient which is a more realistic condition. It will also enable to link the temperature in the assembly to the outdoor conditions. Even though it was shown not necessary to consider the daily variations of outdoor temperature to predict the drying process, it may be interesting to take into account these variations where condensation is possible.

Chapter 4

Guidelines derived from the research program

This section addresses the transfer of knowledge acquired in this research to the designers, and proposes ways to implement the findings of this research in terms of design guidelines and improved details.

4.1 How to transfer building science to the designer

The broad role of science is to provide a portrait of nature by describing and predicting natural phenomena. Building scientists aim at developing the knowledge base of building science to be used by the designer who selects and develops the best intervention for a given situation. However, the designer must be made aware of the value of science in the creation of products (Mayall, 1979). The challenge is to develop tools and packages of information that incorporate scientific knowledge and aid the decision process involved in design. The process of design requires different quantity and quality of inputs during its unfolding. One way to tailor the available information is to cater to the level of intervention in the design process of a building which are recognized to be: 1) Performance specifications (also called program or objectives), 2) Overall architectural concept, 3) Design development, 4) Detailing, and 5) Construction supervision. These five levels overlap each other and strive to fulfill the main purpose of the design process, i.e. the operation and the maintenance of a well-performing building. This process applies as well for new construction or renovation projects.

The following are two exercises to adapt the information gain through the research project to two stages of the design process, concept and detailing.

4.2 Knowledge transfer at the conceptual level of flat roof design

- Components of the roofs

Let us start by a clarification of the nomenclature used to designate the components of a wood-framed roofing system. Simply stated, a roof has four layers: the interior finish which includes the air and vapor barrier, the insulation layer, the deck supported by the main structure, and the roofing membrane to prevent rain ingress, as shown in Figure 4.1



Figure 4.1. Schematic representation of the four basic layers of a light weight flat roof system.

This study considers only flat roofs. However, as the conceptual stage encompasses the choice of the geometry of the roof, three basic geometrical roof configuration are included: (1) both the roofing layer and the interior layer are horizontal, (2) both the roofing layer and the membrane are sloping, (3) the roofing layer is sloping and the under layer is horizontal.

- Conceptual decision process

The most current design alternatives are found in the decision tree represented in Figure 4.2. Two main parameters have to be considered: a vented or not vented assembly, and an insulation below or above the roof deck.

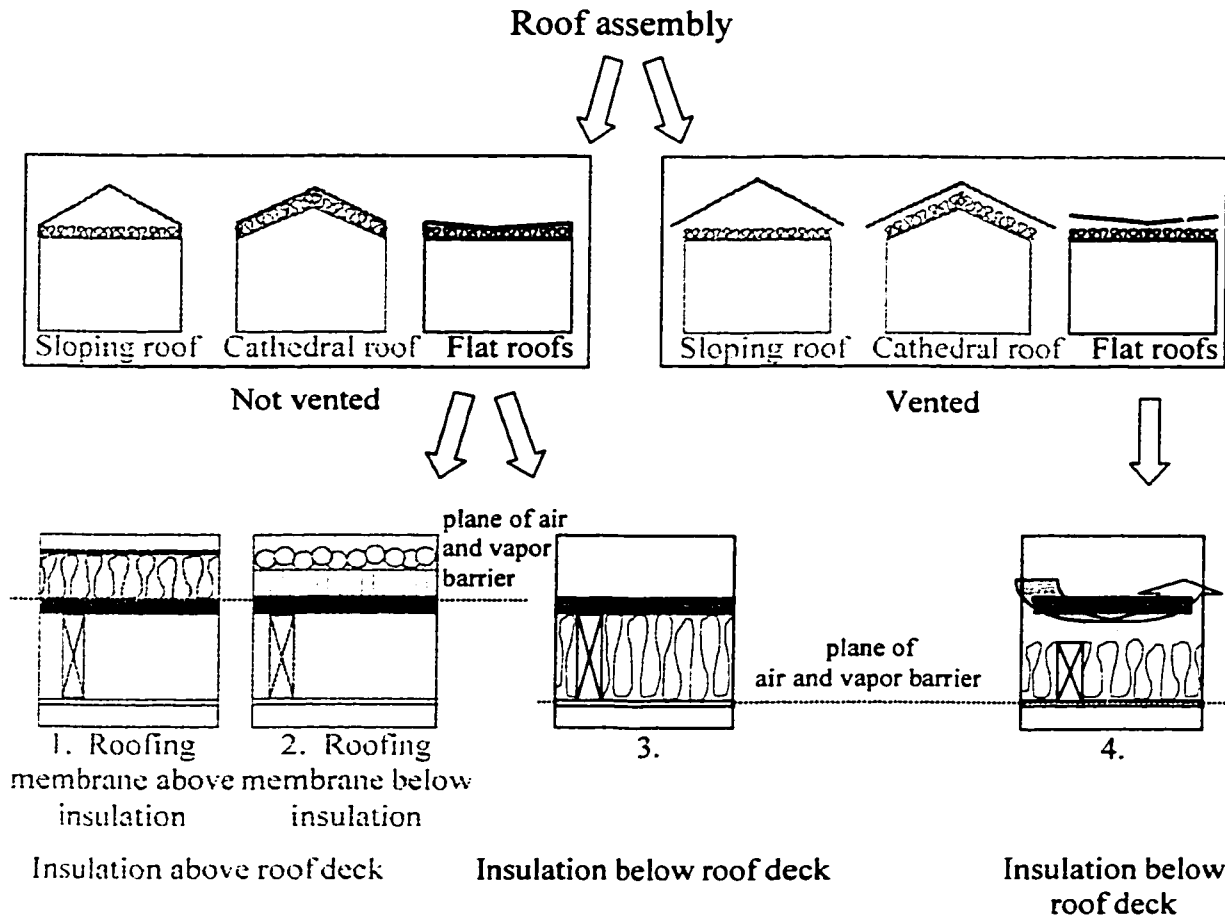


Figure 4.2. Schematic representation of the different flat roof assemblies for wood-framed buildings. 1. insulation above roof deck and below roof membrane, 2. insulation above deck and membrane, 3. insulation below roof deck without ventilation, and 4. insulation below deck, with ventilation in space between insulation and deck,

- Design guidelines

At this level of decision, the following considerations should be taken into account:

- The National Building Code of Canada (1995), in article 9.19.1.1.1, states that, when insulation is placed below the roof deck, a space is required between the insulation

and the deck and that space must be vented to the outside. This requirement makes the choice of ventilation and location of insulation interrelated. When no ventilation is desired nor possible, all the insulation should be put on top of the deck, according to the NBCC.

- The case of existing roofs that undergo renovation is not discussed by the code. The annex to the Code mentions that, where it may be demonstrated that the construction is sufficiently tight, the ventilation for insulation installed below the deck may not be required (NBCC, 1995, art. A-9.19.1.1). This provision targeted pre-manufactured houses but could be applicable elsewhere. Therefore, placing the insulation below the deck requires a very good air barrier strategy that must be assessed at the detail level.
- Once the roof air barrier strategy is taken care of, the control of vapor diffusion becomes a simple task. The solutions may be to use a polyethylene sheet behind the gypsum board or another vapor retarder membrane. In the case of retrofitting, the paint layer can act as the vapor retarder. Older buildings are often painted with oil-based vapor resistant paints and already present a certain level of vapor resistance.
- Thermal bridges must be avoided as they present cold spot within the assemblies where condensation may deposit itself.
- Condensation should not be trapped between two vapor tight materials. However, Handegord (1967) mentions the possibility of deliberately letting moisture accumulate in an absorbing material that can retain condensate until conditions favorable to evaporation prevail. Moisture in insulation will however increase heat flow. Due to the complexity of assessing the behavior of all materials, Handegord

mentioned that such a design should be usually kept for buildings with low indoor relative humidity, which seemed to exclude residential buildings. However, this research supports that some storage of moisture may occur in wood-frame assemblies with complete drying.

- A sound design principle for envelope assemblies is to have redundancy. This requires the deliberate repetition of functions by different elements against the more severe causes of degradation, *i.e.* vapor condensation and water ingress.

4.3 Knowledge transfer at the detailing level of flat roof design

At the detailing level, attention is focused on the components, the systems and the junctions of systems. Design rules must be followed to prevent moisture problems. Problems can rarely be imputed to materials but rather to their assembly and configuration (Handegord 1967).

• Focusing on preventing air leakage

The main lesson from the research work presented here is that air movement may bring large quantities of moisture within assemblies. The air may come from as far as the basement of the building as shown in Figure 4.3. Comparison of the moisture patterns of T2 and T3 illustrate the effect of air movement. While the performance of a central cavity like T3 may be found it acceptable, it is the details at junctions that are critical, as shown in T5. The problems with moisture accumulation in the cellulose are the resultant increase in weight and density and reduction of the thermal conductivity.

However, due to the presence of borax and boric acid, introduced as a flame retarder, in cellulose insulation, fungi cannot grow in cellulose.

While the short-term presence of water in wood has little impact in terms of structural capacity or dimensional changes, in the long term, it leads to the concern of biological degradation of the wood which compromises the structural member. To prevent wood from rotting could be one way to resolve the problem of moisture accumulation. In the test, the two insulated cavities exposed to high moisture content, T5 and L5, have shown no sign of fungi staining or growth found in all the wood surfaces facing the cellulose insulation, which points to the protecting ability of the borax. Cavities T1 and L1, which were not insulated, had their wood deck and some parts of the joist markedly darkened by the presence of fungi. However, the protecting ability of borax does not reach far passed its contact with wood. The presence of fungi was noted on wood surfaces that were not exposed to cellulose, like the top of the joist covered with deck planks and the underside of the joist resting on the top plate of the wall.

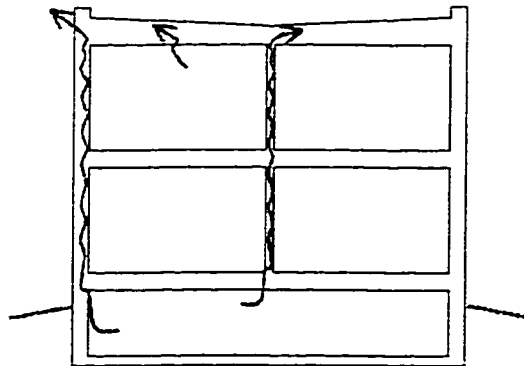


Figure 4.3. Schematic representation of air leakage through a building from basement to roof.

- Building envelope details

The addition of cellulose insulation to fill completely the cavities must be accompanied with the strong improvement of the airtightness at the level of the roof. The air barrier strategy rests on the appropriate detailing of joints. The main details to consider are the junction of the exterior wall with the roof also called parapet, the junction of the roof with internal partitions, the connection of the roof with mechanical parts connection, connection of roof with electrical fixtures or communication wiring. The following figures propose improvement to existing details.

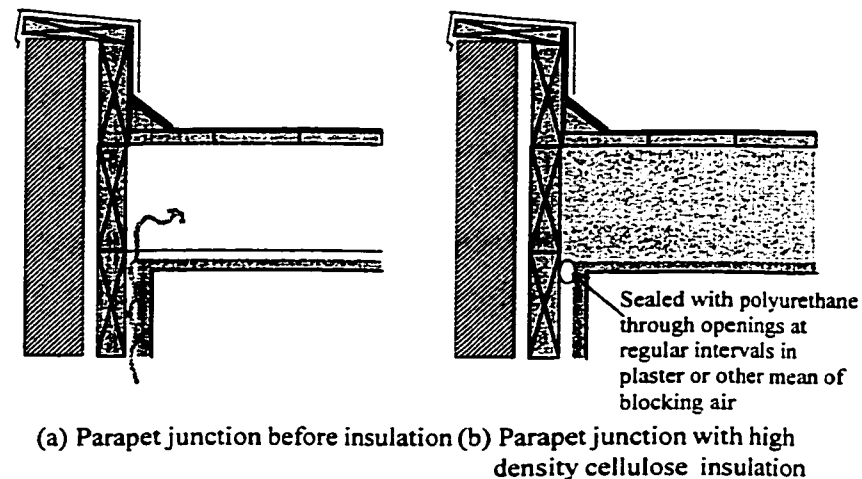


Figure 4.4. Parapet details before and after the installation of the insulation with detailing in order to minimize air flow through the roof.

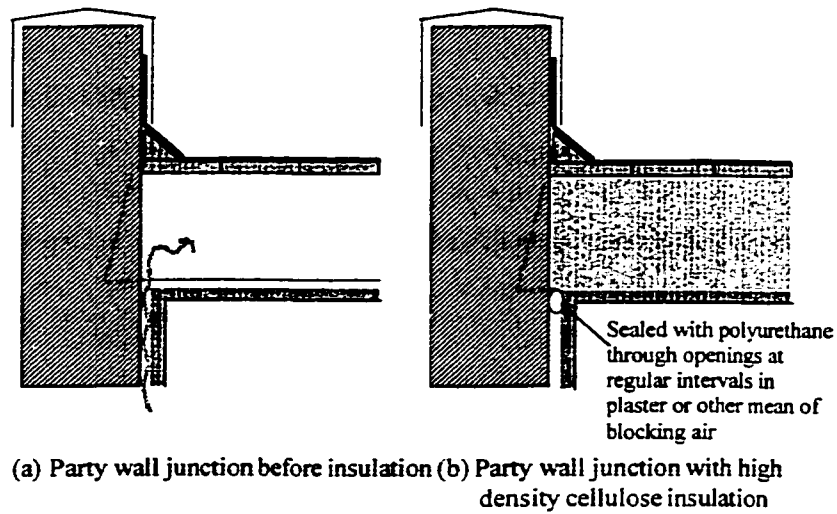


Figure 4.5. Party wall details before and after the installation of the insulation.

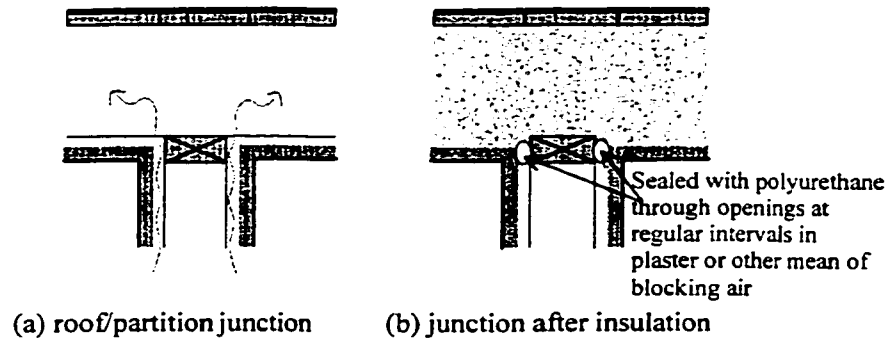


Figure 4.6. Roof/parapet details before and after the installation of the insulation.

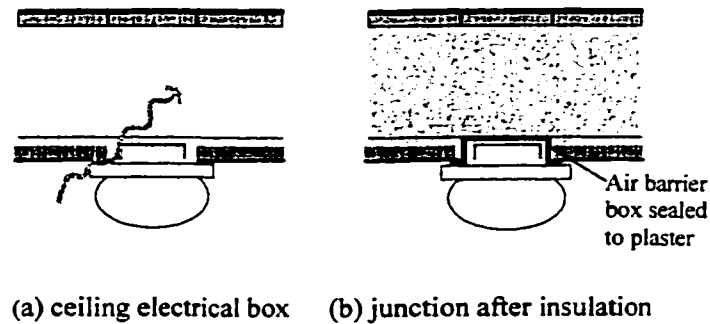


Figure 4.7. Electrical outlet details before and after the installation of the insulation.

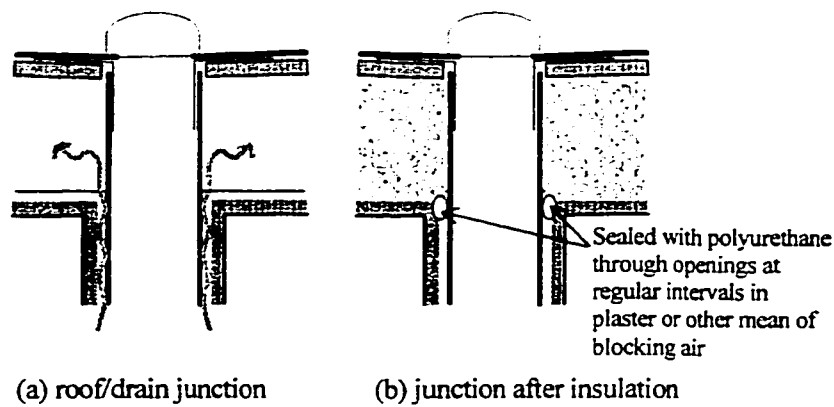


Figure 4.8. Roof drain details before and after the installation of the insulation.

4.4 Conclusion

To produce the information to designers in terms of the decision that they have to take may be the most efficient route to transfer knowledge to the industry. Designers do not always have the time nowadays to study all that there is to know on one specific building assembly, however they are opened to improve their design and integrate new knowledge that could improve their practice. The proposed details should be further developed and implemented where high density cellulose is used to insulate flat roofs.

The guidelines and details proposed here assist the designer in providing a thought-through design from an air barrier point of view. In the scope of a project, other considerations, like membrane reliability, waterproofing details, and climate in terms of rain and snow, may suggest other solutions. Therefore, the details presented here show the principles but are not complete in other aspects and should not be copied directly.

Chapter 5

Conclusion

This investigation on moisture movement through the building envelope has reaffirmed the importance of this field of study and the need to advance its state of knowledge.

In the rapidly evolving field of moisture movement in the building envelope, the most advanced research deals with extensive experimental set-ups to study the interaction of actual assemblies with climate conditions, and modeling work to perform advanced simulation of the heat, air and moisture transfer requiring a large amount of data on material properties and conditions. It is recognized that the field thrives most when experimentation and modeling are combined.

This study has advanced this field of study by developing:

- an experimental procedure and producing the experimental results on 10 flat roof assemblies which can be used to validate current theories;
- a physical model which has been implemented into a computer model that can predict the moisture pattern of the wood planks in the assemblies tested;
- preliminary design guidelines and details to facilitate the transfer of the findings of this study to the design profession and to the construction site.

5.1 Contributions of the research

The experimental program has advanced the field of study of moisture movement through building envelope through the following contributions:

- Development of a novel test procedure for the evaluation of assemblies susceptible to moisture accumulation. The considerations of the research objectives led to the development of an extensive monitoring protocol using both electronic and manual methods, with emphasis on moisture transfer. The test huts reproduced actual roofs as closely as possible.
- Production of a unique set of data on moisture patterns of ten flat roof assemblies subjected to a full wetting-drying cycle. The experiment was held continuously for 190 days. The data collected gathers temperature, moisture content, relative humidity and pressure differentials and the exact location of all points of measurement. This set of data could be used to validate other models as it is one of the only sets of experimental results of an assembly incorporating cellulose insulation.
- Demonstration of performance of flat roof assemblies fully insulated with cellulose in terms of accumulation of moisture and potential to rot. Demonstration of rate of wetting and drying of different assemblies with and without air exfiltration. Data on the performance of cellulose insulation in assemblies exposed to moisture accumulation.

The modeling work has advanced this field through the following contributions:

- Development of a physical model using the water potential gradient as the driving force. The physical model predicts the drying and wetting of wood planks in flat roofs. Its development includes the analytical and experimental determination of the appropriate heat and mass convective transfer and the determination of the effective water conductivity function. The physical model uses full and intermediary adsorption and desorption curves respecting the sorption history of the wood plank being modeled.
- Validation of the physical model with a computer model, modified to implement the developed physical model, used to predict the moisture pattern in the roof wood plank tested. This work validates the use of the water potential approach to model moisture pattern within building envelope assemblies.

The research has contributed to the transfer of information through preliminary design guidelines and details intended to the design profession and the building industry for wood-frame assemblies with a moisture storing insulation layer.

5.2 Recommendations for further work

Through this work, a clearer picture of future work has emerged to guide future research which should direct its effort to provide:

- Measurement on building envelope material to document their hygrothermal properties and the impact of moisture content of these properties.

- Measurement of boundary conditions within assemblies in terms of temperature, relative humidity, air velocity, etc., to allow the determination of the heat and mass transfer coefficients present in the small air spaces and the porous materials within envelope assemblies.
- Experimental data on assemblies containing cellulose insulation to study the impact of moisture accumulation on the thermal resistance of the assembly, specially with moisture conditions that lead to the gradual caking of the cellulose, impact of density of cellulose on thermal resistance and air movement.
- Experimental comparison of behavior of ventilated and non-ventilated roofs insulated with cellulose.
- Application of the model developed to study the impact of different climate conditions, different initial moisture content and to study the impact of the time compression used in the wetting portion of the test presented herein.
- Further development of modeling should aim at modeling condensation and frost thaw to demonstrate the applicability of the water potential gradient to describe capillary action, daily cycle with appropriate adsorption and desorption curves, and interaction of wood and cellulose. Further modifications should allow different boundary conditions on each side and attempt to link condition on both sides of the assembly to the air temperature and relative humidity within the assembly.

5.3 Related publications

- Derome, D. and P. Fazio. Large scale testing of two flat roof assemblies insulated with cellulose, accepted for publication by the Journal of Architectural Engineering (March 2000), ASCE.
- Fazio, P. and Derome, D. (1999) Tested performance of cellulose insulation in flat roofs, Fifth Symposium on Building Physics in the Nordic Countries, Aug. 24-26, Göteborg, Sweden, pp. 401-408.
- Derome, D., Fortin, Y., and Fazio, P. (1999) Détermination des coefficients de transfert de masse et de chaleur pour le transfert d'humidité sous un platelage de toit en bois, IVe Colloque Interuniversitaire Franco-Québécois, Thermique des systèmes à température modérée, May 25-27, Montreal, Quebec, pp. 301-308.
- Fazio, P.; D. Derome; D. Gerbasi; A. Athienitis; and S. Depani. 1998. Testing of flat roofs insulated with cellulosic fiber. *Proceedings of Thermal Performance of the Exterior Envelopes of Buildings VII*, ASHRAE/BETEC/CIBSE/ORNL/DOE/NRCC, Dec.7-11, Clearwater Beach, Fl, USA, ASHRAE, Atlanta, pp.1-11.
- Derome, D., P. Fazio et A. Athienitis. 1997. Techniques de mesures du transfert combiné de la chaleur et de l'humidité à travers des toits plats, Thermique des systèmes à température modérée, Toulouse, May.
- Fazio, P. , D. Derome, A. Athienitis, and J. Rao. 1997. Use of an environmental chamber to investigate large-scale envelope specimen hygrothermal performance, presented to ICBEST '97, Bath, April.

References

- Andersson, A.-C. 1985. Verification of calculation methods for moisture transport in porous building materials, D6:1985, Swedish Council for Building Research, Stockholm, 223 p.
- ASHRAE. 1997. Handbook of Fundamentals, ASHRAE, Atlanta.
- ASTM. 1980. Standard test methods for water vapor transmission of materials. Standard E96, American Society for Testing and Materials, Philadelphia.
- ASTM. 1983. Standard test method for steady-state thermal performance of building assemblies by means of a guarded hot box. Standard C236, American Society for Testing and Materials, Philadelphia.
- ASTM. 1988. Standard test method for determining air leakage rate by fan pressurization. Standard E779. American Society for Testing and Materials, Philadelphia.
- ASTM. 1990. Standard test method for thermal performance of building assemblies by means of a calibrated hot box. Standard C976, American Society for Testing and Materials, Philadelphia.
- ASTM. 1991a. Standard test method for determining the rate of air leakage through exterior windows, curtain walls, and doors under specified pressure differences across the specimens. Standard E283. American Society for Testing and Materials, Philadelphia.
- ASTM. 1991b. Standard test method for determining the rate of air leakage through exterior windows, curtain walls, and doors under specified pressure and temperature differences across the specimen. Standard E1424, American Society for Testing and Materials, Philadelphia.
- ASTM. 1993. Standard test methods for determining air change in a single zone by means of a tracer gas dilution. Standard E741. American Society for Testing and Materials, Philadelphia.
- Athienitis, A. K., M. Stylianou and J. Shou. 1990. A methodology for building thermal dynamics studies and control applications, Transactions, ASHRAE, Vol. 96, SL-90-14-4.
- Auger, J. and Roquet, N. 1998. Mémoires de bâtisseurs du Québec, Éditions du Méridien, Montréal, in print.
- Birley, A.W., Haworth, B., Batchelor, J. 1991. Physics of Plastics Processing, Properties and Materials Engineering, Hanser Publishers, Munich, 1991, 528 p.

- Bomberg, M. and Brown, W.C. 1993. Building envelope: heat, air and moisture interactions, *Journal of Thermal Insulation and Building Envelopes*, Technomic Publishing Co., Mancaster, PA, Vol. 16, April, pp. 306-311.
- Brown, W.C. and Poirier, G.F. 1988. Testing of air barrier systems for wood frame walls, Report no. CR5505.1, Canada Mortgage and Housing Corporation, Ottawa, 81 p.
- Brown, W.C. and Stephenson, D.G. 1993a. A guarded hot box procedure for determining the dynamic response of full-scale wall specimens – part 1, *Transactions, ASHRAE*, V. 99, pt. 1, 3683 (RP-515).
- Brown, W.C. and Stephenson, D.G. 1993b. A guarded hot box measurements of the dynamic heat transmission characteristics of seven wall specimens – part 2, *Transactions, ASHRAE*, V. 99, pt. 2, 3684.
- Bumbaru, D., Jutras, R., Patenaude, A. 1988. Air permeance of building materials, Canada Mortgage and Housing Corporation, Ottawa, 76 p.
- Burch, D.M., Thomas, W.C., Mathena, L.R. 1989. Transient moisture and heat transfer in multilayer non-isothermal walls – comparison of predicted and measured results. *Proceedings of the ASHRAE/DOE/BTECC/ CIBSE Conference. Thermal performance of the exterior envelopes of building IV*, Orlando, Florida, pp. 513-531.
- Burch, D.M., Thomas, W.C. 1992. An analysis of moisture accumulation in a wood-frame wall subjected to winter climate. *Proceedings of the ASHRAE/DOE/BTECC Conference. Thermal performance of the exterior envelopes of building V*, Clearwater Beach, Florida, pp. 467-479.
- Burch, D.M., Chi, J. 1997. MOIST A PC Program for Predicting Heat and Moisture Transfer in Building envelope Release 3.0, NIST Special Publication 917, National Institute of Standards and Technology, Washington, 47 p.
- Catalog of Material Properties. Report Annex XIV.
- CGSB. 1986. Determination of the airtightness of building envelopes by the fan depressurization method. CGSB Standard, 149.10-M86. Canadian General Standards Board, Ottawa.
- Cloutier, A. 1991. Modélisation du séchage du bois basée sur le concept de potentiel hydrique. Ph.D. Thesis, Laval University, Québec, 275 p.
- Cloutier, A. and Fortin, Y. 1991. Moisture content-water potential relationship of wood from saturated to dry conditions, *Wood Science and Technology*, Springer-Verlag, No. 25, pp.263-280.

- Cloutier, A., Fortin, Y., Dhatt, G. 1992. A wood drying finite element model based on the water potential concept, *Drying technology*, Marcel Dekker inc., Vol. 10, No. 5, pp. 1151-1181,s (invited paper on a theme issue on wood).
- Cloutier, A. and Fortin, Y. 1993. A model of moisture movement in wood based on water potential and the determination of the effective water conductivity, *Wood Science and Technology*, Springer-Verlag, No. 27, pp. 95-114.
- Cloutier, A. and Fortin, Y. 1994. Wood drying modelling based on the water potential concept: hysteresis effects. *Drying Technology*, Marcel Dekker inc., Vol.12, No. 8, pp. 1793-1814.
- Cloutier, A. 1995. Wood drying modeling progress report. Project No. 3312K200, Canadian Forest Service No. 26, Forintek Canada Corp., Sainte-Foy, Québec, pp 1-44.
- Colliver, D.G., Murphy, W.E, Sun, W. 1994. Development of a building component air leakage data base. *ASHRAE Transactions* 100(1): 292-305.
- Comstock, G.L. 1963. Moisture diffusion coefficients in wood as calculated from adsorption, desorption, and steady state data. *Forest Products Journal*, March, pp. 97-103.
- CONDENSE. 1998. Program, AutoCAD application, SIRICON, Montreal.
- Darcy, H. 1856. Les fontaines publiques de la ville de Dijon. Exposition et application des principes à suivre et des formules à employer dans les questions de distribution d'eau, Victor Dalmont ed., Paris.
- Desjarlais et al. 1986. Development of a building component air leakage data base. *ASHRAE Technical Data Bulletin Thermal performance of building components - a collection of papers from ASHRAE meetings*, Vol. 2, No. 5, pp. 140-153.
- Desjarlais, A.O., Kyle, D.M., Christian, J.E. 1993. The simulated impact of climate on the drying times of a wetted low-slope roof system. *Journal of Thermal Insulation and building envelopes*, Technomic Publishing Co., Mancaster, PA, USA, Vol. 16 / Jan, pp. 234-245.
- Duff, J.E. 1968. Moisture distribution in wood-frame walls in winter. *Forest Products Journal*, Forest Products Research Society, Vol. 18, No. 1, pp. 60-64.
- Dumont, R. 1993. Wood frame wall moisture accumulation study. Saskatchewan Research Council, SRC Publ. No. 1-4800-25-C-93, 31 p.

- Fazio, P., Athienitis, A.K., Marsh, C., Rao, J. 1997. An environmental chamber for investigation of building envelope performance, ASCE Journal of Architectural Engineering, American Society of Civil Engineers, New York, USA, June, Vol. 3, No. 2, pp. 97-102.
- Forest, T.W. 1989. Moisture transfer through walls, Proceedings of the ASHRAE/DOE/BTECC/ CIBSE Conference. Thermal performance of the exterior envelopes of buildings IV. Orlando, Florida. American Society of Heating, Refrigerating and Air-Conditioning Engineers, pp. 532-542.
- Fortin, Y. 1979. Moisture content-matric potential relationship and water flow properties of wood at high moisture contents. Ph.D. dissertation, The University of British Columbia, Vancouver, 187 p.
- Fournier, F. J.-L. 1976. Diffusion de l'humidité dans le bois de 20° à 95° en fonction de son état de sorption. Note de recherches no. 16, Département d'exploitation et utilisation des bois, Université Laval, Québec, juin, 63 p.
- Gagné, A. 1997. Private communication, November.
- Gerbasi, D. to be published.
- Geving, S., Karagiozis, A., Salonvaara, M. 1997. Measurements and two-dimensional computer simulations of the hygrothermal performance of a wood frame wall, Journal of Thermal insulation and building envelopes, Technomic Publishing Co., Mancaster, PA, USA, Vol. 20 / April, pp. 301-319.
- Glaser, H. 1959. Graphisches Vefrhren zur Untersuchung von Diffusionsvorgangen. Kälte Technik, No. 10, pp. 345-349.
- Goulet, M. 1968. Phénomènes de second ordre de la sorption d'humidité dans le bois au terme d'un conditionnement de trois mois à température normale. Seconde partie: essais du bois d'érable à sucre en compression radiale. Notes de recherches no 3, Département d'Exploitation et Utilisation des bois, Université Laval, Québec, mars, 29 p.
- Hagentoft, C.-E. and Harderup, E. 1995. Moisture conditions in a north-facing wall with cellulose loose-fill insulation : construction with and without a vapor retarder and air leakage. ASHRAE Transactions, ASHRAE, Atlanta, Vol. 101, Part 1, pp. 639-646.
- Hedlin, C.P. 1966. Sorption isotherms of twelve woods at subfreezing temperatures. Forest Products Journal, Dec., Vol. 17, No. 12, pp. 43-48.

- Hedlin, C.P. 1988. Heat transfer in a wet porous thermal insulation in a flat roof, *Journal of Thermal insulation*, Technomic Publishing Co., Mancaster, PA, USA, Vol. 11, January, pp. 165-188.
- Hens, H. 1995. Heat, air, and moisture transfer in envelope parts: the international energy agencies ANNEX 24 common exercises. *Proceedings of the DOE/ORNL/ASHRAE/BETEC Conference, Thermal Performance of the Exterior Envelopes of Buildings VI.*, American Society of Heating, Refrigerating and Air-Conditioning Engineers, Clear Water, Florida, pp. 321-332.
- Hens, H. 1996. IEA ANNEX 24 Heat, air and moisture transfer through new and retrofitted insulated envelope parts (Hamtie) - Final report – Volume 1 - Task 1 Modelling, International energy agency, 90 p.
- Hens, H. and Janssens, A. 1992. EA ANNEX 24 Heat, air and moisture transfer through new and retrofitted insulated envelope parts (Hamtie) - Taks 1 Modelling Enquiry on HAMCaT codes, Report T1-B-92/01, International energy agency, 23 p.
- Hillel, D. 1971. *Soil and water. Physical principles and processes*, Academic Press, New York, London, 288p.
- Hokoi, S. and Kumaran, M.K 1993. Experimental and analytical investigations of simultaneous heat and moisture transport through glass fiber insulation, , *Journal of Thermal Insulation and building envelopes*, Technomic Publishing Co., Mancaster, PA, USA, Vol. 11 /Jan., pp. 263-292.
- Handegord, G.O. 1967. Moisture considerations in roof design. CBD 73, Canadian Building Digest, NRC, DBR Ottawa.
- Hutcheon, N.B. 1966. Requirements for exterior walls. CBD 48. Canadian Building Digest, NRC, DBR Ottawa.
- Hutcheon, N. and Handegord, G. 1983. *Building Science for a Cold Climate*, Construction technology Centre Atlantic inc., Fredericton.
- Incropera, F.P. and DeWitt, D.P. 1996. *Fundamentals of Heat and Mass Transfer*, John Wiley & Sons, New York, 885 p.
- ICA. Institute of Construction and Architecture of SAS, Department of Building Physics, Slovakia, data.
- Janssens, A., Hens, H., Silberstein, A. 1995. A study of parameters influencing the hygric behavior of insulated sloped roofs without air barrier. *Proceedings of the DOE/ORNL/ASHRAE/BETEC Conference, Orlando, FL, Thermal Performance of the Exterior Envelopes of Buildings IV.* 111-118.

- Janssens, A., Hens, H., Silberstein, A., Boulant, J. 1992. The influence of underroof systems on the hygrothermal behavior of sloped insulated roofs. Proceedings of the ASHRAE/DOE/ BTECC Conference. Thermal performance of the exterior envelopes of building V, ASHRAE, Clearwater Beach, Florida, pp. 368-378.
- Karagiozis, A., Salonvaara, M. 1995. Influence of material properties on the hygrothermal performance of a high-rise residential wall. ASHRAE Transactions, ASHRAE, Atlanta, Vol. 101, Part 1, pp. 647-655.
- Kerestecioglu, A. 1989. Detailed simulation of combined heat and moisture transfer in building components. Proceedings of the ASHRAE/DOE/BTECC/ CIBSE Conference. Thermal performance of the exterior envelopes of building IV, American Society of Heating, Refrigerating and Air-Conditioning Engineers, Orlando, Florida, pp. 477-491.
- Kisseloff, P. 1969. Feuchtigkeitsbewegung und Wärmeleitung in Holz. Holz als Roh- und Werkstoff, Vol. 27, No. 7, pp. 245-253. Aussi: 1970, Transmission d'humidité et conduction thermique dans le bois. Traduction no. 10, Département d'Exploitation et Utilisation des Bois, Université Laval, 27 p.
- Kohonen, R. 1984. A method to analyze the transient hygrothermal behaviour of building materials and components. Publication 21, Technical Research Centre of Finland, Espoo, 88 p.
- Kohonen, R. 1985. Thermal effects of airflows and moisture on exterior wall structures. Proceedings of the ASHRAE/DOE/ BTECC Conference. Thermal performance of the exterior envelopes of buildings III, American Society of Heating, Refrigerating and Air-Conditioning Engineers, Clearwater Beach, Florida, pp. 583-605.
- Kollman, F.F.P. and Côté, W.A. 1968. Principles of wood science and technology. Vol. I Solid Wood, Springer-Verlag, New York.
- Kreith, F. 1986. Principles of Heat Transfer. Intext Educational Publishers, New York, 656 p.
- Kübler, H. 1957. Studien über die Holzfeuchtebewegung. Holz als Roh-und Werkstoff, Vol. 15, No. 11, pp. 453-468. Aussi 1958, Studies on the movement of moisture through wood. Translation no. 120, Department of Northern Affairs and national Resources, Forestry Branch, Forest Products Laboratories Division, Canada, 36 p.
- Kumaran, M.K. 1988. Comparison of simultaneous heat and moisture transport through glass-fibre and spray-cellulose insulations. Journal of Thermal Insulation, Technomic Publishing Co., Mancaster, PA, USA, Vol. 12 / July, pp. 6-16.

- Kumaran, M.K. 1992. Heat, air and moisture transport through building materials and components : can we calculate and predict? Proceedings of the 6th conference on Building Science and Technology, University of Waterloo, pp. 103-144.
- Kumaran, K. 1996. Taking guess work out of placing air/vapor barriers. Canadian Consulting Engineer, March/April, pp. 32-34.
- Künzel, H.M. 1995. Simultaneous heat and moisture transport in building components. One- and two-dimensional calculation using simple parameters. IRB Verlag Fraunhofer-Informationszentrum Raum und Bau, Stuttgart, 102 p. + tables and figures.
- Lawton, M. and Quirouette, R.L. 1991. Research project Testing of air barriers construction details, Report no. 30121.OR/2, Canada Mortgage and Housing Corporation, Ottawa, 44 p.
- Leblanc, R. and Patenaude, A. 1991. Airtightness tests on components used to join different or similar materials of the building envelope, Canada Mortgage and Housing Corporation, Ottawa, 69 p.
- Lewis, T., Andert, G., Calder, P., Gamma, E., Pree, W., Rosenstein, L., Schmucker, K., Weinand, A. and Vlissides, J.M. 1995. Object-oriented application frameworks, Manning, Greenwich, CT, 344 p.
- Mahdavi, A. and Lam, K.P. 1993. Dynamic analysis and visualization of water vapor diffusion through building components, ASHRAE Transactions : Research, ASHRAE, Atlanta, Vol. 99, no. 1, pp. 288-296.
- Matsumoto, M. 1994. Simultaneous heat and moisture transfer during freezing-melting in building materials, Proceedings CIB-W40 Sopron meeting, Sept. 6-8 1993, Publication 173, CIB.
- Mayall, W.H. 1979. Principles in design. Van Nostrand Reinhold Company, London, 189 p.
- McKay, M.C., Chevrier, A., Quirouette, R.L. 1993. Research project Testing of air barriers construction details II, Report no. 32173.03/1, Canada Mortgage and Housing Corporation, Ottawa, 24 p.
- Mitalas, G.P. and Arsenault, J.P. 1972. FORTRAN IV program to calculate z-transfer functions for the calculation of transient heat transfer through walls and roofs. DBR Computer Program no. 33. Ottawa, National Research Council.
- Moschler, W.W. and Martin, R.E. 1968. Diffusion equation solutions in experimental wood drying, Wood Science, Vol. 1, No. 1, pp. 47-56.

- Model National Energy Code of Canada for houses. 1997. Canadian Commission on Building and Fire Codes, National research Council of Canada, Ottawa.
- National Building Code for Canada, 1990, Institute for construction, National Research Council of Canada, Ottawa.
- National Building Code for Canada, 1995, Institute for construction, National Research Council of Canada, Ottawa.
- Ojanen, T. 1988. Combined diffusive and convective heat and mass transfer in building structures. Licentiate paper. School of technology, Dep. Of Mech. Eng. , Espoo, 115 p. (referred in Ojanen et al 1989)
- Ojanen, T. and Kohonen, R. 1989. Hygrothermal influence of air convection in wall structures. Thermal performance of the exterior envelopes of buildings IV ASHRAE/DOE/BTECC/ CIBSE, ASHRAE, pp. 234-249.
- Ojanen, T., Salonvaara, M., Kohonen, R., Nieminen, J. 1989. Moisture transfer in building structures : numerical methods /Kosteuden siirtyminen rakenteissa Laskentamenetelmät. Technical Research Center of Finland, Report no. 595, 113 p. (english translation by IRC).
- Ojanen, T. and Kohonen, R.O. 1995. Hygrothermal performance analysis of wind barrier structures, ASHRAE Transactions, ASHRAE, Atlanta, Vol. 101, Part 1, pp. 595-606.
- Ojanen, T. and Simonson, C. 1995. Convective moisture accumulation in structures with additional inside insulation, Proceedings of the DOE/ORN/ASHRAE/BETEC Conference, Thermal Performance of the Exterior Envelopes of Buildings VII, Clearwater, Florida, American Society of heating, Refrigerating and Air-Conditioning, Engineers, Atlanta, pp. 745-752.
- Onysko, D.M. and Jones, S.K. 1989. Airtightness of wall sheathing as a function of lumber drying. Proceedings of the ASHRAE/DOE/BTECC/CIBSE Conference, Orlando, FL, Thermal Performance of the Exterior Envelopes of Buildings IV., 458-474.
- Peralta, P.N. 1995. Sorption of moisture by wood within a limited range of relative humidities. Wood and Fiber Science, Society of Wood Science and Technology, vol. 27, no. 1, pp. 13-21.
- Peralta, P.N. 1996. Moisture sorption hysteresis and the independent-domain theory: the moisture distribution function. Wood and Fiber Science, Society of Wood Science and Technology, vol. 28, no. 4, pp. 406-410.

- Peralta, P.N. and Bangi, A.P. 1998a. Modeling wood sorption hysteresis based on similarity hypothesis. Part I. Direct approach.. Wood and Fiber Science, Society of Wood Science and Technology, vol. 30, no. 1, pp. 48-55.
- Peralta, P.N. and Bangi, A.P. 1998b. Modeling wood sorption hysteresis based on similarity hypothesis. Part II. Capillary-radii approach.. Wood and Fiber Science, Society of Wood Science and Technology, vol. 30, no. 2, pp. 148-154.
- Persily, A.K., Grot, R.A., Fang, J.B., Chang, Y.M. 1988. Diagnostic techniques for evaluating office building envelopes, ASHRAE Transactions, ASHRAE, Atlanta, Vol. 94, Part. 1, pp. 987-1004.
- Regulation respecting energy conservation in buildings. 1992. E-1.1, r. 1, Éditeur officiel du Québec.
- Robinson, T. 1992. Moisture challenges in canadian energy efficient housing, Journal of Thermal Insulation and building envelopes, Technomic Publishing Co., Mancaster, PA, USA, Vol. 16 / Oct, pp. 112-120.
- Rode Pedersen, C. 1990. Combined heat and moisture transfer in building constructions. Report no. 214, Thermal Insulation Laboratory, Technical University of Denmark, Lyngby, 132 p.
- Rode, C. and Burch, D. 1995. Empirical validation of a transient computer model for combined heat and moisture transfer. Proceedings of the DOE/ORNL/ASHRAE/BETEC Conference, Thermal Performance of the Exterior Envelopes of Buildings VI, American Society of Heating, Refrigerating and Air-Conditioning Engineers, Clearwater, Florida, pp. 283-295.
- Rose, W.B., McCaa, D.J. 1998. Temperature and moisture performance of wall assemblies with fiberglass and cellulose insulation. Proceedings of the DOE/ORNL/ASHRAE/ORNL/BETEC/NRCC/CIBSE Conference, Thermal Performance of the Exterior Envelopes of Buildings VII, American Society of Heating, Refrigerating and Air-Conditioning Engineers, Clearwater, Florida, pp. 133-144.
- Rose, W.B. 1995a. The history of attic ventilation regulation and research. Proceedings of the DOE/ORNL/ASHRAE/BETEC Conference, Thermal Performance of the Exterior Envelopes of Buildings VI, American Society of Heating, Refrigerating and Air-Conditioning Engineers, Clearwater, Florida, pp. 125-134.
- Rose, W.B. 1995b. Attic construction with sheathing-applied insulation. Proceedings of the DOE/ORNL/ASHRAE/BETEC Conference, Orlando, Florida, Thermal Performance of the Exterior Envelopes of Buildings VI , 789-798.

- Rose, W.B. 1994. Conditions for mold growth in vaulted ceilings, Proceedings of the First International Conference on Buildings and the Environment, Building Research Establishment, London, Paper 25.
- Rose, W.B. 1992. Measured values of temperature and sheathing moisture content in residential attic assemblies. Proceedings of the ASHRAE/DOE/BTECC Conference, Clearwater, FL, Thermal Performance of the Exterior Envelopes of Buildings V, 379-389.
- Rousseau, J. 1992. Creating effective air barriers materials and techniques. Proceedings of the ASHRAE/DOE/BTECC Conference, Clearwater, FL, Thermal Performance of the Exterior Envelopes of Buildings V, 646-651.
- Salin, J.-G. 1996. Prediction of heat and mass transfer coefficients for individual boards and board surfaces. A review. Proceedings of the 5th Intern. IUFRO Wood Drying Conf., Quebec City, Canada, pp. 49-58.
- Salonvaara, M. 1990. A transient method to determine moisture and heat transport coefficients of porous materials, 2nd Conference on Building Physics in the Nordic Countries, pp. 355-360.
- Salonvaara, M. and Karagiozis, A. 1994. Moisture transport in building envelopes using an approximate factorization solution method. CFD 94 Conference, CFD, Toronto, 10 p.
- Sandberg, P.I. 1992. Determination of the effects of moisture on the thermal transmissivity of cellulose fiber loose-fill insulation. Proceedings of the ASHRAE/DOE/ BTECC Conference. Thermal performance of the exterior envelopes of building V., American Society of Heating, Refrigerating and Air-Conditioning Engineers, Clearwater Beach, Florida, pp. 517-525.
- Scheffer, T.C. 1971. A climate index for estimating potential for decay in wood structures above ground. Forest Products Journal Vol. 21, no. 10, pp. 25-31.
- Scott, M.A. and Lawton, M. 1991. Laboratory experimentation in wood frame wall drying with comparisons to WALLDRY (modified 1986 version), Report no. 39165.OR/2, CMHC, Ottawa, 43 p.
- Setliff, E.C. 1986. Wood decay hazard in Canada based on Scheffer's climate index formula. The Forestry Chronicle, Canadian Institute of Forestry, Ottawa. Ont., Vol. 62, no. 5, pp. 456-459.
- Shaw, C.Y. 1980. Methods for conduction small-scale pressurization tests and air leakage data of multi-storey apartment buildings, ASHRAE Transactions, ASHRAE, Atlanta, Vol. 86, Part. 1, pp. 241-250.

- Shuman, E.C. 1980. Field measurement of heat flux through a roof with saturated thermal insulation and covered with black and white granules, ASTM STP 718, pp. 519-39.
- Siau, J.F. 1984. Transport processes in wood. Springer-Verlag, New York, 245 p.
- Simpson, A. and O'Connor, D.E. 1994. Timber frame wall : Hygrothermal properties and vapour barrier damage, Building Services Engineering Research and Technology, Chartered Institution of Building Services Engineers, Great Britain, Vol. 15, No. 3, pp. 179-184.
- Skarr, C. 1988. Wood-water relations. Springer-Verlag, New York, 283 p.
- Spalt, H.A. 1957. The sorption of water vapor by domestic and tropical woods. Forest Products Journal, Oct., pp. 331-335.
- Spalt, H.A. 1958. The fundamentals of water vapor sorption by wood. Forest Products Journal, Oct., pp. 288-295.
- Spolek, G. A. and Oosternout, G. R. 1989. Prediction of moisture movement in the walls of residences. Bonneville Power Administration, Contract no. DE-A179-86bp64355.
- Stephenson, D.G. and Mitalas, G.P. 1971. Calculation of heat conduction transfer functions for multi-layer slabs, ASHRAE Transactions, ASHRAE, Atlanta, Vol. 77, P. 2, pp. 117-126.
- Stewart, M. B. 1982. An experimental approach to the study of moisture dynamics in walls, Moisture Migration in Buildings, ASTM STP 779, M. Lieff and H.R. Trechsel, Eds, American Society for Testing and Materials, pp. 92-101.
- TenWolde, A. 1985. Steady-state one-dimensional water vapor movement by diffusion and convection in a multilayered wall. ASHRAE Transactions, ASHRAE, Atlanta, Vol. 91, part 1A, pp. 322-342.
- TenWolde, A. 1989. Moisture transfer through materials and systems in buildings, Water vapor transmission through building materials and systems : mechanisms and measurement, ASTM STP 1039, H. R. Trechsel and M. Bomberg, Eds, American Society for Testing and Materials, Philadelphia, pp. 11-18.
- Tiemann, H.D. 1906. Effect of moisture upon the strength and stiffness of wood. USDA for Serv. Bull. 70, 144 p.
- Timusk, J. and Doshi, H.B. 1986. Effect of insulating sheathing on heat and moisture flow. Canadian Journal of Civil Engineers 13, pp. 674-680.

- Trechsel, H.R. 1994. Moisture control handbook, ASTM Manual 18, American Society for Testing and Materials, Philadelphia.
- Trechsel, H.R., Achenbach, P.R., Ebbets, J.R. 1985a. Effect of an exterior air-infiltration barrier on moisture condensation and accumulation within insulated frame wall cavities. ASHRAE Technical Data Bulletin Infiltrometry and Air leakage, Vol. 1, No.2, pp. 23-37.
- Trechsel, H.R., Achenbach, P.R., Knight, H.J., Lou, G.W. 1985b. Evaluation of wind effect on moisture content of frame walls with and without an air-infiltration barrier. Proceedings of the ASHRAE/DOE/BTECC Conference, Clearwater Beach, Florida, Thermal Performance of the Exterior Envelopes of Buildings III, pp. 648-654.
- Tremblay, C. 1999. Détermination expérimentale des paramètres caractérisant les transferts de chaleur et de masse dans le bois lors du séchage. Thèse de doctorat, Département des sciences du bois et de la forêt, Université Laval, Janvier 1999. 243 p.
- Tremblay, C., Cloutier, A., and Fortin, Y. 1996. Moisture content-water potential relationship of red pine sapwood above the fiber saturation point and determination of the effective pore size distribution. Wood Science and Technology, Springer-Verlag, Vol. 5, No. 30, pp. 361-371.
- Tremblay, C., Cloutier, A., and Fortin, Y. 1999a. Determination of the effective water conductivity of red pine sapwood. Accepted for publication in Wood Science and Technology, Springer-Verlag. (10/97)
- Tremblay, C., Cloutier, A., and Fortin, Y. 1999b. Experimental determination of the convective heat and mass transfer coefficients for wood drying. Accepted for publication in Wood Science and Technology, Springer-Verlag. (07/97)
- Tremblay, C., Cloutier, A. and Grandjean, B. 1999c. Experimental determination of the ratio of vapour diffusion to the total water movement in wood during drying. Wood Fiber Science, Vol. 31, No. 3, pp. 253-248.
- Tsongas, G., Burch, D., Ross, C., Cunningham, M. 1995. A parametric study of wall moisture contents using a revised variable indoor relative humidity version of the "MOIST" transient heat and moisture transfer model. Proceedings of the DOE/ORNL/ASHRAE/BETEC Conference, Thermal Performance of the Exterior Envelopes of Buildings VI, American Society of Heating, Refrigerating and Air-Conditioning Engineers, Clearwater, Florida, pp. 307-319.
- Tsongas, G. and Olson, J. 1995. Tri State homes : a case study of extensive decay in the walls of older manufactured homes with exterior vapor retarder. Proceedings of the DOE/ORNL/ASHRAE/BETEC Conference, Thermal Performance of the

Exterior Envelopes of Buildings VI, American Society of Heating, Refrigerating and Air-Conditioning Engineers, Orlando, Florida, pp. 207-218.

Urquhart, A.R. 1960. Sorption isotherms in J.W.S. Hearle and R.H. Peters, eds. *Moisture in Textiles*. Wiley Interscience, New York, NY, pp. 14-32.

Van Krevelen, D.W., and Hoftyzer, P.J. 1972. *Properties of Polymers Correlations with Chemical Structure*. Elsevier Publishing Co., Amsterdam, 1972, 427 p.

Vershoor, J.D.. 1986. Measurement of water vapor migration and storage in composite building construction ASHRAE Technical Data Bulletin, Vol. 2, No. 5, pp. 140-153.

Viitanen, H. and Ritschoff, A.-C. 1991. Mould growth in pine and spruce sapwood in relation to air humidity and temperature. Report no. 221, Swedish University of Agricultural Sciences, Dep. of forest products, Uppsala, 40 p.

Viitanen, H. 1996. Factors affecting the development of mould and brown rot decay in wooden material and wooden structures Effects of humidity, temperature and exposure time. Dissertation, The Swedish University of Agricultural Sciences Department of Forest Products, Uppsala, 58 p. plus 6 papers.

White, J. 1989. Moisture transport in walls: Canadian experience. Water vapor transmission through building materials and systems: mechanisms and measurement, ASTM STP 1039, H. R. Trechsel and M. Bomberg, Eds, American Society for Testing and Materials, Philadelphia, pp. 35-50.

Zarr, R.R., Burch, D.M., Fanney, A.H. 1995. Heat and moisture transfer in wood-based wall construction : Measured versus predicted. National Institute of Standards and Technology, NIST Building Science Series 173, 72 p.

Appendix A

Conversion calculations

As some of the parameters used in this thesis are not commonly used in building science, their conversion from commonly used parameters is presented.

A.1 Water potential

$$\psi = \frac{RT}{M} \ln \left(\frac{p}{p_{\text{sat}}} \right)$$

where R is the gas constant [8.3143 J/mole K]

T is the temperature [K]

M is the molar mass [$\text{kg}_{\text{water}}/\text{mole}$]

P is the vapor pressure [Pa]

P_{sat} is the saturation vapor pressure [Pa]

For example, a temperature of 20°C,

at 99.5%RH, ψ is -135 J/kg

at 99%RH, ψ is -1 360 J/kg

at 90%RH, ψ is -14 240 J/kg

at 75%RH, ψ is -38 900 J/kg

at 50%RH, ψ is -93 700 J/kg

A.2 Saturation percentage

Conversion of moisture content, M , into saturation percentage, Sp .

The relationship is:

$$S_p = \frac{M}{\frac{1}{G_m} - \frac{1}{G_{ws}}}$$

S_p saturation percentage [%]

M moisture content expressed in percentage [$\text{kg}_{\text{water}}/\text{kg}_{\text{oven-dry wood}} \times 100$]

G_{ws} specific gravity of the wood substance (matière ligneuse) , [$1.5\text{g/cm}^3 \Rightarrow 1500$
 kg/m^3 divided by water density = 1.5 kg/m^3]

$$G_{ws} = \frac{w_0}{V_{ows}\rho_w}$$

w_0 oven-dry mass [$\text{kg}_{\text{oven-dry wood}}$]

V_{ows} oven-dry volume of the wood substance [$\text{m}^3_{\text{oven-dry wood substance}}$]

ρ_w density of water [$\text{kg}_{\text{water}}/\text{m}^3_{\text{water}}$]

G_m specific gravity of moist wood, $G_m = G_g/(1-B_v)$

G_g green specific gravity

$$G_m = \frac{w_0}{V_m\rho_w} = \frac{w_0}{V_{\max}(1-B_v)\rho_w}$$

V_m volume of moist wood [$\text{m}^3_{\text{moist wood}}$]

V_{\max} maximum volume of moist wood [$\text{m}^3_{\text{moist wood}}$] (or green wood volume)

B_v volume shrinkage corresponding to M (maximum 11.3 for spruce)

Green specific gravity, of black spruce (green) 406 kg/m^3 , divided by $\rho_w = .406$

Green specific gravity, of white spruce (green) 390 kg/m^3 , divided by $\rho_w = .390$

For completely dry wood, divide by 0.887 $G_m = .458$.

Given that PSF is at 30%M,

For dry wood at 5%, 5/6 of Bv

$$(1/G_m - 1/G_{ws}) = (1/0.451) - (1/1.5) = 1.56$$

$$M = 5\% \text{ yields } S_p = 5 / 1.56 = 3.2 \%$$

For moist wood, 15%, with 30 %M maximum shrinkage

$$(1/G_m - 1/G_{ws}) = (1/0.430) - (1/1.5) = 1.66$$

$$M = 15\% \text{ yields } S_p = 15 / 1.66 = 9 \%$$

For green wood

$$(1/G_m - 1/G_{ws}) = (1/0.406) - (1/1.5) = 1.80$$

$$M = 70\% \text{ yields } S_p = 70 / 1.8 = 39\%$$

A.3 Water effective conductivity

The relationships to convert diffusion coefficient to effective conductivity are presented in section 3.

The coefficients of diffusion measured by Egner for epicea, at 40°C have presented by Kubler after conversion from coefficient of diffusion due to moisture content gradient to coefficients of diffusion due to vapor pressure gradients..

To convert to water effective conductivity due to a gradient of water potential, the following relationship is used

$$K_{eff} = D_{pv} \cdot \frac{\partial HR}{\partial M} \cdot \frac{p_{vs}}{100} \cdot \frac{\partial M}{\partial \psi}$$

The following table presents the values used for the conversion

M	Dp [m/h]	HR/M	pvs/100	dM/dpsi	K
4	5.50E-08	3.30	20.6	0.000111	1.156E-13
6	6.50E-08	5.30	20.6	0.000111	2.189E-13
12	1.90E-07	4.37	20.6	0.000111	5.285E-13
18	8.00E-07	3.33	20.6	0.000111	1.695E-12
24	2.00E-06	1.93	20.6	0.000111	2.454E-12
28	2.50E-06	1.25	20.6	0.0002	3.576E-12

This uses the sorption for spruce by Hedlin, the sorption curve for red pine by Tremblay.

A.4 Conversion of h_h to h_ψ using the Lewis analogy

Starting with $h_h = 5 \text{ W/m}^2 \text{ }^\circ\text{C}$

Assuming a relative humidity of 90% and a temperature of 10°C and wood surface saturated with water the following is calculated

$$\psi_\infty = 13\,750 \text{ J/kg}$$

$$\psi_{\text{surf}} = 0 \text{ J/kg}$$

$$c_\infty = 0.007 \text{ kg}_{\text{water}}/\text{kg}_{\text{air}} \quad c_\infty = 0.0058 \text{ kg}_{\text{water}}/\text{m}^3_{\text{air}} \text{ with } 0.81 \text{ m}^3/\text{kg}$$

$$c_{\text{surf}} = 0.0078 \text{ kg}_{\text{water}}/\text{kg}_{\text{air}} \quad c_\infty = 0.0063 \text{ kg}_{\text{water}}/\text{m}^3_{\text{air}} \text{ with } 0.81 \text{ m}^3/\text{kg}$$

Conversion of h_h to h_{mc}

$$h_{mc} = \frac{h_h}{\cdot c_p \cdot Le^{2/3}} = \frac{5 \frac{W}{m^2 \cdot C}}{1.2 \frac{kg}{m^3} \cdot 1011 \frac{J}{kgK} \cdot 1} = 0.004 m/s$$

Conversion of h_{mc} to $h_{m\psi}$

$$h_m = h_{mc} \left(\frac{c_{surf} - c_{\infty}}{\psi_{surf} - \psi_{\infty}} \right) = 0.004 \frac{0.0005}{13750} = 1.45 \times 10^{-1} \frac{kg^2_{water}}{s \cdot J \cdot m^2_{air}}$$

If $h_h = 4.6$, $h_{\psi} = 1.38 \times 10^{-10}$

If $h_h = 2$, $h_{\psi} = 6.0 \times 10^{-11}$

Appendix B

Legend of sensors used during the experimental test

Most sensors have a three-part tagname, for example: TC_T3_7

First part refers to type of sensors

TC thermocouples

RH relative humidity

M moisture content sensor

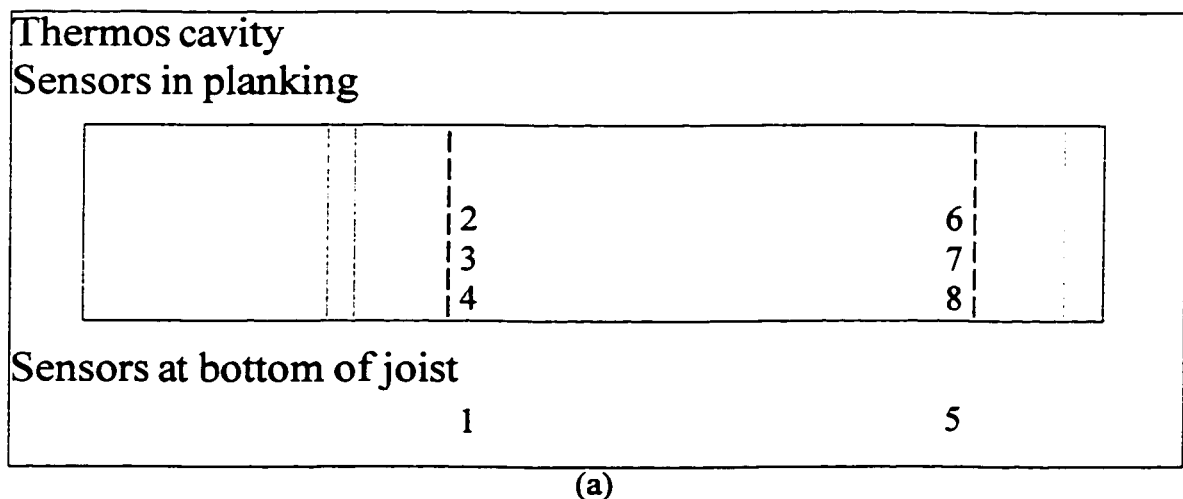
The second part refers to the cavity

T1, T2, T3, T4 and T5 are the five cavities of the thermos hut

L1, L2, L3, L4 and L5 are the five cavities of the lambourdes hut

See figure 2.5 of text

The third part refers to the specific location of the sensor within a cavity as shown in the diagrams of Figure B.1.



Lambourdes cavity

Sensors in planking

		3		15	8	11
		4		16	9	
		5		17	10	12

Sensors at bottom and top of joist

1	13	6
2	14	7

(b)

B.1 Diagrams of layout of sensors.

Appendix C

Calculation results of the convective heat and mass transfer coefficients above wood in a 10mm high tunnel.

Parameters for run 1, 2 and 3

White pine specimens at 12% moisture content

$$\begin{aligned}
 \text{Volume of moist wood} \quad V_h &:= .038 \cdot \text{m} \cdot .295 \cdot \text{m} \cdot .091 \cdot \text{m} & V_h &= 1.02 \cdot 10^{-3} \cdot \text{m}^3 \\
 \text{Mass of moist wood} \quad M_h &:= .3718 \cdot \text{kg} \\
 \text{Density of moist wood} \quad D_m &:= \frac{M_h}{V_h} & D_m &= 364.47 \cdot \text{kg} \cdot \text{m}^{-3} \\
 \text{Specific heat of moist wood} \quad C_{p\text{wood}} &:= 1250 \cdot \frac{\text{joule}}{\text{kg} \cdot \text{degC}} & C_{p\text{water}} &:= 4180 \cdot \frac{\text{joule}}{\text{kg} \cdot \text{degC}} \\
 C_p &:= \left(C_{p\text{wood}} \cdot \frac{100}{112} \right) + \left(C_{p\text{water}} \cdot \frac{12}{112} \right) & C_p &= 1.564 \cdot 10^3 \cdot \text{m}^2 \cdot \text{sec}^{-2}
 \end{aligned}$$

Run 1

Air velocity = 0.3 m/s

Table C.1. Summary of data calculated from run 1

Time [s]	Integral of profile [°C·m]	Heat= Integral x $D_m C_p$ [J/m ²]	$q_{\text{cond}} = 70.85 -$ $0.0222 \cdot t$ [W/m ²]	$\Delta T =$ $T_{\infty} - T_{\text{surf}}$ [°C]	$h_c = q_{\text{cond}} / \Delta T$ [W/m ² ·°C]
0	0.046	26710	70.86	6.99	10.13
651	0.135	77550	56.54	5.02	11.27
1275	0.182	104100	42.81	3.87	11.07
1879	0.213	122100	29.53	2.88	10.24
2492	0.235	134900	16.03	2.16	7.44
3105	0.250	143100	2.54	1.70	1.50
3366	0.255	146000	-3.18	1.53	-2.08
Mean value for 4 first values					10.6

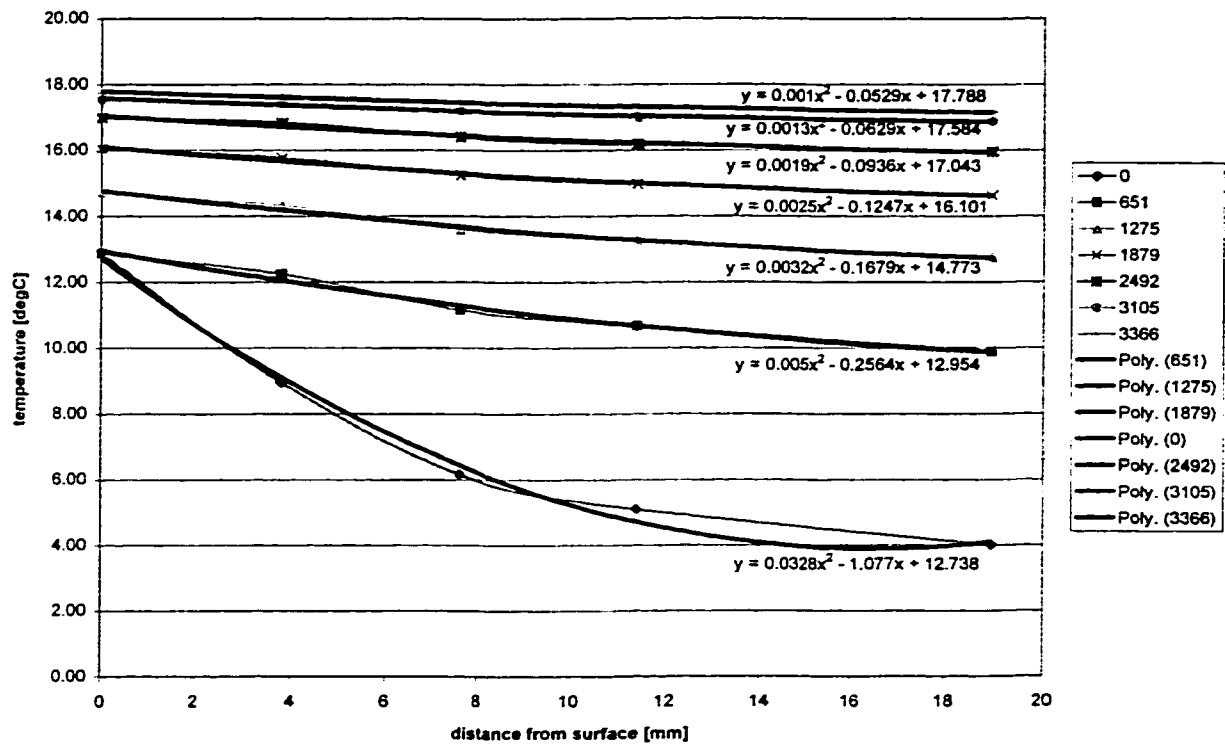


Figure C.1. Temperature profiles for run 1

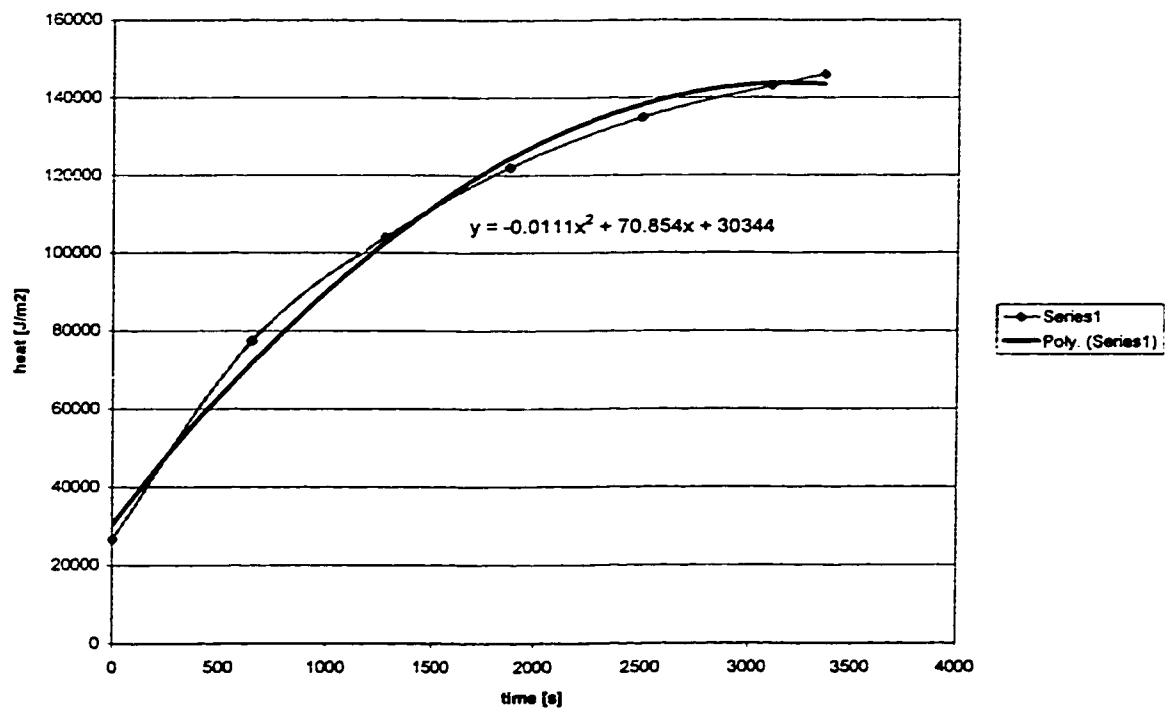


Figure C.2 – Heat per square meter of wood as a function of time for run 1

Run 2

Air velocity = 0.3 m/s

Table C.2. Summary of data calculated from run 2

Time [s]	Integral of profile [$^{\circ}\text{C}\cdot\text{m}$]	Heat= Integral $\times D_m C_p$ [J/m^2]	$q_{\text{cond}}=90.24-0.026\cdot t$ [W/m^2]	$\Delta T = T_{\infty}-T_{\text{surf}}$ [$^{\circ}\text{C}$]	$h_c = q_{\text{cond}}/\Delta T$ [$\text{W}/\text{m}^2\cdot^{\circ}\text{C}$]
0	0.043	24400	90.24	9.29	9.72
563	0.152	86870	75.60	7.34	10.29
1205	0.223	127500	58.90	5.78	10.18
1848	0.269	153200	42.19	4.31	9.80
2450	0.299	170300	26.54	3.29	8.06
3102	0.320	182600	9.58	2.03	4.71
3714	0.331	188600	-6.33	1.37	-4.61
3915	0.335	190900	-11.55	1.53	-7.56
Mean value for 5 first values					9.6

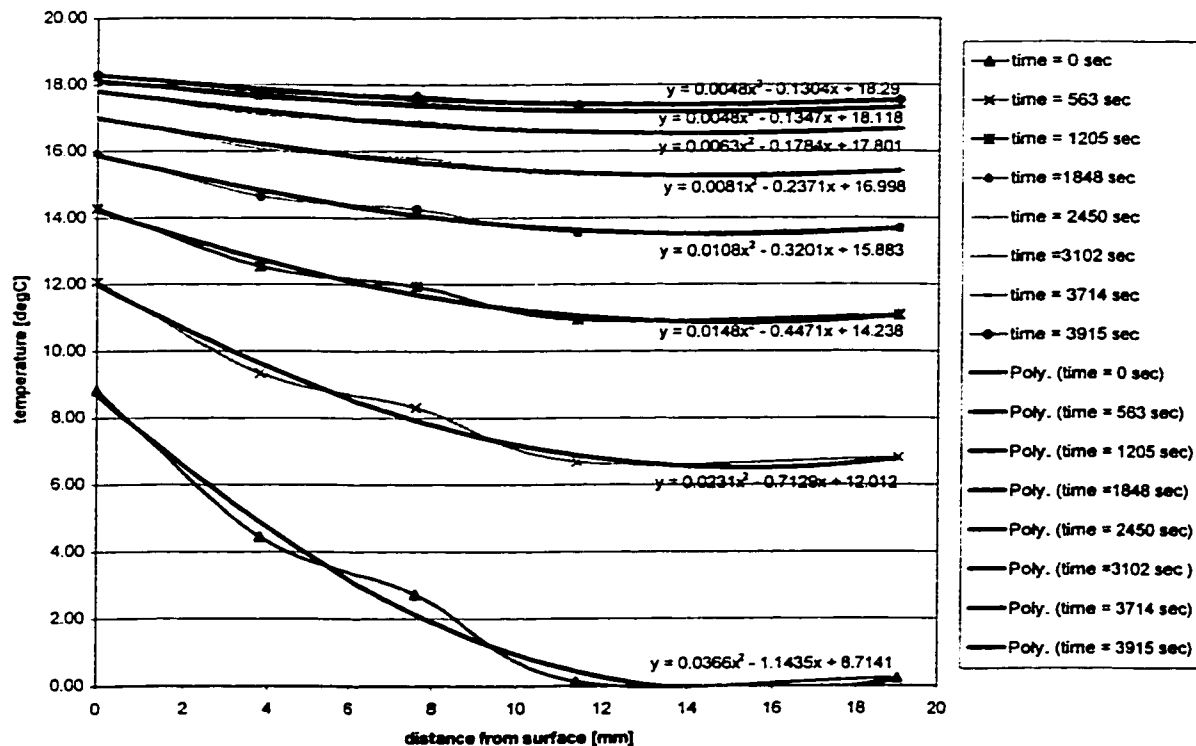


Figure C.3. Temperature profiles for run 2

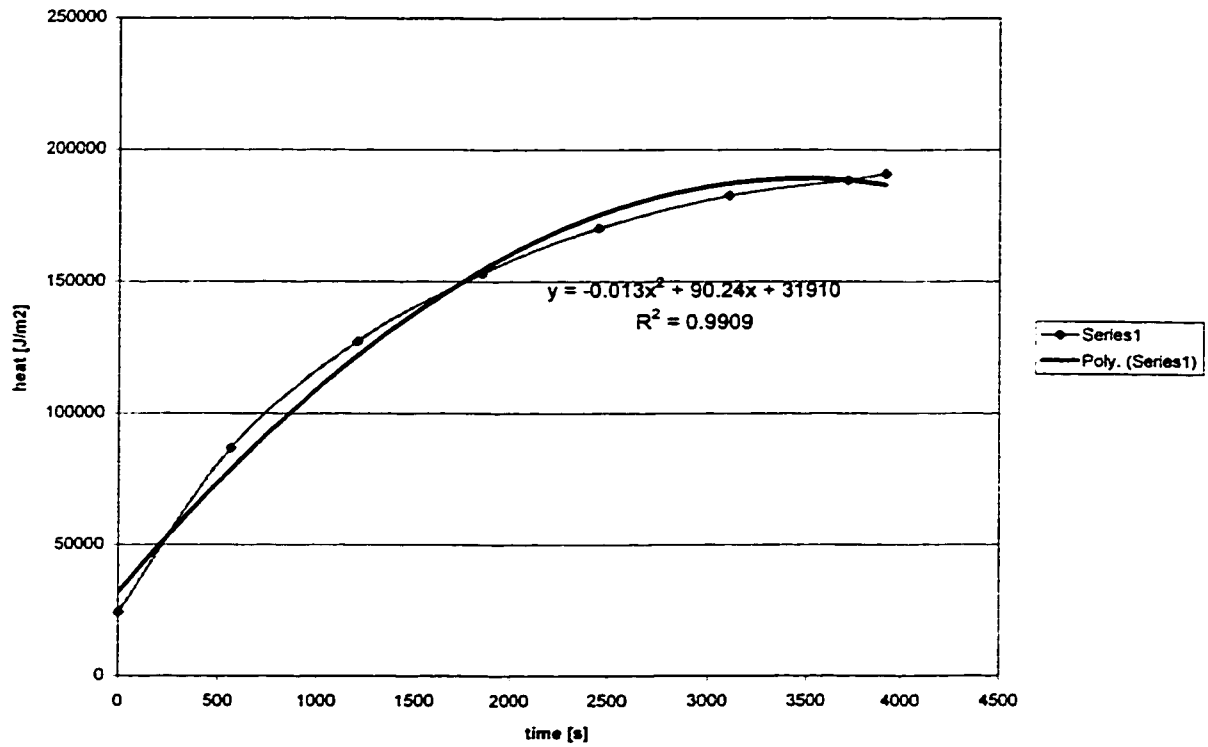


Figure C.4 – Heat per square meter of wood as a function of time for run 2

Run 3

Air velocity = 0.15 m/s

Table C.3. Summary of data calculated from run 3

Time [s]	Integral of profile [°C·m]	Heat= Integral $\times D_m C_p$ [J/m²]	$q_{\text{cond}} = 52.69 -$ $0.0108 \cdot t$ [W/m²]	$\Delta T =$ $T_{\infty} - T_{\text{surf}}$ [°C]	$h_c =$ $q_{\text{cond}} / \Delta T$ [W/m²·°C]
623	0.135	77460	45.97	12.64	3.64
1236	0.182	104700	39.34	9.52	4.13
1849	0.224	128300	32.72	7.69	4.25
2462	0.253	145300	26.10	6.35	4.11
3076	0.275	157900	19.47	5.35	3.64
3689	0.292	167400	12.85	4.35	2.95
4302	0.304	174400	6.23	3.65	1.71
4516	0.310	177600	3.92	3.55	1.10
Mean value for 6 first values					3.8

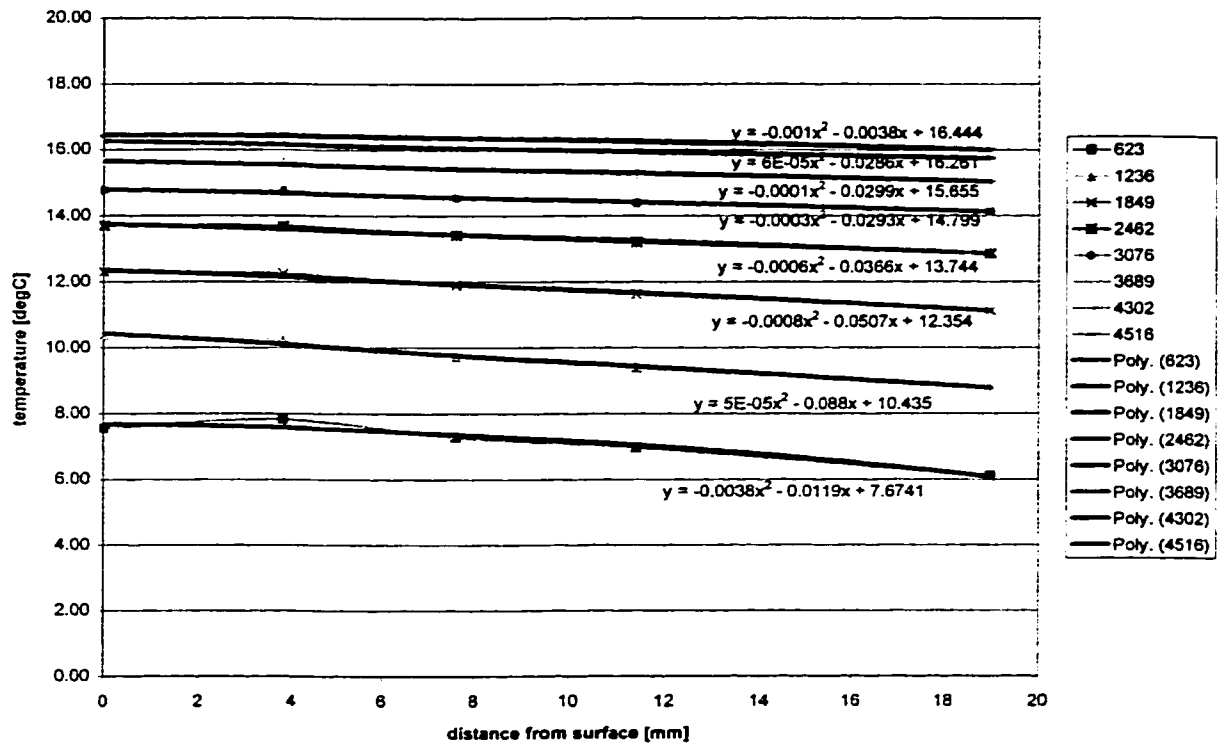


Figure C.5. Temperature profiles for run 3

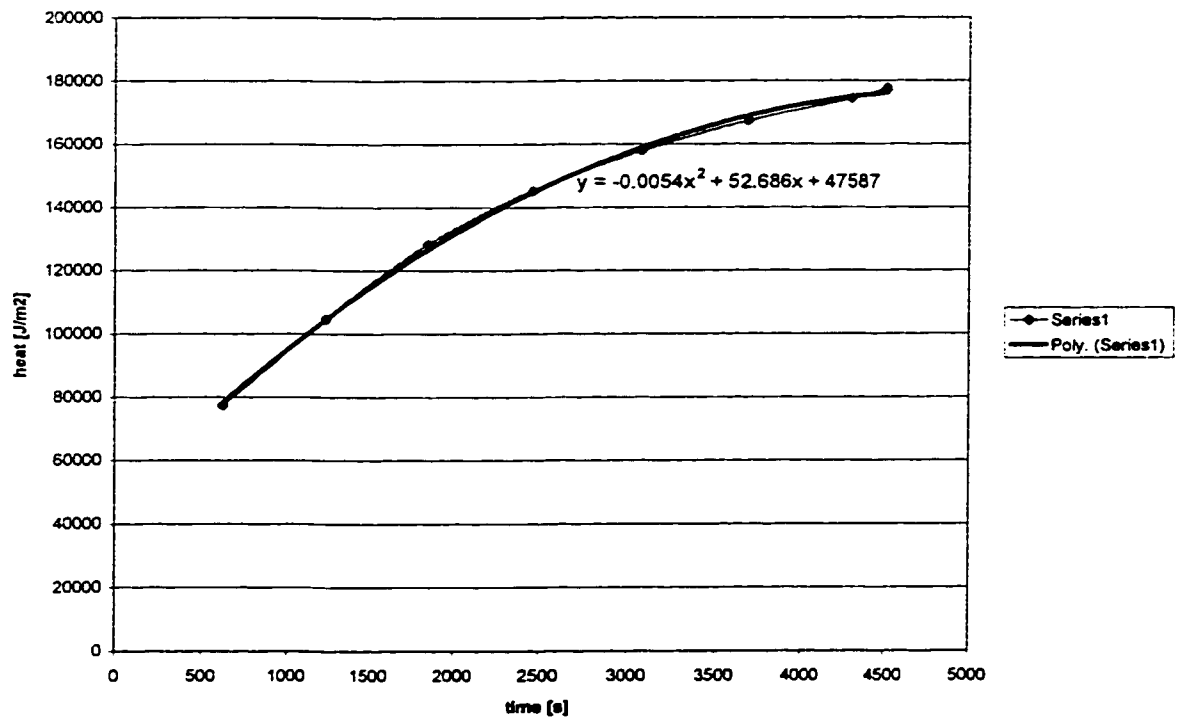


Figure C.6 – Heat per square meter of wood as a function of time for run 3

Run 4

Air velocity 0.15 m/s

M := 75.5 %

Volume of moist wood $.040 \cdot m \cdot .295 \cdot m \cdot .093 \cdot m = 1.097 \cdot 10^{-3} \cdot m^3$ $V_h := 1.086 \cdot 10^{-3} \cdot m^3$

Mass of moist wood $M_h := .705 \cdot kg$

Density of moist wood $D_m := \frac{M_h}{V_h}$ $D_m = 649.171 \cdot kg \cdot m^{-3}$

Specific heat of moist wood $C_{pwood} := 1250 \cdot \frac{joule}{kg \cdot degC}$ $C_{pwater} := 4180 \cdot \frac{joule}{kg \cdot degC}$

$$C_p := \left(C_{pwood} \cdot \frac{100}{175.5} \right) + \left(C_{pwater} \cdot \frac{75.5}{175.5} \right) \quad C_p = 2.51 \cdot 10^3 \cdot m^2 \cdot sec^{-2}$$

Heat taken by evaporation

$$q := \left(1.46 \cdot 10^{-5} \cdot \frac{kg}{sec \cdot m^2} \right) \quad h_{vap} := 2454.66 \cdot 1000 \cdot joule \cdot kg^{-1} \quad q_m := q \cdot h_{vap} \quad q_m = 35.838 \cdot m^{-2} \cdot watt$$

During drying of specimen

Table C.4. Summary of data calculated from run 4

Time [s]	Integral of profile [°C·m]	Heat= Integral x $D_m C_p$ [J/m ²]	$q_{cond} = 130.04 -$ $0.114t +$ $2.7 \times 10^{-5} t^2$ [W/m ²]	$q_{tot} =$ $q_{cond} + q_m$ [W/m ²]	$\Delta T =$ $T_{\infty} - T_{surf}$ [°C]	$h_c =$ $q_{cond} / \Delta T$ [W/m ² ·°C]
1085.4	0.223	363500.0	38.11	73.95	4.8	15.57
1357.2	0.229	372600.0	25.05	60.89	4.9	12.34
1912.7	0.230	380900.0	10.77	46.61	4.7	9.97
2455.9	0.234	387700.0	12.92	48.75	4.8	10.24
2727.7	0.238	391600.0	19.97	55.81	4.7	11.91
Mean value for 5 values						12.01

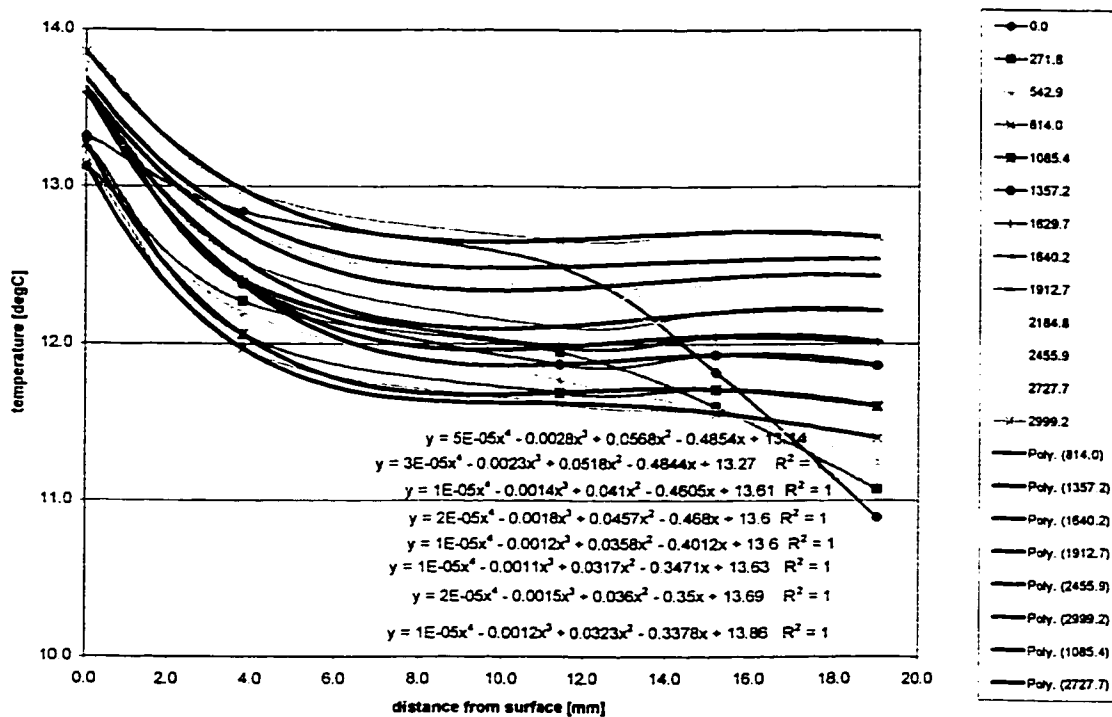


Figure C.7 Temperature profiles for run 4

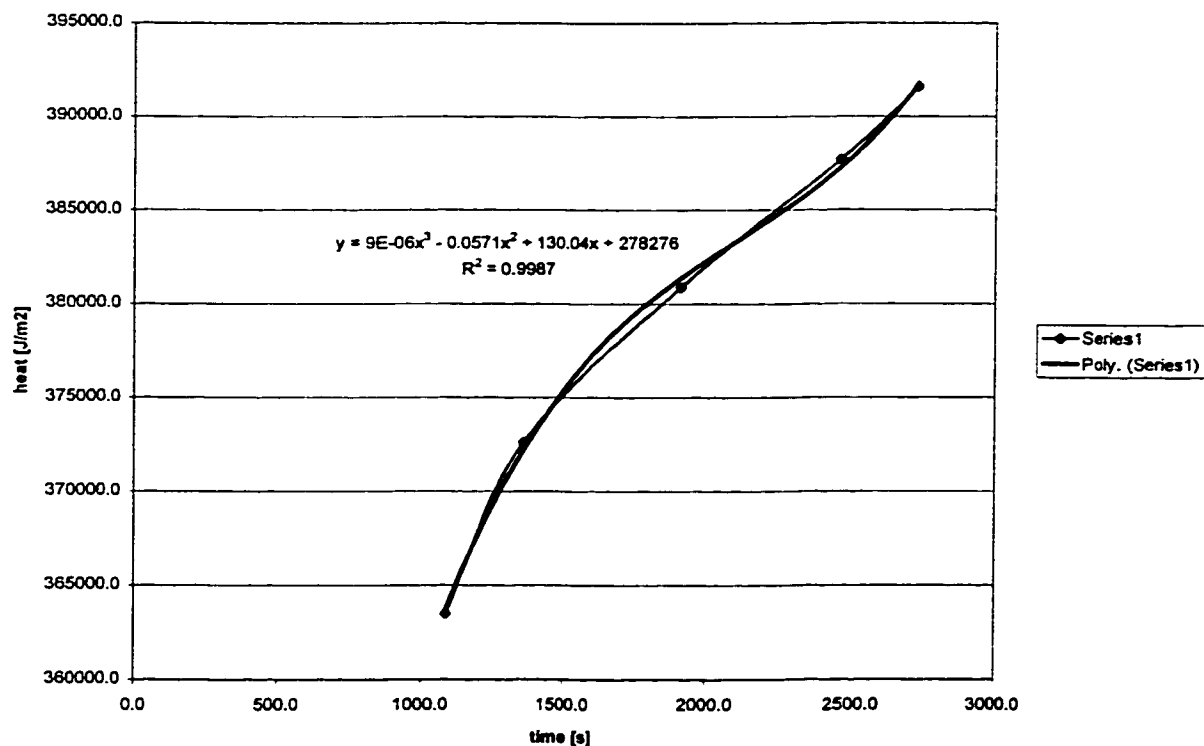


Figure C.8. Heat per square meter of wood as a function of time for run 4

Warming in wet conditions

Resulting in gain of weight due to condensation

Heat brought by condensation

$$q := \frac{0.004 \cdot \text{kg}}{3600 \cdot \text{sec} \cdot 2 \cdot 0.093 \cdot \text{m} \cdot 0.295 \cdot \text{m}} \quad q = 2.025 \cdot 10^{-5} \cdot \text{kg} \cdot \text{m}^{-2} \cdot \text{sec}^{-1}$$

Heat flux

$$q_m := q \cdot h_{\text{vap}} \quad h_{\text{vap}} = 2.455 \cdot 10^6 \cdot \text{kg}^{-1} \cdot \text{joule} \quad q_m = 49.707 \cdot \text{m}^{-2} \cdot \text{watt}$$

By integration of profiles, it is found that heat flux to wood is completely due to condensation. So there was no convective transfer.

Table C.5. Summary of data calculated from run 4

Time [s]	Integral of profile [°C·m]	Heat= Integral x D _m C _p [J/m ²]	q _{cond} =--·t [W/m ²]
0	0.092	78810	discarted*
324	0.099	85170	discarted*
952	0.114	98320	42.20
1580	0.139	119200	43.58
2208	0.167	143800	44.96
2837	0.194	166700	46.35
3444	0.215	184700	47.68

*impact of defrost at center of specimen was too strong at those times

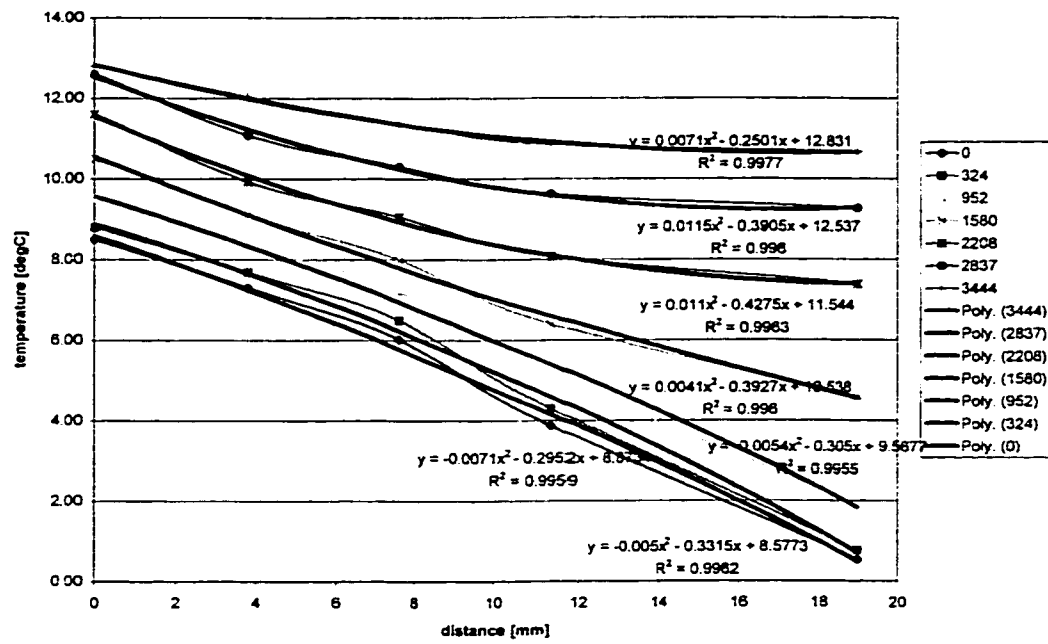


Figure C.9. Temperature profiles for warming in wet conditions

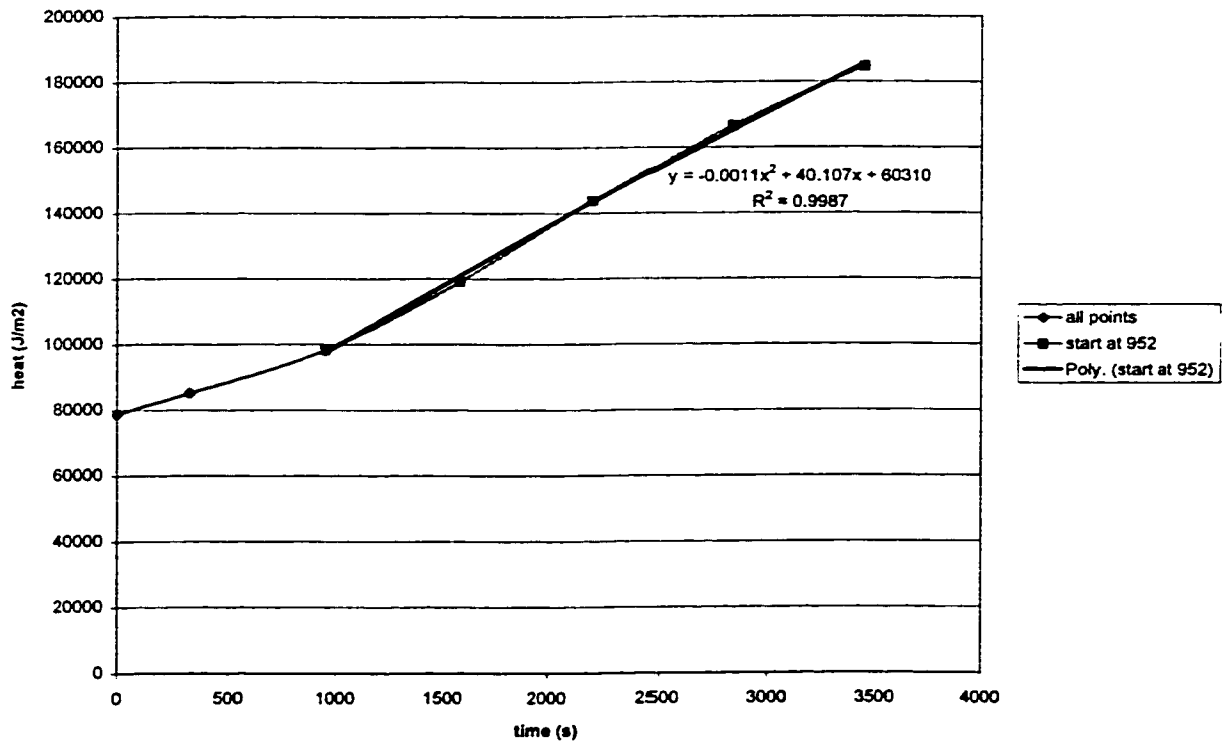


Figure C.10 – Heat per square meter of wood as a function of time for warming on wet conditions

Mass transfer coefficient

Run 5

$$A := 2 \cdot 0.093 \cdot 0.295 \cdot \text{m}^2 \quad A = 0.055 \cdot \text{m}^2$$

From graph, find slope $\text{flux} := 8.046 \cdot 10^{-7} \cdot \text{kg} \cdot \text{sec}^{-1}$

$$q_m := \frac{\text{flux}}{A} \quad q_m = 1.466 \cdot 10^{-5} \cdot \text{kg} \cdot \text{m}^{-2} \cdot \text{sec}^{-1}$$

$$R := 8.3143 \cdot \text{joule} \cdot \text{mol}^{-1} \cdot \text{degK}^{-1} \quad M := 0.0180153 \cdot \text{kg} \cdot \text{mol}^{-1} \quad T := (273 + 19.5) \cdot \text{degK} \quad \text{RH} := 70$$

$$\psi_{\text{air}} := R \cdot \frac{T}{M} \cdot (\ln(\text{RH} \cdot 0.01)) \quad \psi_{\text{air}} = -4.815 \cdot 10^4 \cdot \text{joule} \cdot \text{kg}^{-1}$$

$$\psi_{\text{surface}} := -800 \cdot \text{joule} \cdot \text{kg}^{-1}$$

$$h_\psi := \frac{q_m}{(\psi_{\text{surface}} - \psi_{\text{air}})} \quad h_\psi = 3.097 \cdot 10^{-10} \cdot \text{kg}^2 \cdot \text{m}^{-2} \cdot \text{sec}^{-1} \cdot \text{joule}^{-1}$$

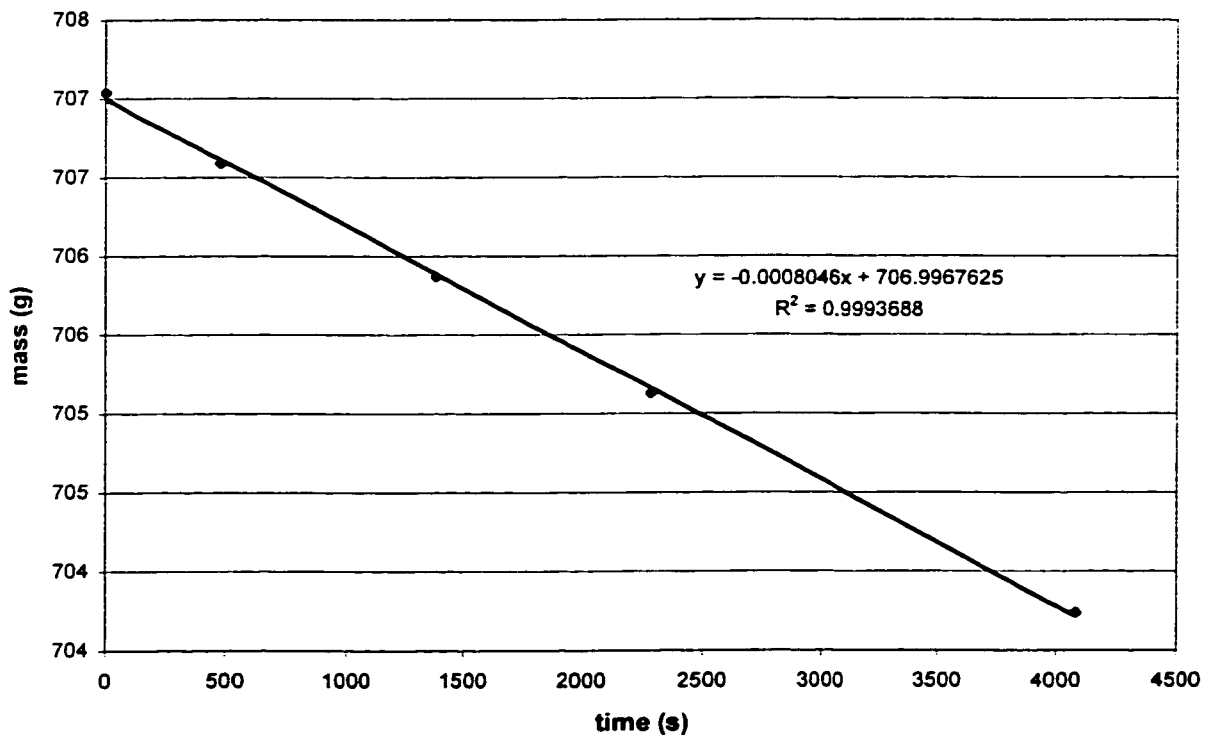


Figure C.11. Results of the drying test to determine the convective mass transfer coefficient

Appendix D

Schematic representation of finite element mesh

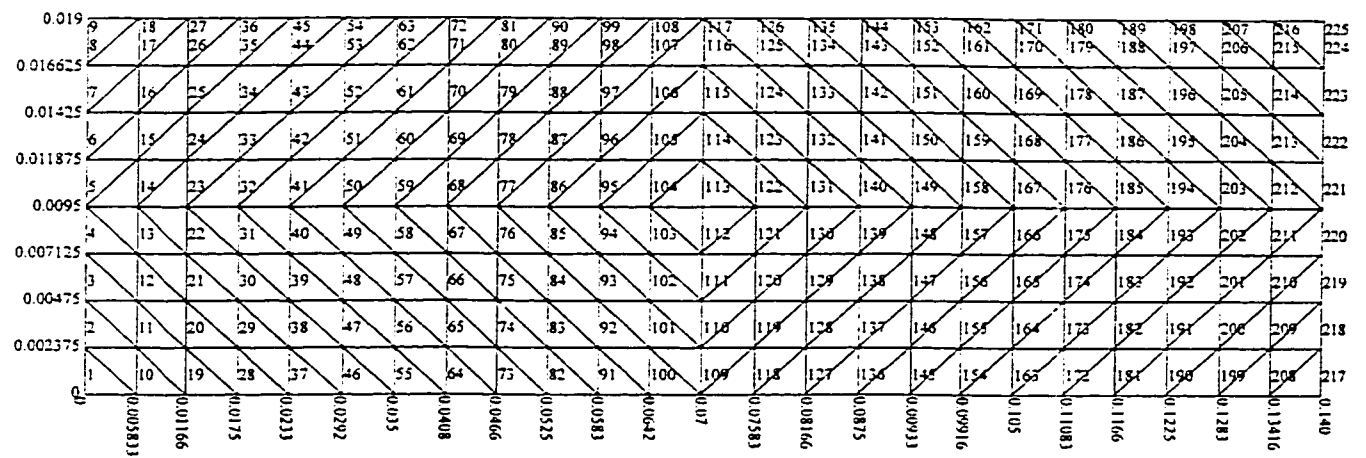


Figure D.1. Schematic representation of finite element mesh.